Fatigue life improvement of DOT-CFFC composite cylinders

December 2015

Prepared for

United States Department of Transportation
Pipeline and Hazardous Materials Safety Administration
Mark Toughiry, PE
1200 New Jersey Avenue, SE
Washington, DC 20590-0001
(202) 366-4545

Prepared by

Digital Wave Corporation
Brian Burks PhD, Steven Ziola PhD, Michael Gorman PhD
13760 East Arapahoe Road
Centennial, CO 80121
(303) 790-7559

Synopsis

- **Forty (40) of the forty (40) DOT-CFFC cylinders which were reautofrettaged and then subjected to 10,000 fatigue cycles (20 years of additional service life) achieved the required 10,000 fatigue cycles without leaking.**
- **Ten (10) of the ten (10) cylinders which were subjected to a block loading fatigue test protocol sustained an additional 24,000 fatigue cycles without the 6061-T6 aluminum liner leaking.**
- **All fifty cylinders subjected to extended service life simulation burst above the minimum required pressure for virgin manufactured DOT-CFFC cylinders.**

Executive Summary

In this research program, the efficacy of a reautofrettage process for improving the fatigue performance of past service life DOT-CFFC composite overwrapped Type III pressure cylinders was evaluated. Previous research has found that hard water exposure of the 6061 T6 aluminum liner associated with the DOT-CFFC cylinder design had a detrimental effect on the fatigue life of the liner. The hard water exposure facilitates an ion exchange between the mineral rich water and the 6061 aluminum alloy which leads to intercrystalline cracking. Hard water exposure of the aluminum liner is characterized by a discoloration of the liner, with a small flaw initiation site at a grain boundary; when subjected to pressure fatigue cycles the flaw eventually grows through wall, rendering the cylinder incapable of holding pressure. It is pointed out that DOT-CFFC cylinders are designed in a leak-before burst fashion and are thus a fail-safe design. However, in breathing air applications a leak is still an adverse failure mechanism.

Through the use of a coupled laminated plate theory, fracture mechanics, and fatigue life estimation analysis, a reautofrettage method was proposed to mitigate the effects of hard water exposure and enhance the fatigue life performance of past service life DOT-CFFC cylinders. To validate the reautofrettage method, forty (40) expired service life DOT-CFFC cylinders were reautofrettaged and then subjected to 10,000 fatigue cycles to maximum developed pressure during fast fill. All forty (40) expired service life cylinders successfully achieved an additional 10,000 fatigue cycles (equivalent to 20 years of additional service life per ISO 11119.2:2002). Post fatigue cycle testing, all forty (40) cylinders were burst test, and it was found that all forty (40) cylinders had a burst strength above what is required for newly manufactured DOT-CFFC composite pressure cylinders.

Further, an additional ten (10) expired service life DOT-CFFC cylinders were subjected to the reautofrettage process and then subjected to a block loading fatigue test program. The block loading fatigue test program was meant to more realistically simulate a typical five (5) year service life interval for a composite cylinder, in which the cylinder would be filled to normal operating pressure for 5 contiguous years (2,500 cycles per ISO 11119.2:2002) and then subjected to a test pressure

cycle as is the case when the cylinder is requalified. Using this fatigue testing protocol, all ten (10) cylinders which had already experienced a fifteen (15) year service life achieved 24,000 fatigue cycles to maximum developed pressure during fast fill (which qualifies a cylinder for infinite service life per ISO 11119.2:2002). Moreover, the ten (10) cylinders which were subjected to 24,000 fatigue cycles to maximum developed pressure after a fifteen (15) year service life were subsequently burst test, and all ten (10) cylinders met the minimum required burst pressure for newly manufactured DOT-CFFC pressure cylinders.

During the fatigue testing and burst pressurization of all fifty (50) cylinders, Modal Acoustic Emission (MAE) was utilized to monitor the damage mechanisms accumulating within the composite microstructure. During fatigue cycle testing, minimal new damage accumulation was detected as all cylinders had achieved their characteristic damage state and were not progressing to failure. During the burst pressurization, it was again found that through the use of a Background Energy Oscillation metric the burst pressure of a specific cylinder could be predicted at an average of 60% of the ultimate strength of a cylinder. Such a predictive capability allows composite pressure cylinders with compromised strength to be removed from service at the time of requalification, improving the safety of the public in the presence of hazardous materials.

Through the use of a reautofrettage method, it has been found that the effects of hard water exposure on the liners of DOT-CFFC cylinders can be mitigated and the fatigue life performance of the cylinder can be safely and reliably improved. With this breakthrough it is concluded that DOT-CFFC designed cylinders may safely be granted an additional fifteen (15) years of service life without compromising the fatigue life performance, the reliability for pressure containment, or the ultimate strength of the cylinder.

Contents

1. Introduction

1.1 *Scope*

The purpose of this research program was to evaluate the efficacy of a reautofrettage process aimed at improving the fatigue life performance of DOT-CFFC aluminum liners. Through the results presented herein, a solid engineering assessment of the viability of extending the service life of DOT-CFFC cylinders may be made relative to the ability to withstand an additional fifteen (15) years of service life.

1.2 *Background Information*

Over the past few decades, DOT-CFFC type III carbon fiber composite cylinders have been in use by firefighters, hazardous materials personnel, and first responders as part of Self Contained Breathing Apparatus (SCBA) units due to their exceptional breathing air to weight ratio. In the United States the design and testing standard that governs the manufacture of these cylinders is known as the "Basic requirements for fully wrapped carbon-fiber reinforced aluminum lined cylinders (DOT-CFFC)" [1]. In the DOT-CFFC design document the permissible materials' of construction, the required cylinder burst strength, and the method of construction are covered. Furthermore, clause 3 of the DOT-CFFC document grants a fifteen (15) year service life, and allows for the potential of a 30 year service life provided certain requirements are met [1]. Where the service life limitation or the engineering analysis to support such a decision is never provided nor referenced.

Based upon the design requirements of the DOT-CFFC document, the carbon fiber composite overwrap (the primary strength member of the design) must operate at a stress level (< 30% of the ultimate fiber strength) which from a fatigue perspective keeps the cylinder in an infinite life regime. Data from previous research programs focused on DOT-CFFC cylinders which had experienced full fifteen (15) year service lives has confirmed that cylinders designed to DOT-CFFC requirements possess the same strength after fifteen (15) years of service life as the day the cylinder was manufactured [2]. Furthermore, it was established that the strength of the composite overwrap was not diminished after a full fifteen (15) year service life and a simulated twenty (20) additional years of service life [2]. Moreover, in the aforementioned research program a non-destructive evaluation technique known as Modal Acoustic Emission (MAE) was found to properly assess the structural integrity of DOT-CFFC cylinders far more reliably than the currently accepted practice of elastic expansion measurement. It has been repeatedly proven that MAE reliably detects cylinders with compromised burst strengths, enabling them to be removed from service at the time of requalification and/or life extension.

A final potential concern relative to extending the life of the DOT-CFFC cylinder design emanates from the possibility of the aluminum liner leaking after a sufficient number of fatigue cycles. It has been found that DOT-CFFC cylinders which are exposed to hard water for "prolonged periods of time" have the potential to develop pits within the 6061-T6 aluminum liner, and when fatigue cycled the pits act as a flaw initiation site and grow through wall causing the cylinder to leak [3, 2]. It is important to note that the hard water exposure may very well happen at the time of manufacture during the initial autofrettage pressurization. Based upon data provided in [3], it is purported that cylinders which have been subjected to hard water exposure may very likely leak in less than 5,000 cycles; such data indicate that cylinders would have the possibility of leaking within ten (10) years of service life. Yet, after nearly twenty (20) years of DOT-CFFC cylinders being in service, reports of cylinder leakage are nowhere to be found.

In this research program the fundamental mechanism behind why DOT-CFFC cylinders which have been subjected to hard water exposure do not leak and are eligible for extended service life will be shown to be due to the effects of crack closure which occur because of the tensile overloading of the 6061-T6 aluminum liner associated with the five (5) year requalification test pressure cycle. In this research program, a theoretical fatigue life estimation model is proposed which elucidates the effects of periodic tensile overloads on the fatigue life performance of the 6061-T6 aluminum liners. Further, a reautofrettage process has been proposed to mitigate the effects of the potential for liner leakage due to the intercrystalline cracking of the 6061-T6 aluminum alloy when subjected to hard water. A test program consisting of the reautofrettage procedure and subsequent fatigue test pressure cycling of forty (40) end of service life DOT-CFFC cylinders was conducted to gain a high level of confidence in the ability to extend the service life of DOT-CFFC cylinders an additional fifteen (15) years.

Finally, ten (10) end of service life cylinders were subjected to the reautofrettage process and then a block loading fatigue cycle test procedure as shown in Figure 1.1 for a maximum of up to 24,000 fatigue cycles (infinite life as specified in ISO 11119.2:2002) [4]. The block loading fatigue cycle schedule shown in Figure 1.1 more realistically simulates the in service loading that DOT-CFFC cylinders experiences. By accounting for the test pressure cycle which occurs every twenty-five hundred cycles or five years, it is postulated that liner leakage will not be an issue. By subjecting the cylinder to test pressure every five years, any crack that may exist within the aluminum liner develops a significant plastic zone around the crack tip and the neighboring material is left in compression, significantly retarding crack growth. Such block loading is far more realistic of what cylinders experience in service as compared to the fatigue test procedures specified in relevant standards documents (e.g., ISO 11119.2:2002, and DOT-CFFC), and should potentially be adopted by such standards documents to gain a more realistic view of cylinder fatigue life performance.

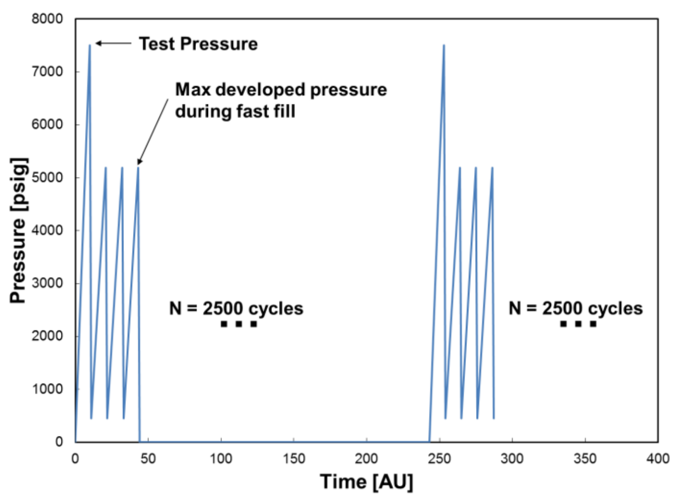

Figure 1.1 – Block loading fatigue cycle schedule intended to directly mimic the in service loading experienced by COCs which are required to requalified every five (5) years.

2. Test Protocols

2.1 *10k fatigue testing*

Prior to any physical testing, forty (40) cylinders were visually inspected per the guidelines of CGA C-6.2 [5]. Results of the internal and external visual inspections are summarized in Section 4. Subsequently, cylinders were reautofrettaged to 113.3% of their designed test pressure. As Section 3 will show, the application of a tensile overload will put any pre-existing flaw into residual compression and significantly retard crack growth.

During the reautofrettage process hydraulic pressure was monitored via a Wika A10 pressure transducer (S/N 11020E6Z), all cylinders were instrumented with a Micro Measurements CEA-06-500UW-120 hoop oriented strain gage located in the cylinder side wall (Figure 2.1), and three Digital Wave Corporation B1025 MAE transducers, one located at the top cylinder-to-side wall transition and two located at the bottom cylinder-to-sidewall transition. The hoop oriented strain gage enabled a plastic deformation measurement of the aluminum liner to be made, and the MAE transducers enabled the structural integrity of the cylinders to be assessed during the reautofrettage process.

Figure 2.1 – Hoop oriented strain gage, and three broadband MAE transducers were placed on each SCBA cylinder during the reautofrettage process, and subsequent cyclic fatigue testing.

During the cyclic fatigue testing, ten cylinders were pressurized in parallel from 400 psig to at least 5,192 psig (maximum developed pressure during fast fill[1]) for a maximum of 10,000 cycles per the fatigue testing requirements of Section 8.5.5 of ISO 11119.2:2002 [4]. Per Section 8.5.5.1.3 of ISO 11119.2:2002, 10,000 fatigue cycles to maximum developed pressure is equivalent to twenty (20) years of service life. The cyclic fatigue frequency was set to approximately 0.02 Hz, resulting in a quasi-static stress state developed within the cylinder during each fatigue cycle. Water with a corrosion inhibitor was used as the pressurizing media. Pressure was monitored via a Wika A10 pressure transducer (S/N 11020E6Z), all cylinders were instrumented with a hoop oriented Micro Measurements CEA-06-500UW-120 strain gage located in the cylinder side wall (Figure 2.1), and three Digital Wave Corporation B1025 MAE transducers, one located at the top cylinder-to-side wall transition and two located at the bottom cylinder-to-sidewall transition. The hoop oriented strain gage enabled the hoop modulus as a function of the number of applied cycles to be monitored, and the MAE transducers enabled the structural integrity of the cylinders to be assessed during the cyclic fatigue test.

2.2 *24k fatigue testing*

Prior to any physical testing, ten (10) cylinders were visually inspected per the guidelines of CGA C-6.2 [5]. Results of the internal and external visual inspections are summarized in Section 4. Subsequently, cylinders were reautofrettaged to 113.3% of their designed test pressure. As Section 3 will show, the application of a tensile overload will put any pre-existing flaw into residual compression and significantly retard crack growth.

During the reautofrettage process hydraulic pressure was monitored via a Wika A10 pressure transducer (S/N 11020E6Z), all cylinders were instrumented with a Micro Measurements CEA-06-500UW-120 hoop oriented strain gage located in the cylinder side wall (Figure 2.1), and three Digital Wave Corporation B1025 MAE transducers, one located at the top cylinder-to-side wall transition and two located at the bottom cylinder-to-sidewall transition. The hoop oriented strain gage enabled a plastic deformation measurement of the aluminum liner to be made, and the MAE transducers enabled the structural integrity of the cylinders to be assessed during the reautofrettage process.

During the cyclic fatigue testing, ten cylinders at a time were pressurized in parallel from 400 psig to at least 5,192 psig (maximum developed pressure during fast fill) for 2,500 cycles (equivalent to a five (5) year service life). After the 2,500 fatigue cycles to maximum developed pressure during fast fill, a test pressure cycle to 5/3^{rds} of the cylinder's service pressure was performed; the application of a test pressure cycle was representative of the pressurization that is required per the respective special permits every five (5) years to requalify a cylinder to be transported in commerce. The block loading sequence (Figure 1.1) was repeated until each cylinder was subjected to 24,000 cycles. Per Section 8.5.5.1.3 of ISO 11119.2:2002, 24,000 fatigue cycles to maximum developed pressure is equivalent to an unlimited service life.

---

[1] Maximum developed pressure for this research project is developed pressure of breathing air at 65 ˚C that may occur during fast filling.

The cyclic fatigue frequency was set to approximately 0.02 Hz, resulting in a quasi-static stress state developed within the cylinder during each fatigue cycle. Water with a corrosion inhibitor was used as the pressurizing media. Pressure was monitored via a Wika A10 pressure transducer (S/N 11020E6Z), all cylinders were instrumented with a hoop oriented Micro Measurements CEA-06-500UW-120 strain gage located in the cylinder side wall (Figure 2.1), and three Digital Wave Corporation B1025 MAE transducers, one located at the top cylinder-to-side wall transition and two located at the bottom cylinder-to-sidewall transition. The hoop oriented strain gage enabled the hoop modulus as a function of the number of applied cycles to be monitored, and the MAE transducers enabled the structural integrity of the cylinders to be assessed during the cyclic fatigue test.

2.3 *EOL burst testing*

After a cylinder was subjected to the respective fatigue cycle regimen described in Sections 2.1 or 2.2, it was subjected to an End of Life (EOL) burst test. All pressurizations were performed at a rate of 2500 psi/min, such that a quasi-static stress state was experienced by the pressure cylinder. Prior to the ramp-up to ultimate burst, cylinders were subjected to two excursions to the hydrostatic test pressure of the cylinder, imitating the test procedure in ASME Section X and the Digital Wave Corporation's DOT-SP's 15720, 16190, and 16343 [6, 7, 8, 9]. The entire EOL burst pressure schedule is shown in Figure 2.2. During the two pressurization cycles up to the hydrostatic test pressure, MAE waveforms were continually monitored and the accept/reject criteria of DOT SP's 15720, 16190, and 16343 were evaluated to determine whether or not the cylinder would have been granted a five year life extension [7, 8, 9]. MAE waveforms from a single transducer were captured during the burst pressure ramp to gain insight into the sequence of damage processes that occur within composite overwrapped pressure cylinders during failure.

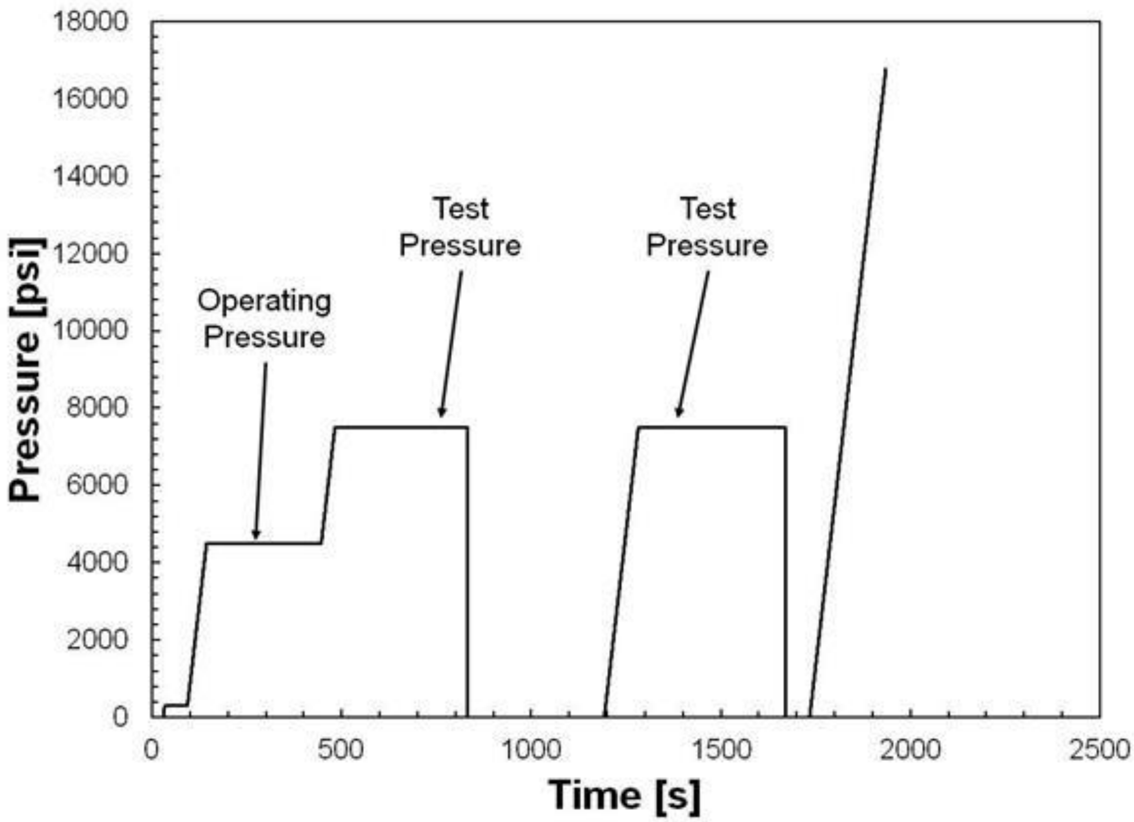

Figure 2.2 – Pressure schedule used during all EOL burst tests.

During EOL burst testing the mechanical response of the SCBA cylinders was monitored. Two Micro Measurements CEA-06-500UW-120 strain gages were mounted onto the cylindrical portion of the SCBA cylinder, as shown in Figure 2.3, such that the stiffness response in the principal directions could be measured. Each strain gage was wired in a quarter bridge configuration, using a three wire lead technique to compensate for lead resistance.

Figure 2.3 – Strain gage orientation for EOL burst tests.

Further, the hydrostatic pressure within the cylinder was measured using an Omegadyne 33,000 psi pressure transducer (Omegadyne Model PX02S1 – 30KG10T, S/N 254895). The principal membrane stresses at the strain gage locations were calculated using the thin wall pressure cylinder equations, i.e.

$$\sigma_{HOOP} = \frac{pr}{t} \tag{2.1}$$

$$\sigma_{AXIAL} = \frac{pr}{2t}. \tag{2.2}$$

where p is the hydrostatic pressure, r is the radius of the cylinder, and t is the pressure cylinder wall thickness. Using the calculated stresses and the measured strains the mechanical stiffness values in both principal directions was determined before and after the hydrostatic test pressure.

3. LPT, fracture mechanics, and fatigue life estimation analysis

3.1 *Stress intensity factor formulation*

To perform a proper fatigue life estimation analysis of the aluminum liner, an adequate stress intensity factor for an internally pressurized thin-walled cylinder is required. To this end, the K solutions of [10, 11, 12, 13] were utilized. The stress intensity factor (K) for a thin walled cylinder with an axially oriented notch subjected to internal pressure may be expressed as

$$K = \sigma\alpha\sqrt{\frac{\pi a}{Q}} \tag{3.1}$$

where σ is the hoop stress within the aluminum liner, a is the current crack depth, Q is the flaw shape parameter, and α is defined as

$$\alpha = \left(\frac{t}{R}\right)\left(\frac{r^2}{(r^2 - R^2)}\right)\left[2H_0 - 2H_1\left(\frac{a}{R}\right) + 3H_2\left(\frac{a}{R}\right)^2 - 4H_3\left(\frac{a}{R}\right)^3\right]. \tag{3.2}$$

In equation 3.2 r and R are the inner and outer radius of the aluminum liner, respectively, t is the thickness of the aluminum liner, and H_i is a function of R/t, a/c, a/t, and the angle within the crack face. As Liu proposed [10], letting $\frac{\alpha}{\sqrt{Q}}$ be equated to a parameter, F, equation (3.1) may be written as

$$K = \sigma F\sqrt{\pi a}. \tag{3.3}$$

Figure 3.1 provides the relationship between F and the ratio of crack depth to liner thickness for a flaw with a ratio a/c equal to 0.6, and a ratio of R/t = 30 for both 0° and 90° of the crack face, taken from Table 17 of [10].

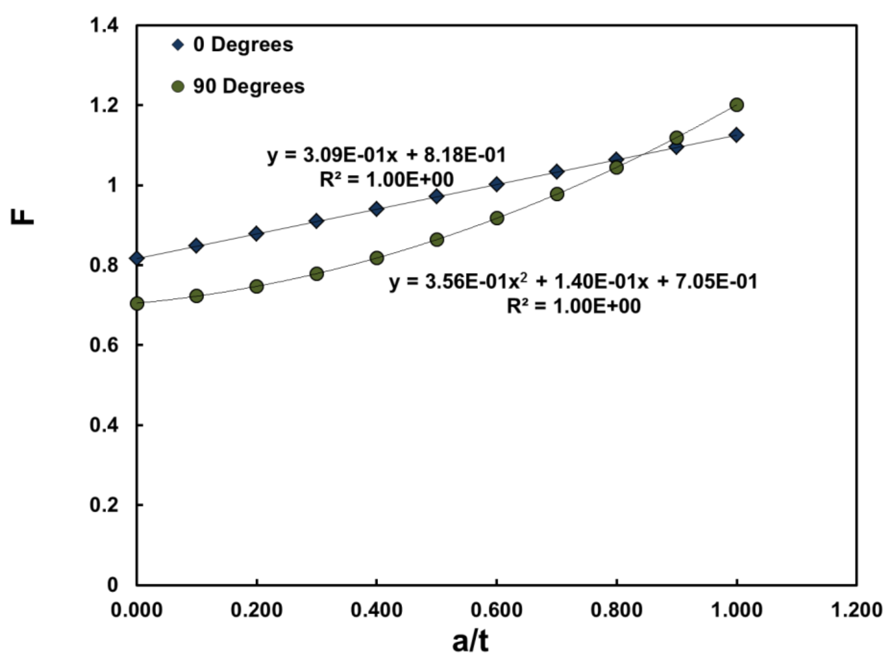

Figure 3.1 – Relationship between F and a/t for R/t = 30, and a/c = 0.6, as reported in Liu [10].

3.2 *Classical Laminated Plate Theory (CLPT) analysis*

To properly determine σ within the aluminum liner in equations (3.1) and (3.3), the distribution of stresses through the thickness of the composite overwrapped pressure cylinder laminate must be considered. To this end, we utilize an anisotropic classical laminated plate theory (CLPT) analysis to calculate the distribution of stresses through the thickness of the laminated plate, and extract the state of stress within the aluminum liner. Table 3.1 summarizes the ply material, ply orientation, and ply thickness for a 45 minute, 4500 psi DOT-CFFC pressure cylinder. Table 3.2 provides the elastic constants used in the CLPT analysis, while Figure 3.2a provides a schematic of the SCBA COPV laminate lay-up (excluding the non-structural sacrificial glass fiber layers). To obtain the maximum hoop stress in the aluminum liner, a representative stress element of the entire laminate was subjected to biaxial tensile traction loads (Figure 3.2b) that were equivalent to what the cylindrical portion of the SCBA pressure cylinder experiences at maximum developed pressure (5192 psi).

Table 3.1 – Summary of the laminate definition used in the CLPT analysis.

Ply material	Ply orientation [degrees]	Ply thickness [inch]
S2/913	90	0.016
S2/913	16	0.008
S2/913	-16	0.008
T700/913	90	0.063
T700/913	16	0.040
T700/913	-16	0.040
T700/913	90	0.047
6061-T6 Aluminum	-	0.100

Table 3.2 – Lamina constants used in CLPT analysis

Ply material	T800/913	S2/913	6061-T6 Aluminum
E_{11} [Msi]	22.06	7.83	10.00
E_{22} [Msi]	0.96	2.32	10.00
G_{12} [Msi]	0.61	1.02	3.85
G_{23} [Msi]	0.31	0.87	3.85
ν_{12}	0.25	0.25	0.30

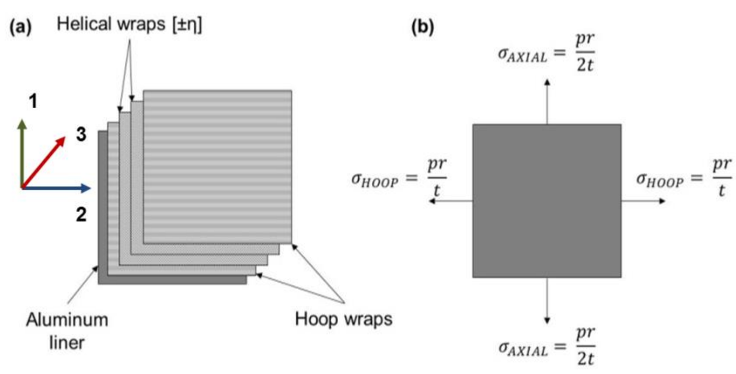

Figure 3.2 – (a) Schematic of the SCBA pressure cylinder laminate, and (b) biaxial loads applied to a representative stress element to simulate the state of stress within the cylindrical portion of the pressure cylinder due to internal pressure.

Figure 3.3 shows the 11 (axial) principal stress, while Figure 3.4 shows the 22 (hoop) principal stress. From Figure 3.4 it can be seen that the maximum hoop stress within the aluminum liner at the maximum developed pressure was found to be 225 MPa (31.9 ksi), which is the value for the hoop stress within the aluminum liner that will be used in all subsequent fatigue life estimation analyses.

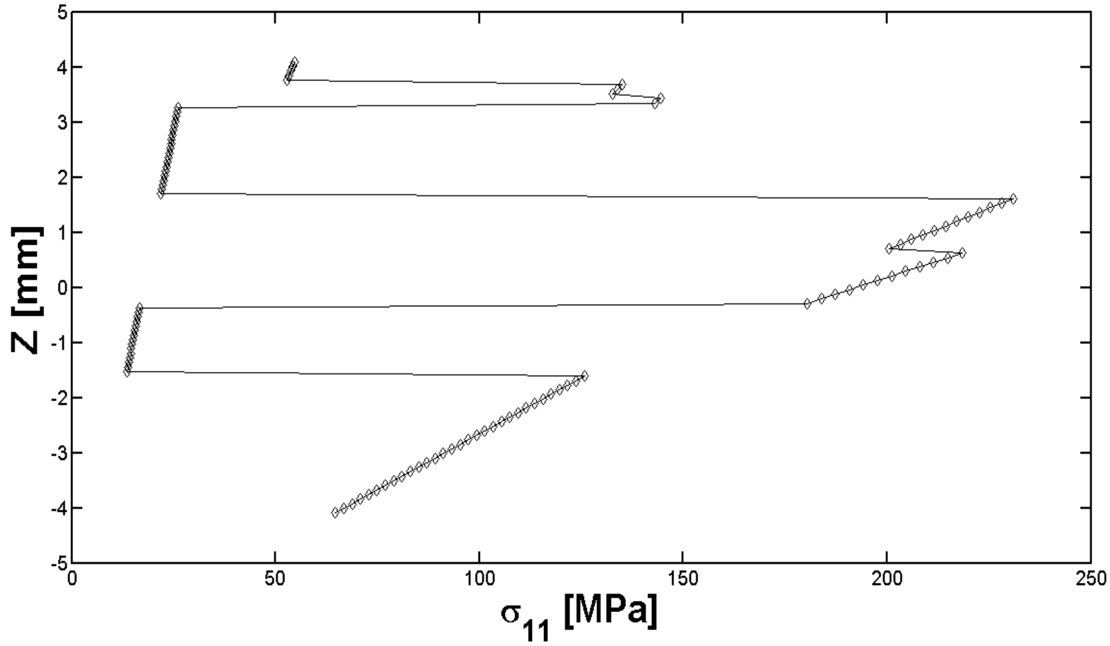

Figure 3.3 – Distribution of axial stress through the laminate thickness for a representative SCBA CFFC pressure cylinder at maximum developed pressure during fast fill (5,192 psi).

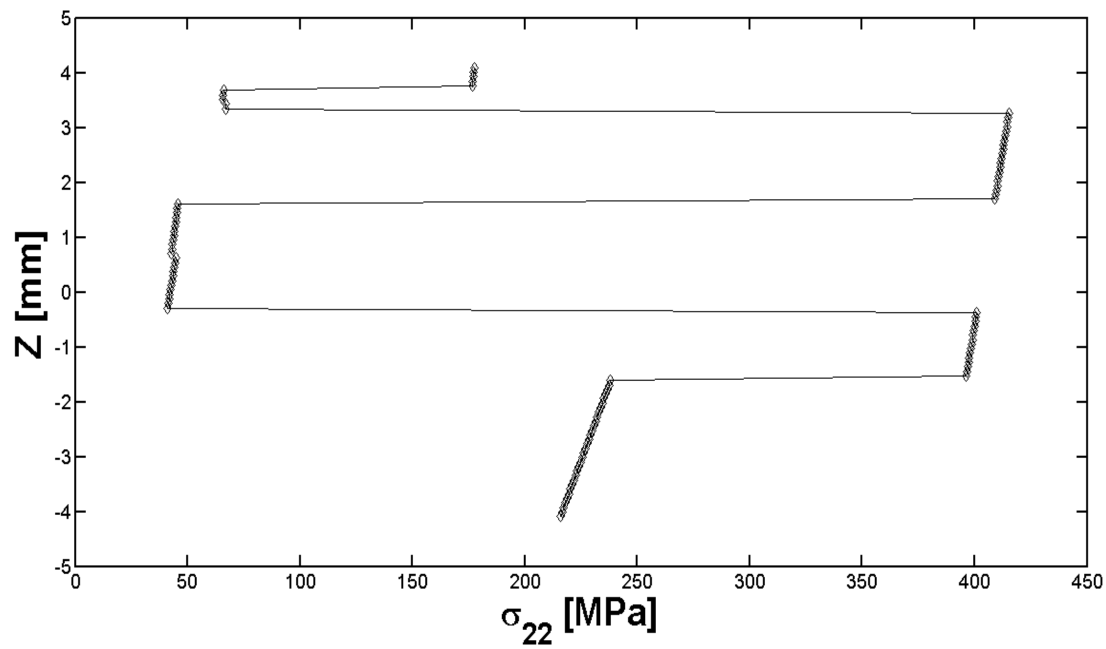

Figure 3.4 – Distribution of hoop stress through the laminate thickness for a representative SCBA CFFC pressure cylinder at maximum developed pressure during fast fill (5,192 psi).

3.3 *Fatigue Life Prediction*

To estimate the fatigue life of a DOT-CFFC composite cylinder, and the effects of the reautofrettage process consider the case of a cylinder which was not reautofrettaged, and had a semi-elliptical flaw axially oriented in the cylindrical portion of the pressure cylinder with an initial depth (a_0) of 0.005", and initial width ($2c_0$) of 0.018". The remaining life of the aluminum liner may then be determined using the standard Paris law equation

$$\frac{da}{dN} = A\Delta K^M \tag{3.4}$$

where $\frac{da}{dN}$ is the crack growth rate, A and M are the Paris law constants for 6061-T6 Aluminum, and ΔK is the stress intensity factor range during a given fatigue cycle. Values of A (3.7086E-12) and M (4.2) were taken from [13]. With the proper material constants equation (3.4) may be integrated numerically for a given number of cycles (N) to determine the final crack length as

$$a_N = a_0 + \sum_{i=1}^{N} A\Delta K^M. \tag{3.5}$$

To consider the effects of the reautofrettage process and crack tip blunting, the crack tip plasticity model of Wheeler was used [14]. In Wheeler's model the plastic zone size at the crack tip under plane stress conditions is calculated as

$$2r = \frac{1}{4\pi}\left(\frac{\Delta K}{S_y}\right)^2 \tag{3.6}$$

in which r is the radius of the plastic zone size, and S_y is the yield strength of the aluminum liner. In Wheeler's model, the plastic zone size is calculated for the tensile overload (r_{OL}), as well as on the i^{th} fatigue cycle (r_i), and then used to determine the retardation parameter C_i

$$C_i = \left[\frac{r_i}{(a_{OL} + r_{OL}) - a_i}\right]^q. \tag{3.7}$$

In equation (3.7) a_{OL} is the crack length at the overload cycle, a_i is the crack length on the i^{th} cycle, and q is a material constant. The value of q was taken from [15], and was 1.67. Using the retardation parameter for the i^{th} cycle (C_i), the crack length for N cycles of fatigue loading is then computed as

$$\frac{da}{dN} = C_i A\Delta K^M. \tag{3.8}$$

Equation (3.8) may be evaluated numerically by separating variables, and integrating through N cycles to determine the resulting crack length (a_N)

$$a_N = a_0 + \sum_{i=1}^{N} C_i A\Delta K^M. \tag{3.9}$$

Figure 3.5 provides the crack length as a function of the number of cycles to maximum developed for the representative DOT-CFFC cylinders that were and were not reautofrettaged, as well as a cylinder which was reautofrettaged and then subjected to a test pressure cycle every 2,500 cycles (or 5 years of service life). The Paris law model predicts that the considered initial flaw (a_0 = 0.005", $2c_0$ = 0.018") would grow to a depth of 0.076" in 10,000 cycles. A slightly larger flaw (only one to two thousandths of an inch deeper) would grow through the remaining 0.024" before 10,000 cycles, resulting in leakage of the aluminum liner.

The Wheeler model predicts reduced crack growth behavior (as compared to cylinders which did not experience the tensile overload). This reduced crack growth rate behavior is due to all existing cracks being blunted and put into residual compression upon the removal of the tensile overload; such behavior is what enables the enhanced fatigue behavior. Finally, from Figure 3.5 it is apparent that the application of a test pressure cycle every 2,500 cycles predicts even greater fatigue life performance than a cylinder which was only reautofrettaged, and exceptional fatigue life performance as compared to a cylinder which has not experienced any form of a tensile overload once a flaw initiation site was present.

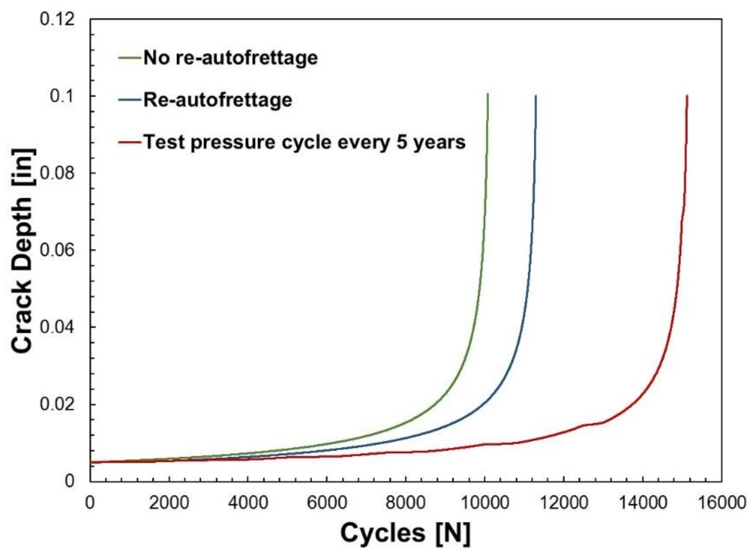

Figure 3.5 – Crack depth as a function of the number of cycles to maximum developed pressure for Aluminum liners that were and were not reautofrettaged, as well as a cylinder which was subjected to a test pressure cycle every 5 years of service life.

It is noted that several influencing factors should be considered in light of the preceding illustrative example. First, the initial flaw size (a_0 = 0.005", $2c_0$ = 0.018") was estimated from visual inspection of aluminum liners using 10x magnification. The effect of the initial flaw size will greatly influence the number of cycles which can be obtained by a given Aluminum liner. Figure 3.6 shows the effect of the initial flaw depth (a_0) on the number of cycles to maximum developed pressure before the crack grows through the aluminum liner. Clearly, for equivalent sized flaws, by reautofrettaging the DOT-CFFC pressure cylinder the number of obtainable cycles prior to leakage is increased. Furthermore, the application of a test pressure cycle every 2,500 cycles appears to drastically improve the fatigue performance of DOT-CFFC cylinders.

Second, the position of the flaw could have a significant effect on whether or not an aluminum liner leaks. The work presented herein only considers the case when a flaw is located on the cylindrical portion of the pressure cylinder. If a flaw were oriented at one of the transitions in the pressure cylinder, the stress state will be magnified (due to the local bending moment caused by the requirement of continuity of deformations), which would increase the crack driving force (ΔK), resulting in diminished fatigue life. To properly analyze such a scenario a more sophisticated analysis (non-linear finite element analysis) would be required to quantify ΔK. Finally, the Paris law parameters taken from [14] were developed for 6061-T651 Aluminum while the crack was growing in air. These material constants were selected as they provide for realistic crack growth rates during service; not accelerated crack growth rates due to the crack being submerged in water [15], as was the case in this experimental test program. Thus, true in-service fatigue lives may be longer than what has been experimentally measured in previous reports [2].

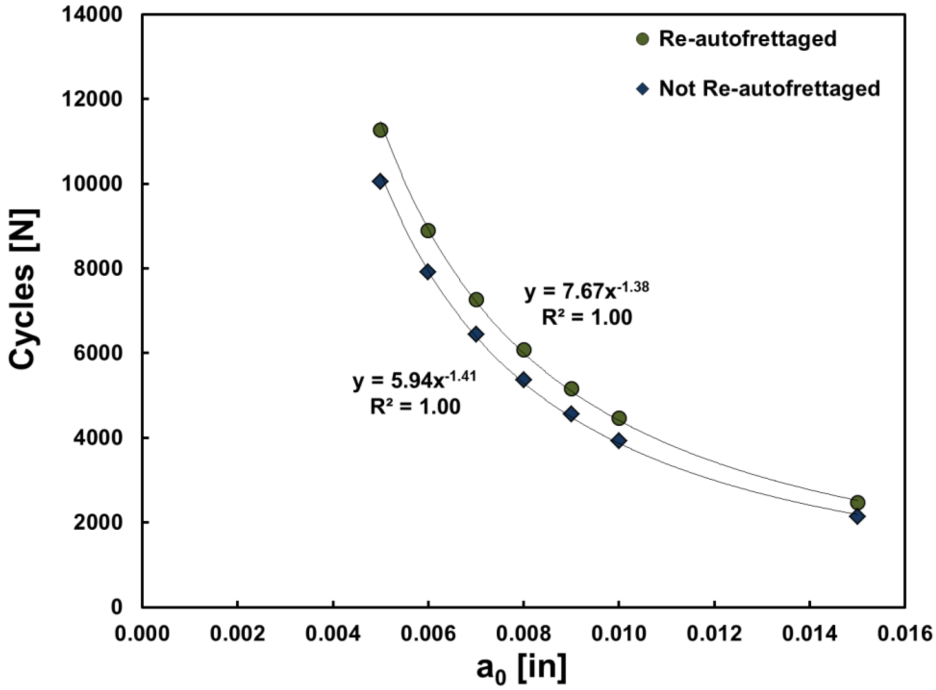

Figure 3.6 – Effect of the initial flaw depth (a_0) on the total number of obtainable fatigue cycles to maximum developed pressure prior to the flaw growing through the aluminum liner.

4. Visual Inspection results

Table 4.1 provides a summary of pertinent cylinder information, manufacture date, cylinder volume, cylinder service pressure, the special permit under which the cylinder was operated, and the results of the internal and external visual inspections. It is pointed out that several of the tested cylinders were donated from some of the busiest fire departments in the United States (e.g., FDNY, Houston FD, Fairfax FD, etc.), likely experiencing some of the most demanding service life's that DOT-CFFC cylinders are subjected to. From Table 4.1, it was observed that forty-three (43) of the fifty (50) cylinders met the acceptance criteria of CGA C-6.2 [5], and would not have been condemned upon a visual examination.

Table 4.1 – Summary of pertinent cylinder identification information, manufacture date, volume, and visual inspection results.

Cylinder S/N	Mfg Date	Volume [min]	Special Permit	External Visual Inspection	Internal Visual Inspection	Visual Inspection [Pass/Fail]
ALT695 - 3646	Jun-98	45	10945	L3 chips on BD, L2 chips on PD	Corrosion indications throughout with mineral deposits.	Fail
ALT695 - 5497	Sep-98	45	10945	L2 abrasions on BD, L2 abrasions and cuts on cylinder sidewall	Corrosion indications throughout with mineral deposits.	Pass
ALT695 - 4396	Jul-98	45	10945	L2 abrasions throughout	Corrosion indications throughout with mineral deposits.	Pass
ALT695 - 4482	Jul-98	45	10945	L2 abrasions throughout	Hard water stains throughout	Pass
ALT695 - 4775	Jul-98	45	10945	L3 abrasions on BD	Corrosion indications throughout with mineral deposits.	Fail
ALT695 - 3575	Jun-98	45	10945	L2 abrasions and cuts throughout, significant near label	Corrosion indications throughout with mineral deposits.	Pass
ALT695 - 3798	Jun-98	45	10945	L2 abrasions and cuts throughout	Water stains and minor corrosion indications throughout	Pass
ALT639 - 4101	Oct-97	30	10945	L2 chips on BD and PD, L1 abrasions throughout	Corrosion indications throughout with mineral deposits.	Pass
ALT639 - 5224	Nov-97	30	10945	L2 chips on BD, L1 abrasions throughout	Water stains and minor corrosion indications throughout	Pass
ALT639 - 4610	Nov-97	30	10945	L2 abrasion on BD and side wall, L1 abrasions throughout	Corrosion indications throughout with mineral deposits	Pass
ALT695 - 4734	Jan-98	45	10945	L3 abrasions on BD, L2 abrasions on cylinder side wall	Minor corrosion indications throughout	Fail
ALT695 - 5641	Sep-98	45	10945	L2 abrasions on BD, L1 impacts throughout, L1 cuts throughout	Corrosion indications throughout with mineral deposits	Pass
ALT695 - 5558	Sep-98	45	10945	L2 abrasions throughout BD, L3 cut on BD transition	Corrosion indications on cylinder side wall and port dome	Fail
ALT695 - 3771	Jun-98	45	10945	L2 abrasions on BD and side wall	Minor corrosion indications throughout	Pass
ALT604 - 5553	Nov-98	60	10945	L2 abrasions throught BD, L3 chips in PD transition near label	Stained liner, no corrosion	Fail
ALT639 - 9435	Feb-98	30	10945	L2 abrasions on PD transition, L1 impacts on BD	Light flaw indications on BD	Pass
ALT639 - 18682	Jan-99	30	10945	L1 abrasions throughout	Good liner, Good threads	Pass
ALT639 - 40136	Dec-99	30	10945	L2 chip and L1 abrasions on BD, L1 cuts throughout	Corrosion indications throught with mineral deposits	Pass
ALT639 - 18594	Jan-99	30	10945	L2 abrasion on BD	Corrosion indications throught with mineral deposits	Pass
ALT639 - 23993	Mar-99	30	10945	Two L2 abrasions on cylinder side wall near label	Corrosion indications throught with mineral deposits	Pass
IL2705	Jun-98	45	10915	L1 impacts on cylinder side wall, L2 chips on cylinder side wall	Water stains of aluminum liner	Pass
IL2722	Jun-98	45	10915	L3 chip on BD	Minor flaw indications on BD	Fail
ALT639-69988	Nov-00	30	10945	Good	Minor corrosion indications on BD	Pass
ALT639-34005	Aug-99	30	10945	L1 chip on BD, L1 cuts throughout	Scratches/flaw indications on BD	Pass
ALT695-3224	May-98	45	10945	L2 abrasions and chips on BD and cylinder side wall	Corrosion indications throughout with mineral deposits	Pass
ALT695-4944	Aug-98	45	10945	L2 chips and abrasions on BD, L2 cut on cylinder transition near BD, L3 cut on cylinder side wall	Corrosion indications throughout with mineral deposits	Fail
IL2933	Jun-98	45	10915	L1 cuts throughout cylinder	Water stains of aluminum liner	Pass
ON3146	Jun-98	60	10915	L1 cuts throughout cylinder	Scaling of the aluminum liner observed	Pass
ALT604-6707	Dec-98	60	10945	L2 abrasionsons on PD, L1 cuts throughout	Minor corrosion indications	Pass
ALT604-5561	Nov-98	60	10945	L2 chips on BD and PD, L1 abrasions throughout	Corrosion indications throughout with mineral deposits	Pass
ALT695-4379	Jul-98	45	10945	L2 chips on BD, L1 abrasions throughout	Discoloration on BD od aluminum liner, not corrosion	Pass
ALT695-3881	Jun-98	45	10945	L2 chips on BD, L1 abrasions throughout	Corrosion indications throughout with mineral deposits	Pass
ALT639-19008	Jan-99	30	10945	L1 abrasions on BD	Good liner, Good threads	Pass
ALT695-1862	Mar-98	45	10945	L2 abrsions on BD, L1 cuts throughout	Corrosion indications throughout with mineral deposits	Pass
ALT695-6041	Sep-98	45	10945	L2 chips on cylinder side wall, L2 abrasions on BD	Corrosion indications with mineral deposits on cylinder side wall	Pass
ON3077	Jun-98	60	10915	L2 chips on BD, L1 scratches on PD	Water stains throughout	Pass
ALT639-9528	Feb-98	30	10945	L1 abrasions on BD and PD, L2 abrasions on transition	Good liner, Good threads	Pass
ALT639-9941	Feb-98	30	10945	L1 abrasions on BD and PD	Good liner, Good threads	Pass
IH667	Apr-98	30	10915	L1 abrasion on BD	Minor corrsion indications throughout with mineral deposits	Pass
IL3334	Aug-98	45	10915	L1 chips on BD, L1 impacts on BD transition	Flaw indication on BD, not related to corrosion	Pass
ALT639-17714	Dec-98	30	10945	L1 abrasions on BD and PD	Good liner	Pass
ALT639-38556	Nov-99	30	10945	L1 abrasion on BD and PD	Good liner	Pass
ALT695-3313	Jun-98	45	10945	L2 abrasions throughout BD, L2 cuts and abrasions throughout cylinder side wall, L3 cut on cylinder side wall	Corrosion indications throughout	Fail
ALT695-3936	Jun-98	45	10945	L2 abrasions on cylinder BD, L1 abrsions throughout cylinder side wall	Corrosion indications throughout	Pass
ALT695-4492	Jul-98	45	10945	L1 abrasions on BD and cylinder side wall	Minor corrosion indications throughout with mineral deposits	Pass
ALT604-5155	Sep-98	60	10945	L1 abrasions throughout, L2 cuts on cylinder BD	Good liner	Pass
OK85342	4-Feb	30	10915	L1 impacts on cylinder side wall, L2 cuts on cylinder BD, possible burn indications	Appear to be shot peen marks on aluminum liner, possibly from manufacture	Pass
ALT639-24574	Apr-99	30	10945	L1 abrasions throughout, L2 cuts on cylinder side wall	Scratches on cylinder BD, corrosion indications on BD	Pass
ALT639-22931	Feb-99	30	10945	L1 abrasions throughout	Scratches on cylinder BD, corrosion indications on cylinder side wall	Pass
ALT695-4469	Jul-98	45	10945	L2 abrasions on BD, L1 abrasions throughout cylinder side wall	Corrosion indications throughout	Pass

5. Physical Testing Results

5.1 *10k fatigue testing*

Table 5.1 summarizes all pertinent cylinder information, residual hoop strain due to the reautofrettage process, and the number of fatigue cycles to maximum developed pressure achieved by each cylinder.

Table 5.1 – Summary of cylinder information, number of fatigue cycles achieved, and residual hoop strain accumulated due to the reautofrettage process.

Cylinder S/N	Mfg Date	Volume [min]	Special Permit	Visual Inspection [Pass/Fail]	Number of Cycles	Residual Hoop Strain [$\mu\varepsilon$]
ALT695 - 3646	Jun-98	45	10945	Fail	10K	0
ALT695 - 5497	Sep-98	45	10945	Pass	10K	178
ALT695 - 4396	Jul-98	45	10945	Pass	10K	125
ALT695 - 4482	Jul-98	45	10945	Pass	10K	85
ALT695 - 4775	Jul-98	45	10945	Fail	10K	133
ALT695 - 3575	Jun-98	45	10945	Pass	10K	75
ALT695 - 3798	Jun-98	45	10945	Pass	10K	-
ALT639 - 4101	Oct-97	30	10945	Pass	10K	133
ALT639 - 5224	Nov-97	30	10945	Pass	10K	178
ALT639 - 4610	Nov-97	30	10945	Pass	10K	-
ALT695 - 4734	Jan-98	45	10945	Fail	10K	145
ALT695 - 5641	Sep-98	45	10945	Pass	10K	145
ALT695 - 5558	Sep-98	45	10945	Fail	10K	138
ALT695 - 3771	Jun-98	45	10945	Pass	10K	0
ALT604 - 5553	Nov-98	60	10945	Fail	10K	187
ALT639 - 9435	Feb-98	30	10945	Pass	10K	90
ALT639 - 18682	Jan-99	30	10945	Pass	10K	170
ALT639 - 40136	Dec-99	30	10945	Pass	10K	230
ALT639 - 18594	Jan-99	30	10945	Pass	10K	138
ALT639 - 23993	Mar-99	30	10945	Pass	10K	169
IL2705	Jun-98	45	10915	Pass	10K	181
IL2722	Jun-98	45	10915	Fail	10K	185
ALT639-69988	Nov-00	30	10945	Pass	10K	58
ALT639-34005	Aug-99	30	10945	Pass	10K	234
ALT695-3224	May-98	45	10945	Pass	10K	73
ALT695-4944	Aug-98	45	10945	Fail	10K	98
IL2933	Jun-98	45	10915	Pass	10K	186
ON3146	Jun-98	60	10915	Pass	10K	121
ALT604-6707	Dec-98	60	10945	Pass	10K	133
ALT604-5561	Nov-98	60	10945	Pass	10K	124
ALT695-4379	Jul-98	45	10945	Pass	10K	25
ALT695-3881	Jun-98	45	10945	Pass	10K	25
ALT639-19008	Jan-99	30	10945	Pass	10K	62
ALT695-1862	Mar-98	45	10945	Pass	10K	22
ALT695-6041	Sep-98	45	10945	Pass	10K	34
ON3077	Jun-98	60	10915	Pass	10K	34
ALT639-9528	Feb-98	30	10945	Pass	10K	108
ALT639-9941	Feb-98	30	10945	Pass	10K	108
IH667	Apr-98	30	10915	Pass	10K	78
IL3334	Aug-98	45	10915	Pass	10K	87

From Table 5.1, it is observed that of the forty (40) end of service life cylinders which were reautofrettaged and subsequently subjected to 10,000 fatigue cycles, all forty (40) cylinders achieved 10,000 fatigue cycles to maximum developed pressure. By imparting on average 113 $\mu\varepsilon$ of additional plastic deformation to the 6061-T6 aluminum liner, any flaw initiation site which was present was put into residual compression and allowed the cylinder to achieve an additional twenty (20) years of simulated service life.

To insure that the composite overwrap was not accumulating damage and losing stiffness during the fatigue cycle testing, the hoop stiffness of the cylinder was monitored throughout the entire fatigue test. The hoop modulus for a given cycle was determined via a least squares linear fit of the hoop stress versus the hoop strain, a representative plot for cylinder ALT639-4101 is shown in Figure 5.1. Next, the hoop modulus on the i^{th} cycle (E_i) was divided by the hoop modulus on the initial cycle (E_0), as shown in Figure 5.2. As observed from Figure 5.2, the value of E_i/E_0 for cylinder ALT639-4101 stays at a value of 1 indicating that the stiffness of the composite cylinder did not change and the cylinder was not accumulating microstructural damage as more fatigue cycles were applied to the cylinder. Plots of E_i/E_0 as a function of number of applied cycles for all fatigue cycled cylinders may be found in Appendix A.

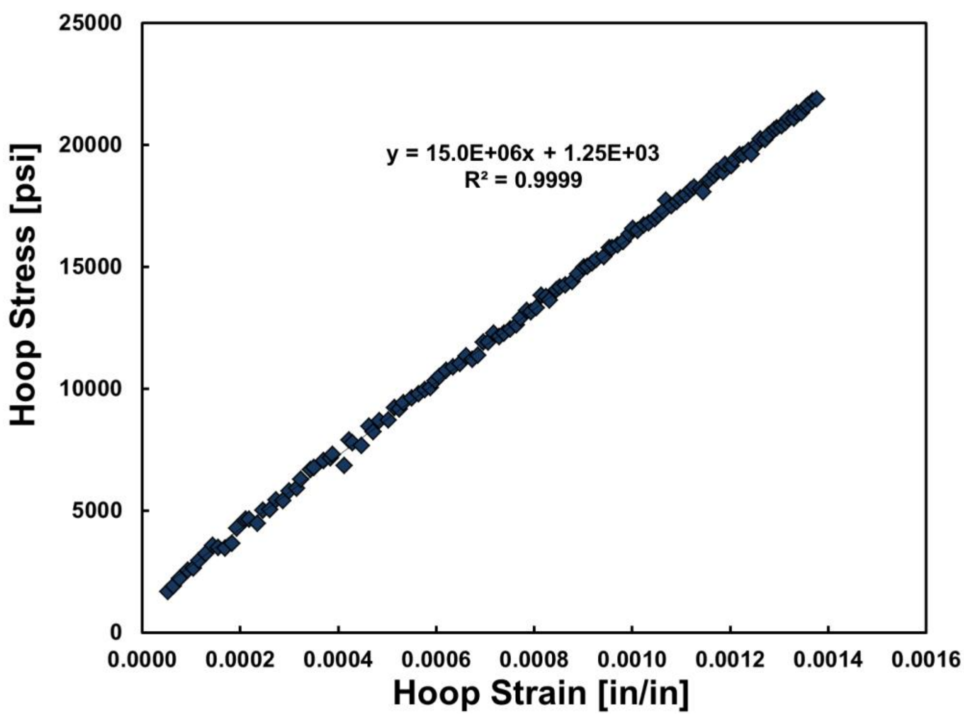

Figure 5.1 – Plot of hoop stress versus hoop strain on a single cycle during the fatigue cycling of ALT639-4101.

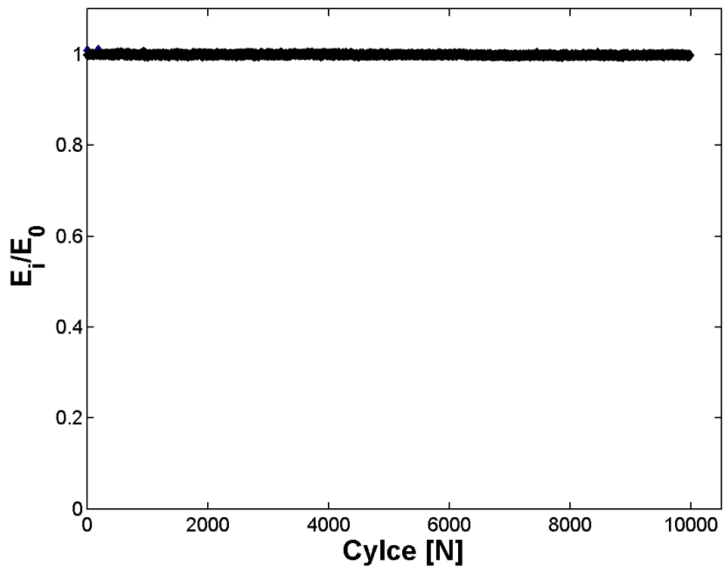

Figure 5.2 – Hoop modulus on the ith cycle (E_i) divided by the hoop modulus on the initial cycle (E_0) as a function of the number of applied fatigue cycles for cylinder ALT639-4101.

To further insure that cylinders were not accumulating microstructural damage and progressing towards failure, MAE waveforms were captured during the entire fatigue cycle testing of all cylinders. Several previous works have shown the power of MAE in the ability to identify the source mechanism in anisotropic composite structures (e.g., fiber fracture, matrix splitting, interfacial failure, delamination, etc.) through the confirmation of forward predictive elastodynamics modeling [16, 17, 18, 19, 20, 21]. During the cyclic fatigue pressurizations, no damage accumulation was detected via MAE due to the fact that cylinders were only stressed to 30% of their nominal strength. Because of the 15 year service life that the cylinders had already experienced, the characteristic damage state had been established [22], and the cylinders were not accumulating any new damage.

5.2 *24k fatigue testing*

Table 5.2 summarizes all pertinent cylinder information, residual hoop strain due to the reautofrettage process, and the number of fatigue cycles to maximum developed pressure achieved by each cylinder.

Table 5.2 - Summary of cylinder information, number of fatigue cycles achieved, and residual hoop strain accumulated due to the reautofrettage process for all cylinders subjected to the block loading fatigue test.

Cylinder S/N	Mfg Date	Volume [min]	Special Permit	Visual Inspection [Pass/Fail]	Number of Cycles	Residual Hoop Strain [με]
ALT639-17714	Dec-98	30	10945	Pass	24k	44
ALT639-38556	Nov-99	30	10945	Pass	24k	9
ALT695-3313	Jun-98	45	10945	Fail	24k	68
ALT695-3936	Jun-98	45	10945	Pass	24k	77
ALT695-4492	Jul-98	45	10945	Pass	24k	56
ALT604-5155	Sep-98	60	10945	Pass	24k	69
OK85342	4-Feb	30	10915	Pass	24k	163
ALT639-24574	Apr-99	30	10945	Pass	24k	86
ALT639-22931	Feb-99	30	10945	Pass	24k	67
ALT695-4469	Jul-98	45	10945	Pass	24k	11

From Table 5.2, it is observed that of the ten (10) end of service life cylinders which were reautofrettaged and subsequently subjected to a 24,000 fatigue cycles in 2,500 cycle block loading increments, all ten (10) cylinders achieved 24,000 fatigue cycles to maximum developed pressure. By imparting on average 65 με of additional plastic deformation to the 6061-T6 aluminum liner, as well as subjecting the cylinders to a test pressure cycle every 2,500 cycles, any flaw initiation site which was present was put into residual compression and allowed the cylinder to achieve an unlimited simulated service life even after fifteen (15) years of real world service.

To insure that the composite overwrap was not accumulating damage and losing stiffness during the fatigue cycle testing, the hoop stiffness of the cylinder was monitored throughout the entire fatigue test. The hoop modulus for a given cycle was determined via a least squares linear fit of the hoop stress versus the hoop strain, a representative plot for cylinder ALT639-17714 is shown in Figure 5.3. Next, the hoop modulus on the ith cycle (E_i) was divided by the hoop modulus on the initial cycle (E_0), as shown in Figure 5.4. As observed from Figure 5.4, the value of E_i/E_0 for cylinder ALT639-17714 stays at a value of 1 indicating that the stiffness of the composite cylinder did not change and the cylinder was not accumulating microstructural damage as more fatigue cycles were applied to the cylinder. Plots of E_i/E_0 for all 24,000 fatigue cycled cylinders may be found in Appendix A.

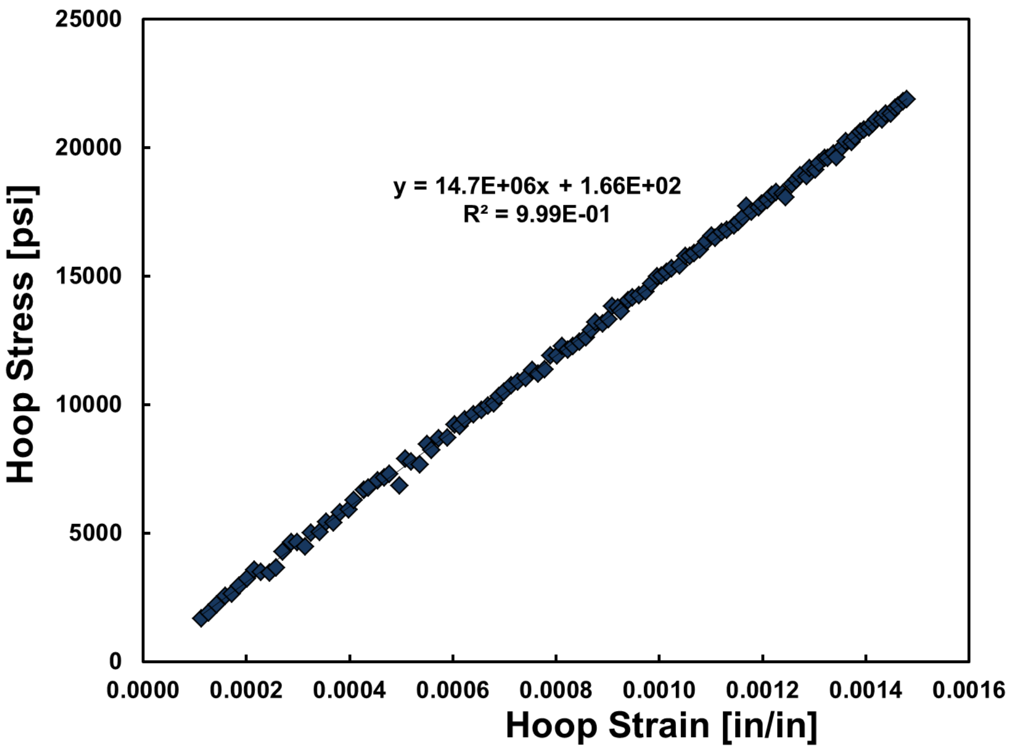

Figure 5.3 – Plot of hoop stress versus hoop strain on a single cycle during the fatigue cycling of ALT639-17714.

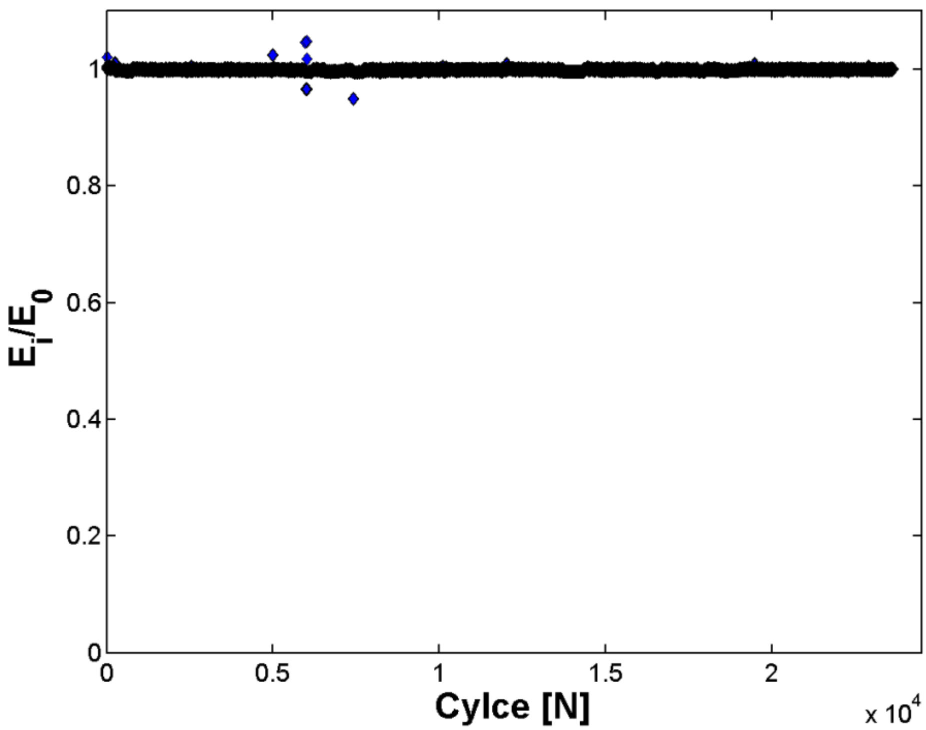

Figure 5.4 – Hoop modulus on the ith cycle (E_i) divided by the hoop modulus on the initial cycle (E_0) as a function of the number of applied fatigue cycles for cylinder ALT639-17714.

To further insure that cylinders were not accumulating microstructural damage and progressing towards failure, MAE waveforms were captured during the entire fatigue cycle testing of all cylinders subjected to the 24,000 cycle block loading fatigue test. Similar to the findings with the cylinders that were subjected to 10,000 fatigue cycles, due to the fact that the cylinders subjected to block loading fatigue test were not accumulating any new damage, no significant MAE waveforms were detected.

5.3 *10k burst testing*

After successfully achieving 10,000 fatigue cycles, all forty (40) cylinders were subjected to an end of life (EOL) burst test. Table 5.3 summarizes pertinent cylinder information, cylinder stiffness information, cylinder burst strength, whether the cylinder met the MAE acceptance criteria of DOT SP's 15720, 16190, 16343, and the background energy oscillation pressure (BEOP) of each cylinder determined on the burst pressurization ramp.

From Table 5.3, it is observed that all forty (40) cylinders which experienced a full fifteen (15) year real world service life, and a simulated twenty (20) additional years of service all burst above the minimum required burst pressure of [1]. Clearly, cycling DOT-CFFC cylinders to the maximum developed pressure during fast fill does not compromise the structural integrity of the composite cylinder. Photos of all EOL burst cylinders are provided in Appendix B.

Table 5.3 – Summary of pertinent cylinder information, cylinder stiffness during burst pressurization, burst strength, MAE evaluation result during test pressure cycles, and BEOP value on the burst pressurization for all cylinders subjected to 10,000 fatigue cycles.

Cylinder S/N	Mfg Date	Volume [min]	Special Permit	Visual Inspection [Pass/Fail]	Number of Cycles	Primary Hoop Modulus [Msi]	Secondary Hoop Modulus [Msi]	Primary Axial Modulus [Msi]	Secondary Axial Modulus [Msi]	Burst Pressure [psig]	Background Energy Oscillation Pressure [psig]	BEOP/P_B [%]	MAE Life Extension [Pass/Fail]
ALT695 - 3646	Jun-98	45	10945	Fail	10K	16.2	11.4	10.6	5.8	15870	10630	67%	Pass
ALT695 - 5497	Sep-98	45	10945	Pass	10K	14.8	10.7	12.1	6.8	15680	8648	55.2%	Pass
ALT695 - 4396	Jul-98	45	10945	Pass	10K	15.1	12.1	11.0	6.3	17430	12190	69.9%	Pass
ALT695 - 4482	Jul-98	45	10945	Pass	10K	15.0	11.4	12.2	7.2	17970	12210	67.9%	Pass
ALT695 - 4775	Jul-98	45	10945	Fail	10K	14.8	11.3	10.6	5.9	19125	11120	58.1%	Pass
ALT695 - 3575	Jun-98	45	10945	Pass	10K	16.5	12.6	11.0	6.2	19330	12720	65.8%	Pass
ALT695 - 3798	Jun-98	45	10945	Pass	10K	15.5	12.0	11.7	6.5	19300	10100	52.3%	Pass
ALT639 - 4101	Oct-97	30	10945	Pass	10K	14.9	11.5	15.1	8.9	19550	12360	63.2%	Pass
ALT639 - 5224	Nov-97	30	10945	Pass	10K	15.6	11.1	13.7	7.6	19450	13150	67.6%	Pass
ALT639 - 4610	Nov-97	30	10945	Pass	10K	15.2	11.3	13.2	7.3	19360	13250	68.4%	Pass
ALT695 - 4734	Jan-98	45	10945	Fail	10K	13.7	10.1	11.4	6.6	20380	11000	54.0%	Pass
ALT695 - 5641	Sep-98	45	10945	Pass	10K	14.9	11.9	11.2	6.7	20500	12940	63.1%	Pass
ALT695 - 5558	Sep-98	45	10945	Fail	10K	14.3	10.7	10.7	6.3	19910	11230	56.4%	Pass
ALT695 - 3771	Jun-98	45	10945	Pass	10K	16.9	12.2	12.3	8.2	18580	10020	53.9%	Pass
ALT604 - 5553	Nov-98	60	10945	Fail	10K	15.8	13.2	13.1	9.6	17125	10850	63.4%	Pass
ALT639 - 9435	Feb-98	30	10945	Pass	10K	14.8	10.8	12.5	6.7	17755	10650	60.0%	Pass
ALT639 - 18682	Jan-99	30	10945	Pass	10K	16.2	12.7	13.5	7.8	20565	12250	59.6%	Pass
ALT639 - 40136	Dec-99	30	10945	Pass	10K	14.2	8.7	14.1	7.7	20000	13490	67.5%	Pass
ALT639 - 18594	Jan-99	30	10945	Pass	10K	18.2	14.0	13.8	7.7	19120	10240	53.6%	Pass
ALT639 - 23993	Mar-99	30	10945	Pass	10K	15.4	10.6	13.0	7.1	18020	10340	57.4%	Pass
IL2705	Jun-98	45	10915	Pass	10K	14.4	9.9	12.5	6.8	19260	11500	59.7%	Pass
IL2722	Jun-98	45	10915	Fail	10K	14.7	10.5	12.6	6.3	19210	10140	52.8%	Pass
ALT639-69988	Nov-00	30	10945	Pass	10K	15.7	11.1	13.8	8.8	19120	11160	58.4%	Pass
ALT639-34005	Aug-99	30	10945	Pass	10K	14.9	10.8	13.0	7.2	20070	12240	61.0%	Pass
ALT695-3224	May-98	45	10945	Pass	10K	15.4	12.2	12.1	6.8	19080	10320	54.1%	Pass
ALT695-4944	Aug-98	45	10945	Fail	10K	15.8	11.8	7.7	4.8	18780	9596	51.1%	Fail
IL2933	Jun-98	45	10915	Pass	10K	13.4	10.4	12.0	6.4	19300	13980	72.4%	Pass
ON3146	Jun-98	60	10915	Pass	10K	16.6	12.8	11.5	4.8	16920	9937	58.7%	Pass
ALT604-6707	Dec-98	60	10945	Pass	10K	13.0	11.8	14.5	10.5	18680	11300	60.5%	Pass
ALT604-5561	Nov-98	60	10945	Pass	10K	15.9	14.3	13.3	9.5	18780	11050	58.8%	Pass
ALT695-4379	Jul-98	45	10945	Pass	10K	15.6	12.4	12.2	6.6	19160	11500	60.0%	Pass
ALT695-3881	Jun-98	45	10945	Pass	10K	16.4	12.1	12.6	6.8	17270	11040	63.9%	Pass
ALT639-19008	Jan-99	30	10945	Pass	10K	14.3	9.9	13.6	5.9	20580	12070	58.6%	Pass
ALT695-1862	Mar-98	45	10945	Pass	10K	13.9	10.7	12.4	6.5	18950	12810	67.6%	Pass
ALT695-6041	Sep-98	45	10945	Pass	10K	15.2	11.8	11.5	6.1	19610	11400	58.1%	Pass
ON3077	Jun-98	60	10915	Pass	10K	17.2	9.4	11.4	7.0	18420	9840	53.4%	Pass
ALT639-9528	Feb-98	30	10945	Pass	10K	15.0	11.3	12.3	6.8	18380	13330	72.5%	Pass
ALT639-9941	Feb-98	30	10945	Pass	10K	15.3	12.4	12.0	6.3	20050	11620	58.0%	Pass
IH667	Apr-98	30	10915	Pass	10K	15.2	11.7	11.1	5.1	17900	11270	63.0%	Pass
IL3334	Aug-98	45	10915	Pass	10K	14.2	10.3	12.8	6.3	18980	10350	54.5%	Pass

In agreement with previous studies of DOT-CFFC cylinders, it was found that each cylinder responded in a bi-modulus fashion in each of the principal directions during the burst pressurization. Figure 5.5 shows an illustrative example of cylinder ALT695-5497. While pressure levels were below the autofrettage pressure of the cylinder (8,500 psig for these particular cylinders) the cylinder exhibits a stiffer primary modulus in which the 6061-T6 aluminum liner is responding elastically and contributing to the stiffness of the cylinder. Once the autofrettage pressure has been exceeded, the 6061-T6 aluminum liner has yielded, is deforming plastically and is contributing minimal stiffness to the cylinder resulting in a more compliant secondary modulus. All primary and secondary moduli for cylinders which were subjected to 10,000 fatigue cycles and an EOL burst pressurization are summarized in Table 5.3. Photos of all stress-strain curves are provided in Appendix C.

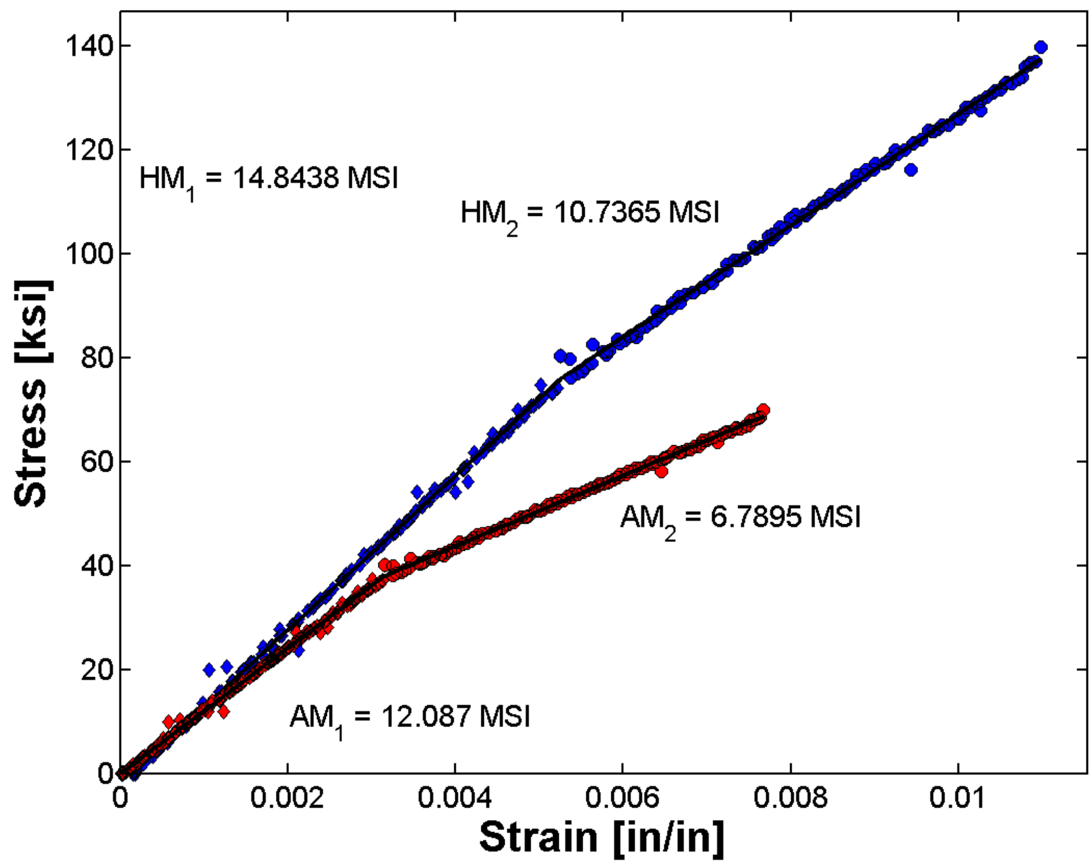

Figure 5.5 – Principal moduli determination during the burst pressurization of ALT695-5497. Note: Blue data points represent hoop response and red data points represent axial response.

From a Modal Acoustic Emission standpoint a majority of the cylinders simply did not emit during the two test pressure cycles prior to the EOL burst, due to the fact that they had established their characteristic damage state and were not accumulating any new damage. Thirty-nine (39) of the forty (40) cylinders met the MAE acceptance criteria of DOT SP's 15720, 16190, and 16343, while all forty (40) cylinders burst above the minimum pressure of the at time of manufacture DOT-CFFC requirement [1].

The lone cylinder which was rejected by the MAE acceptance criteria was cylinder ALT695-4944, and the cylinder was rejected due to an event on the second test pressure cycle which exceeded the partial fiber tow fracture energy. Figure 5.6 presents the time domain waveform as well as a time-frequency representation of the detected partial fiber tow fracture event which failed the cylinder. Based upon the location of the transducer (3" below the top cylinder-to-side wall transition) relative to the location of the Level 3 cut on the cylinder side wall (Table 4.1) and a wave ranging analysis, it is confirmed that the Level 3 cut was a significant enough stress concentrator that upon the application of a test pressure cycle, portions of neighboring fiber tows failed. Thus, the MAE acceptance criteria has once again shown to provide an exceptionally conservative examination of DOT-CFFC cylinders that is in good agreement with visual observations of defects within the cylinders.

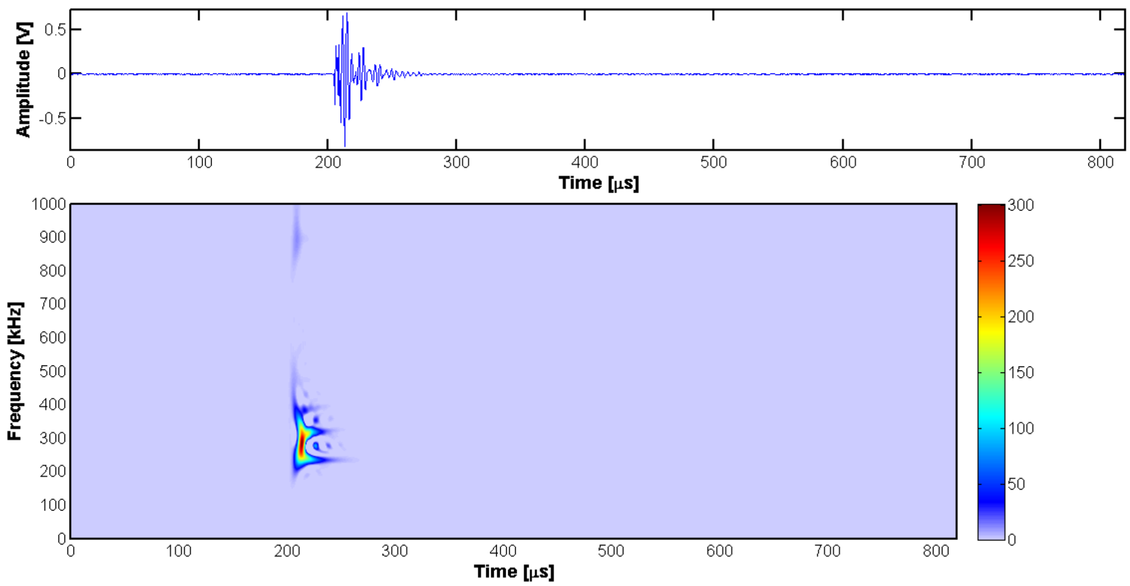

Figure 5.6 – (top) Time domain waveform, and (bottom) time-frequency representation of the partial fiber tow fracture event that occurred on the second test pressure cycle which failed cylinder ALT695-4944.

During the burst pressurization of the forty (40) cylinders which were subjected to 10,000 fatigue cycles, the background energy oscillation pressure was monitored for each cylinder. The background energy oscillation pressure is defined in [19]. Figure 5.7 provides a representative background energy oscillation plot superimposed on the pressure vs. time for cylinder IL3334. Background energy oscillation plots for all cylinders burst test after being subjected to 10,000 fatigue cycles are included in Appendix D.

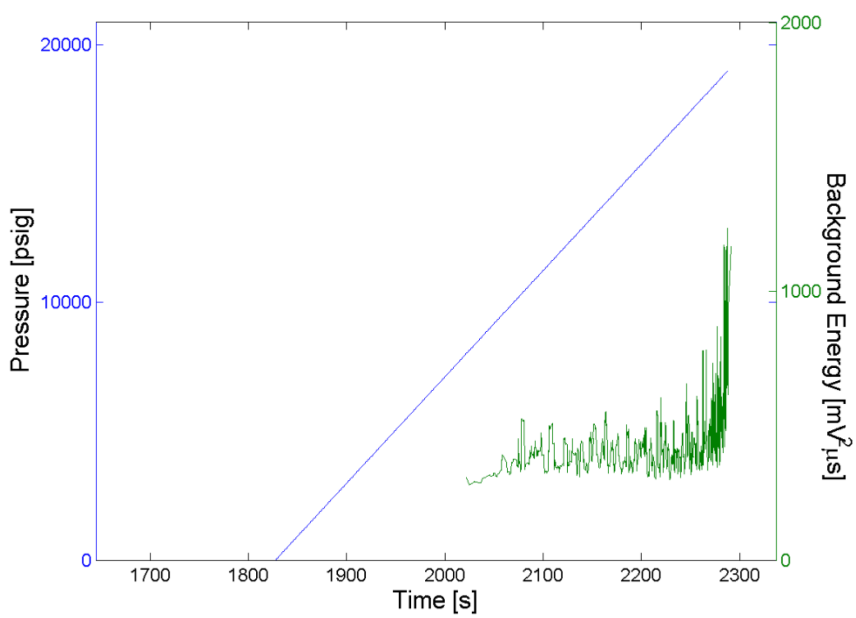

Figure 5.7 – Background energy oscillation vs time superimposed on the pressure vs time plot of the burst pressurization of cylinder IL3334.

Also monitored during the EOL burst pressurization of the cylinders which were subjected to 10,000 fatigue cycles to maximum developed pressure were the waveforms detected as the cylinder began to accumulate damage and progress to failure. To condense the immense amount of information contained within a single waveform (i.e., respective mode content, wave dispersion, frequency content, etc.) frequency domain scalar metrics have been proposed that have the capability when coupled with a forward predictive model of classifying the source mechanism [2, 16, 23]. In this work the metrics proposed in [2] were used for source mechanism classification, and a representative plot of partial power versus weighted peak frequency is shown in Figure 5.8 for cylinder IL3334. Partial power versus weighted peak frequency plots for all cylinders burst test after being subjected to 10,000 fatigue cycles are included in Appendix E.

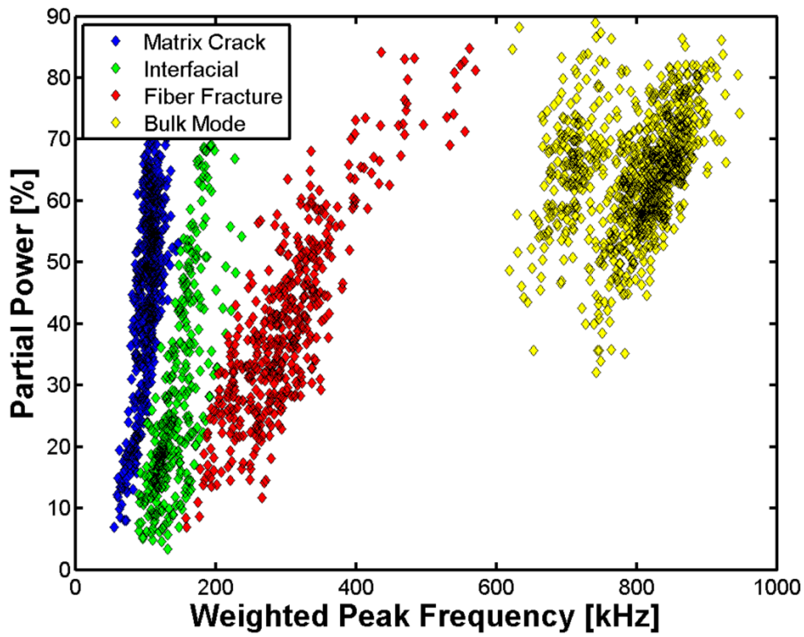

Figure 5.8 – Partial power vs weighted peak frequency for all waveforms detected during the EOL burst pressurization of IL3334.

5.4 *24k burst testing*

After successfully achieving 24,000 cycles in the block loading fatigue test, all ten (10) cylinders were subjected to an end of life (EOL) burst test. Table 5.4 summarizes pertinent cylinder information, cylinder stiffness information, cylinder burst strength, whether the cylinder met the MAE acceptance criteria of DOT SP's 15720, 16190, 16343, and the background energy oscillation pressure (BEOP) of each cylinder determined on the burst pressurization ramp.

From Table 5.4, it is observed that all ten (10) cylinders which experienced a full fifteen (15) year real world service life, and a simulated forty-eight (48) additional years of service all burst above the minimum required burst pressure of [1]. Clearly, cycling DOT-CFFC cylinders to the maximum developed pressure during fast fill 24,000 times, while performing a test pressure cycle every 2,500 cycles does not compromise the structural integrity of the composite cylinder.

Table 5.4 – Summary of pertinent cylinder information, cylinder stiffness during burst pressurization, burst strength, MAE evaluation result during test pressure cycles, and BEOP value on the burst pressurization for all cylinders subjected to 24,000 cycles in the block loading fatigue test.

Cylinder S/N	Mfg Date	Volume [min]	Special Permit	Visual Inspection [Pass/Fail]	Number of Cycles	Primary Hoop Modulus [Msi]	Secondary Hoop Modulus [Msi]	Primary Axial Modulus [Msi]	Secondary Axial Modulus [Msi]	Burst Pressure [psig]	Background Energy Oscillation Pressure [psig]	BEOP/P_B [%]	MAE Life Extension [Pass/Fail]
ALT639-17714	Dec-98	30	10945	Pass	24k	17.5	12.9	13.6	7.4	21960	14610	66.5%	Pass
ALT639-38556	Nov-99	30	10945	Pass	24k	15.5	11.6	13.6	7.0	19950	10800	54.1%	Pass
ALT695-3313	Jun-98	45	10945	Fail	24k	11.7	6.4	7.8	5.9	18740	11480	61.3%	Pass
ALT695-3936	Jun-98	45	10945	Pass	24k	15.3	12.4	11.8	6.8	21140	13730	64.9%	Pass
ALT695-4492	Jul-98	45	10945	Pass	24k	14.8	11.2	10.7	5.8	19850	13420	67.6%	Pass
ALT604-5155	Sep-98	60	10945	Pass	24k	15.4	13.3	12.4	8.9	20880	14000	67.0%	Pass
OK85342	4-Feb	30	10915	Pass	24k	14.0	10.7	11.4	5.4	19340	12390	64.1%	Pass
ALT639-24574	Apr-99	30	10945	Pass	24k	13.8	7.6	8.1	6.3	20500	10110	49.3%	Pass
ALT639-22931	Feb-99	30	10945	Pass	24k	15.8	11.6	13.2	7.3	20000	10720	53.6%	Pass
ALT695-4469	Jul-98	45	10945	Pass	24k	15.5	11.9	11.8	7.3	16160	9867	61.1%	Pass

In agreement with previous studies of DOT-CFFC cylinders, it was found that each cylinder responded in a bi-modulus fashion in each of the principal directions during the burst pressurization Figure 5.9 provides an illustrative example for cylinder ALT695-3936. While pressure levels were below the autofrettage pressure of the cylinder (8,500 psig for these particular cylinders) the cylinder exhibits a stiffer primary modulus in which the 6061-T6 aluminum liner is responding elastically and contributing to the stiffness of the cylinder. Once the autofrettage pressure has been exceeded, the 6061-T6 aluminum liner has yielded, is deforming plastically and is contributing minimal stiffness to the cylinder resulting in a more compliant secondary modulus. All primary and secondary moduli for cylinders which were subjected to 24,000 fatigue cycles and an EOL burst pressurization are summarized in Table 5.4.

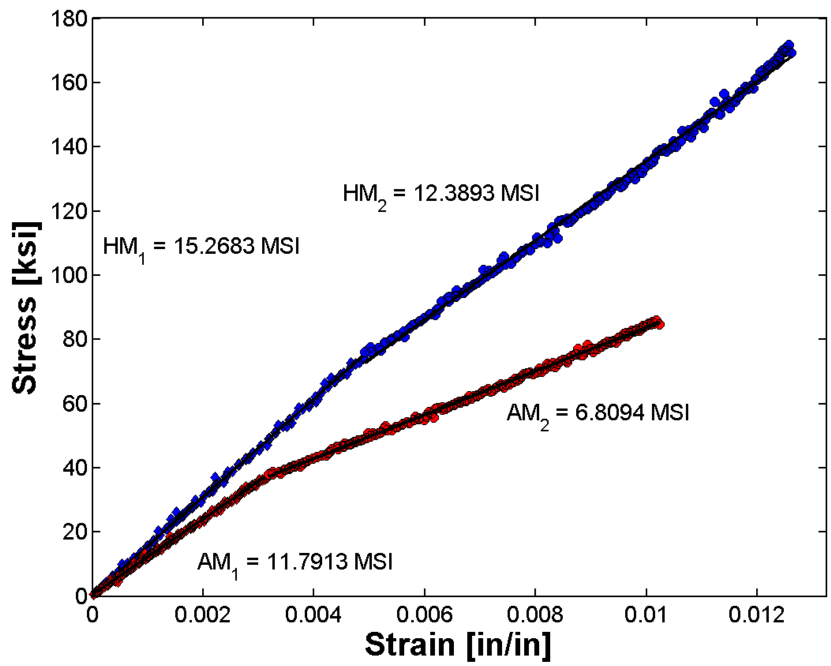

Figure 5.9 – Principal moduli determination during the burst pressurization of ALT695-3936. Note: Blue data points represent hoop response and red data points represent axial response.

From a Modal Acoustic Emission standpoint all of the cylinders simply did not emit during the two test pressure cycles prior to the EOL burst, due to the fact that they had established their characteristic damage state and were not accumulating any new damage. Ten (10) of the ten (10) cylinders met the MAE acceptance criteria of DOT SP's 15720, 16190, and 16343, while all ten (10) cylinders burst above the minimum pressure of the at time of manufacture DOT-CFFC requirement [1].

During the burst pressurization of the ten (10) cylinders which were subjected to 24,000 cycles in a block loading fatigue test, the background energy oscillation pressure was monitored for each cylinder. The background energy oscillation pressure is defined in [19]. Figure 5.10 provides a representative background energy oscillation plot superimposed on the pressure vs. time for cylinder ALT639-24574. Background energy oscillation plots for all cylinders burst test after being subjected to 24,000 cycles in the block loading fatigue test are included in Appendix D.

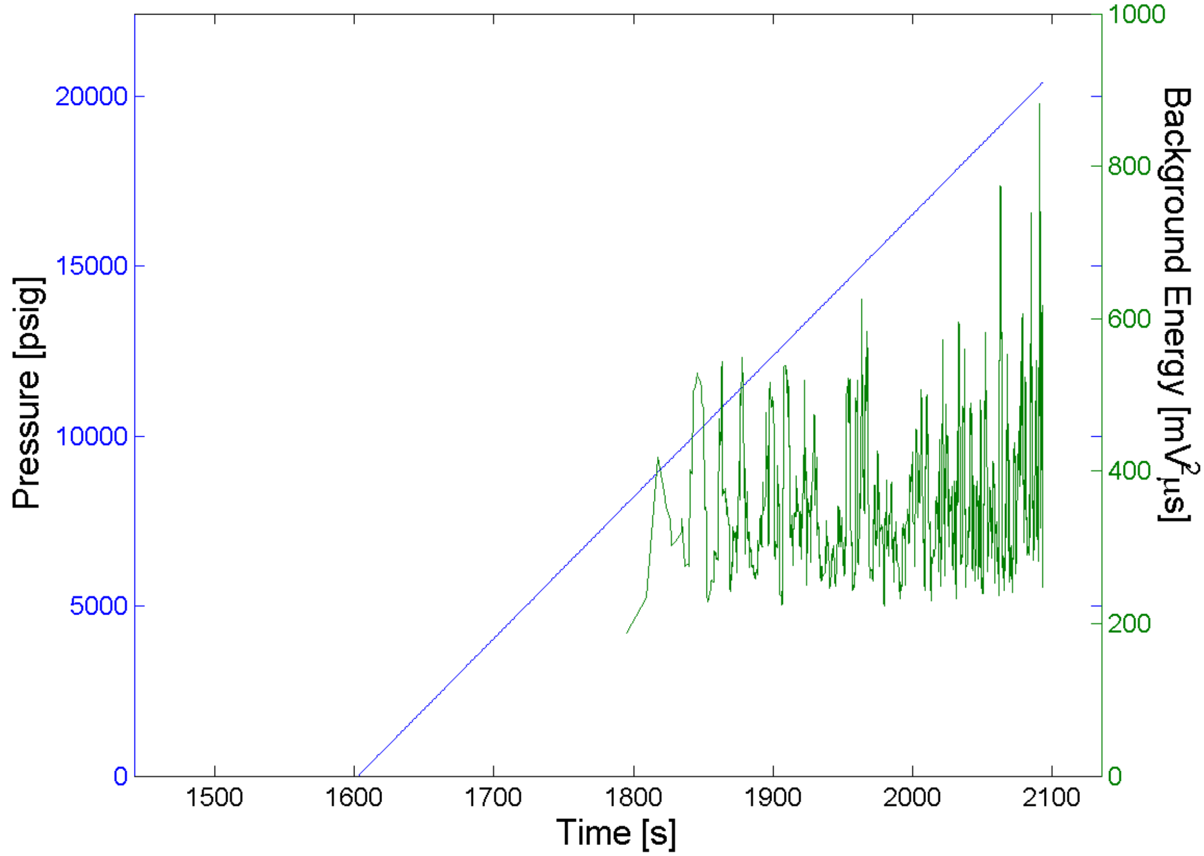

Figure 5.10 – Background energy oscillation vs time superimposed on the pressure vs time plot of the burst pressurization of cylinder ALT639-24574.

Also monitored during the EOL burst pressurization of the cylinders which were subjected to 24,000 cycles in the block loading fatigue test were the waveforms detected as the cylinder began to accumulate damage and progress to failure. To condense the immense amount of information contained within a single waveform (i.e., respective mode content, wave dispersion, frequency content, etc.) frequency domain scalar metrics have been proposed that have the capability when coupled with a forward predictive model of classifying the source mechanism [2, 16, 23]. In this work the metrics proposed in [2] were used for source mechanism classification, and a representative plot of partial power versus weighted peak frequency is shown in Figure 5.11 for cylinder ALT639-24574. Partial power versus weighted peak frequency plots for all cylinders burst test after being subjected to 24,000 cycles in the block loading fatigue test are included in Appendix E.

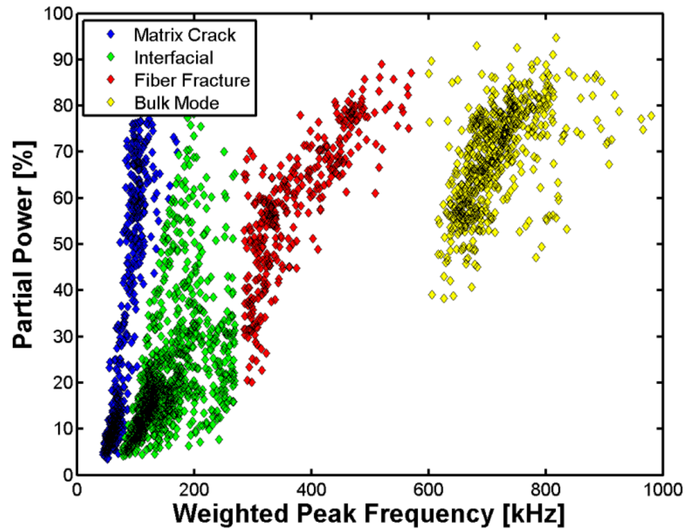

Figure 5.11 – Partial power vs weighted peak frequency for all waveforms detected during the EOL burst pressurization of ALT639-24574.

5.5 *Burst pressure predictive capability of MAE*

In previous research programs the background energy oscillation pressure has been found to occur at an average of 60% of the ultimate burst strength of the cylinder [2, 24]. Similarly, in this study the background energy oscillation pressure was found to occur at an average of 60.6% of the burst pressure of the cylinder, with a standard deviation of 5.9%. Figure 5.12 shows the ratio of background energy oscillation pressure to cylinder burst pressure for all fifty cylinders considered in this study. From Figure 5.12, a clear ability through the use of MAE to predict the burst strength of a composite pressure cylinder exists; such a capability facilitates the ability to remove a cylinder with compromised strength from service at the time of requalification (regardless of the age of the cylinder – whether it be at the time of manufacture or with 60+ years of service life experienced).

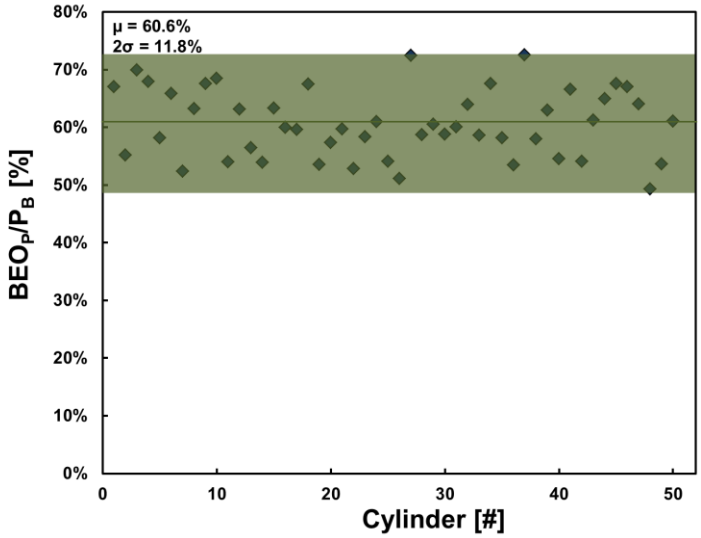

Figure 5.12 – Ratio of background energy oscillation pressure to the cylinder burst pressure for all fifty (50) cylinders tested in this research program.

5.6 *Statistical analysis of fatigue cycled cylinders*

A previous research program has shown that a two parameter Weibull distribution well models the burst strength distribution of DOT-CFFC cylinders [2]. The totality of burst strength distributions available for end of service life DOT-CFFC cylinders was considered by incorporating data from [2] in the current analysis. The effect of service life length (i.e., number of fatigue cycles placed upon a DOT-CFFC cylinder) will be investigated via considering three (3) populations of cylinders:

1. Twenty-five (25) DOT-CFFC cylinders which experienced a fifteen (15) year real world service life. All burst strength data was taken from [2].
2. Sixty-one (61) DOT-CFFC cylinders which experienced a fifteen (15) year real world service life and then twenty (20) additional years of simulated service life. Data was taken from the present study and [2].
3. Ten (10) DOT-CFFC cylinders which experienced a fifteen (15) year real world service life and then forty-eight (48) additional years of simulated service life (which ISO 11119.2:2002 states may be considered an infinite fatigue life [4]). Data was taken exclusively from this report.

Figure 5.13 shows the three (3) Weibull distributions for the aforementioned cylinder populations, while Table 5.5 provides the shape and scale parameters for the respective Weibull distributions. Examination of Figure 5.13 indicates that additional fatigue cycles to maximum developed pressure does not diminish the burst strengths of DOT-CFFC composite cylinders. Further, Figure 5.13 shows that all cylinders which were subjected to a simulated extended service life possessed burst strength distributions that fall well above the minimum required burst strength at the time of manufacture (15,300 psi) [1].

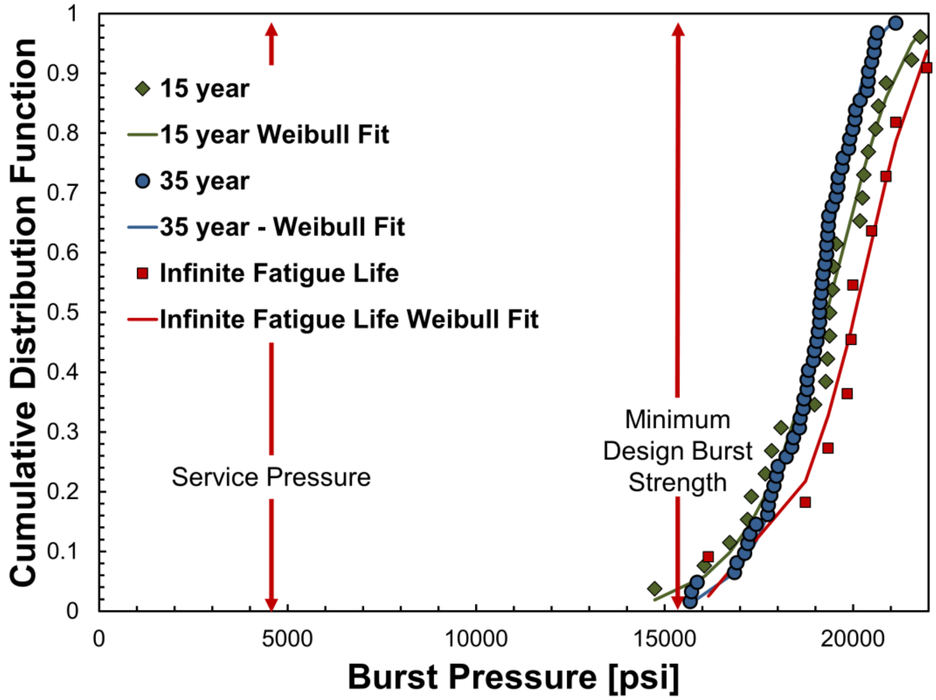

Figure 5.13 – Burst strength data and corresponding Weibull distribution fits for 15 year service life, 35 year service life, and infinite fatigue life DOT-CFFC cylinders.

Table 5.5 – Summary of Weibull distribution parameters for 15 year service life, 35 year service life, and infinite fatigue life DOT-CFFC cylinders.

Population	Shape Parameter (κ)	Scale Parameter (λ, psi)
15 year service life	13.3	19840
35 year service life	19.0	19430
Infinite service life	15.3	20545

Of the ninety-six (96) cylinders considered herein, a single cylinder did not meet the minimum required burst strength [2]. Furthermore, directly prior to the burst pressurization of the compromised strength cylinder, the cylinder was rejected by the MAE analysis of DOT SP's 15720, 16190, and 16343, signifying that the cylinder would have been condemned and removed from service [2].

6. Conclusions

From the entirety of the data presented herein several key points should be taken away.

- The proposed reautofrettage process significantly improved the fatigue performance of the 6061-T6 aluminum liner of DOT-CFFC cylinders, when evaluated for extended service life.

- Forty (40) of the forty (40) DOT-CFFC cylinders which were reautofrettaged and then subjected to 10,000 fatigue cycles (20 years of additional service life) achieved the required 10,000 fatigue cycles without leaking.

- Forty (40) of the forty (40) DOT-CFFC cylinders which were reautofrettaged and then subjected to 10,000 fatigue cycles (20 years of additional service life) burst above the minimum required pressure at the time of manufacture as set forth in [1].

- By utilizing a block loading fatigue test procedure that accounted for the test pressure cycle which occurs at the five (5) year requalification interval, end of service life DOT-CFFC cylinders can sustain an additional 24,000 fatigue cycles to maximum developed pressure (infinite life as defined by [4]). All ten (10) of the cylinders which were subjected to the block loading fatigue test protocol sustained an additional 24,000 fatigue cycles without the 6061-T6 aluminum liner leaking. Such findings indicate that a block loading fatigue test program may more appropriately represent real world cylinder fatigue performance, and should therefore be adopted into design qualification testing and standards.

- Ten (10) of the ten (10) cylinders which were subjected to the 24,000 cycle block loading fatigue test protocol burst above the minimum required burst pressure at the time of manufacture for DOT-CFFC cylinders [1].

- Modal Acoustic Emission (MAE) again showed the ability to predict the burst strength of DOT-CFFC composite pressure cylinders, facilitating the ability to remove a cylinder with compromised strength from service (regardless of the age of the cylinder – whether it be at the time of manufacture or with 60+ years of service life experienced).

7. References

[1] Department of Transportation, "Basic requirements for fully wrapped carbon-fiber reinforced aluminum lined cylinders (DOT-CFFC)," DOT, 2007.

[2] Digital Wave Corporation (DWC), "Use of Modal Acoustic Emission (MAE) for life extension of civilian self-contained breathing apparatus (SCBA) DOT-CFFC cylinders," DOT/PHMSA, Centennial, CO, 2014.

[3] Compressed Gas Association (CGA), "CGA C-22 Water Corrosion of Composites AA6061 Liners," Compressed Gas Association, Inc., Chantilly, VA, 2012.

[4] (ISO), International Standards Organization, "11119.2 Gas cylinders of composite construction - specification and test methods Part 2: Fully wrapped fibre reinforced composite gas cylinders with load-sharing metal liners," ISO, Geneva, Switzerland, 2002.

[5] C. G. A. (CGA), "CGA C-6.2 - 2013 Standard for Visual Inspection and Requalification of Fiber Reinforced High Pressure Cylinders," CGA, Chantilly, VA, 2013.

[6] American Society of Mechanical Engineers (ASME), "Boiler and Pressure Vessel Code," in *Section X: Fiber Reinforced Plastic Pressure Vessels*, New York, NY, 2013, pp. 129-134.

[7] Department of Transportation, "DOT-SP 15720," Washington D.C., 2013.

[8] Department of Transportation, "DOT-SP 16190," DOT, Washington D.C., 2015.

[9] Department of Transportation, "DOT-SP 16343," Washington, DC, 2015.

[10] A. Liu, "Summary of stress-intensity factors," in *ASM Handbook Volume 19, Fatigue and Fracture*, Materials Park, OH, ASM International, 1996, pp. 980-1000.

[11] J. Newman Jr., "Fracture analysis of surface and through cracks in cylindrical pressure vessels," NASA TN D-8325, 1976.

[12] I. Raju and J. Newman Jr., "Stress-intensity factors for internal and external surface cracks in cylindrical vessels," *Journal of Pressure Vessel Technology, Transactions of ASME*, vol. 104, pp. 293-298, 1982.

[13] A. Riberio, A. Jesus and A. Fernandes, "Fatigue crack propagation rates of the aluminum alloy 6061-T651," in *18th International Congress of Mechanical Engineering*, Ouro Preto, 2005.

[14] R. I. Stephens, A. Fatemi, R. R. Stephens and H. O. Fuchs, Metal Fatigue in Engineering 2nd

Edition, New York: Wiley Inter-Science, 2001.

[15] B. Sheu and P. Song, "Shaping exponent in Wheeler model under a single overload," *Engineering Fracture Mechanics,* vol. 51, no. 1, pp. 135-143, 1995.

[16] B. Burks and M. Kumosa, "A modal acoustic emission signal classification scheme derived from finite element simulation," *International Journal of Damage Mechanics,* vol. 23, no. 1, pp. 43-62, 2014.

[17] B. Burks and M. Hamstad, "The impact of solid-fluid interaction on transient stress wave propagation due to Acoustic Emissions in multi-layer plate structures," *Composite Structures,* pp. 411-422, 2014.

[18] M. Gorman, "Plate Wave Acoustic Emission," *Journal of Acoustical Society of America,* vol. 90, no. 1, pp. 358-364, 1990.

[19] M. Gorman, "Modal AE analysis of fracture and failure in composite materials, and the quality and life of high pressure composite cylinders," *Journal of Acoustic Emission,* vol. 29, pp. 1-28, 2011.

[20] D. Guo, A. Mal and M. Hamstad, "AE wavefield calculations in a plate," in *Progress in Acoustic Emission,* Hawaii, 1998.

[21] M. Sause, M. Hamstad and S. Horn, "Finite element modeling of lamb wave propagation in anisotropic hybrid materials," *Composites: Part B,* pp. 249-257, 2013.

[22] J. Masters and K. Reifsnider, "An investigation of cumulative damage development in quasi-isotropic graphite/epoxy laminates," *ASTM STP775,* pp. 40-62, 1982.

[23] M. Sause and S. Horn, "Simulation of acoustic emission in planar carbon fiber reinforced plastic specimens," *Journal of Nondestructive Evaluation,* vol. 29, pp. 123-142, 2010.

[24] Digital Wave Corporation, "SCBA Materials and Modal Acoustic Emission Testing Life Extension Report," Digital Wave Corporation, Centennial, CO, 2012.

8. Appendix A – Fatigue modulus plots

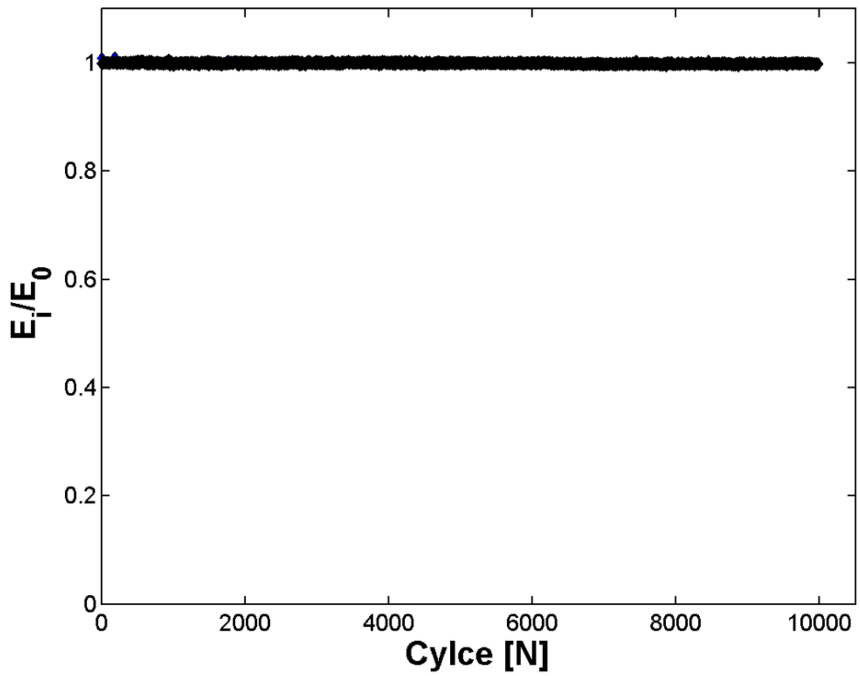

Figure A.1 – Fatigue modulus monitoring of cylinder ALT639-4101.

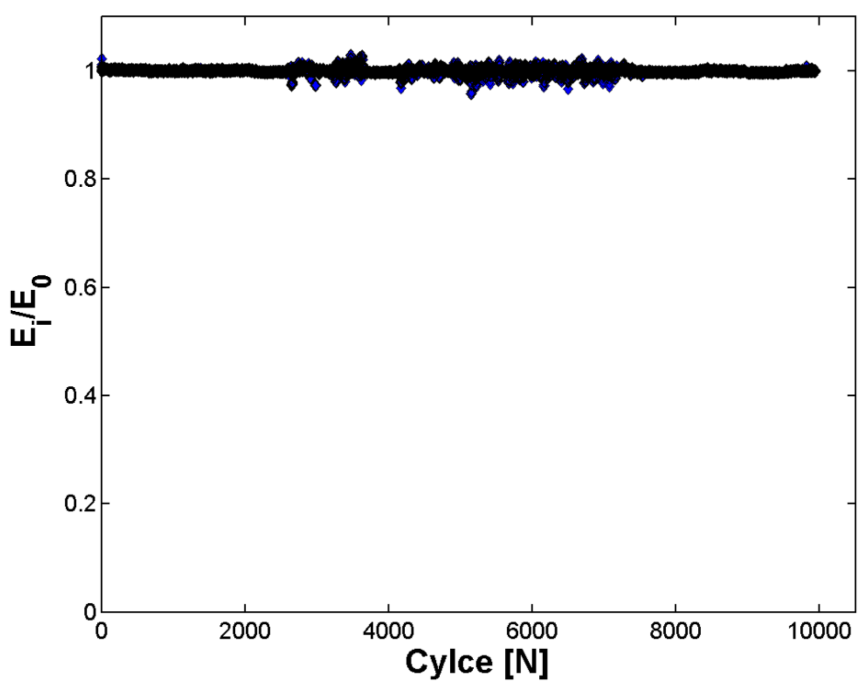

Figure A.2 – Fatigue modulus monitoring of cylinder ALT639-9435.

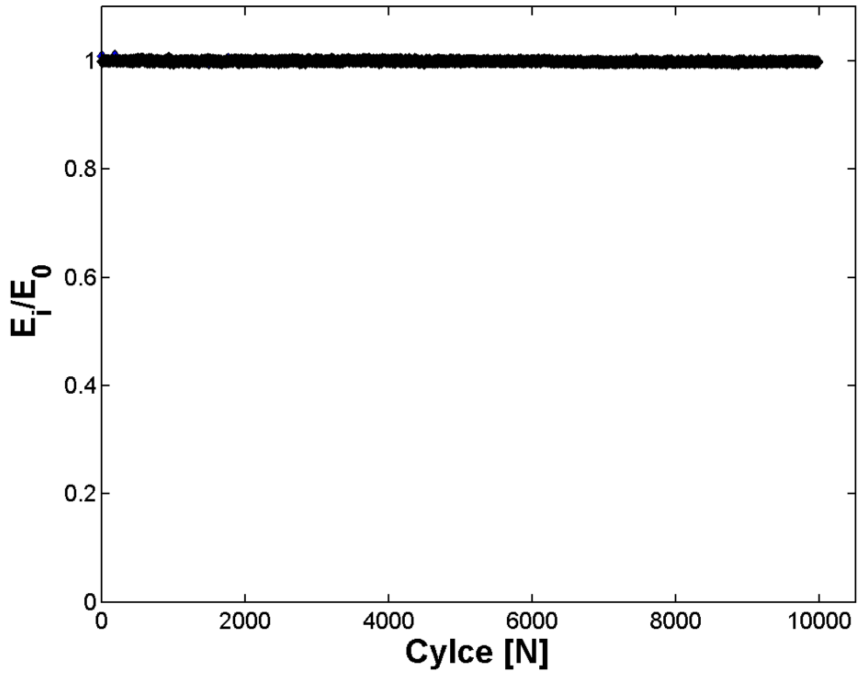

Figure A.3 – Fatigue modulus monitoring of cylinder ALT639-9528.

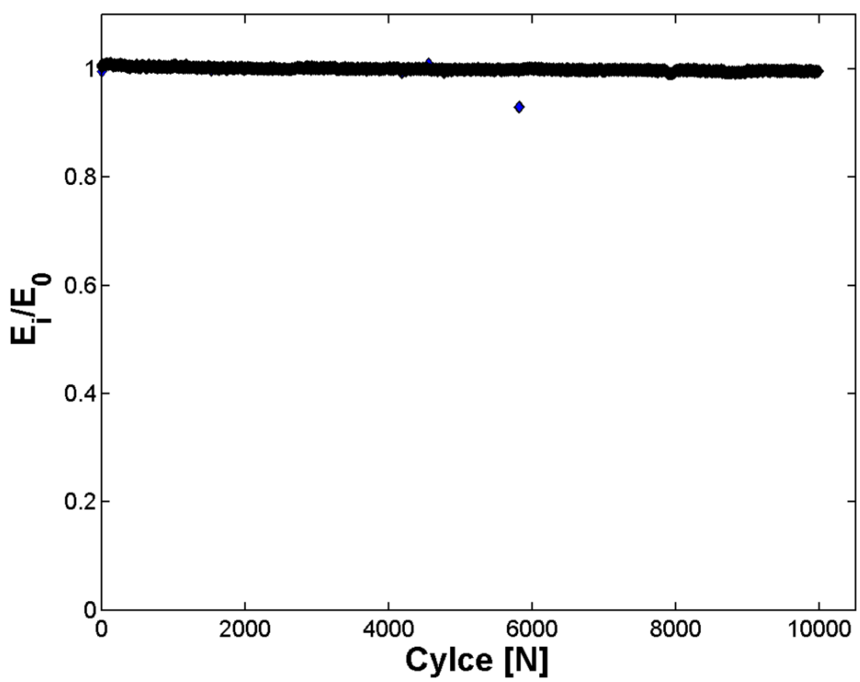

Figure A.4 – Fatigue modulus monitoring of cylinder ALT639-9941.

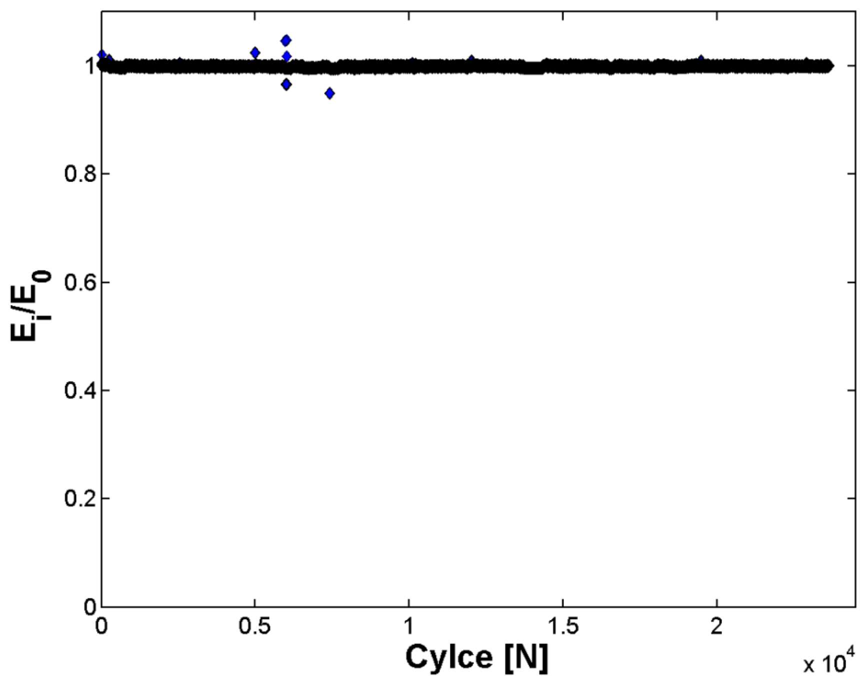

Figure A.5 – Fatigue modulus monitoring of cylinder ALT639-17714.

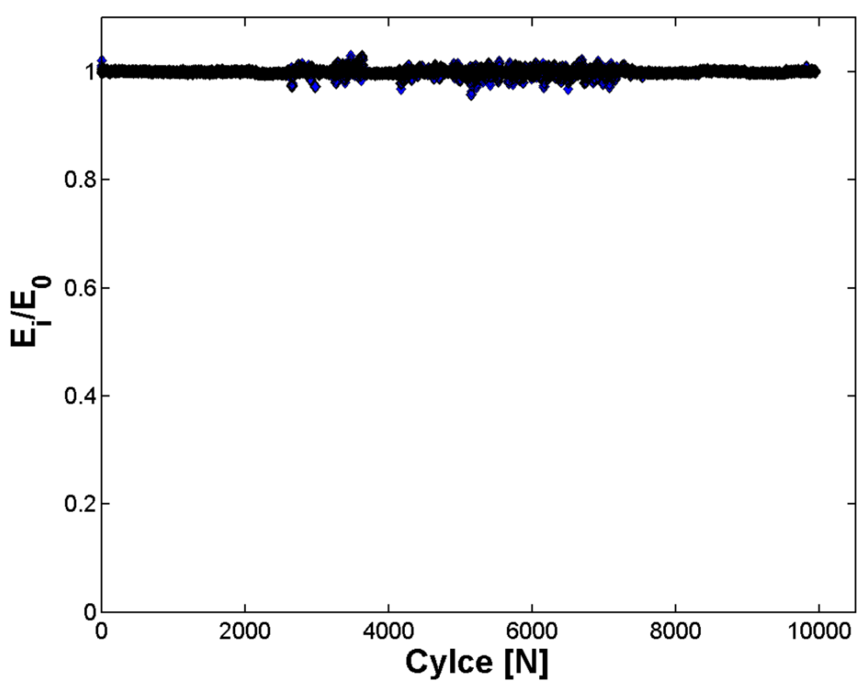

Figure A.6 – Fatigue modulus monitoring of cylinder ALT639-18594.

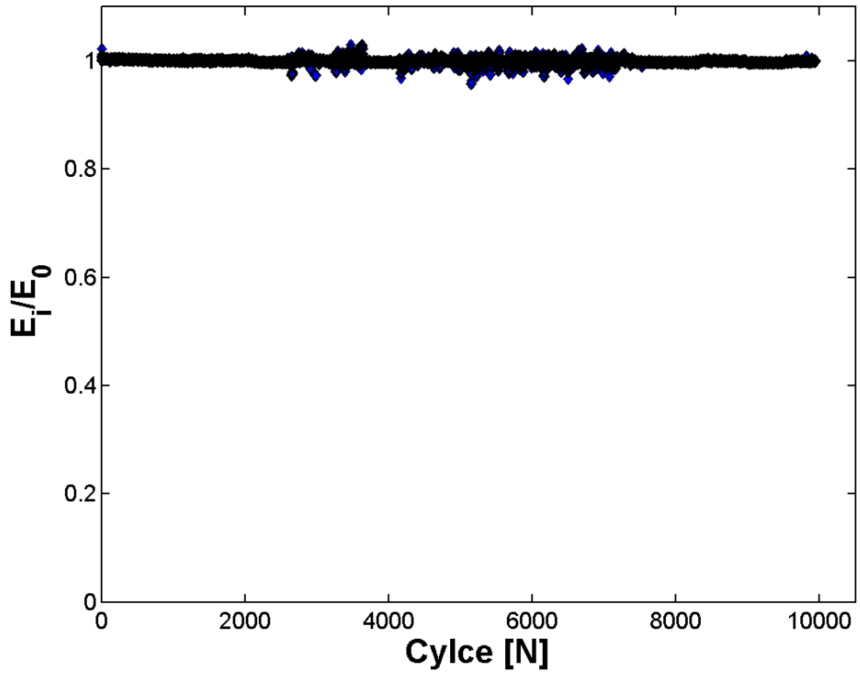

Figure A.7 – Fatigue modulus monitoring of cylinder ALT639-18682.

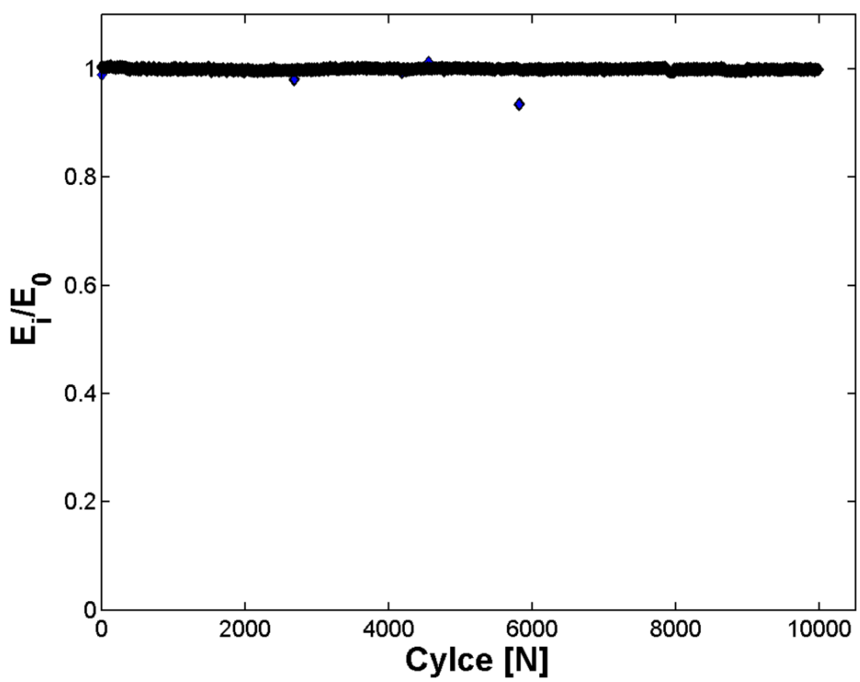

Figure A.8 – Fatigue modulus monitoring of cylinder ALT639-19008.

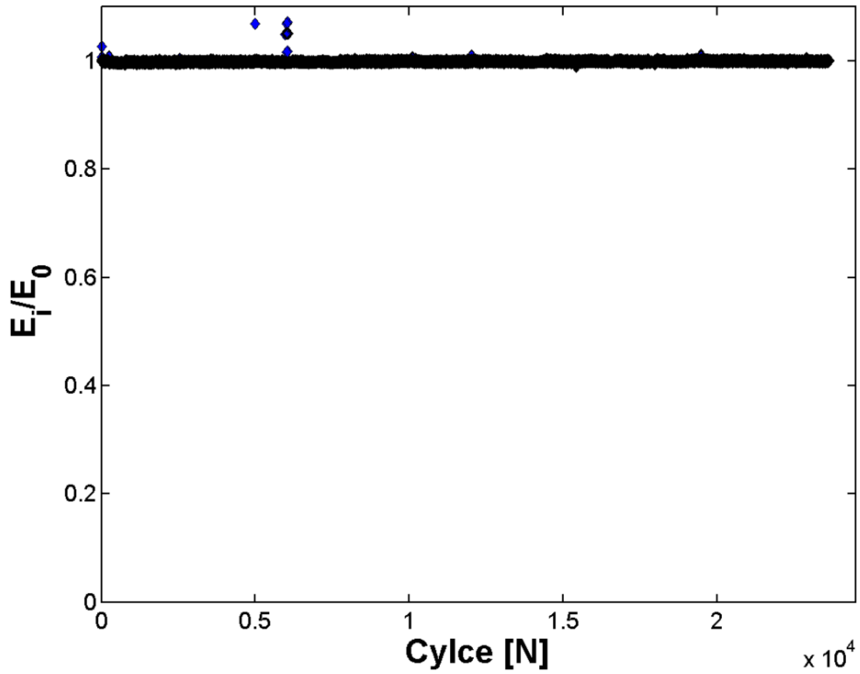

Figure A.9 – Fatigue modulus monitoring of cylinder ALT639-22931.

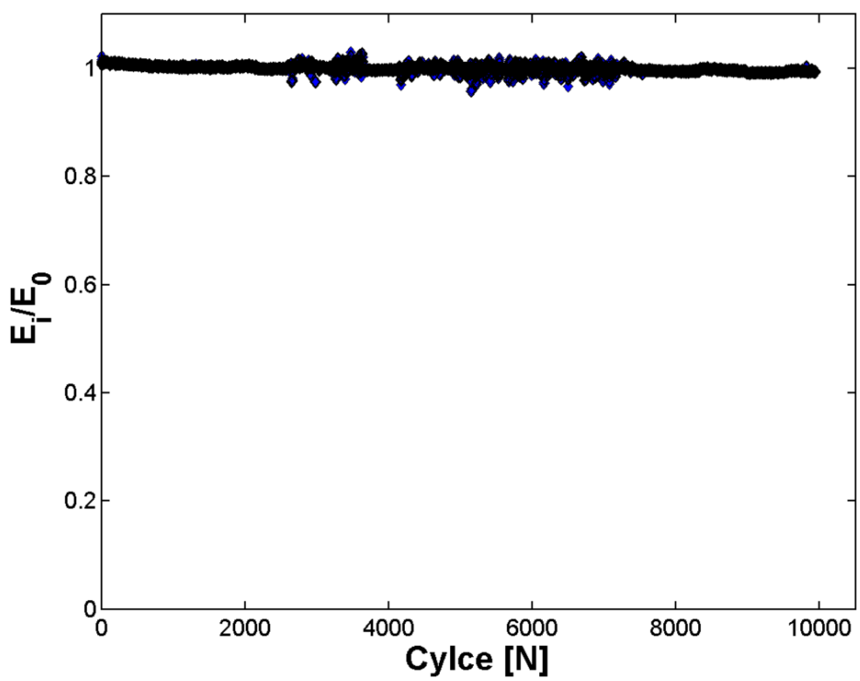

Figure A.10 – Fatigue modulus monitoring of cylinder ALT639-23993.

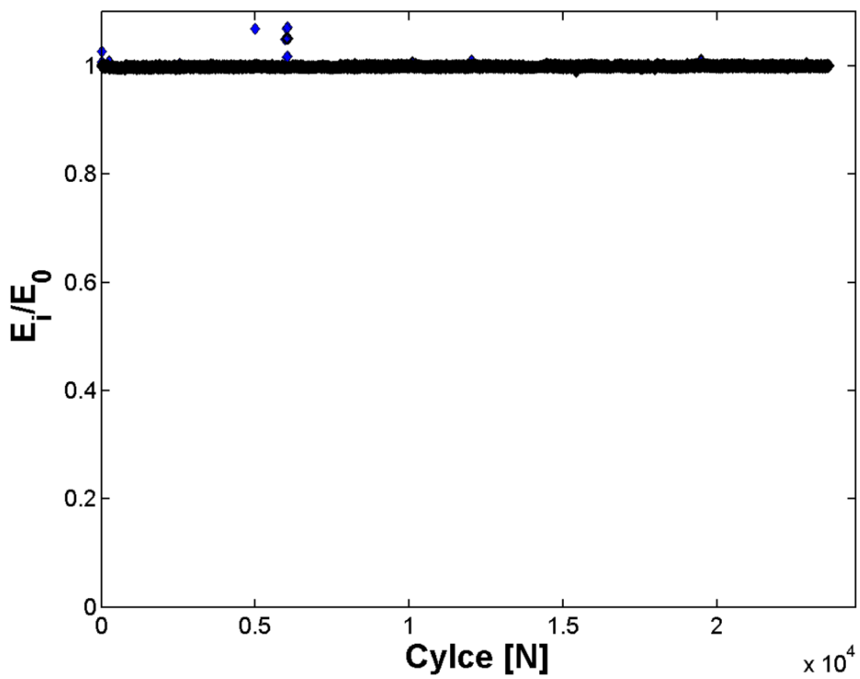

Figure A. 11 – Fatigue modulus monitoring of cylinder ALT639-24574.

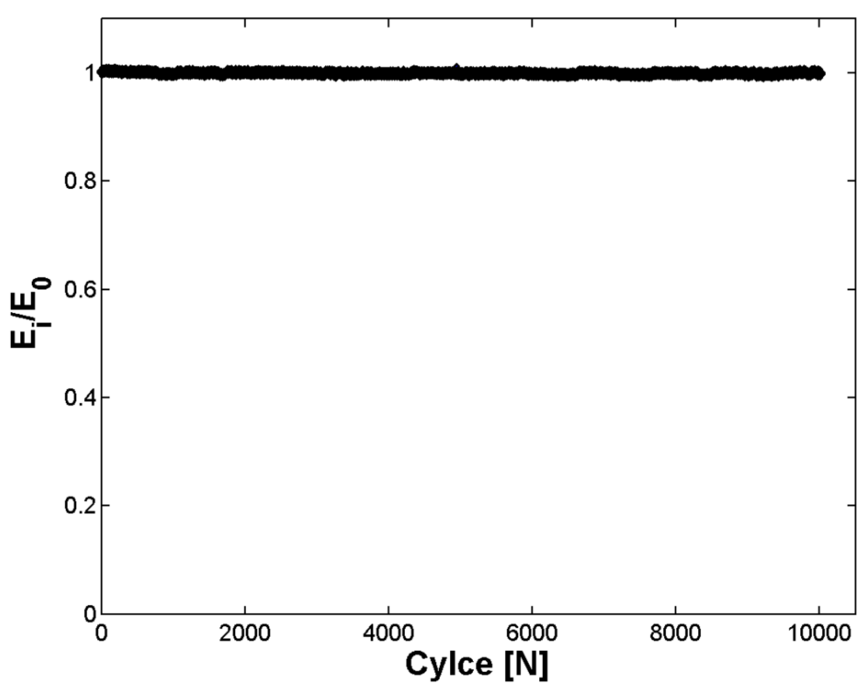

Figure A.12 – Fatigue modulus monitoring of cylinder ALT639-34005.

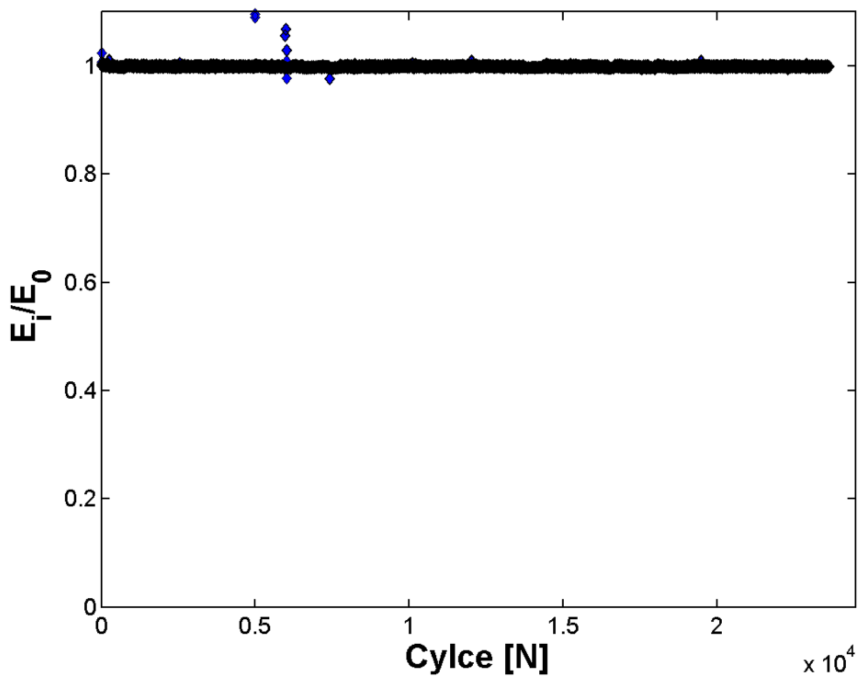

Figure A.13 – Fatigue modulus monitoring of cylinder ALT639-38566.

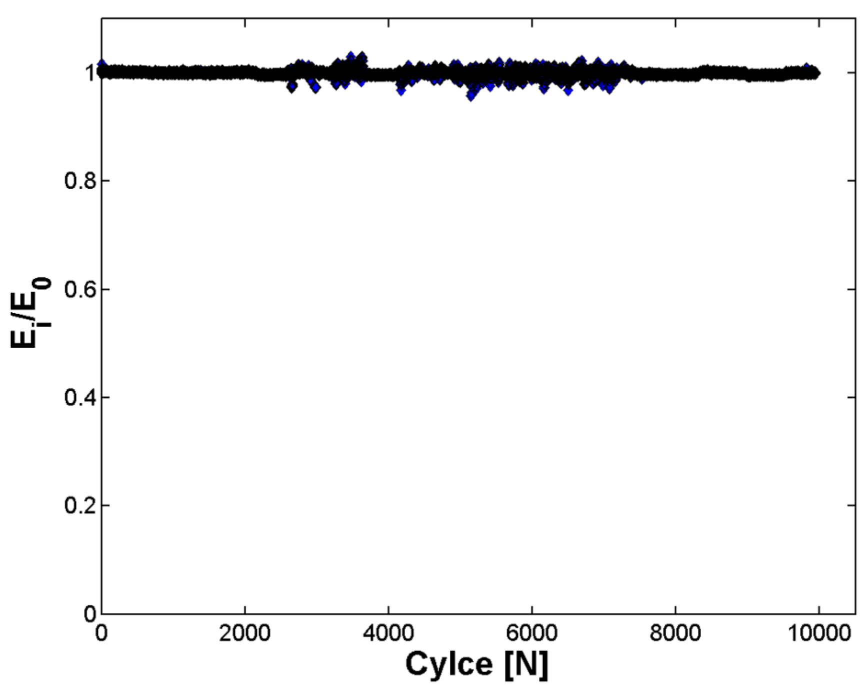

Figure A.14 – Fatigue modulus monitoring of cylinder ALT639-40136.

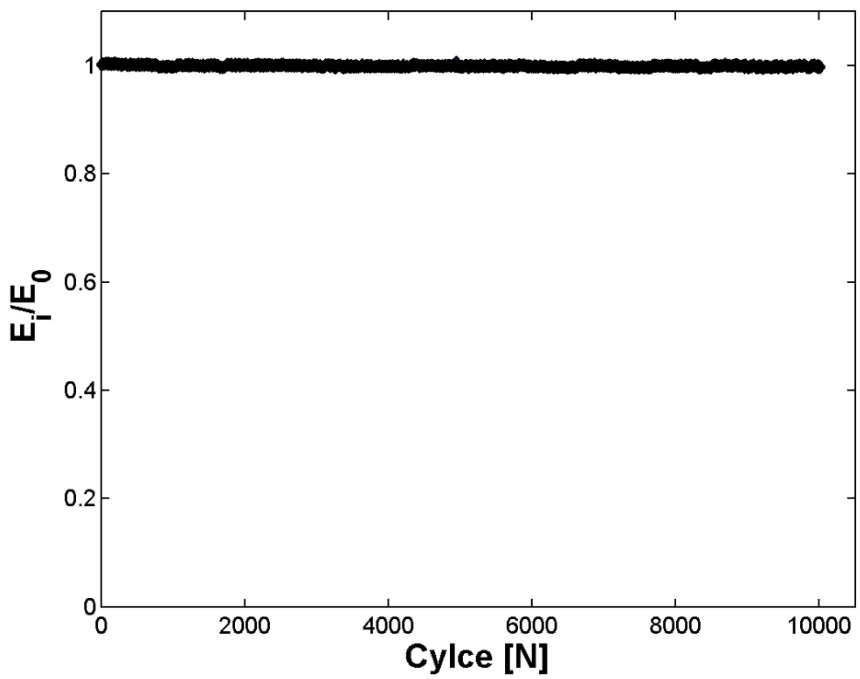

Figure A.15 – Fatigue modulus monitoring of cylinder ALT639-69988.

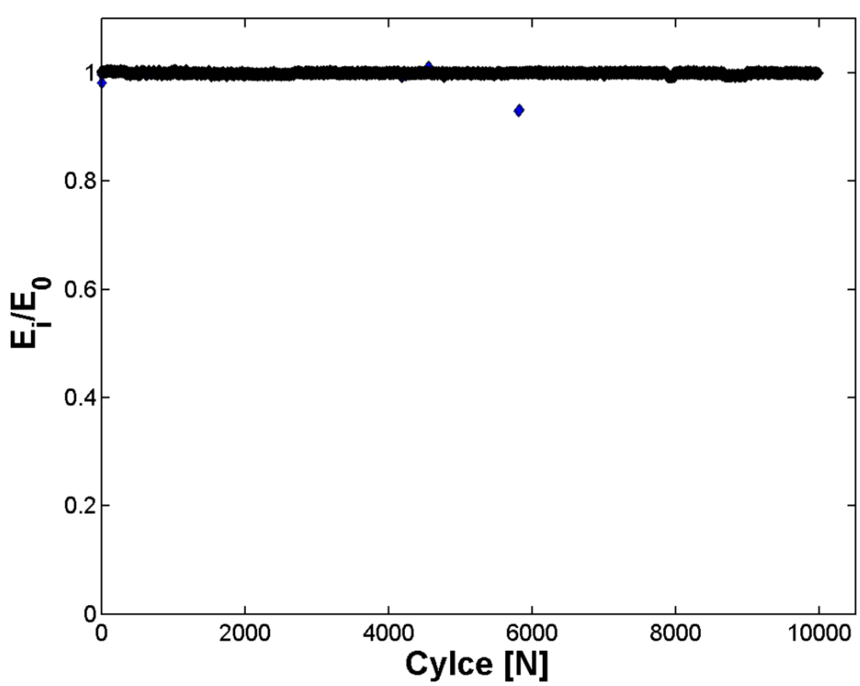

Figure A.16 – Fatigue modulus monitoring of cylinder ALT695-1862.

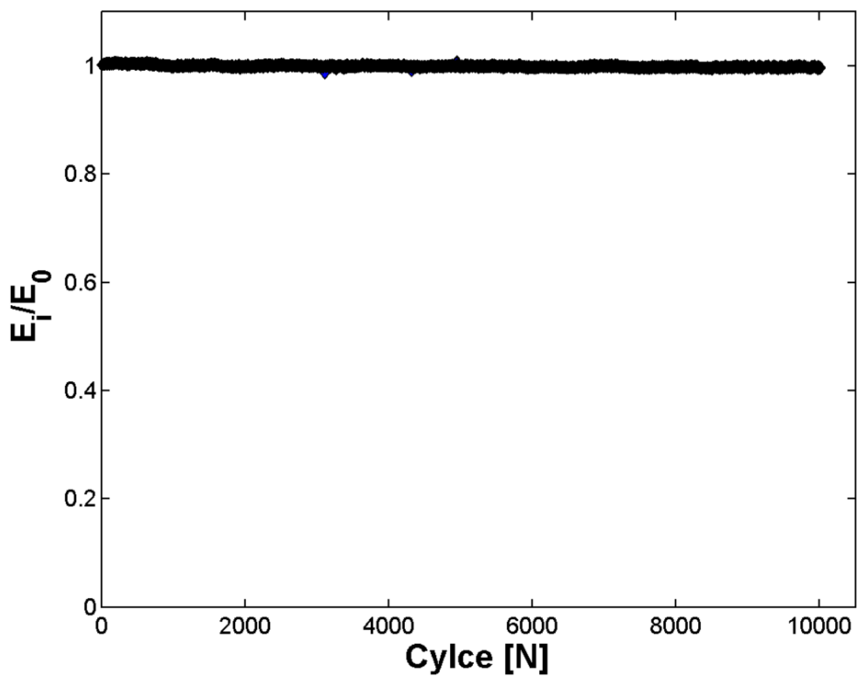

Figure A.17 – Fatigue modulus monitoring of cylinder ALT695-3224.

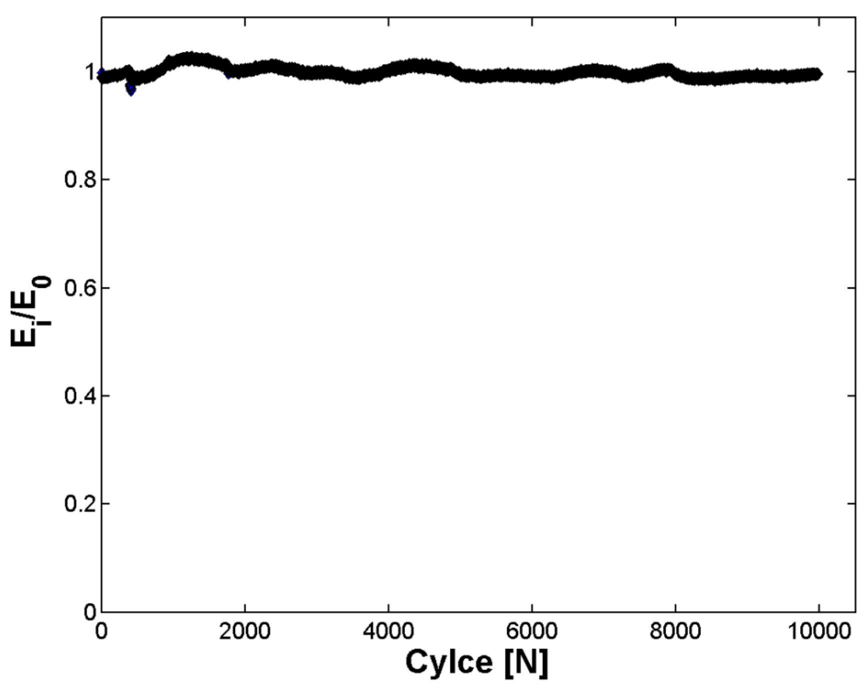

Figure A.18 – Fatigue modulus monitoring of cylinder ALT695-3575.

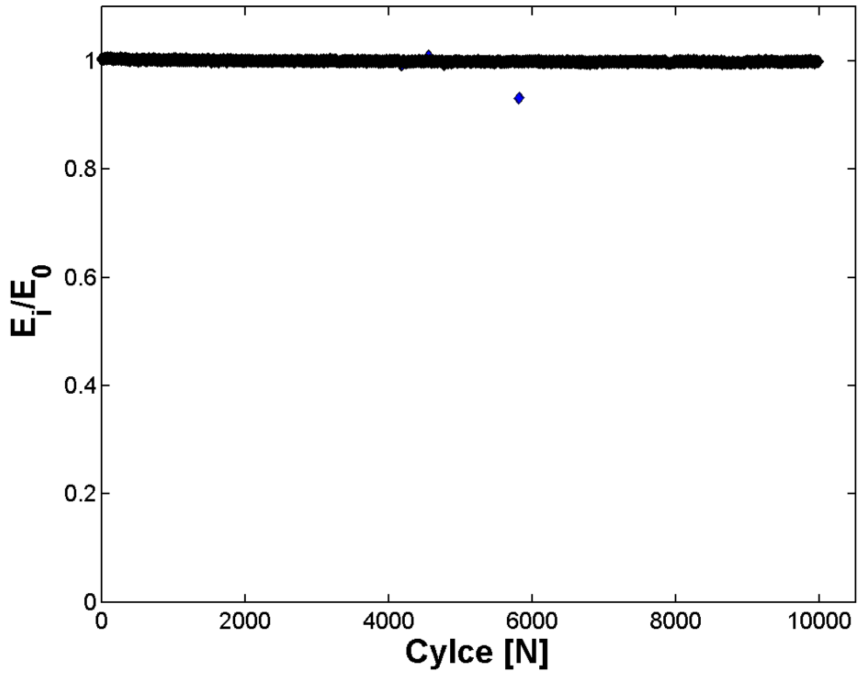

Figure A.19 – Fatigue modulus monitoring of cylinder ALT695-3881.

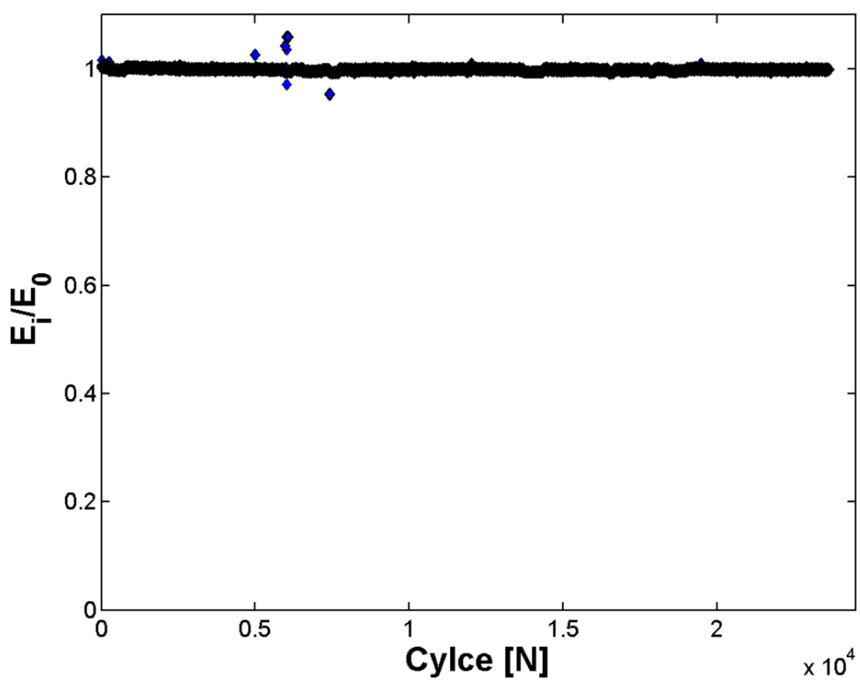

Figure A.20 – Fatigue modulus monitoring of cylinder ALT695-3936.

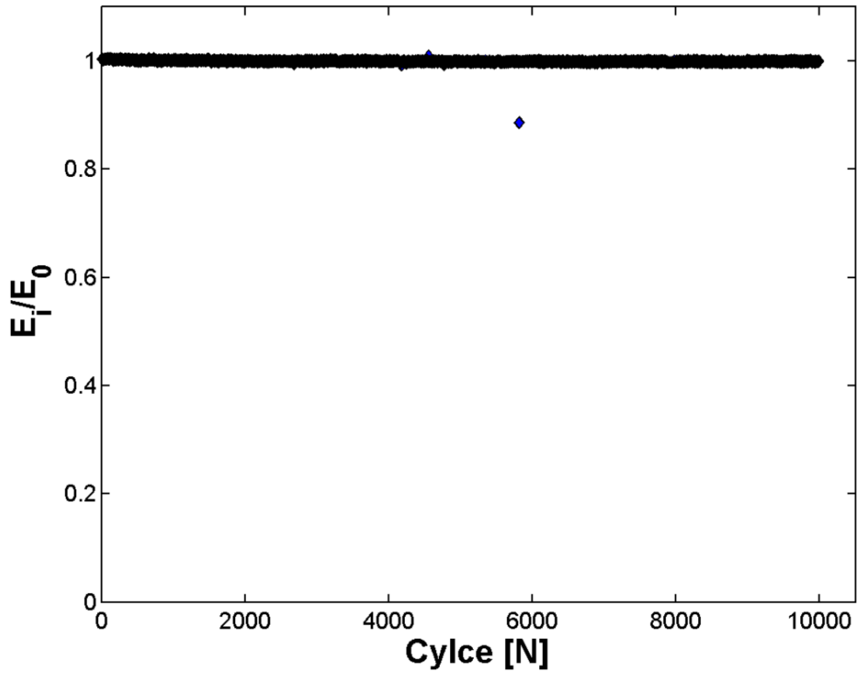

Figure A.21 – Fatigue modulus monitoring of cylinder ALT695-4379.

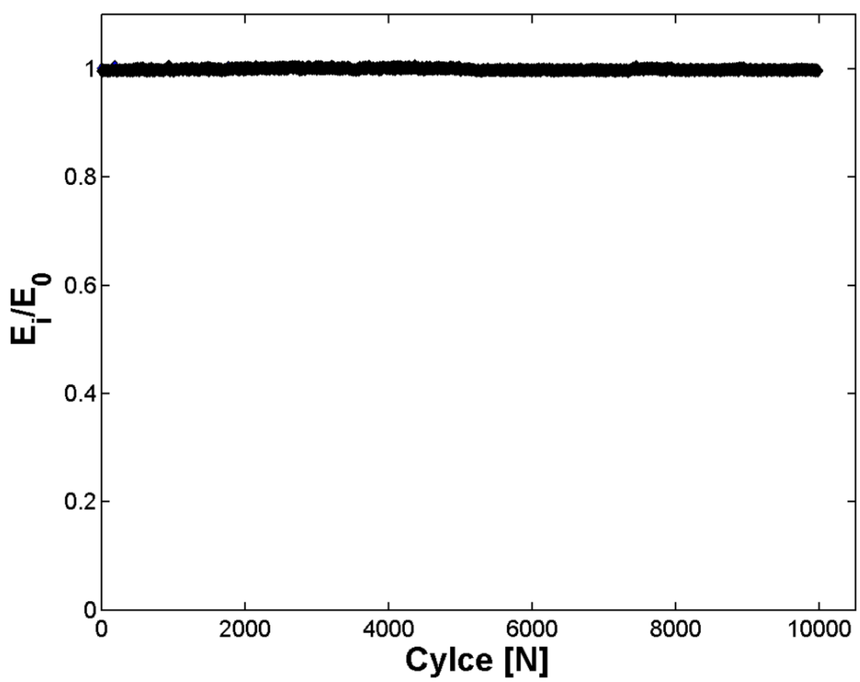

Figure A.22 – Fatigue modulus monitoring of cylinder ALT695-4396.

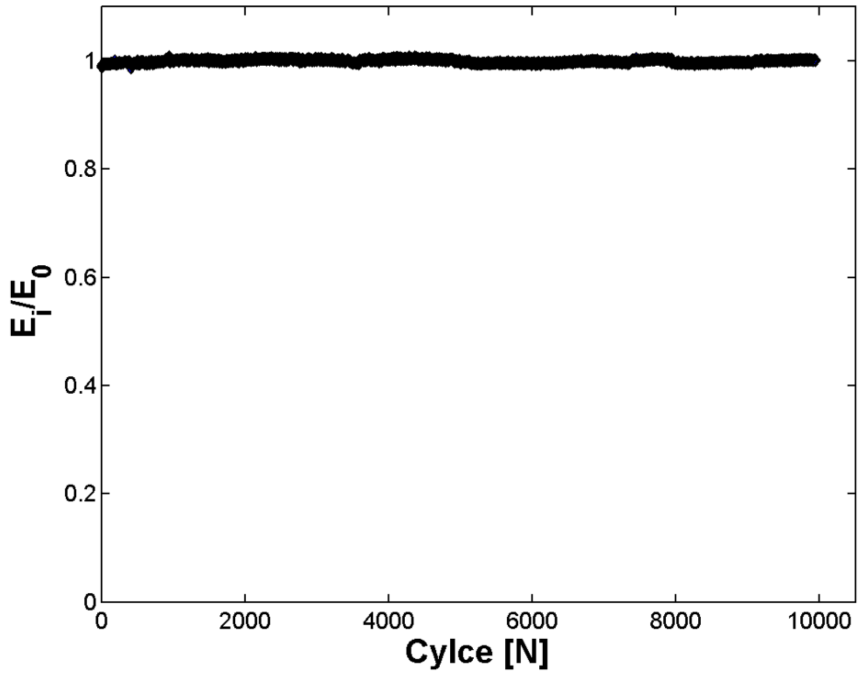

Figure A.23 – Fatigue modulus monitoring of cylinder ALT695-4482.

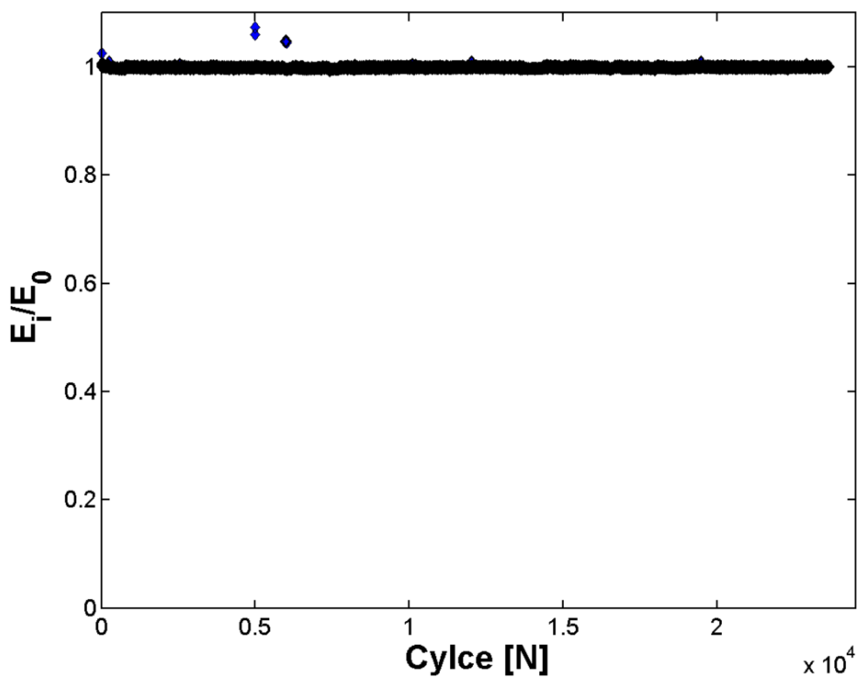

Figure A.24 – Fatigue modulus monitoring of cylinder ALT695-4492.

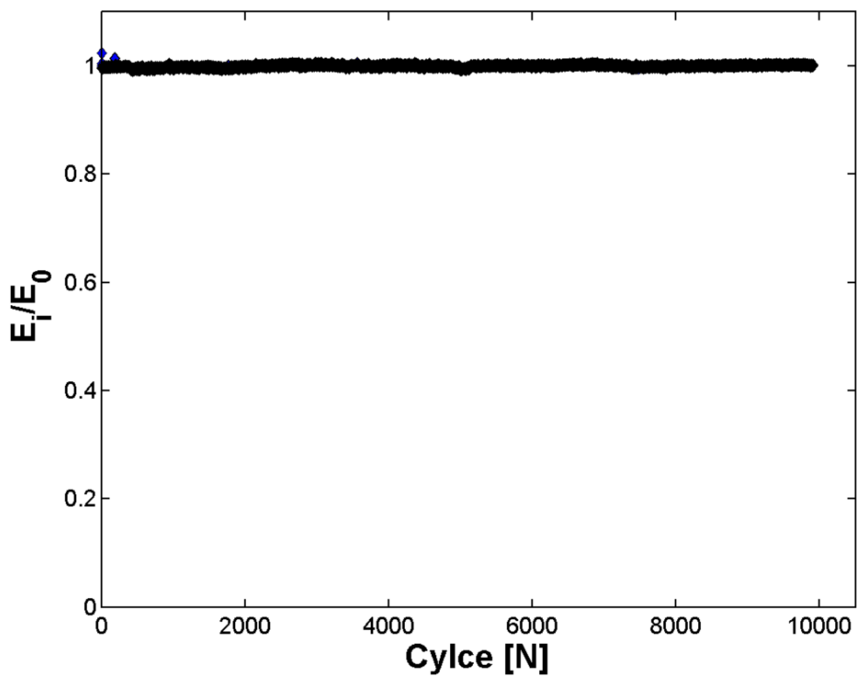

Figure A.25 – Fatigue modulus monitoring of cylinder ALT695-4636.

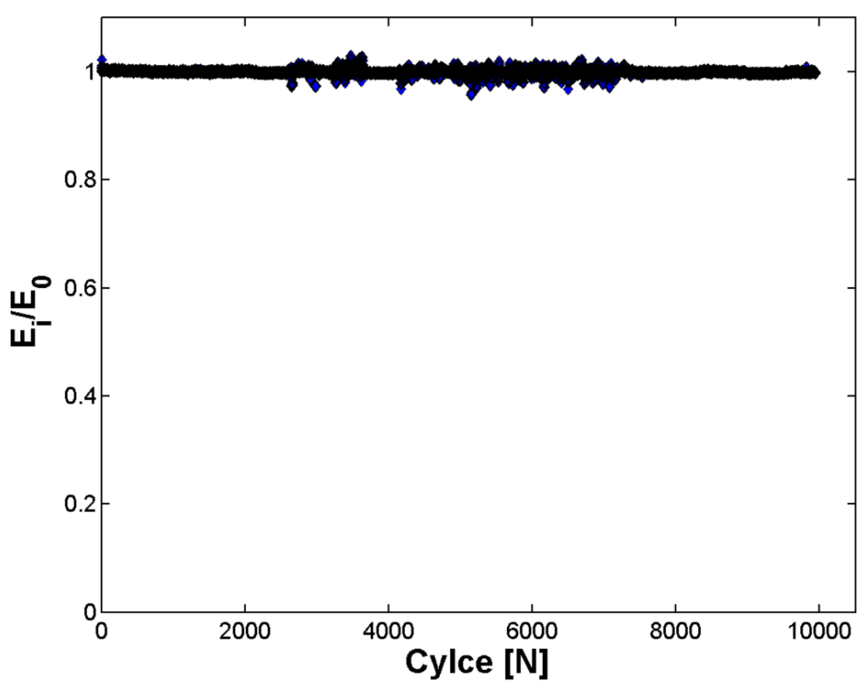

Figure A.26 – Fatigue modulus monitoring of cylinder ALT695-4734.

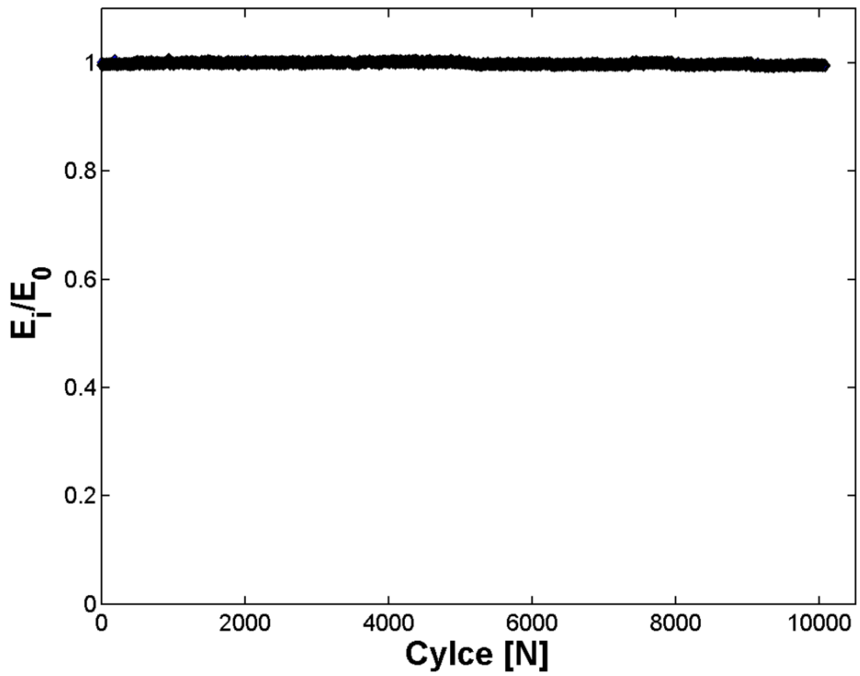

Figure A.27 – Fatigue modulus monitoring of cylinder ALT695-4775.

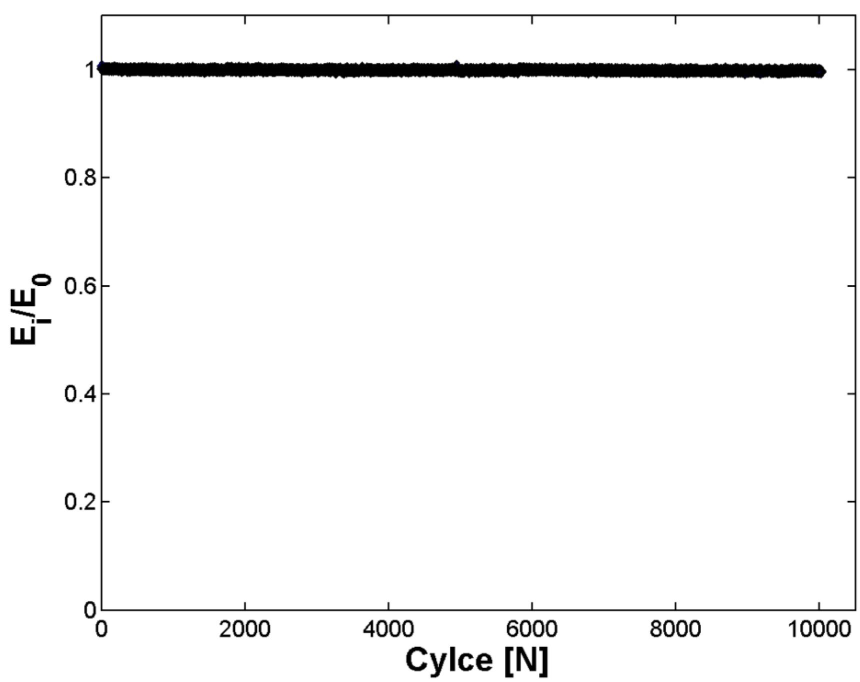

Figure A.28 – Fatigue modulus monitoring of cylinder ALT695-4944.

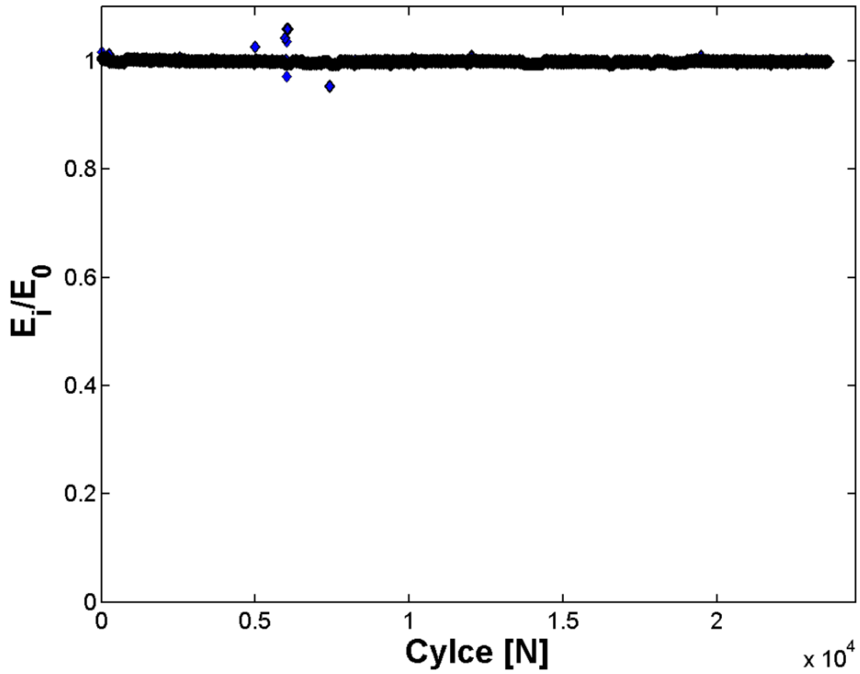

Figure A.29 – Fatigue modulus monitoring of cylinder ALT695-5155.

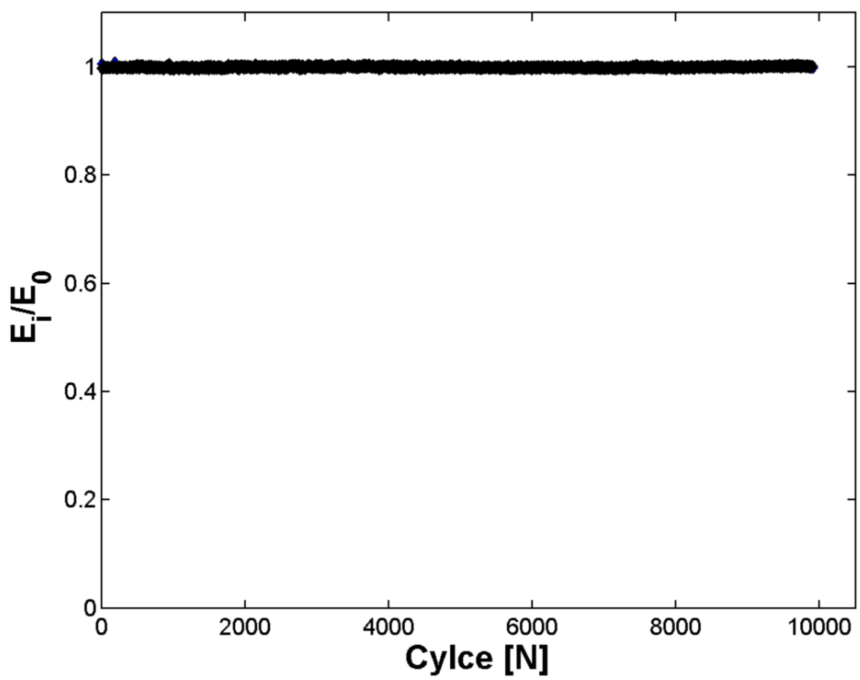

Figure A.30 – Fatigue modulus monitoring of cylinder ALT695-5224.

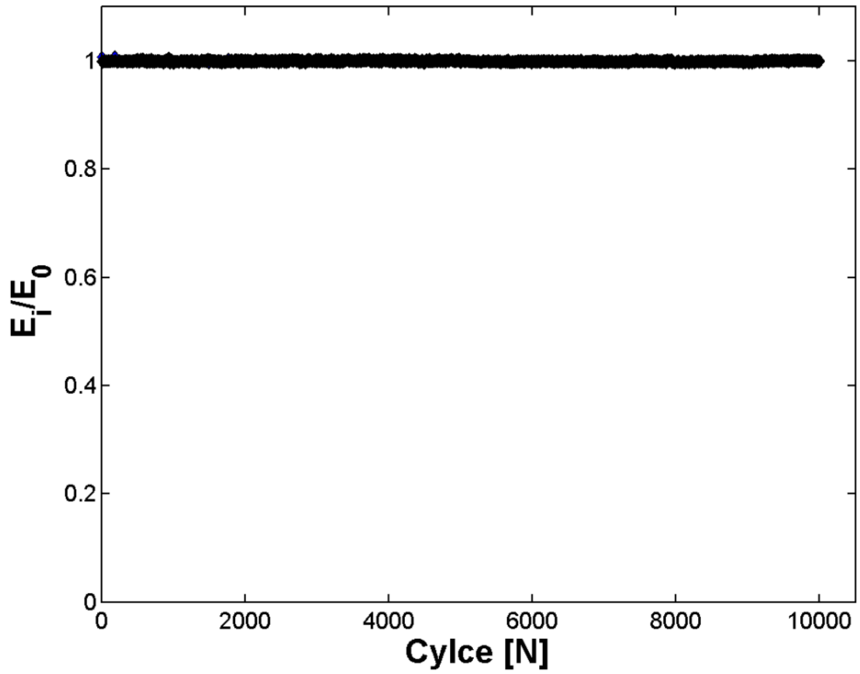

Figure A.31 – Fatigue modulus monitoring of cylinder ALT695-5497.

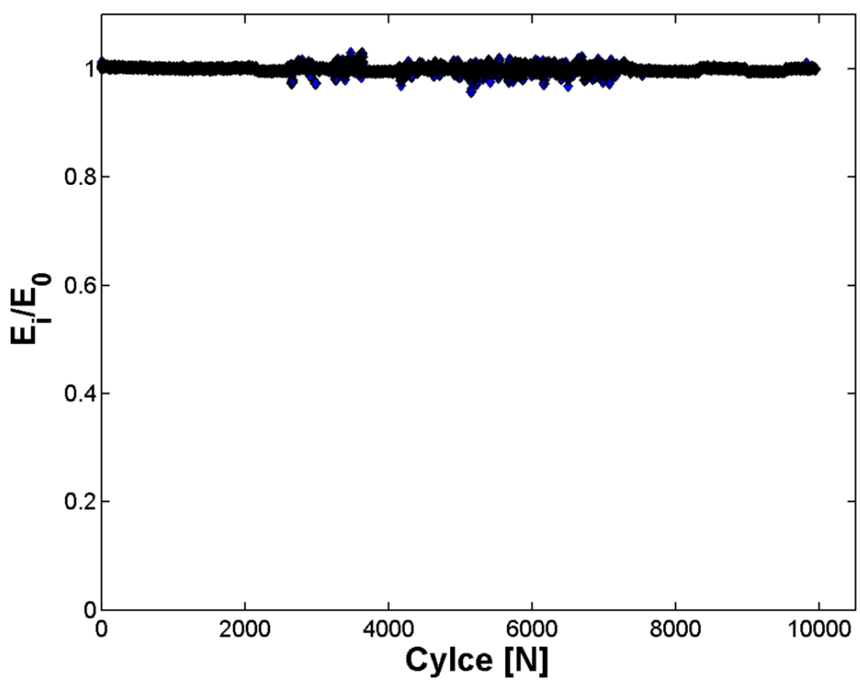

Figure A.32 – Fatigue modulus monitoring of cylinder ALT695-5558.

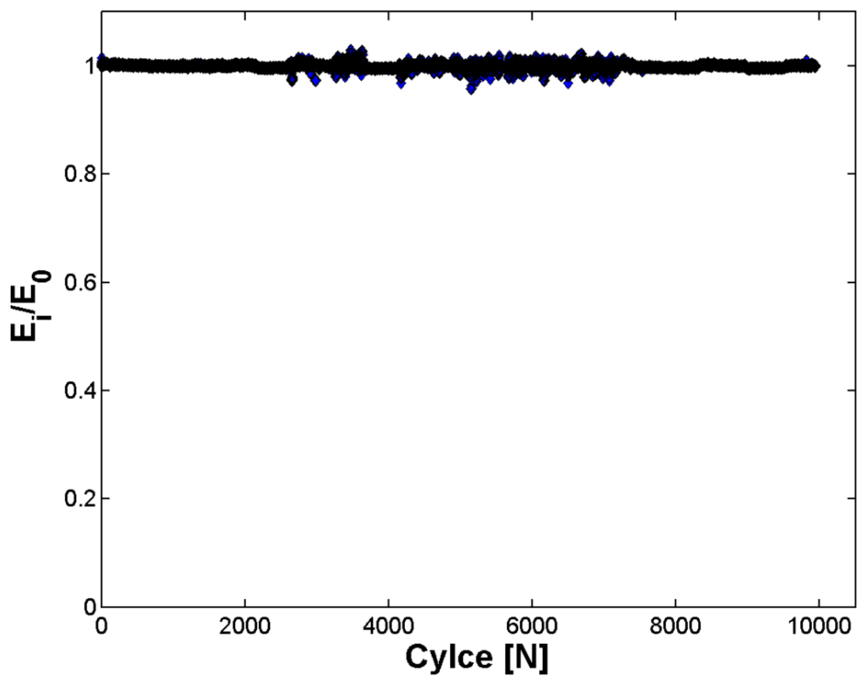

Figure A.33 – Fatigue modulus monitoring of cylinder ALT695-5641.

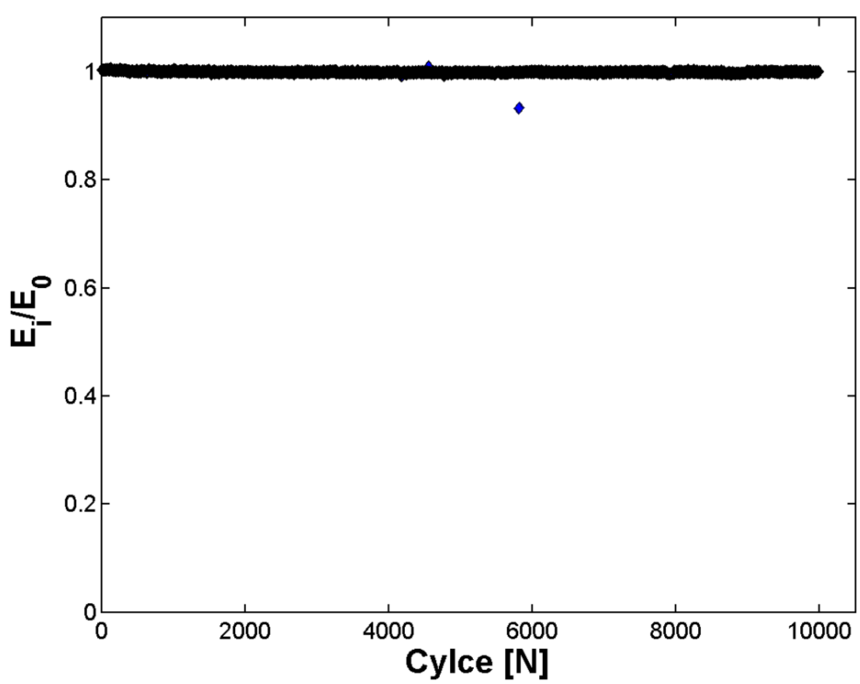

Figure A.34 – Fatigue modulus monitoring of cylinder ALT695-6041.

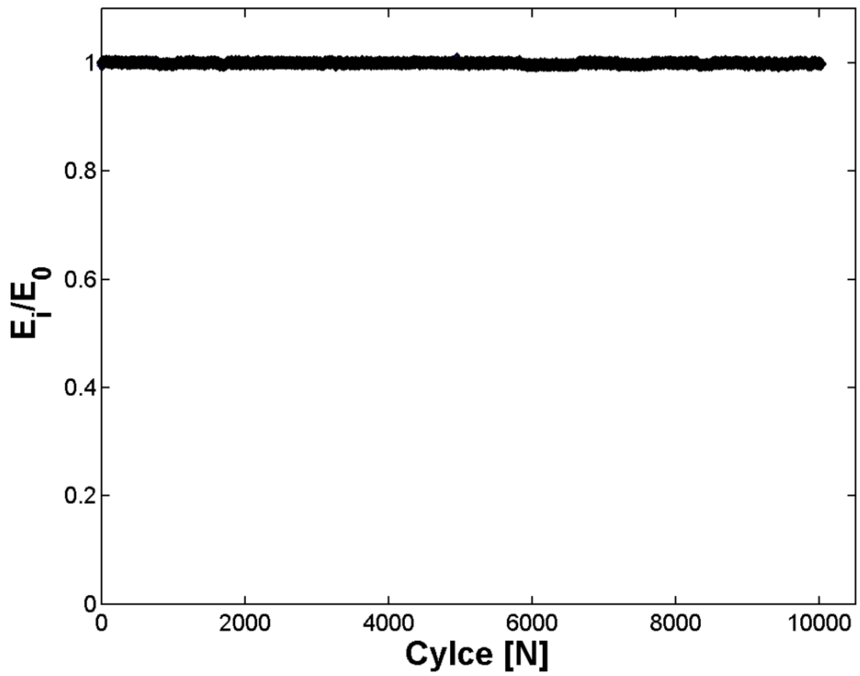

Figure A.35 – Fatigue modulus monitoring of cylinder IL2705.

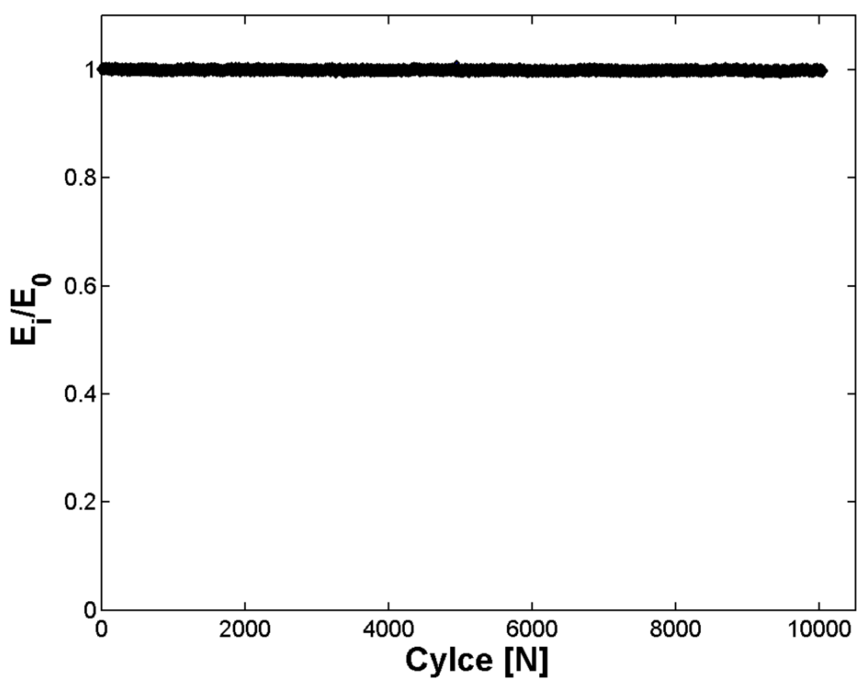

Figure A.36 – Fatigue modulus monitoring of cylinder IL2722.

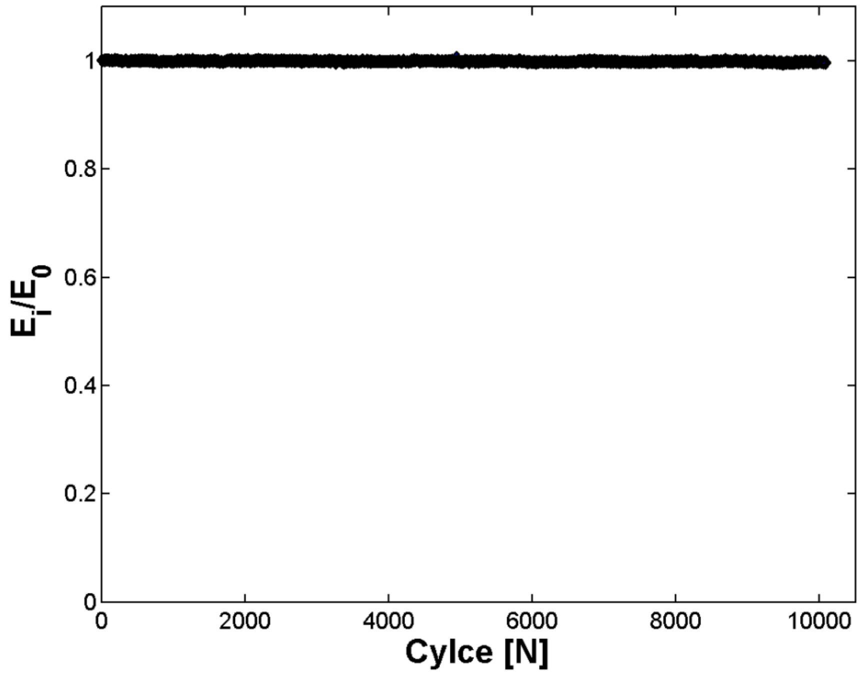

Figure A.37 – Fatigue modulus monitoring of cylinder IL2933.

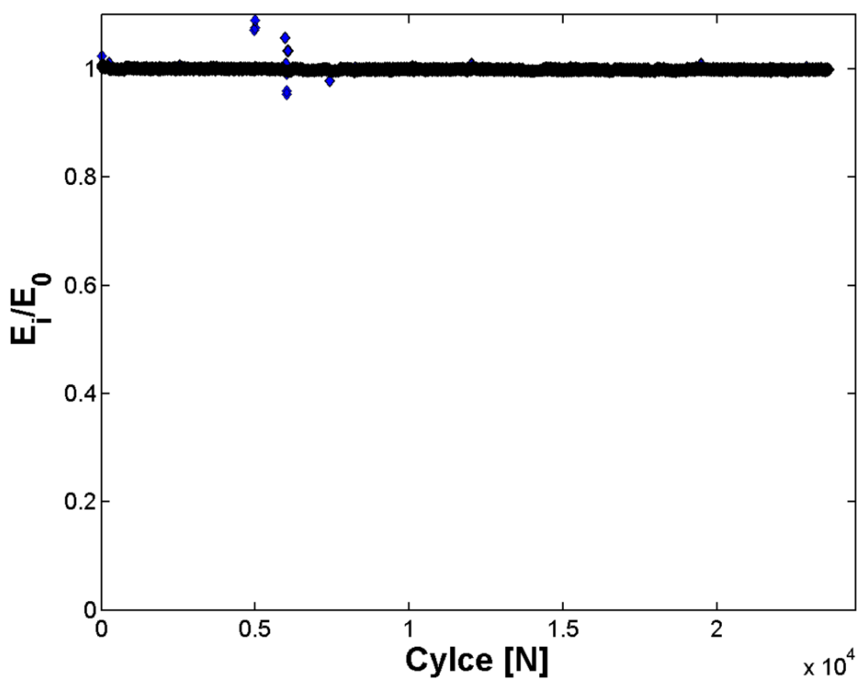

Figure A.38 – Fatigue modulus monitoring of cylinder OK85342.

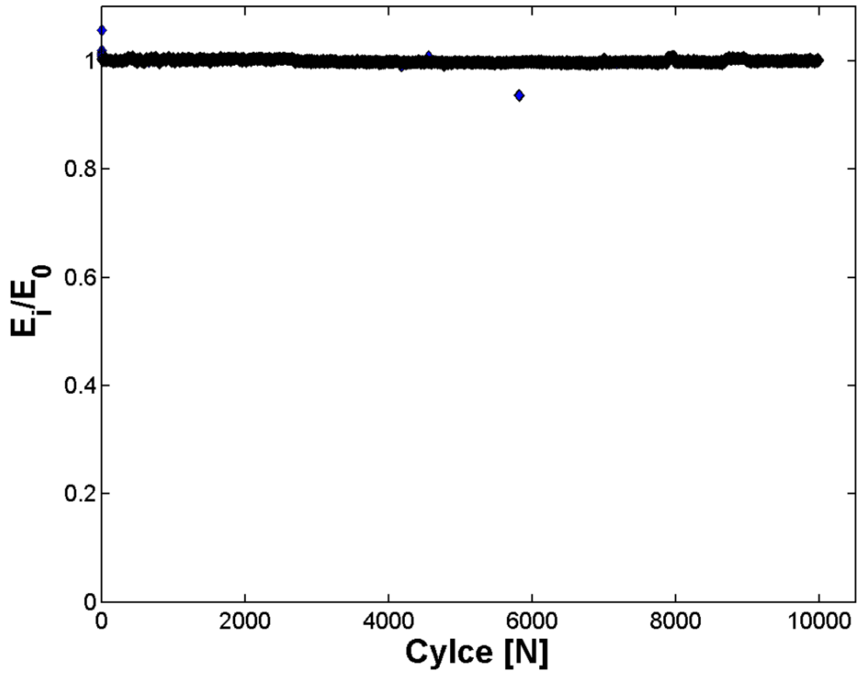

Figure A.39 – Fatigue modulus monitoring of cylinder ON3077.

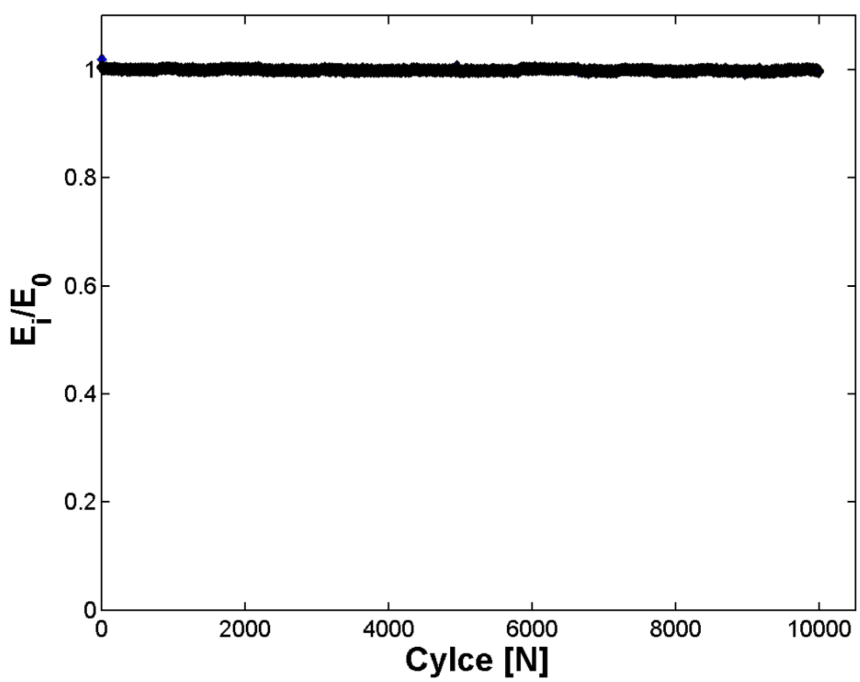

Figure A.40 – Fatigue modulus monitoring of cylinder ON3146.

9. Appendix B – EOL burst photos

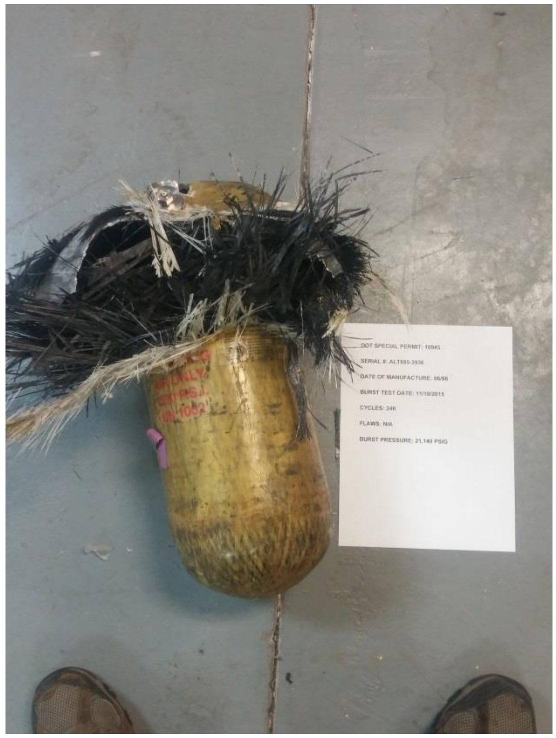

Figure B.1 – EOL burst photo of ALT604-3936.

Figure B.2 – EOL burst photo of ALT604-5155.

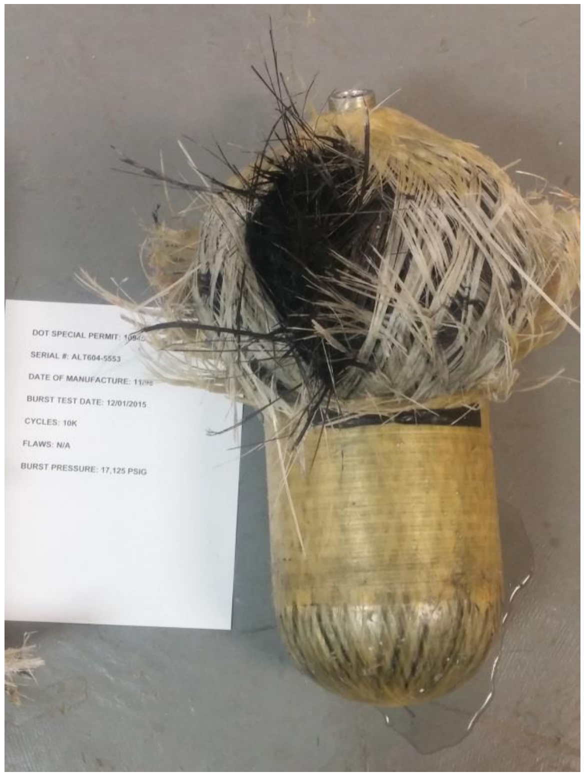

Figure B.3 – EOL burst photo of ALT604-5553.

Figure B.4 – EOL burst photo of ALT604-5561.

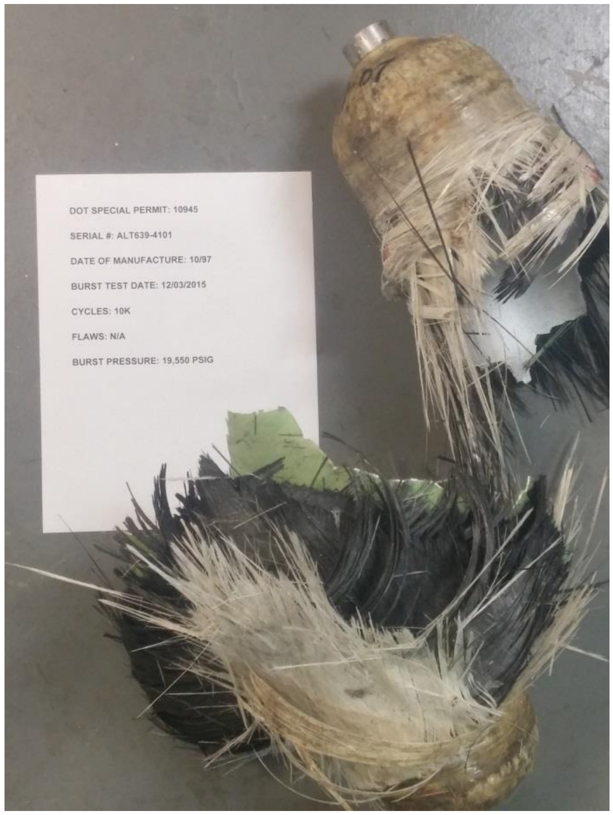

Figure B.5 – EOL burst photo of ALT639-4101.

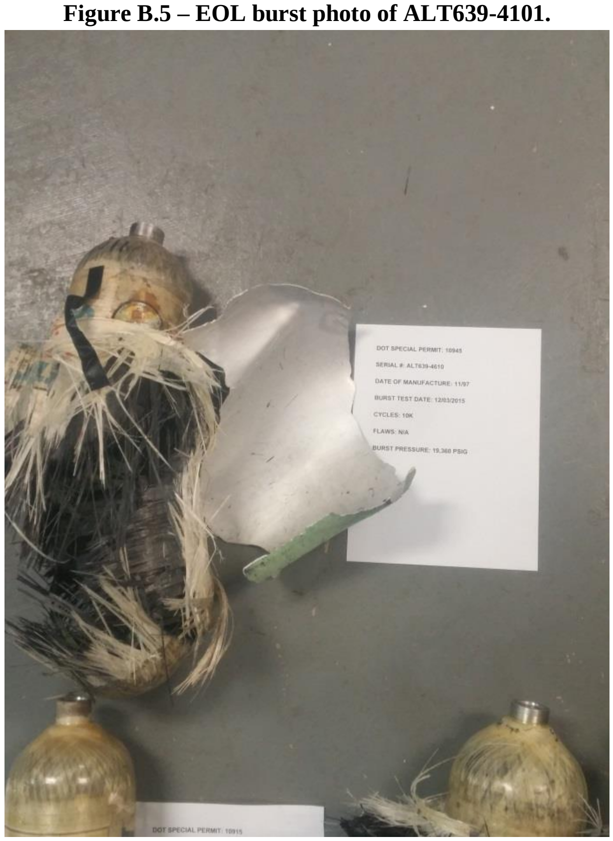

Figure B.6 – EOL burst photo of ALT639-4610.

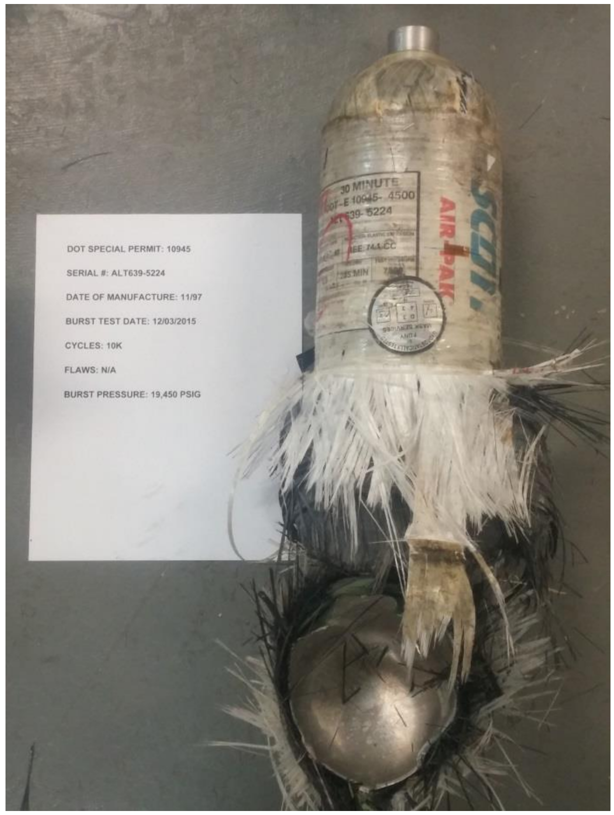

Figure B.7 – EOL burst photo of ALT639-5224.

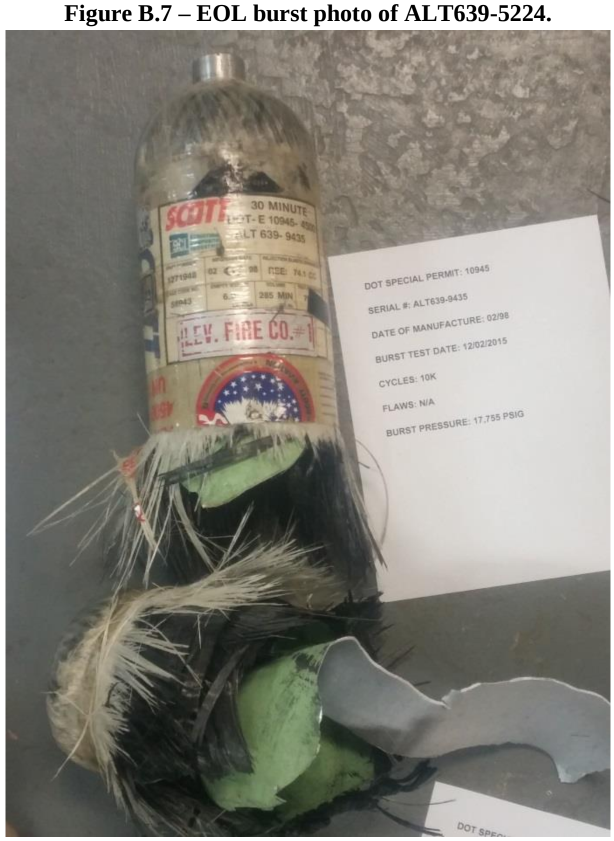

Figure B.8 – EOL burst photo of ALT639-9435.

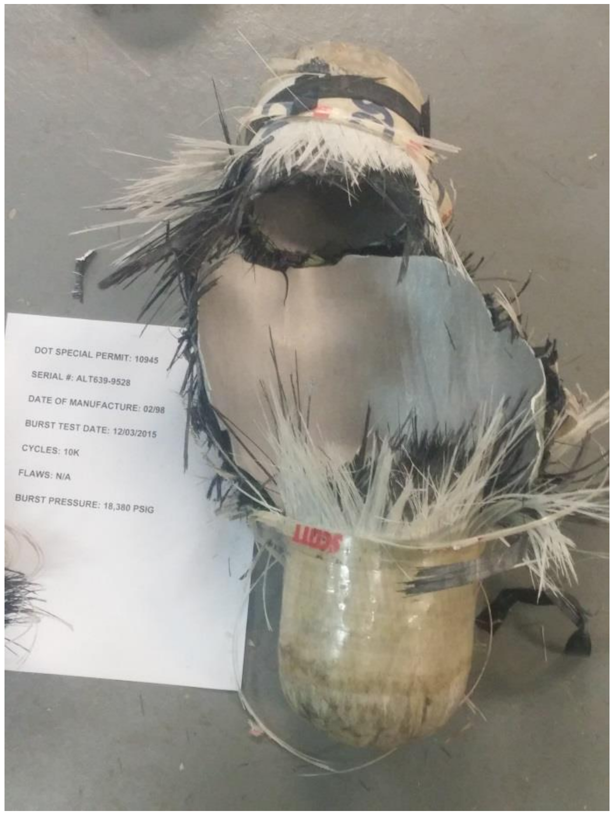

Figure B.9 – EOL burst photo of ALT639-9528.

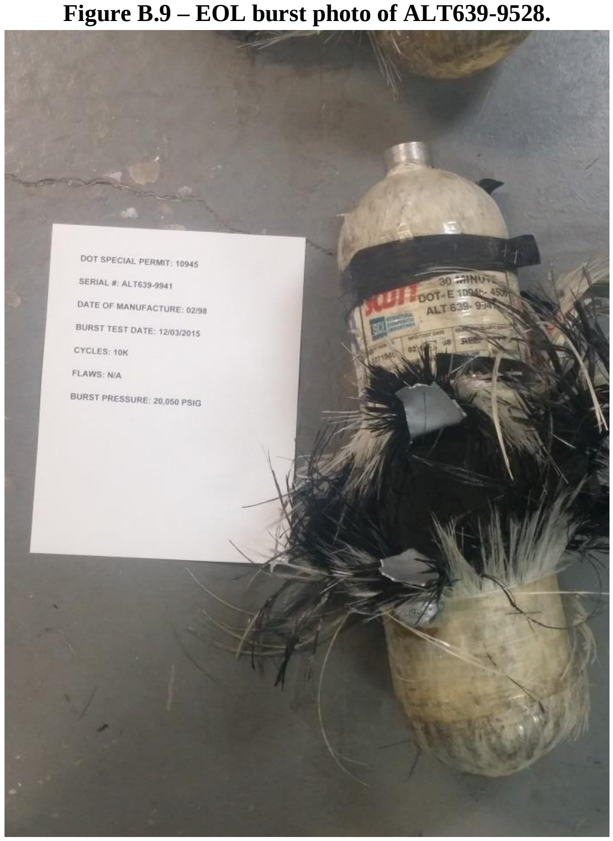

Figure B.10 – EOL burst photo of ALT639-9941.

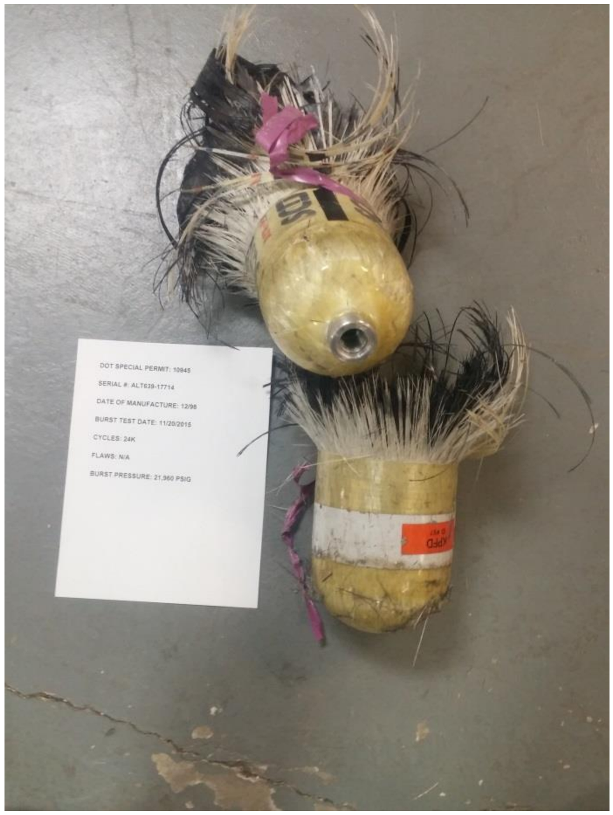

Figure B.11 – EOL burst photo of ALT639-17714.

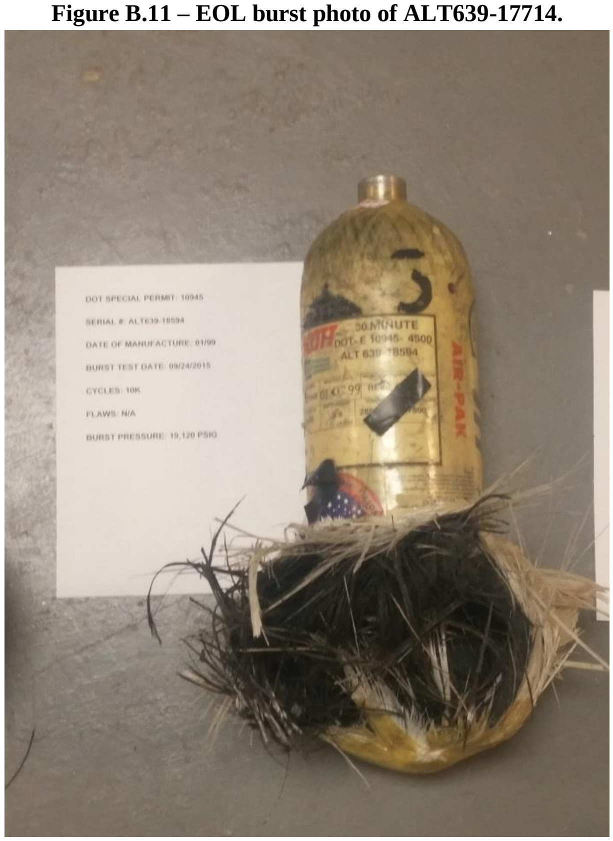

Figure B.12 – EOL burst photo of ALT639-18594.

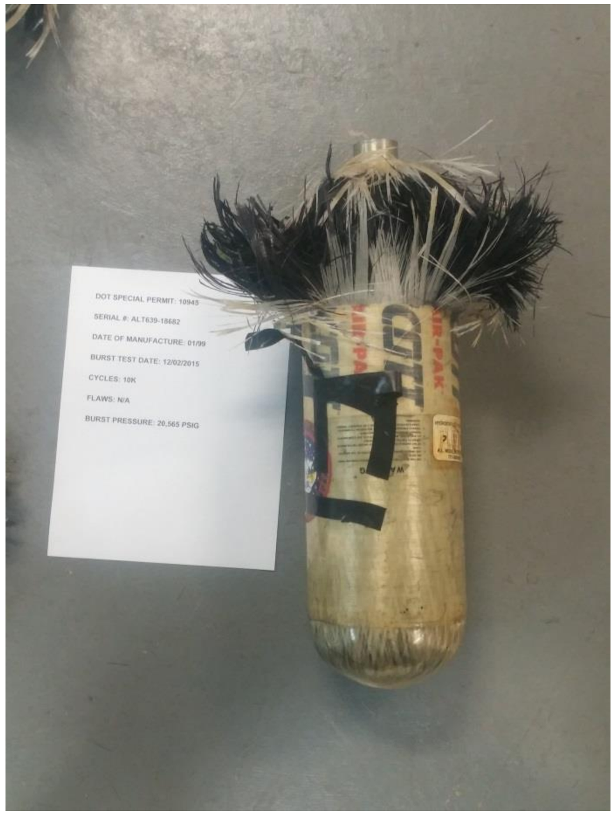

Figure B.13 – EOL burst photo of ALT639-18682.

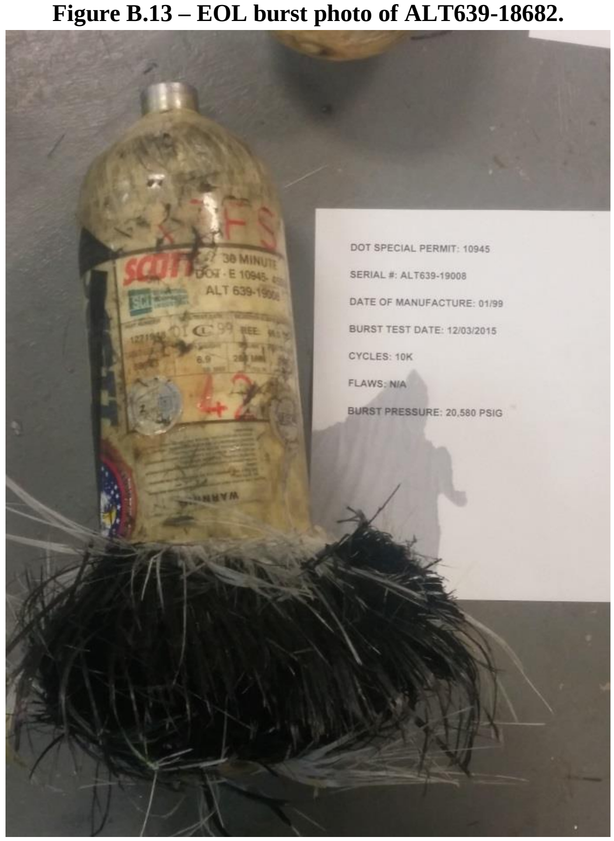

Figure B.14 – EOL burst photo of ALT639-19008.

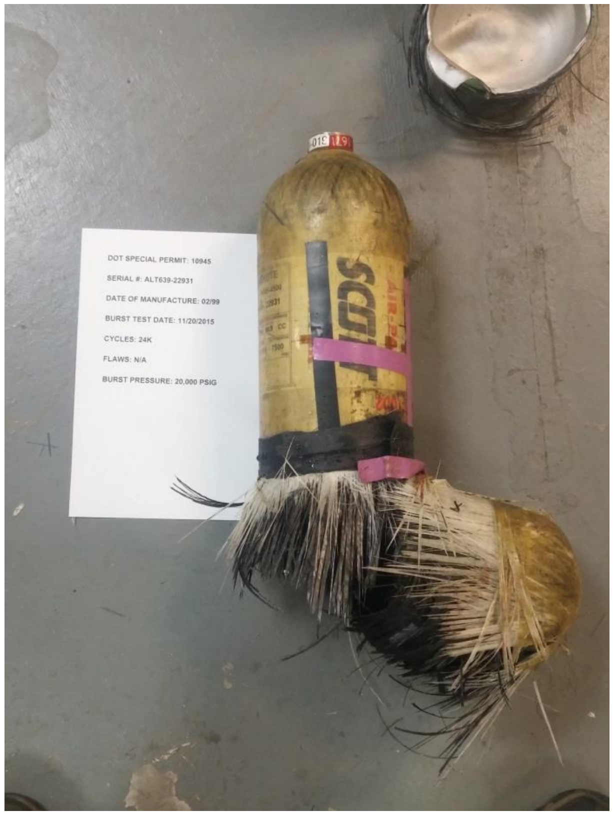

Figure B.15 – EOL burst photo of ALT639-22931.

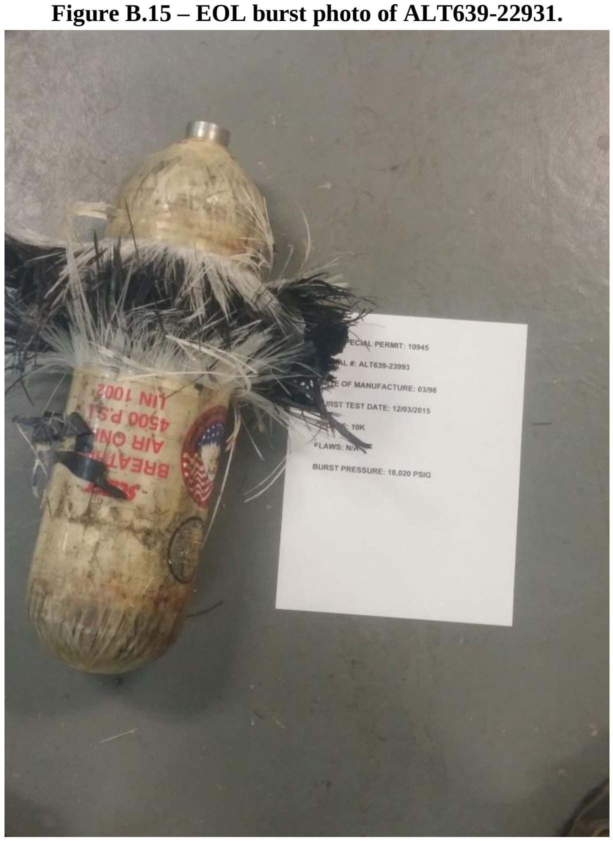

Figure B.16 – EOL burst photo of ALT639-23993.

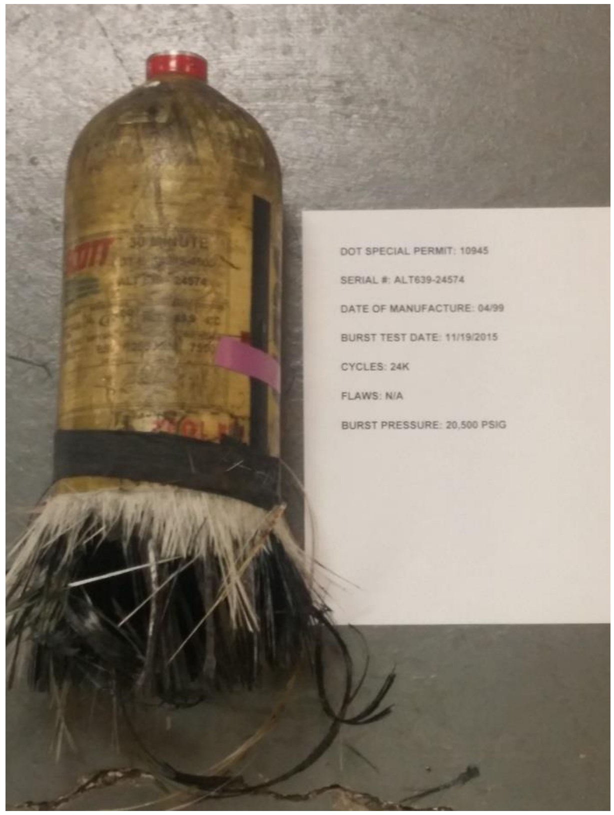

Figure B.17 – EOL burst photo of ALT639-24574.

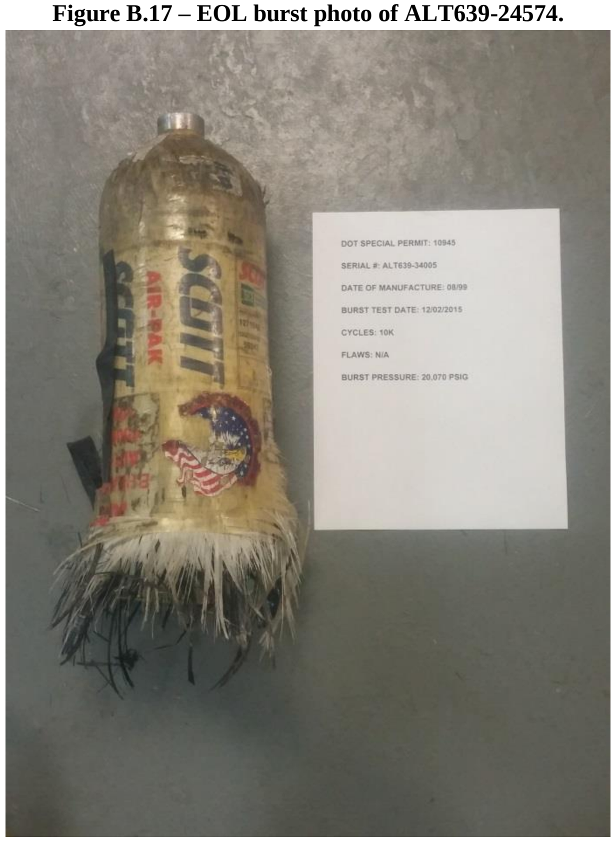

Figure B.18 – EOL burst photo of ALT639-34005.

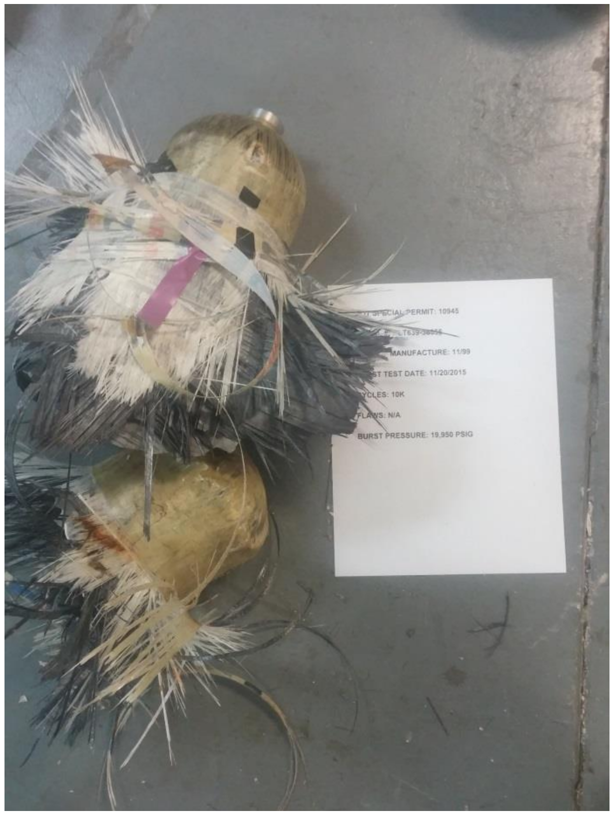

Figure B.19 – EOL burst photo of ALT639-38566.

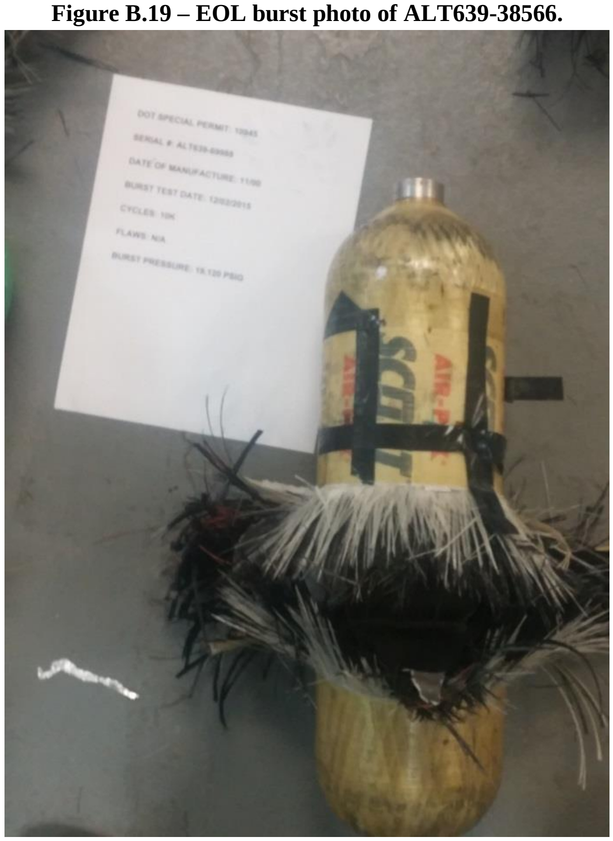

Figure B.20 – EOL burst photo of ALT639-69988.

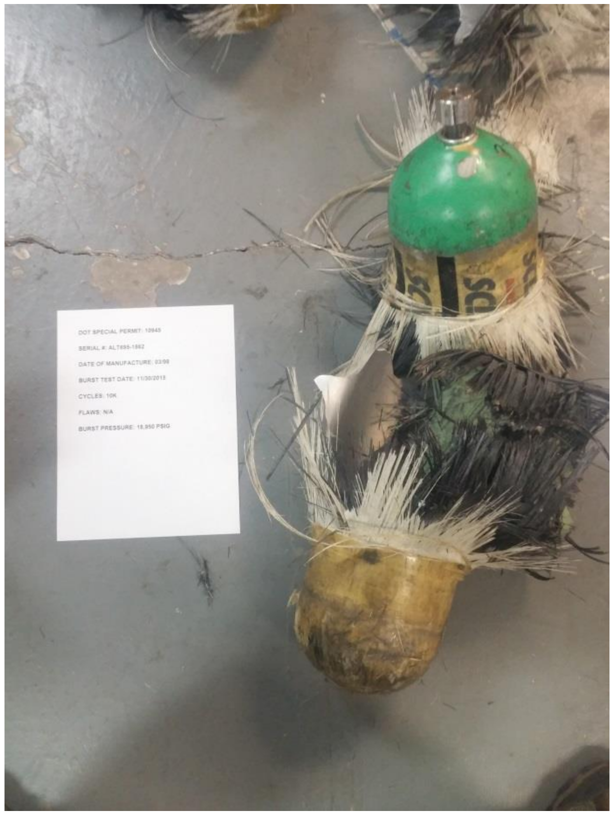

Figure B.21 – EOL burst photo of ALT695-1862.

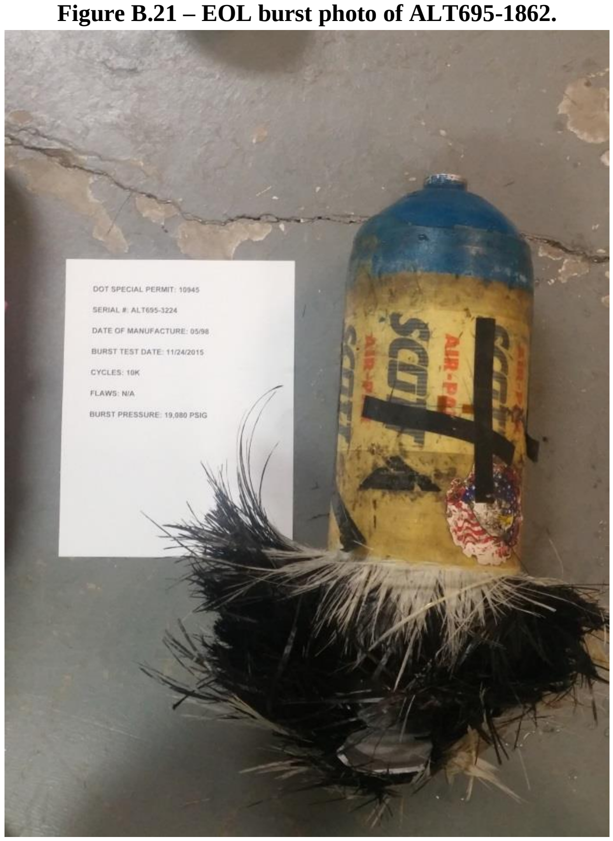

Figure B.22 – EOL burst photo of ALT695-3224.

Figure B.23 – EOL burst photo of ALT695-3313.

Figure B.24 – EOL burst photo of ALT695-3575.

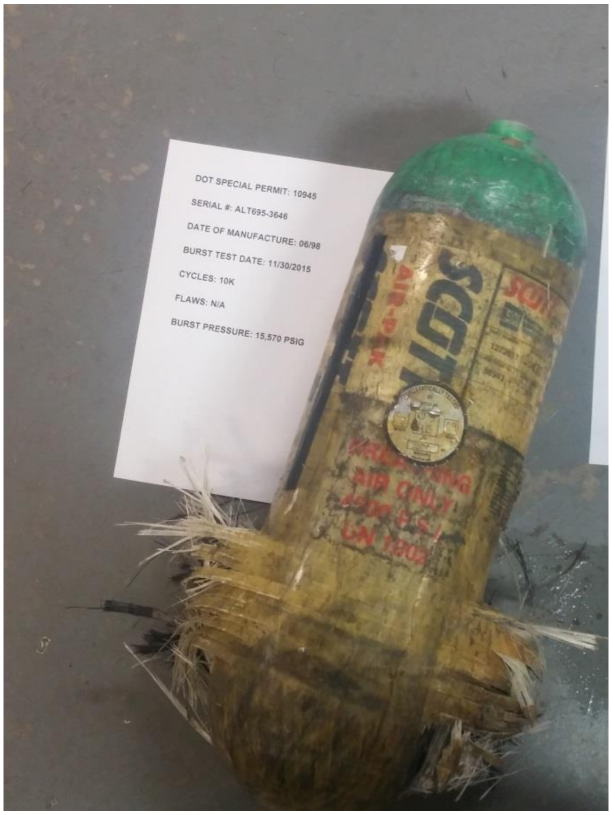

Figure B.25 – EOL burst photo of ALT695-3646.

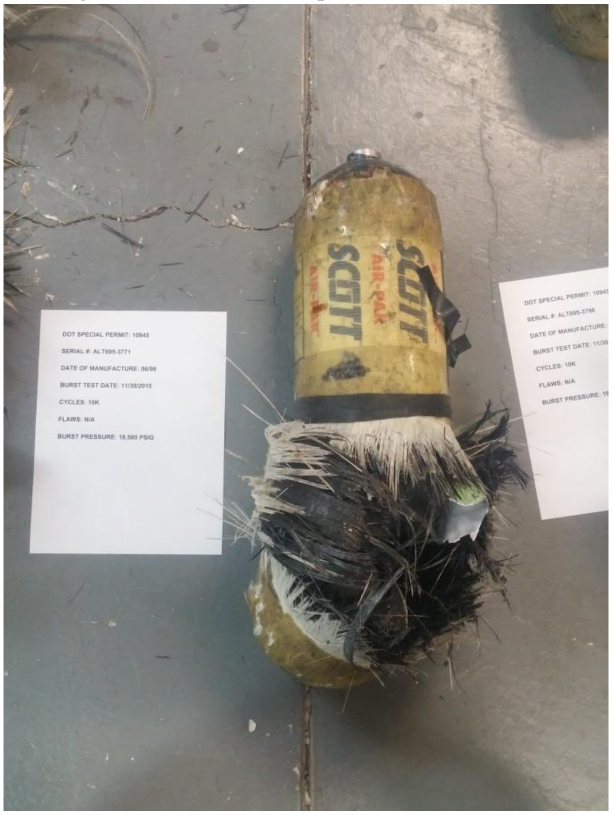

Figure B.26 – EOL burst photo of ALT695-3771.

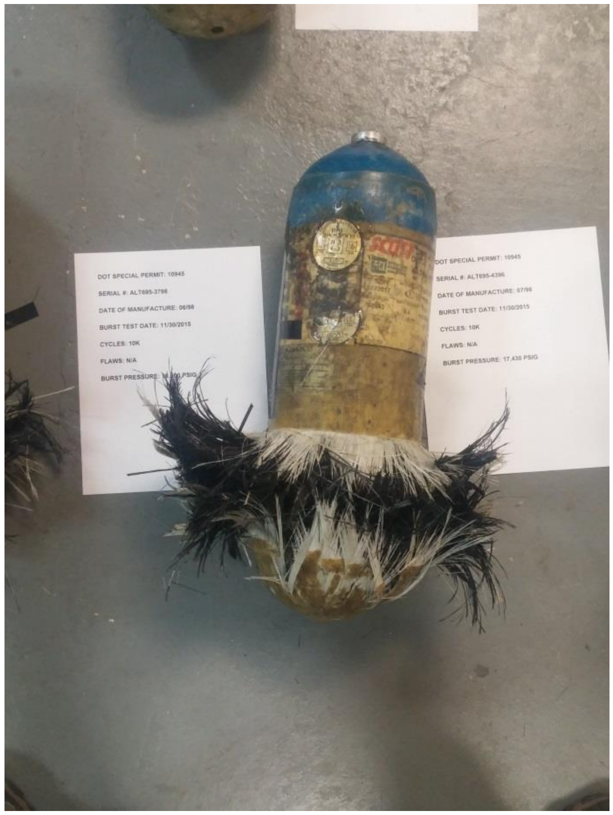

Figure B.27 – EOL burst photo of ALT695-3798.

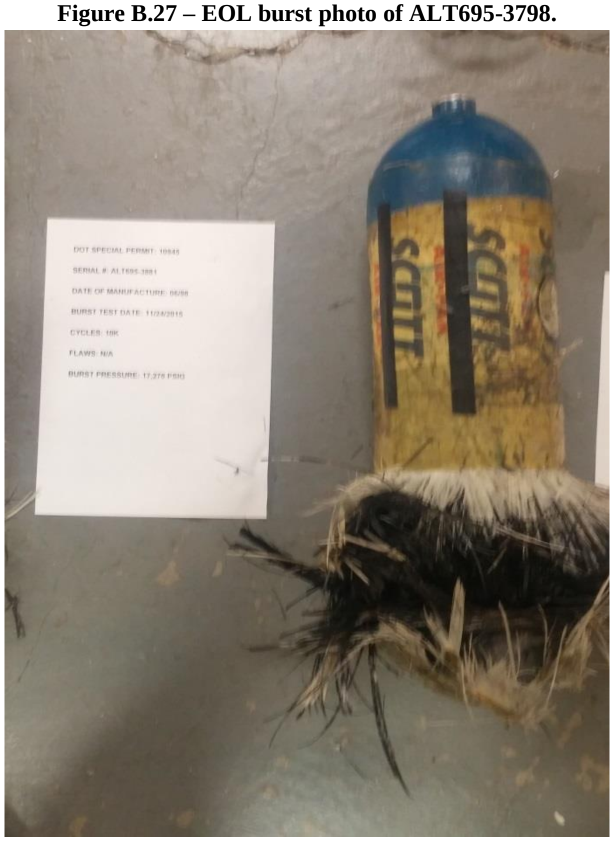

Figure B.28 – EOL burst photo of ALT695-3881.

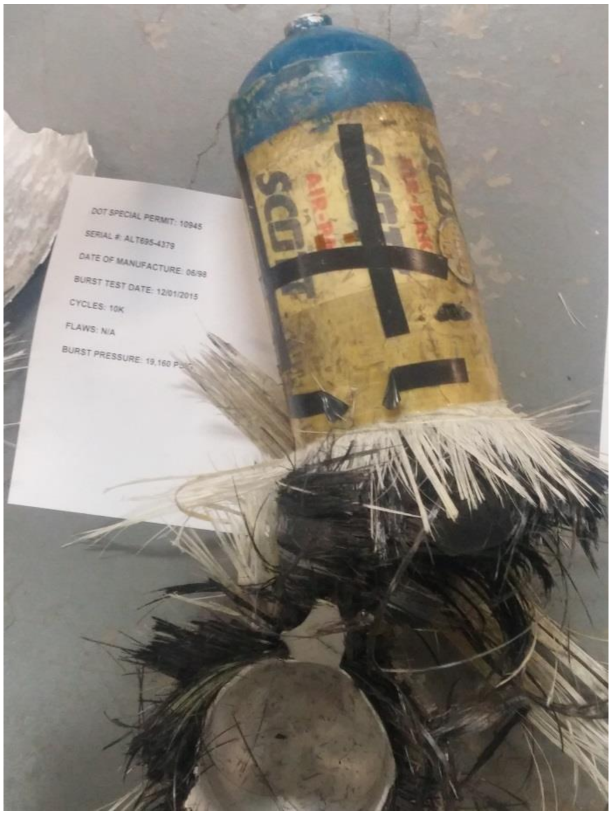

Figure B.29 – EOL burst photo of ALT695-4379.

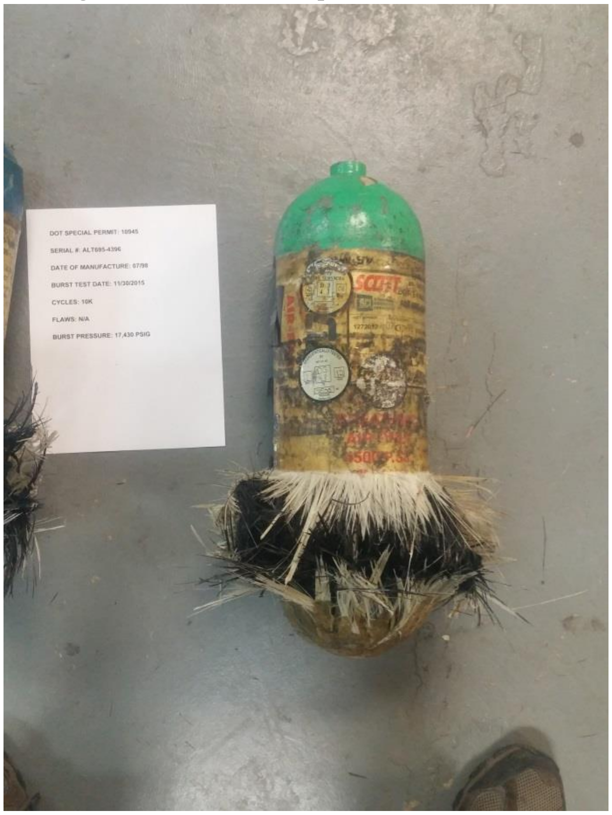

Figure B.30 – EOL burst photo of ALT695-4396.

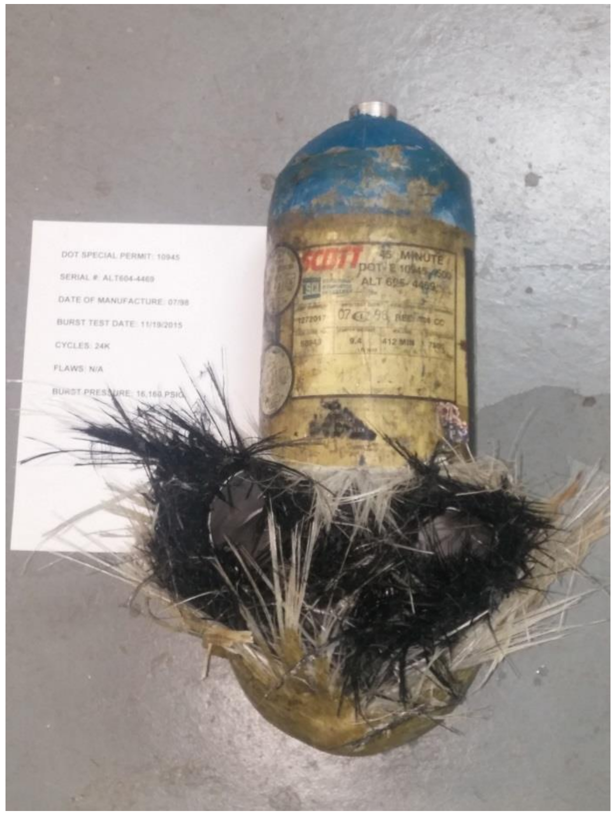

Figure B.31 – EOL burst photo of ALT695-4469.

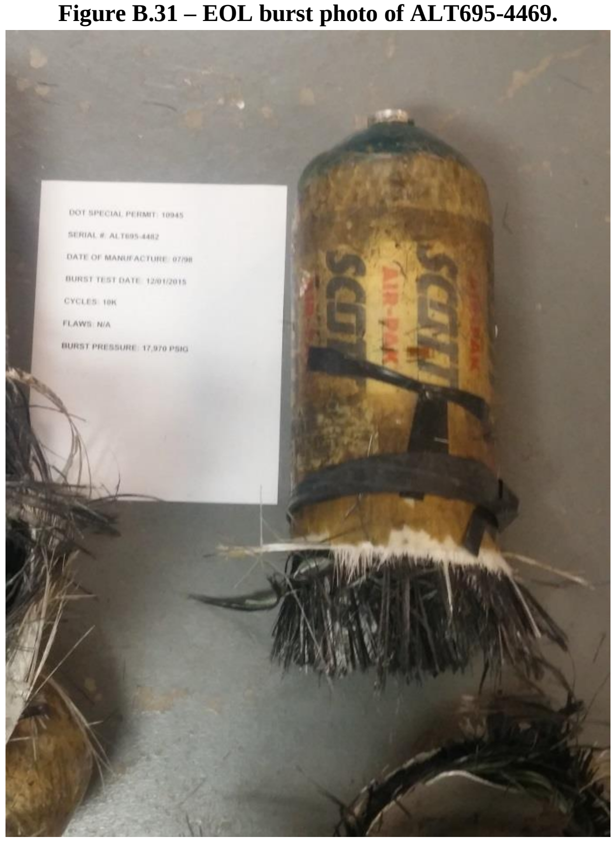

Figure B.32 – EOL burst photo of ALT695-4482.

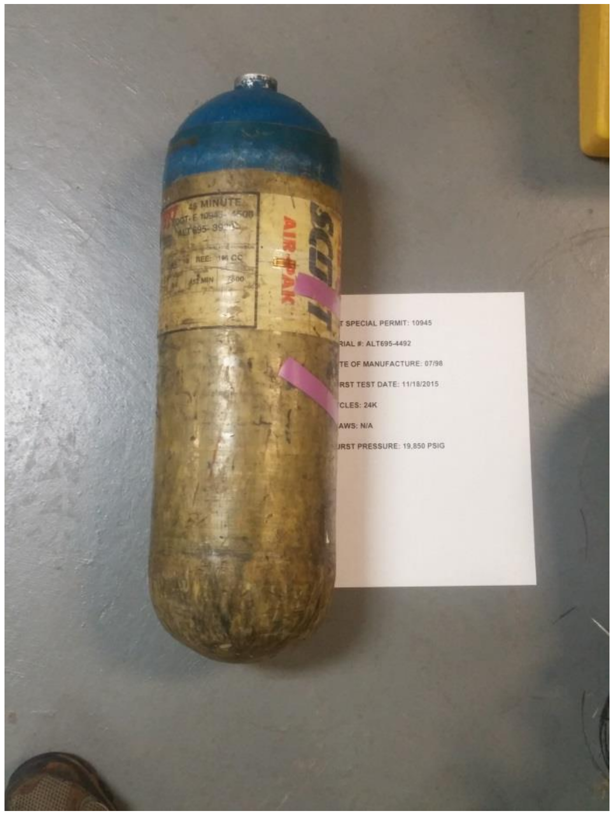

Figure B.33 – EOL burst photo of ALT695-4492.

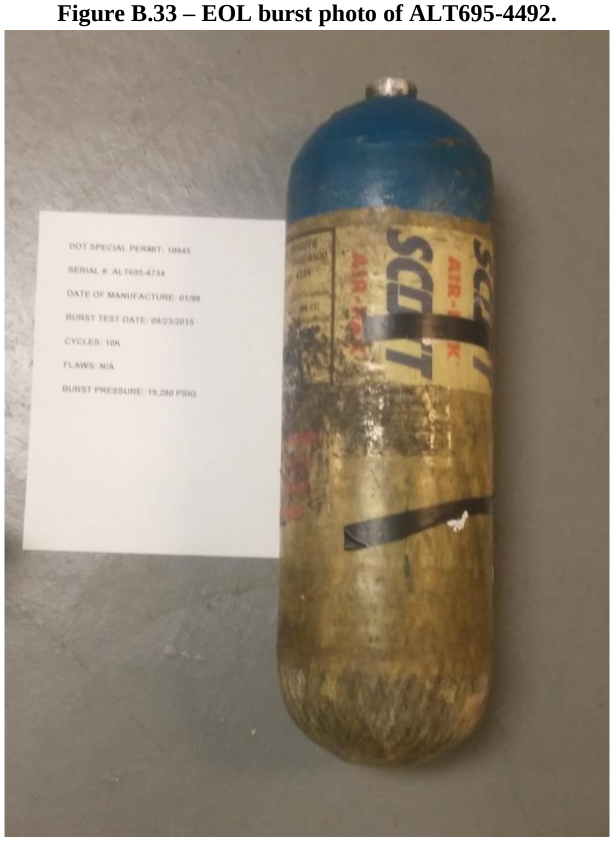

Figure B.34 – EOL burst photo of ALT695-4734.

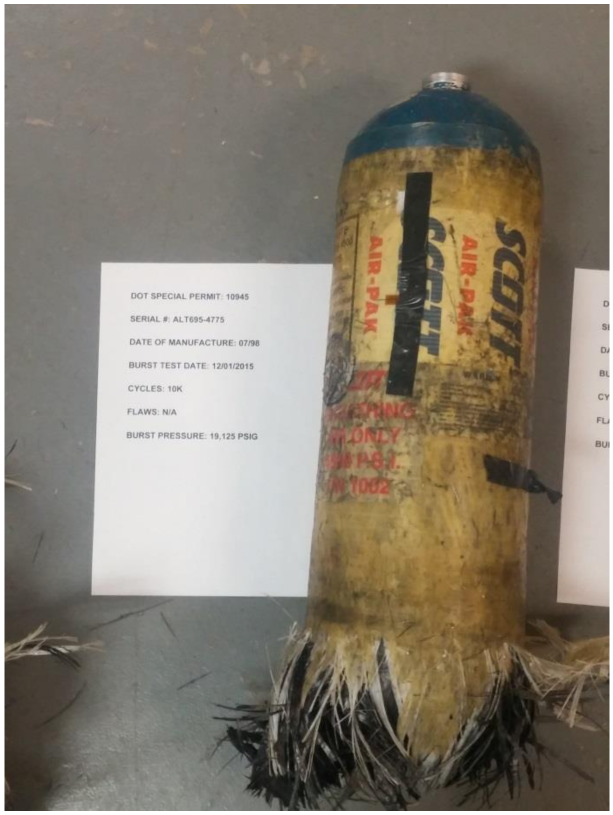

Figure B.35 – EOL burst photo of ALT695-4775.

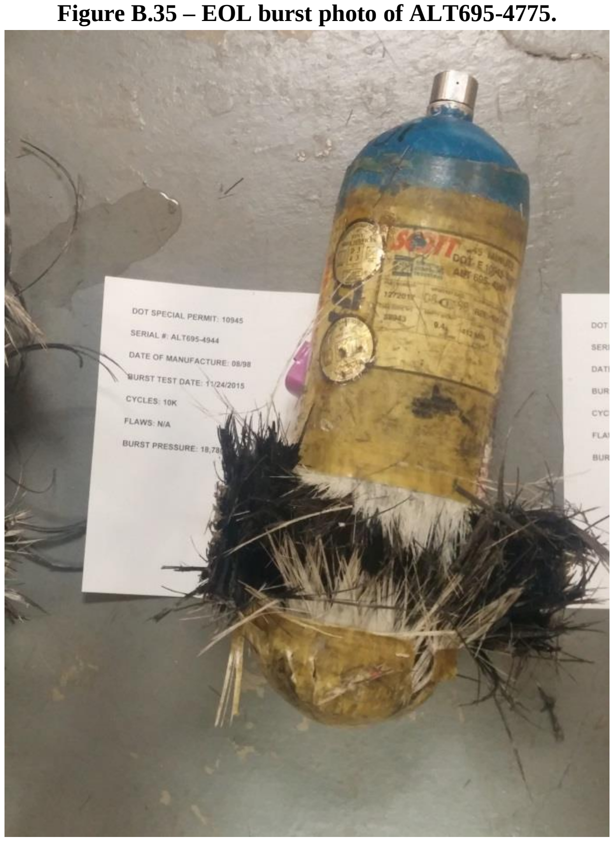

Figure B.36 – EOL burst photo of ALT695-4944.

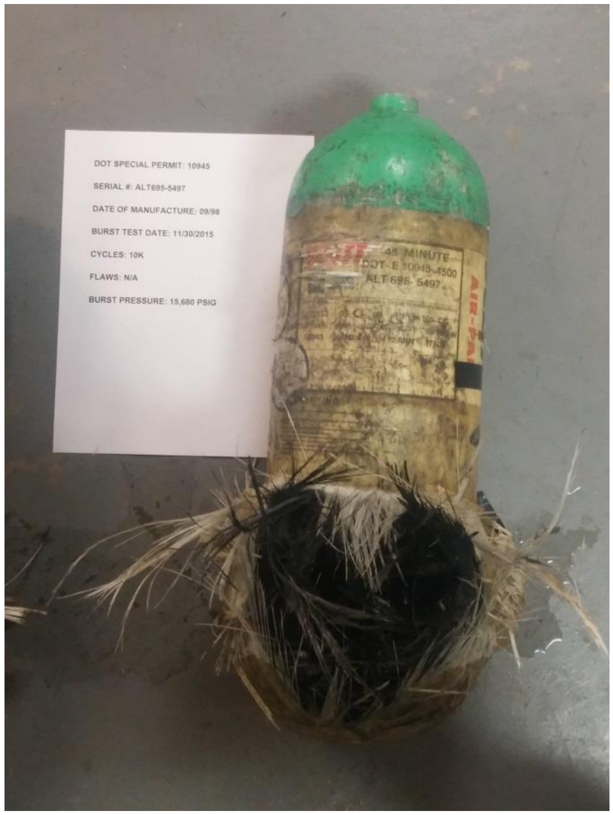

Figure B.37 – EOL burst photo of ALT695-5497.

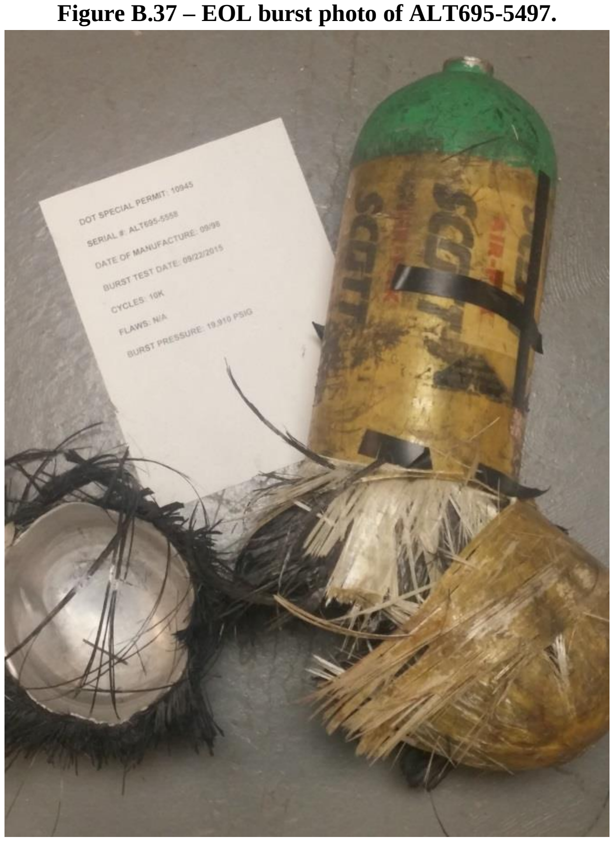

Figure B.38 – EOL burst photo of ALT695-5558.

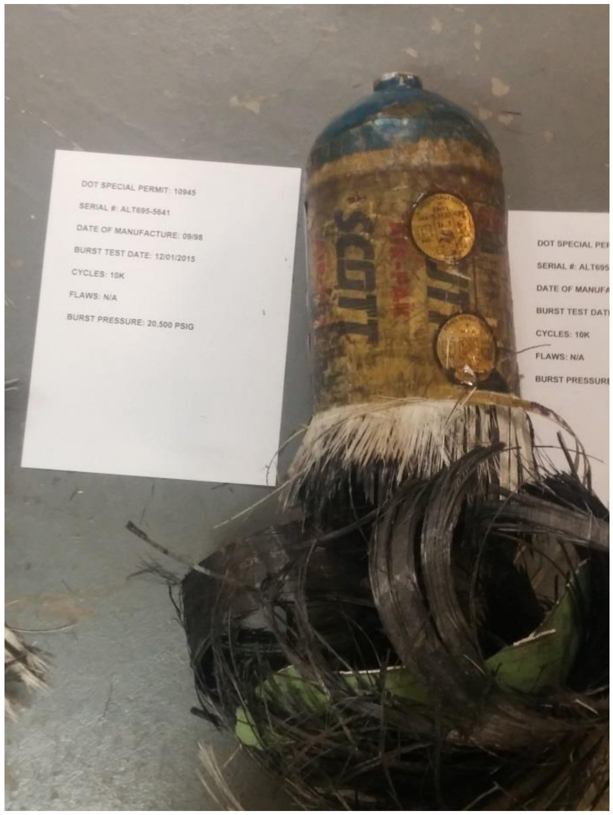

Figure B.39 – EOL burst photo of ALT695-5641.

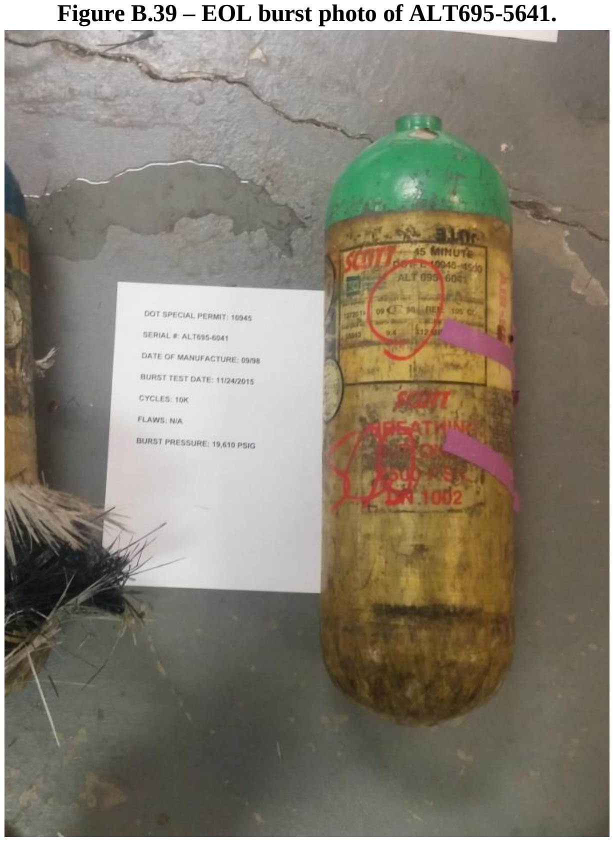

Figure B.40 – EOL burst photo of ALT695-6041.

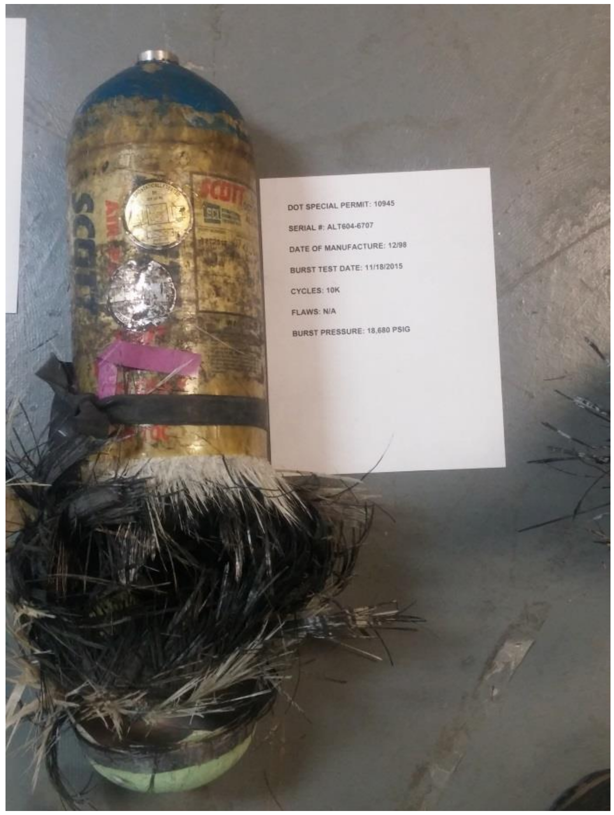

Figure B.41 – EOL burst photo of ALT695-6707.

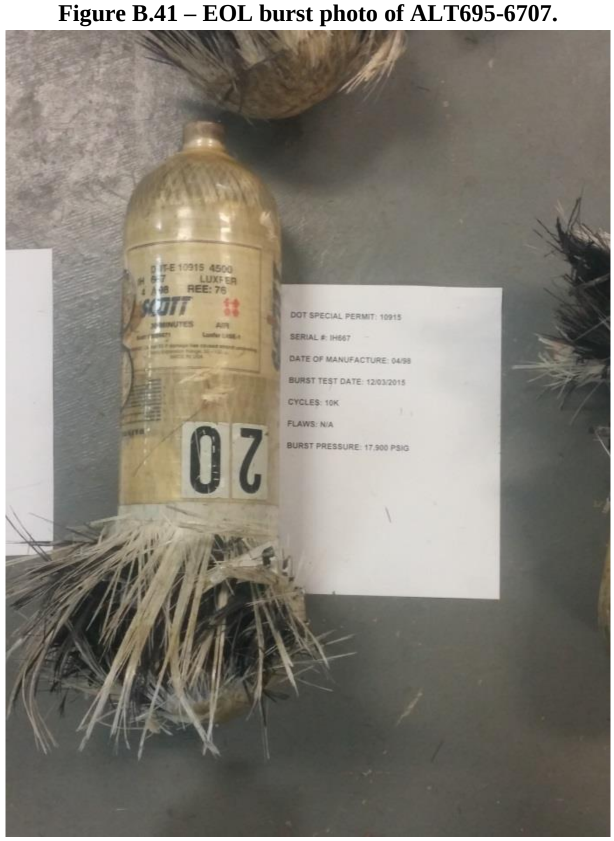

Figure B.42 – EOL burst photo of IH667.

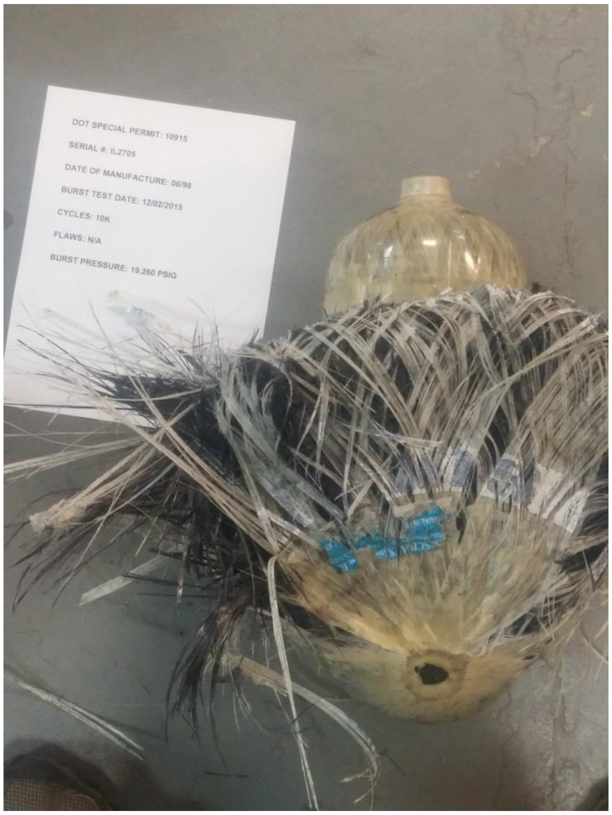

Figure B.43 – EOL burst photo of IL2705.

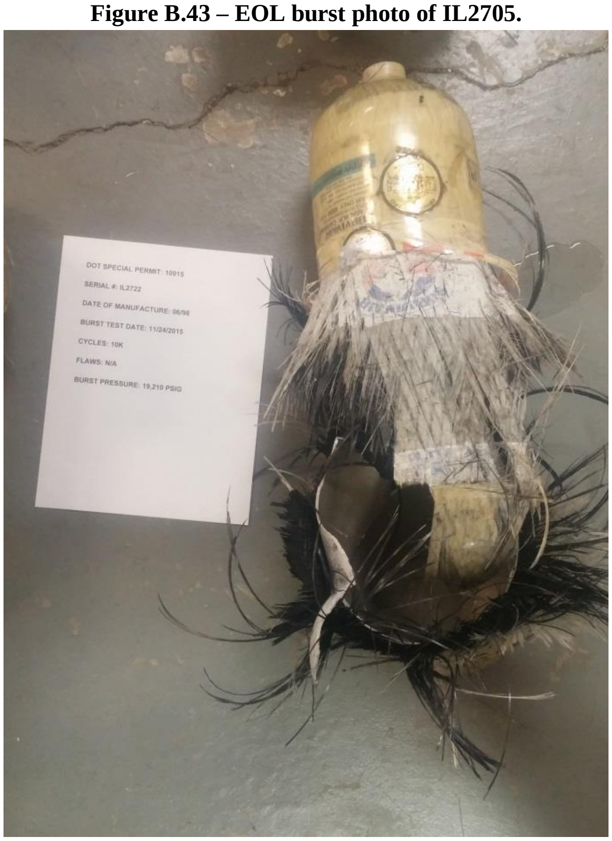

Figure B.44 – EOL burst photo of IL2722.

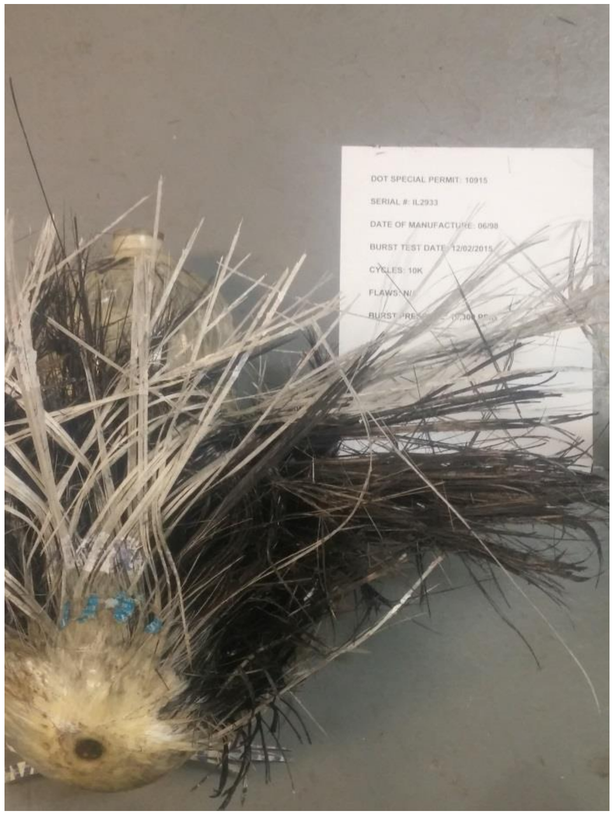

Figure B.45 – EOL burst photo of IL2933.

Figure B.46 – EOL burst photo of IL3334.

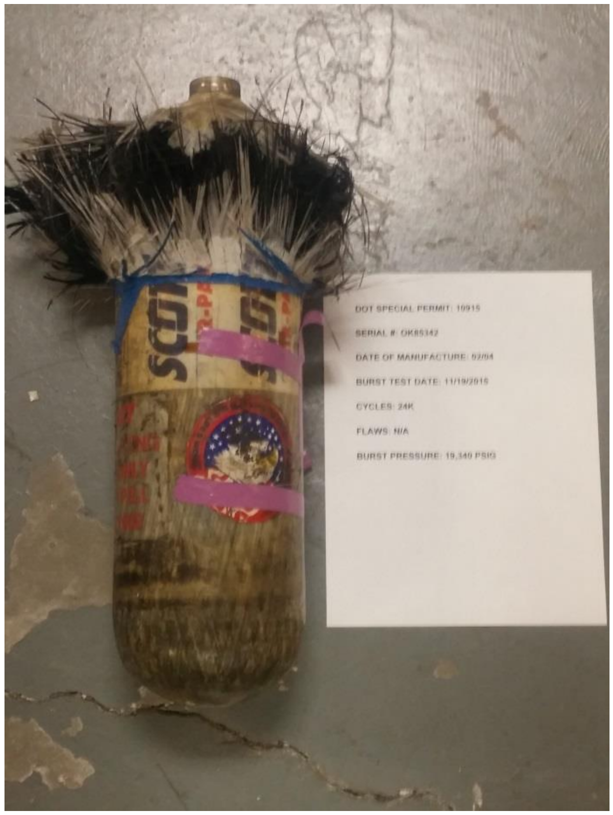

Figure B.47 – EOL burst photo of OK85342.

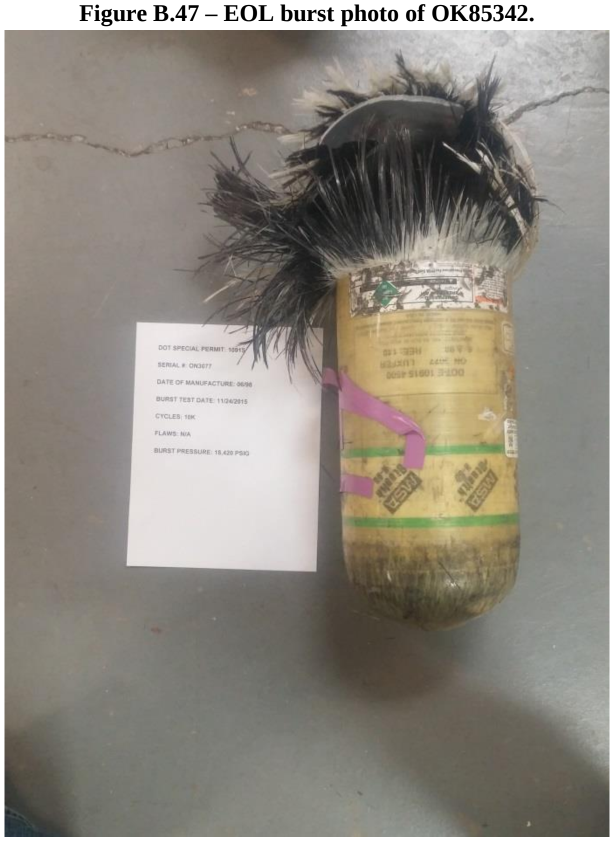

Figure B.48 – EOL burst photo of OM3077.

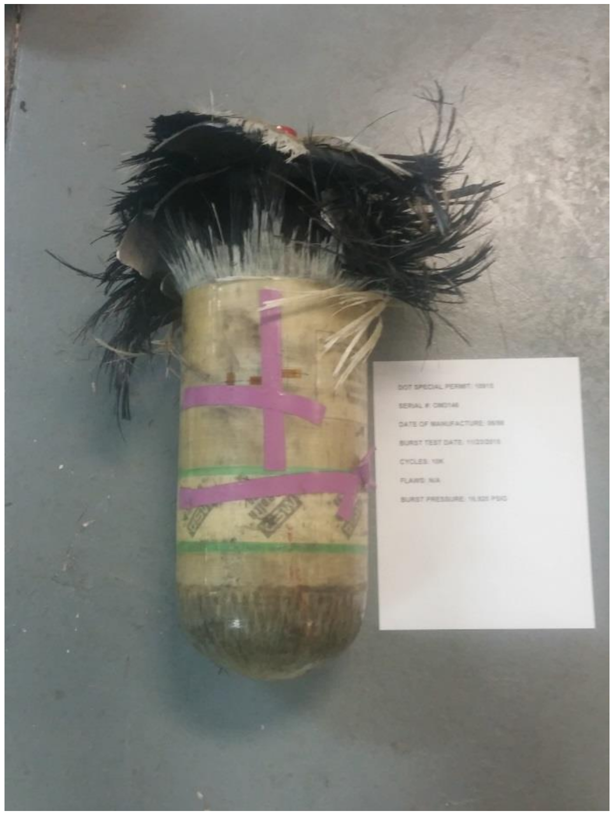

Figure B.49 – EOL burst photo of OM3146.

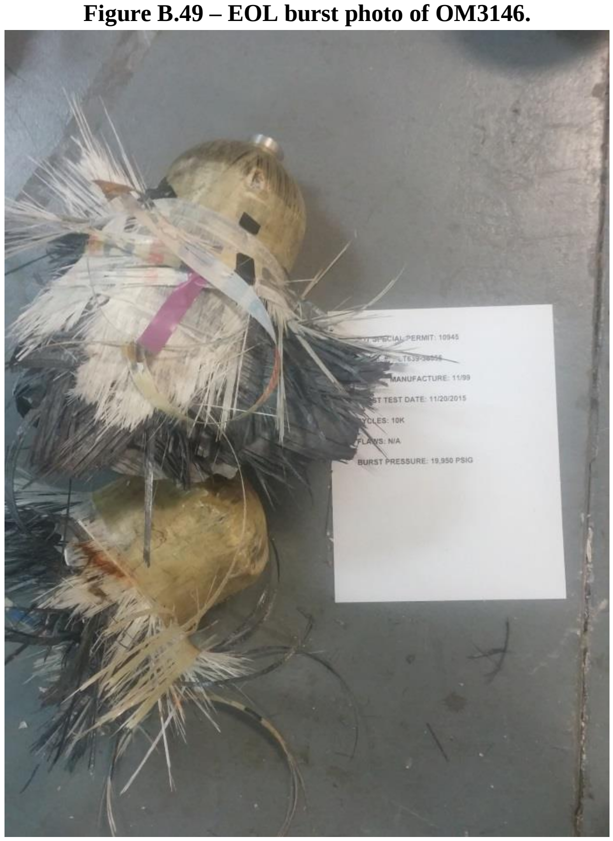

Figure B.50– EOL burst photo of ALT639-40136.

10. Appendix C – Burst stress-strain plots

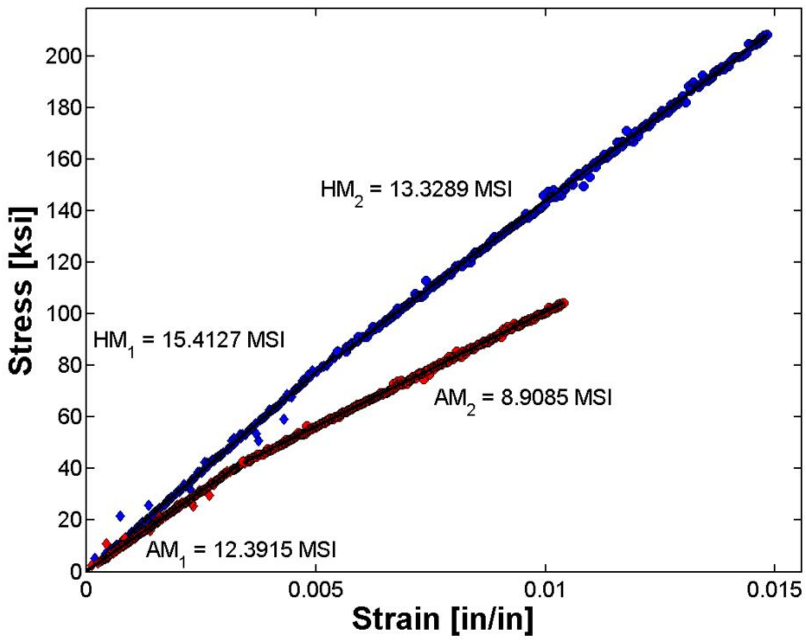

Figure C.1 Principal stress strain response of cylinder ALT604-5155. Note: Blue data points represent hoop response and red data points represent axial response.

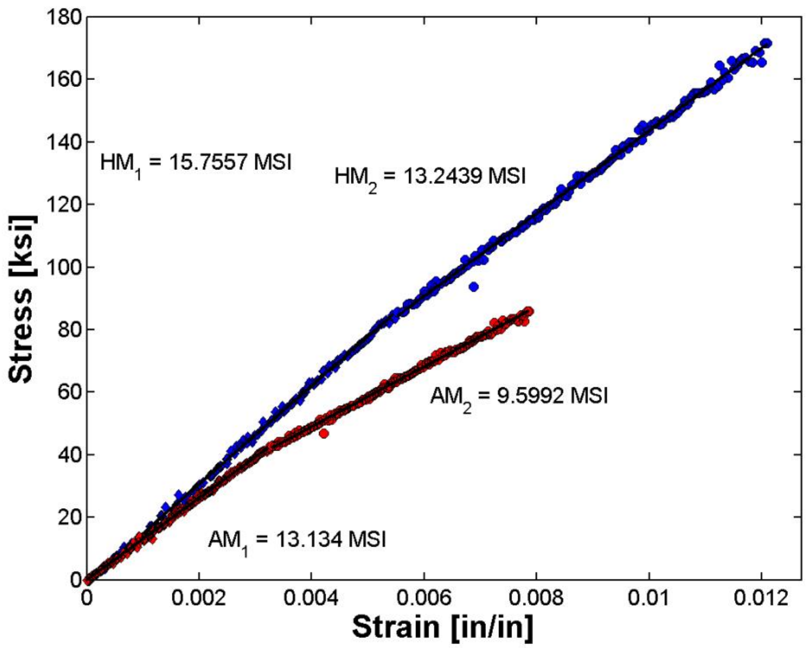

Figure C.2 Principal stress strain response of cylinder ALT604-5553. Note: Blue data points represent hoop response and red data points represent axial response.

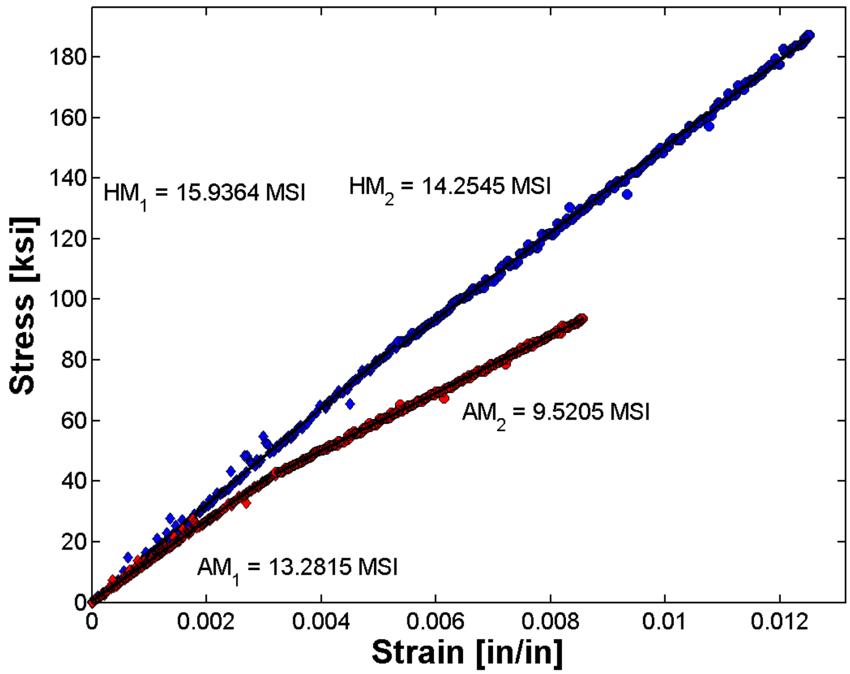

Figure C.3 Principal stress strain response of cylinder ALT604-5561. Note: Blue data points represent hoop response and red data points represent axial response.

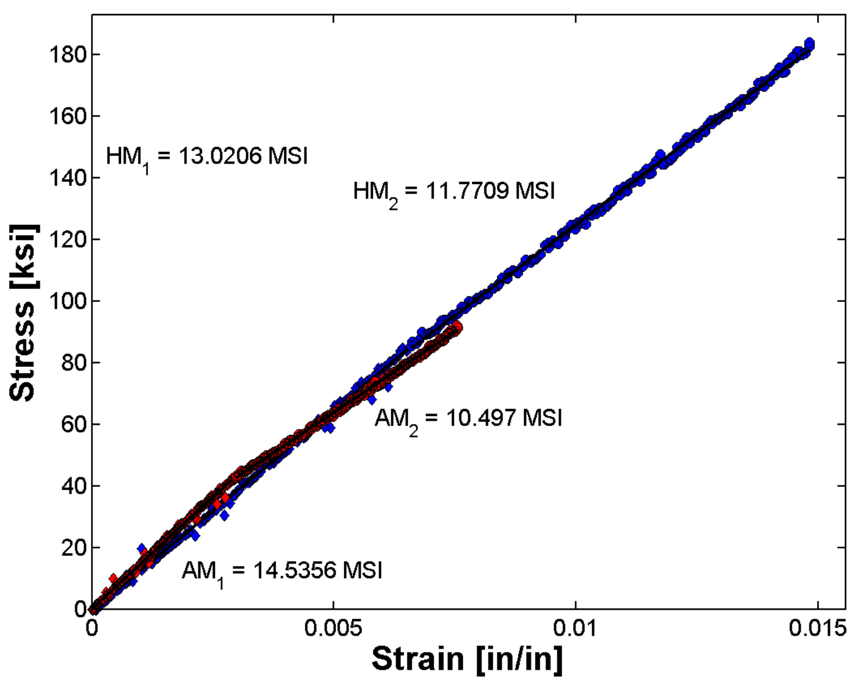

Figure C.4 Principal stress strain response of cylinder ALT604-6707. Note: Blue data points represent hoop response and red data points represent axial response.

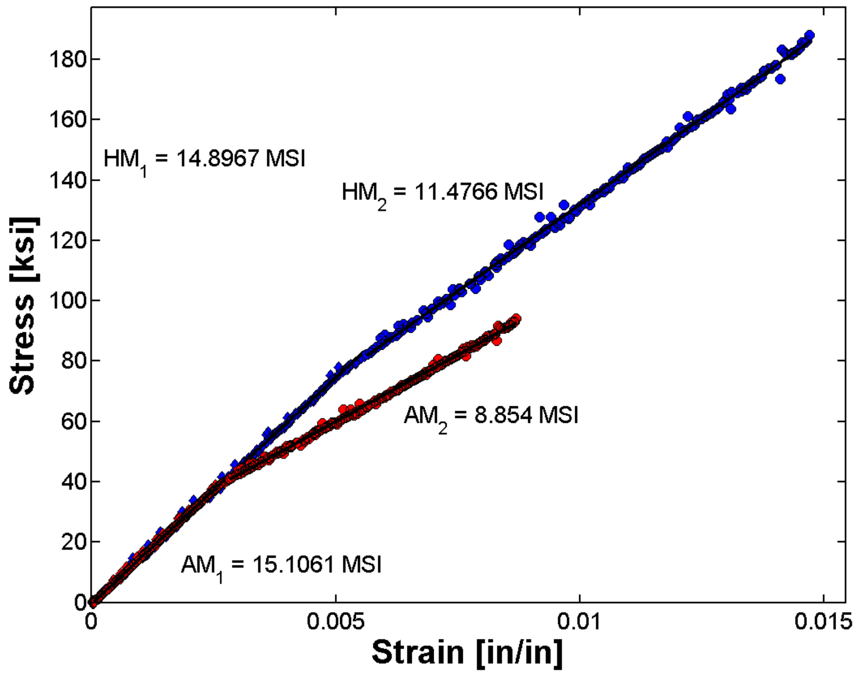

Figure C.5 Principal stress strain response of cylinder ALT639-4101. Note: Blue data points represent hoop response and red data points represent axial response.

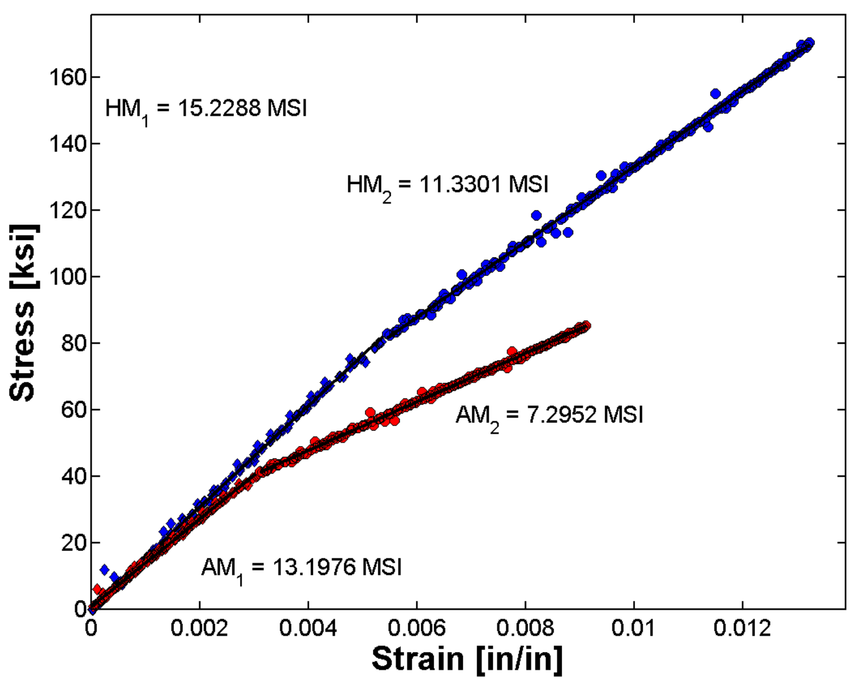

Figure C.6 Principal stress strain response of cylinder ALT639-4610. Note: Blue data points represent hoop response and red data points represent axial response.

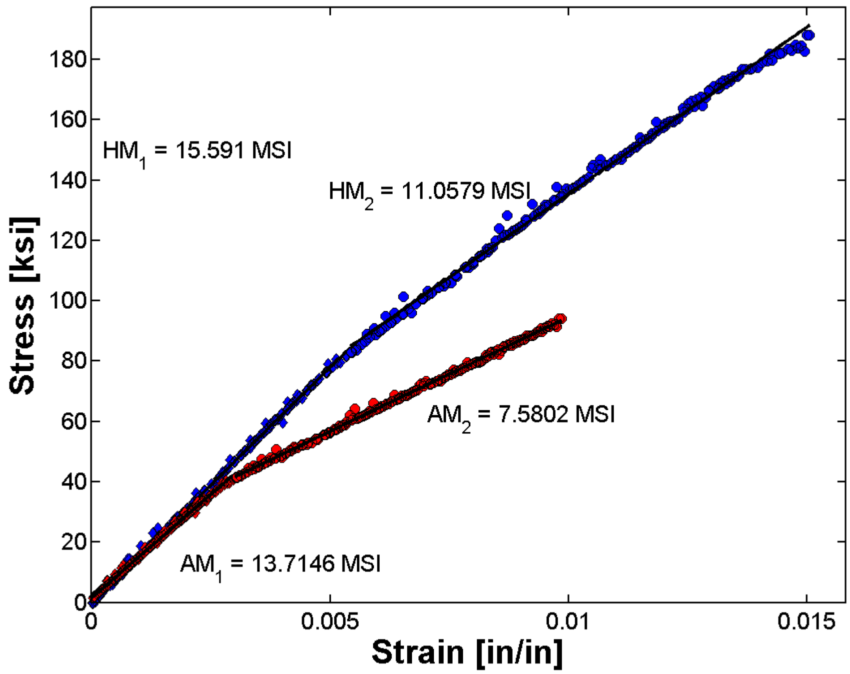

Figure C.7 Principal stress strain response of cylinder ALT639-5224. Note: Blue data points represent hoop response and red data points represent axial response.

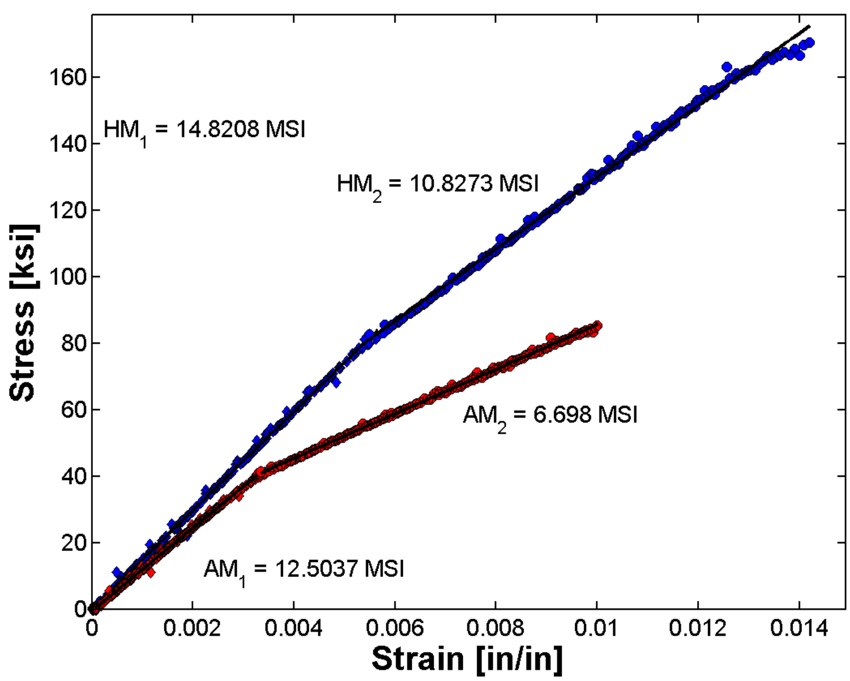

Figure C.8 Principal stress strain response of cylinder ALT639-9435. Note: Blue data points represent hoop response and red data points represent axial response.

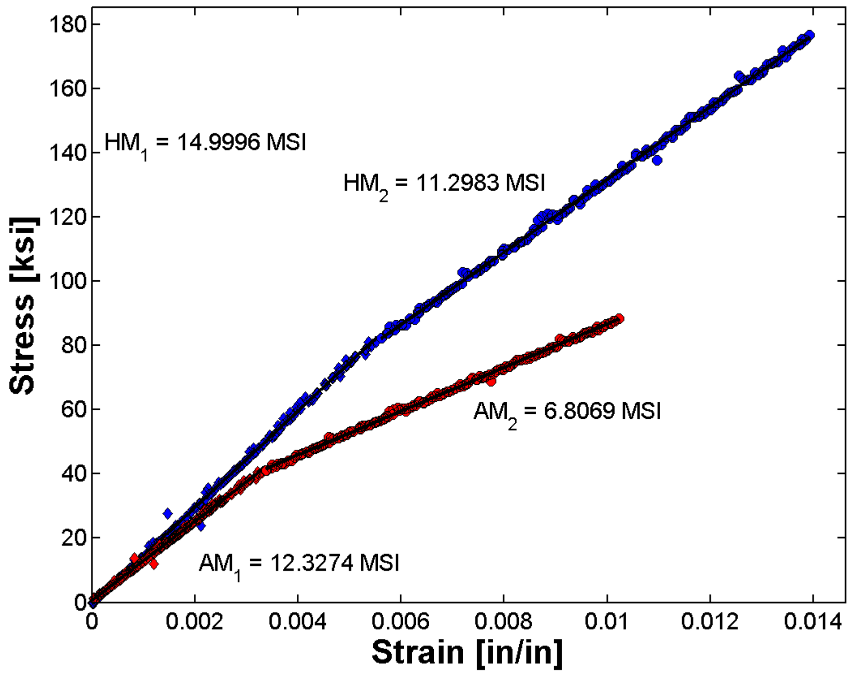

Figure C.9 Principal stress strain response of cylinder ALT639-9528. Note: Blue data points represent hoop response and red data points represent axial response.

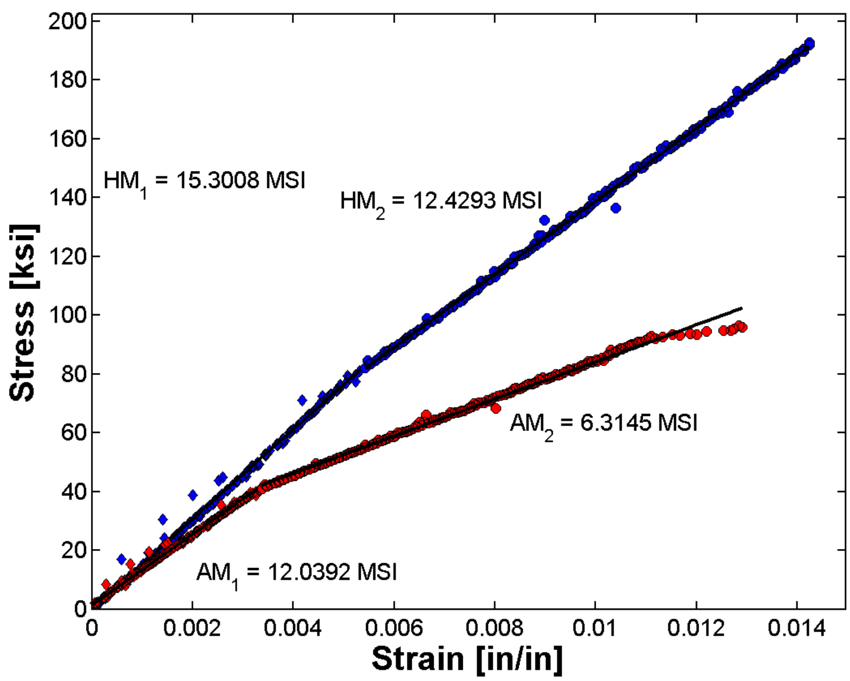

Figure C.10 Principal stress strain response of cylinder ALT639-9941. Note: Blue data points represent hoop response and red data points represent axial response.

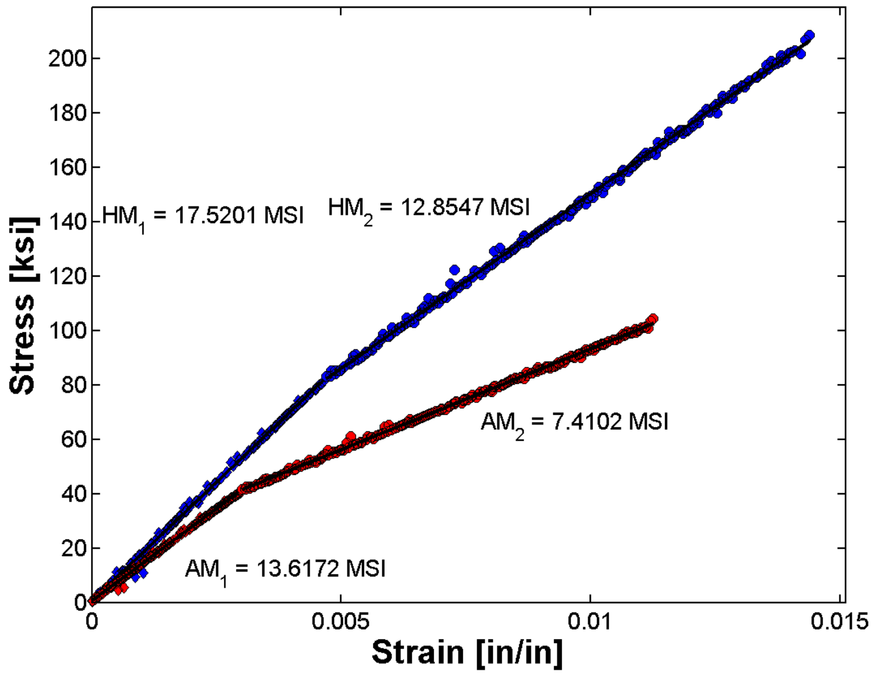

Figure C.11 Principal stress strain response of cylinder ALT639-17714. Note: Blue data points represent hoop response and red data points represent axial response.

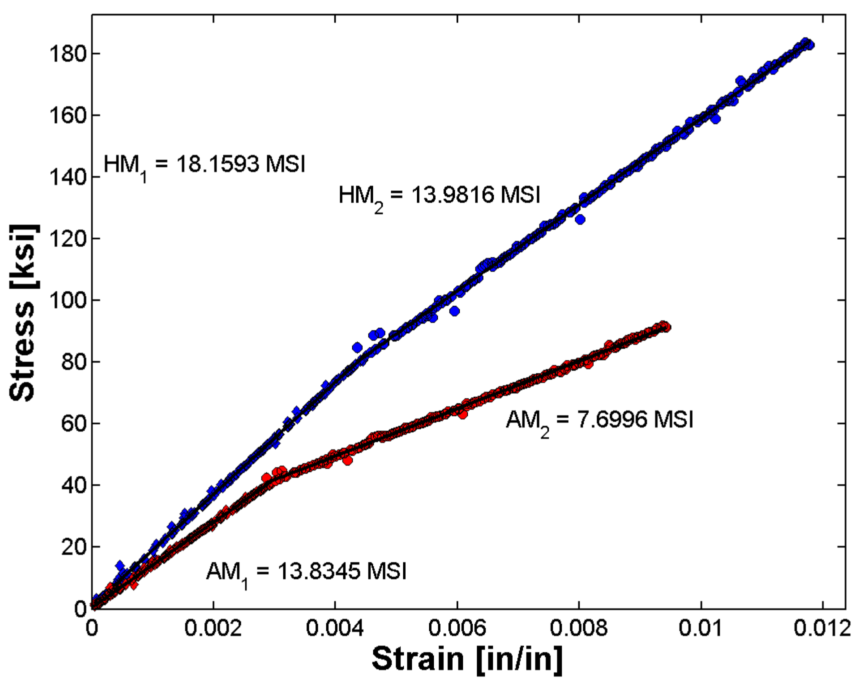

Figure C.12 Principal stress strain response of cylinder ALT639-18594. Note: Blue data points represent hoop response and red data points represent axial response.

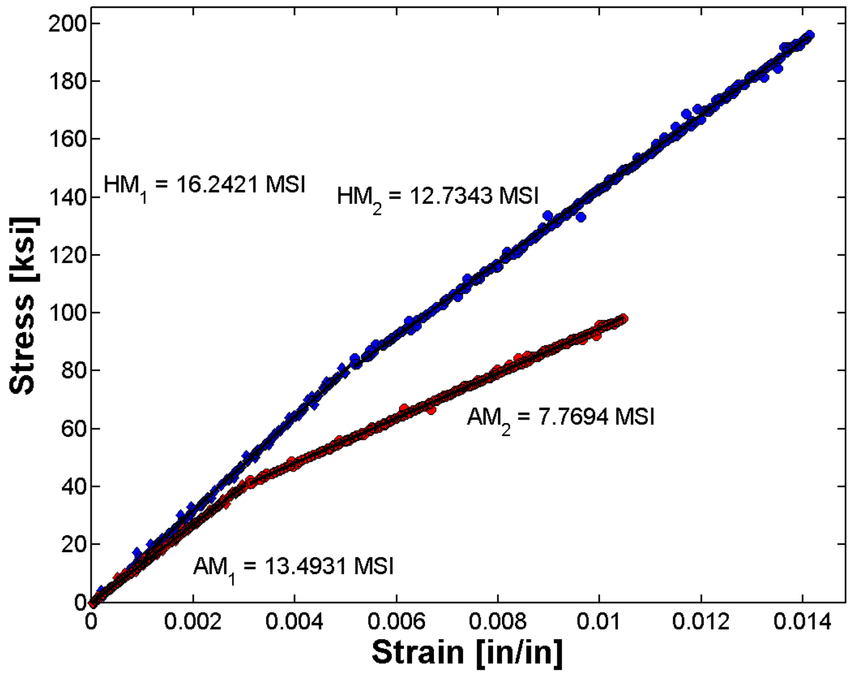

Figure C.13 Principal stress strain response of cylinder ALT639-18682. Note: Blue data points represent hoop response and red data points represent axial response.

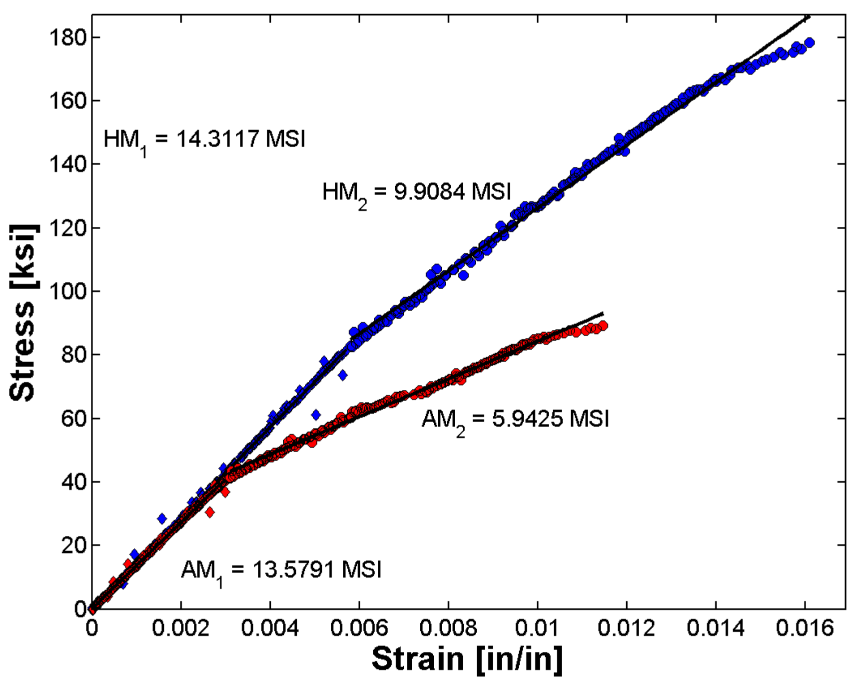

Figure C.14 Principal stress strain response of cylinder ALT639-19008. Note: Blue data points represent hoop response and red data points represent axial response.

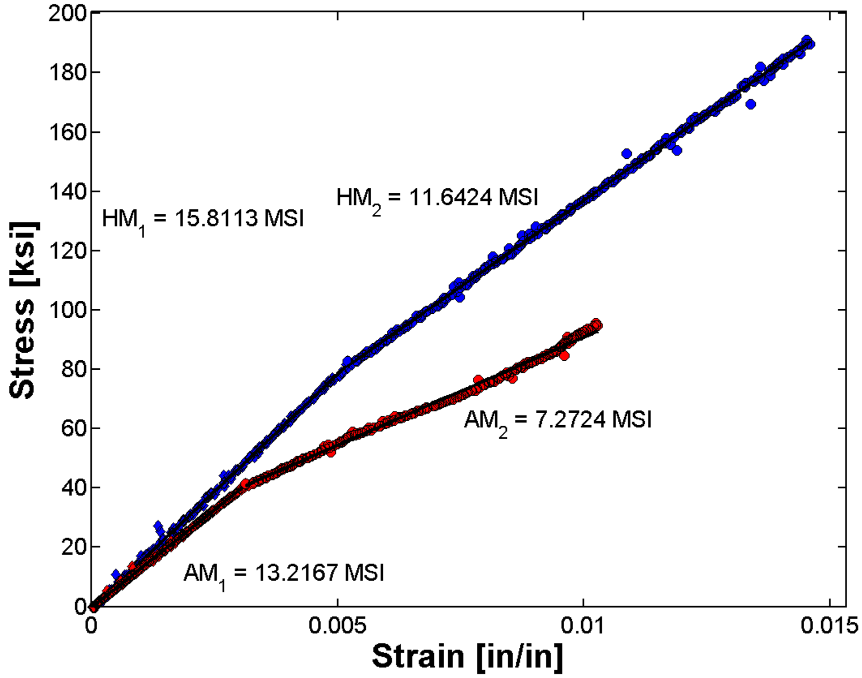

Figure C.15 Principal stress strain response of cylinder ALT639-22931. Note: Blue data points represent hoop response and red data points represent axial response.

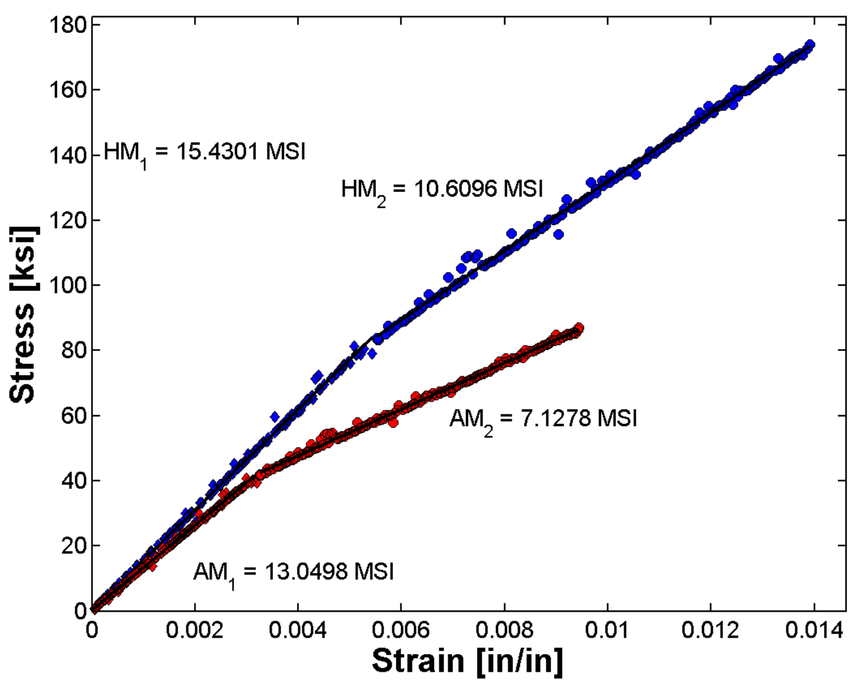

Figure C.16 Principal stress strain response of cylinder ALT639-23993. Note: Blue data points represent hoop response and red data points represent axial response.

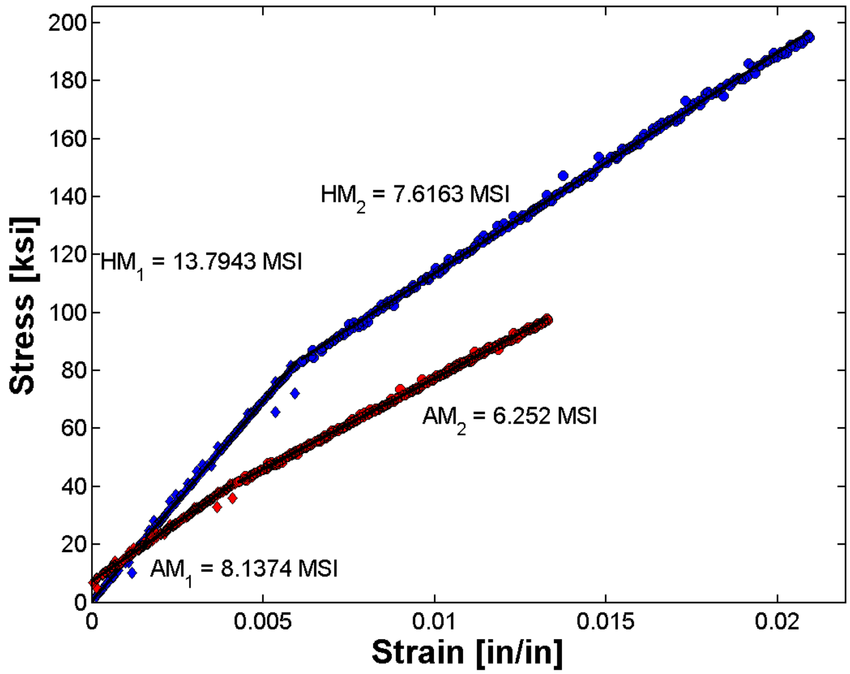

Figure C.17 Principal stress strain response of cylinder ALT639-24574. Note: Blue data points represent hoop response and red data points represent axial response.

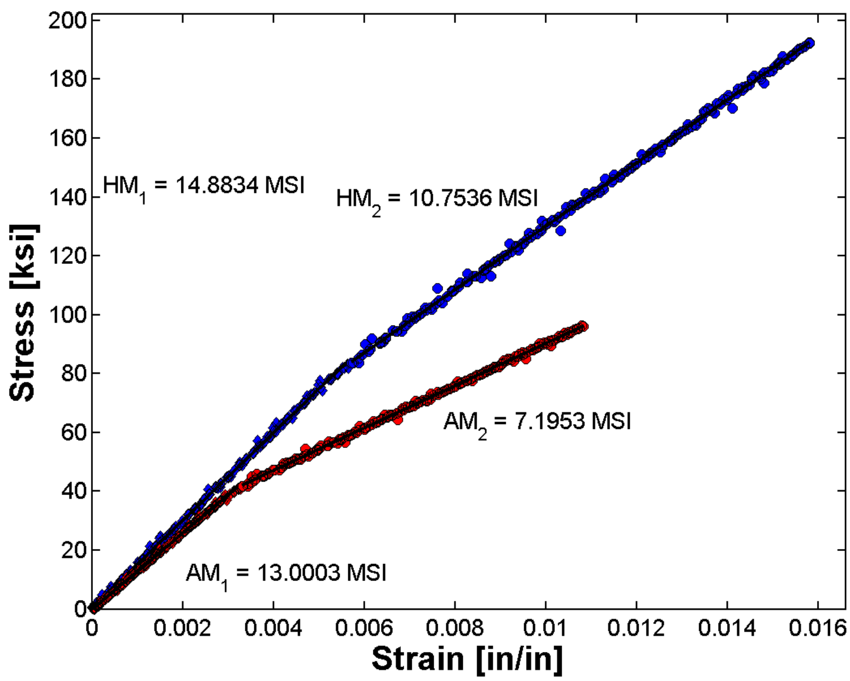

Figure C.18 Principal stress strain response of cylinder ALT639-34005. Note: Blue data points represent hoop response and red data points represent axial response.

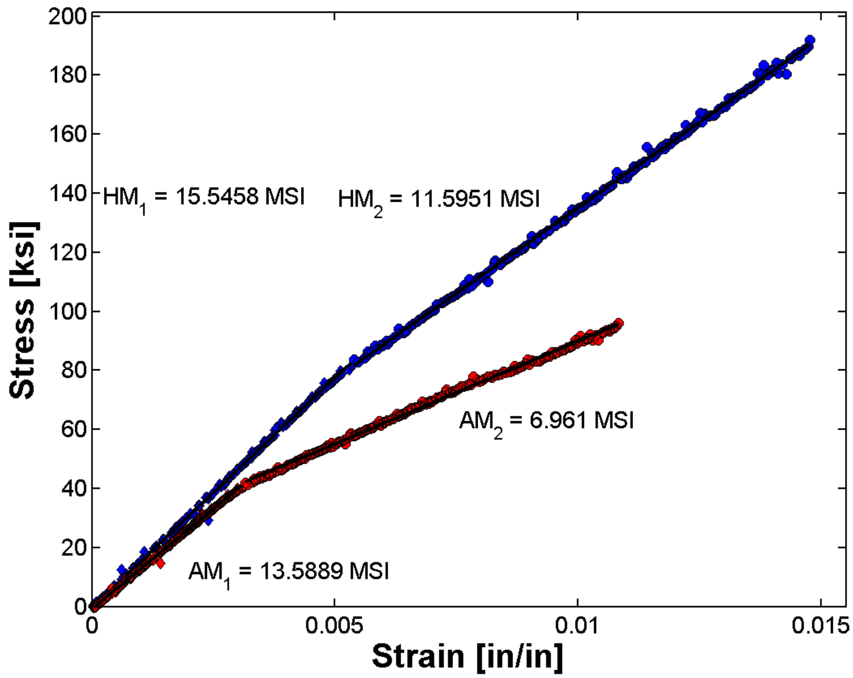

Figure C.19 Principal stress strain response of cylinder ALT639-38556. Note: Blue data points represent hoop response and red data points represent axial response.

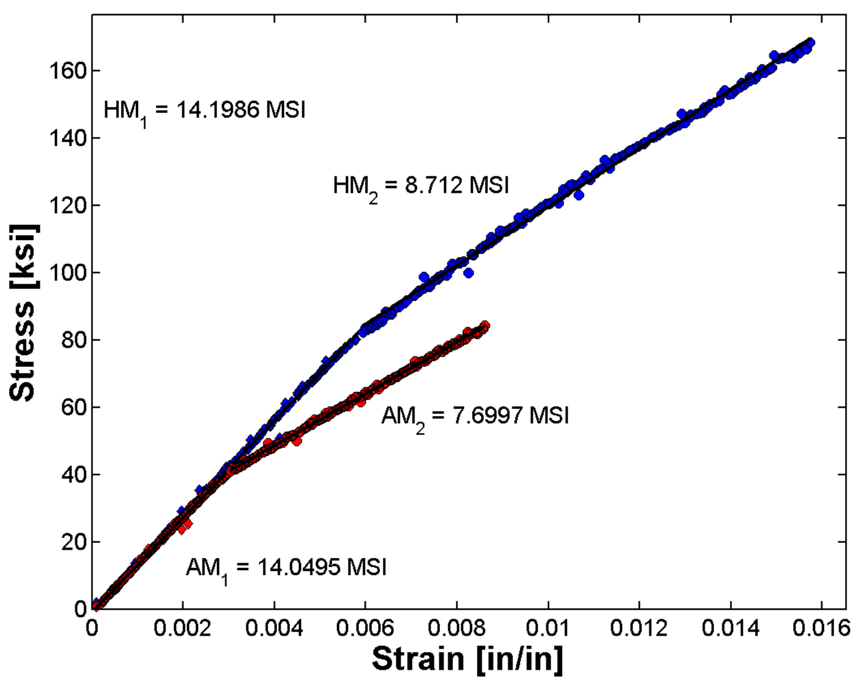

Figure C.20 Principal stress strain response of cylinder ALT639-40136. Note: Blue data points represent hoop response and red data points represent axial response.

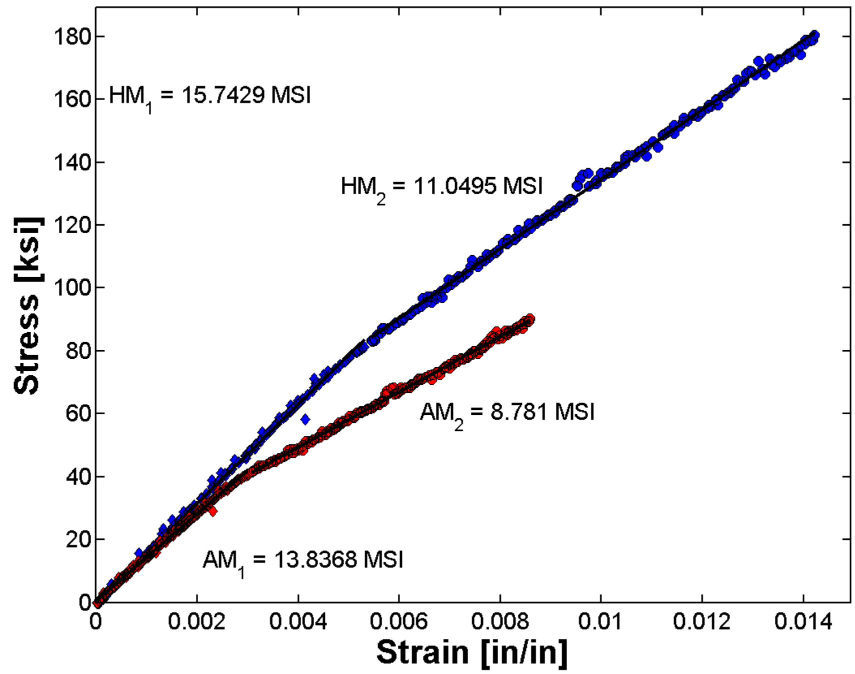

Figure C.21 Principal stress strain response of cylinder ALT639-69988. Note: Blue data points represent hoop response and red data points represent axial response.

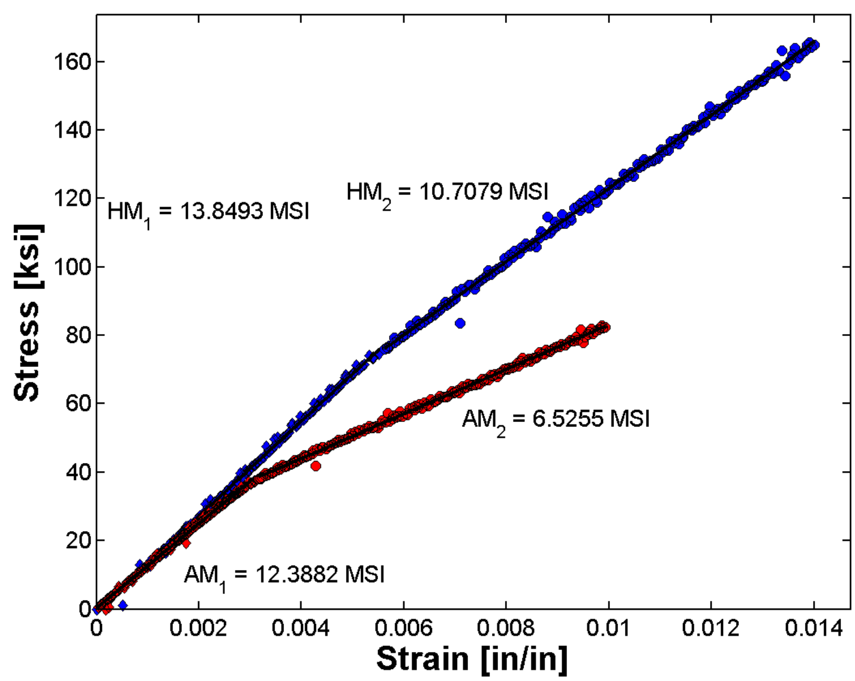

Figure C.22 Principal stress strain response of cylinder ALT695-1862. Note: Blue data points represent hoop response and red data points represent axial response.

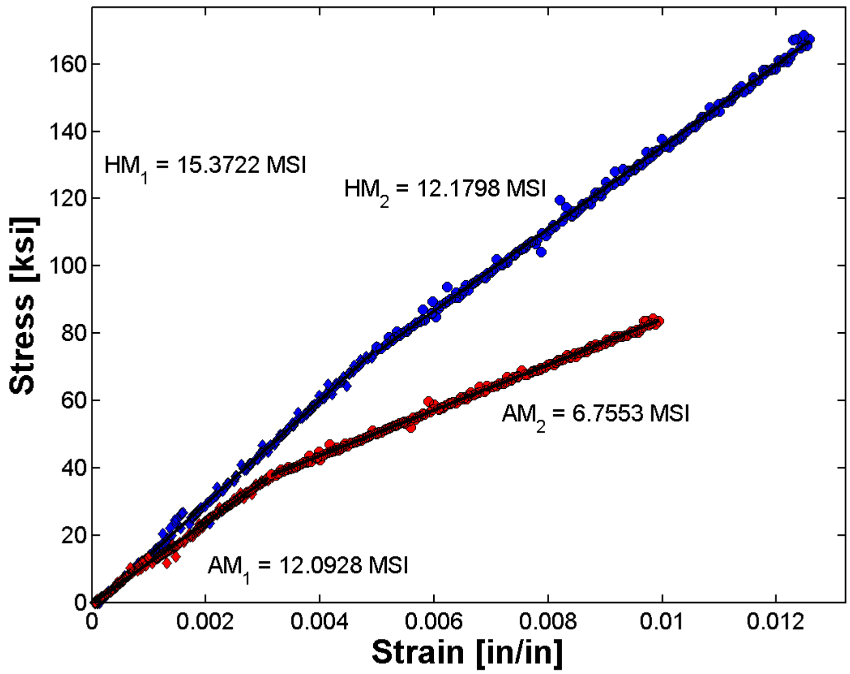

Figure C.23 Principal stress strain response of cylinder ALT695-3224. Note: Blue data points represent hoop response and red data points represent axial response.

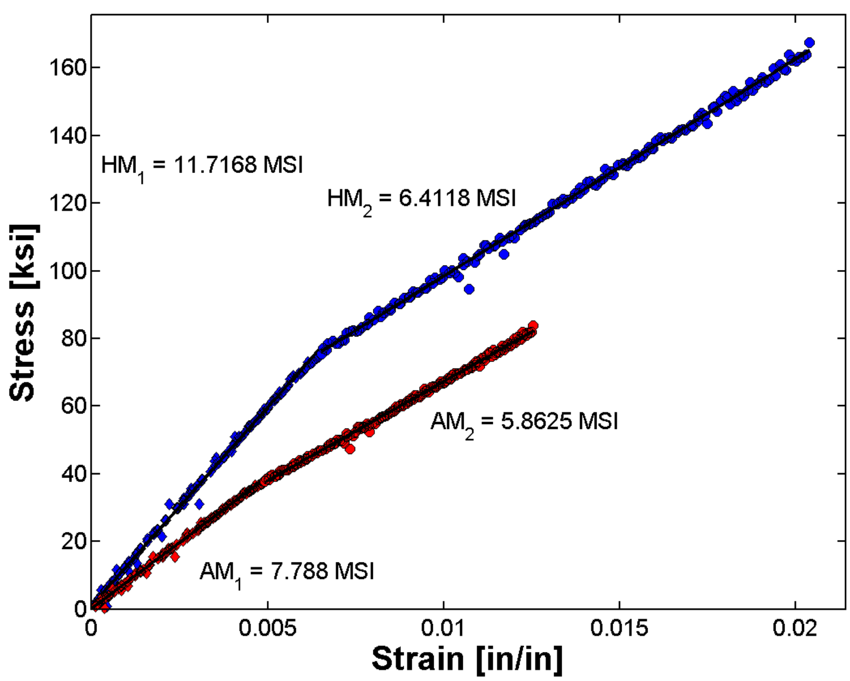

Figure C.24 Principal stress strain response of cylinder ALT695-3313. Note: Blue data points represent hoop response and red data points represent axial response.

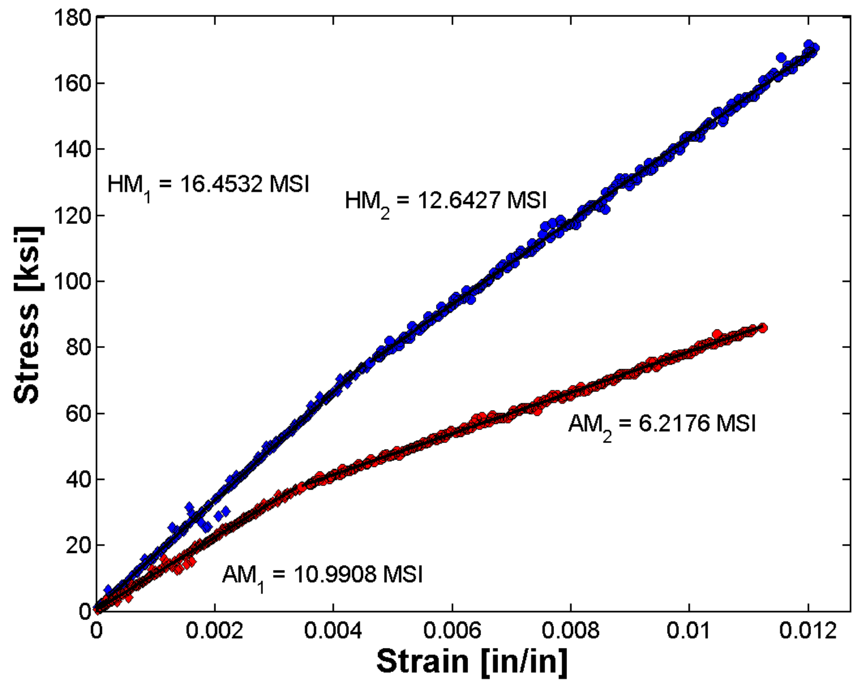

Figure C.25 Principal stress strain response of cylinder ALT695-3575. Note: Blue data points represent hoop response and red data points represent axial response.

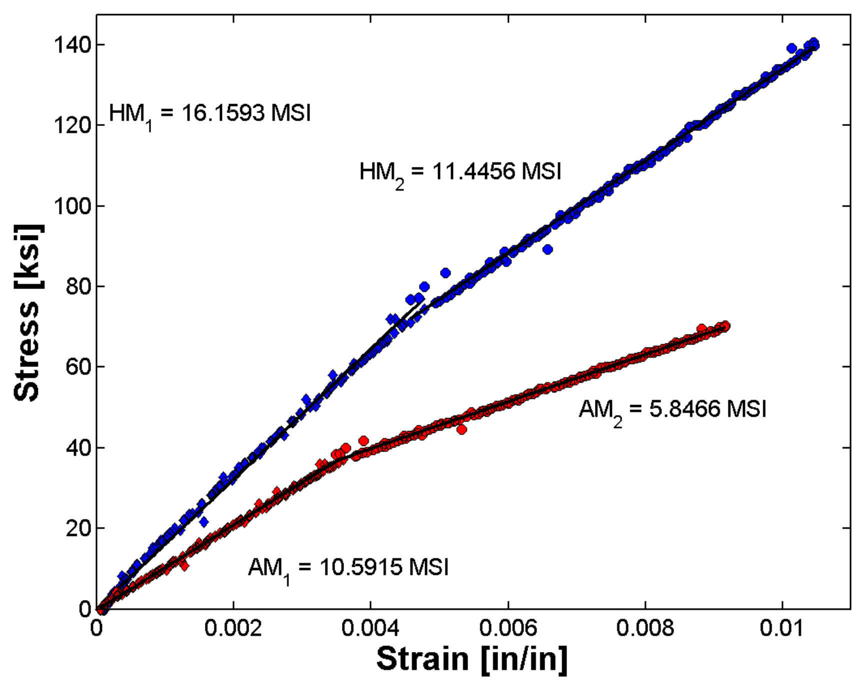

Figure C.26 Principal stress strain response of cylinder ALT695-3646. Note: Blue data points represent hoop response and red data points represent axial response.

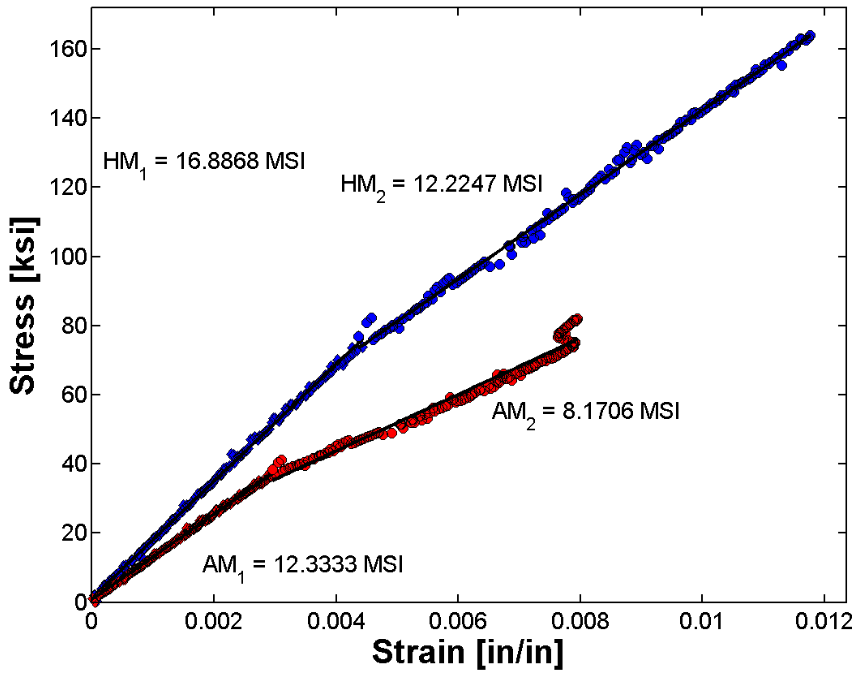

Figure C.27 Principal stress strain response of cylinder ALT695-3771. Note: Blue data points represent hoop response and red data points represent axial response.

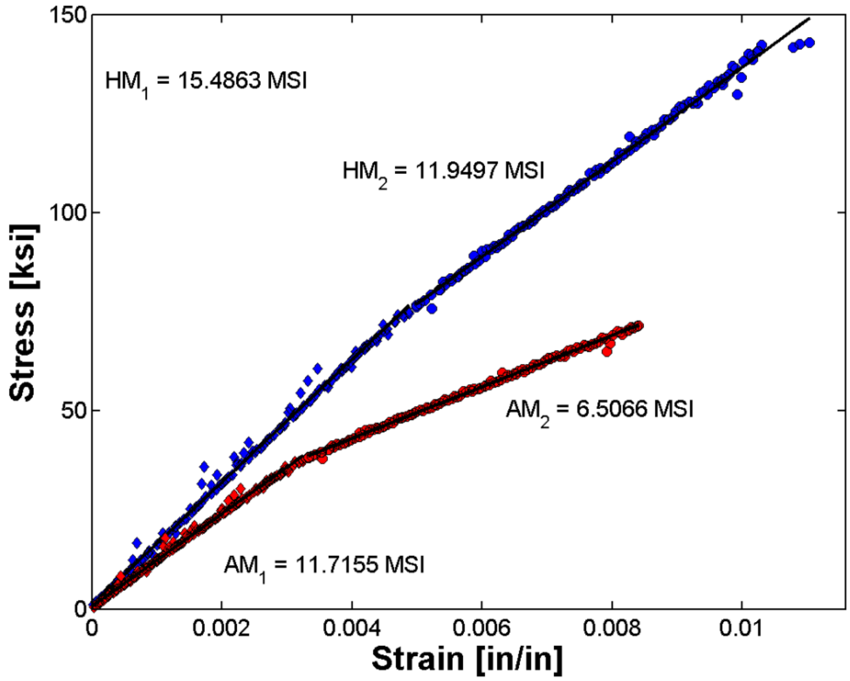

Figure C.28 Principal stress strain response of cylinder ALT695-3798. Note: Blue data points represent hoop response and red data points represent axial response.

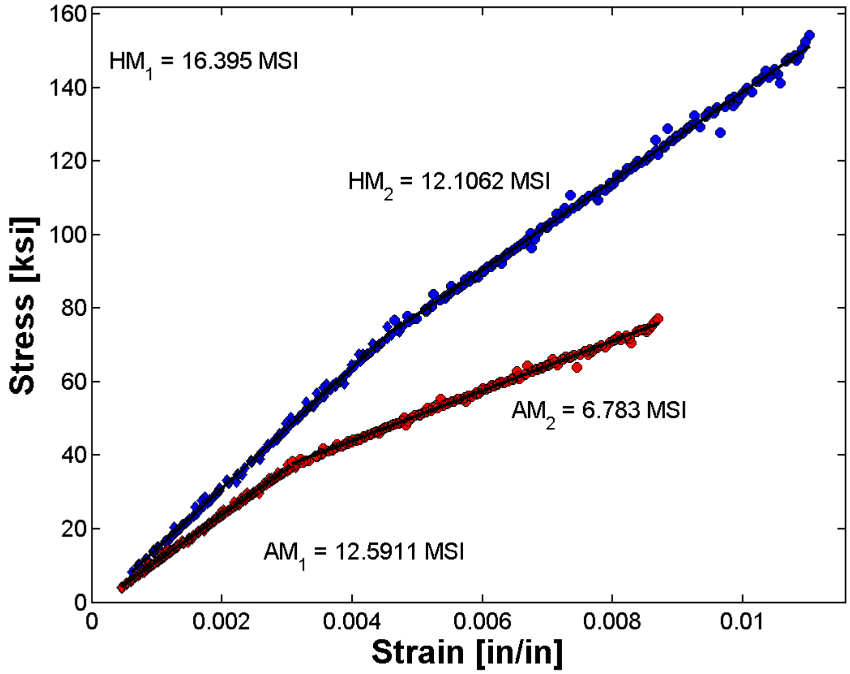

Figure C.29 Principal stress strain response of cylinder ALT695-3881. Note: Blue data points represent hoop response and red data points represent axial response.

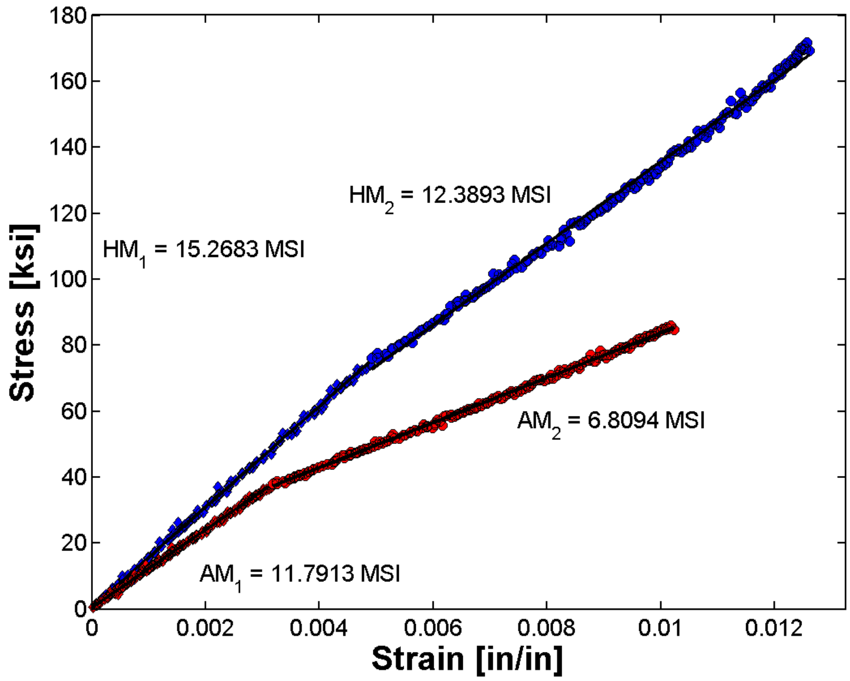

Figure C.30 Principal stress strain response of cylinder ALT695-3936. Note: Blue data points represent hoop response and red data points represent axial response.

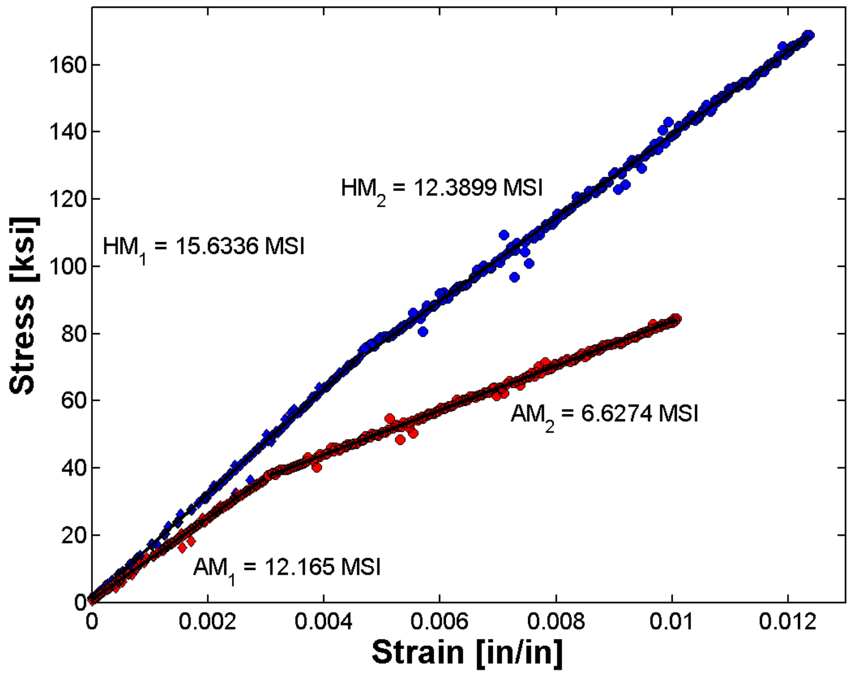

Figure C.31 Principal stress strain response of cylinder ALT695-4379. Note: Blue data points represent hoop response and red data points represent axial response.

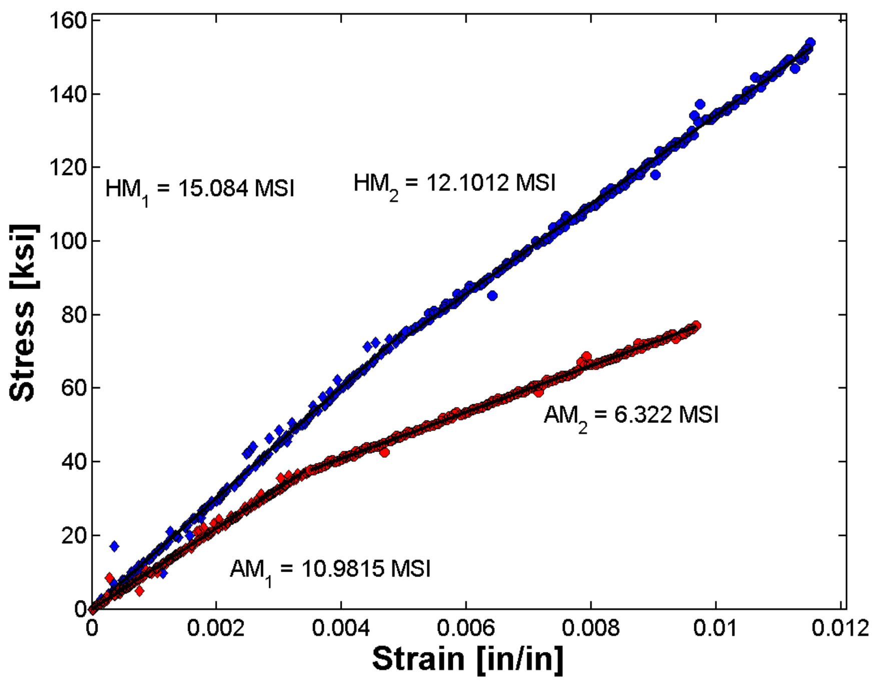

Figure C.32 Principal stress strain response of cylinder ALT695-4396. Note: Blue data points represent hoop response and red data points represent axial response.

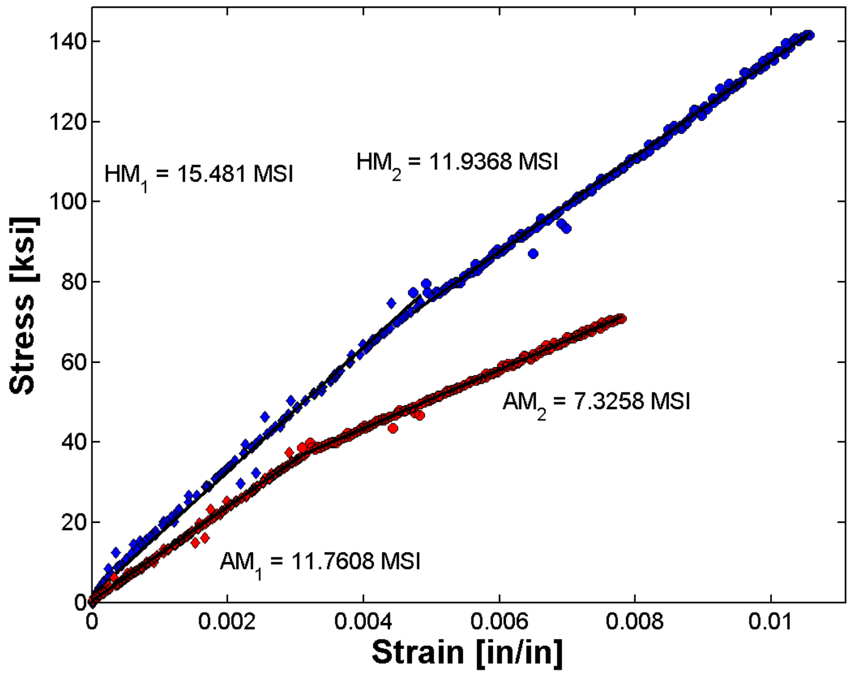

Figure C.33 Principal stress strain response of cylinder ALT695-4469. Note: Blue data points represent hoop response and red data points represent axial response.

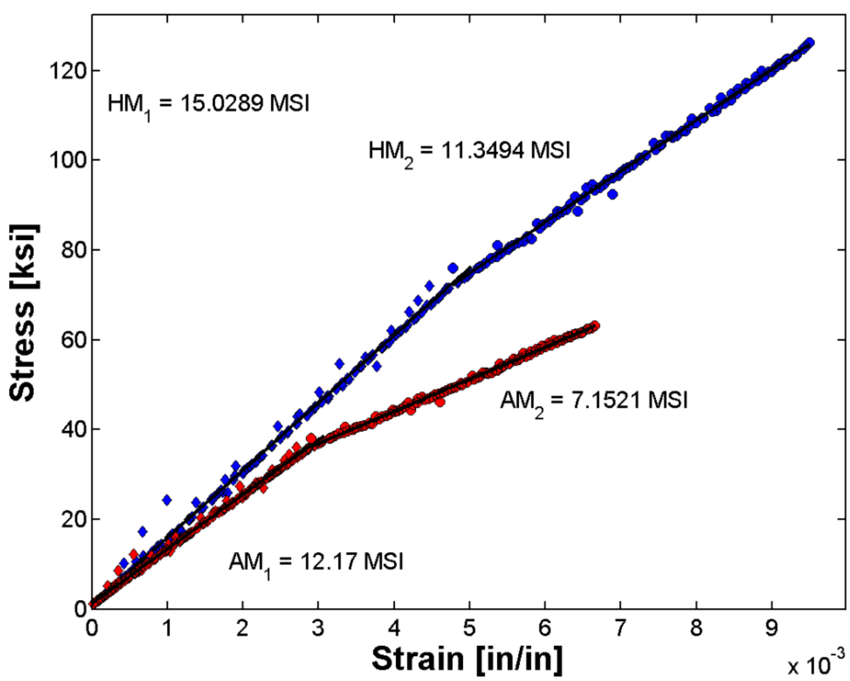

Figure C.34 Principal stress strain response of cylinder ALT695-4482. Note: Blue data points represent hoop response and red data points represent axial response.

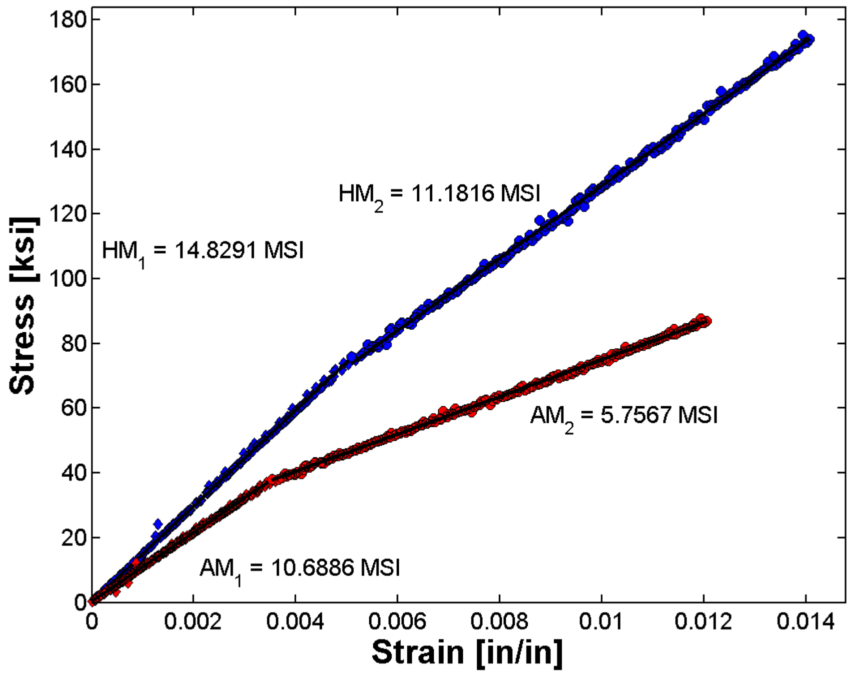

Figure C.35 Principal stress strain response of cylinder ALT695-4492. Note: Blue data points represent hoop response and red data points represent axial response.

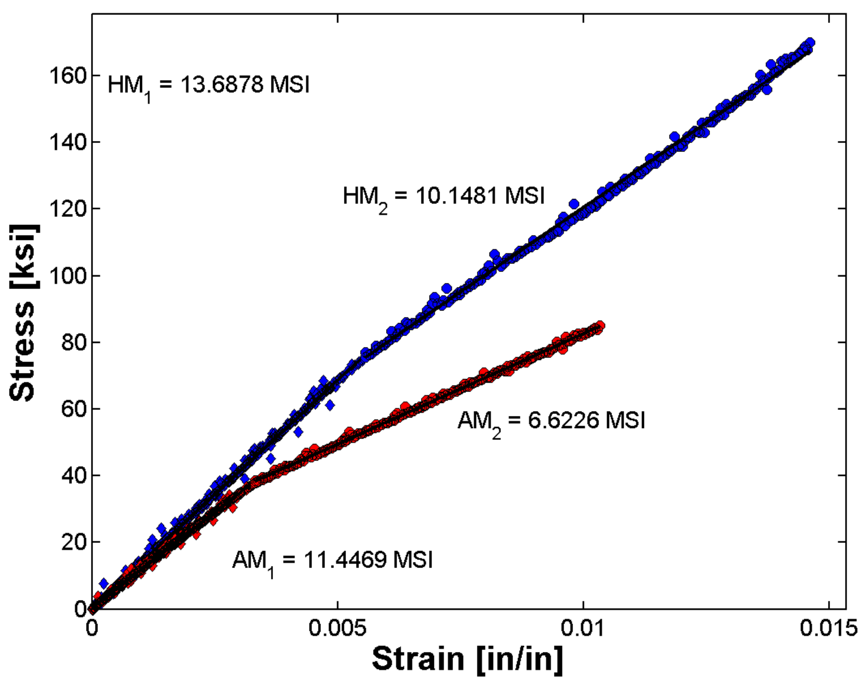

Figure C.36 Principal stress strain response of cylinder ALT695-4734. Note: Blue data points represent hoop response and red data points represent axial response.

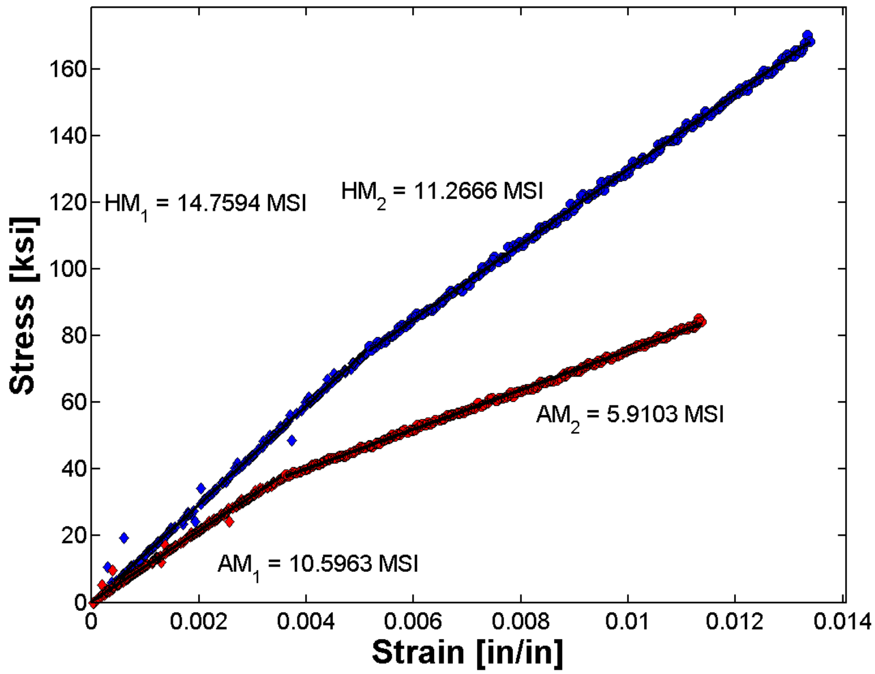

Figure C.37 Principal stress strain response of cylinder ALT695-4775. Note: Blue data points represent hoop response and red data points represent axial response.

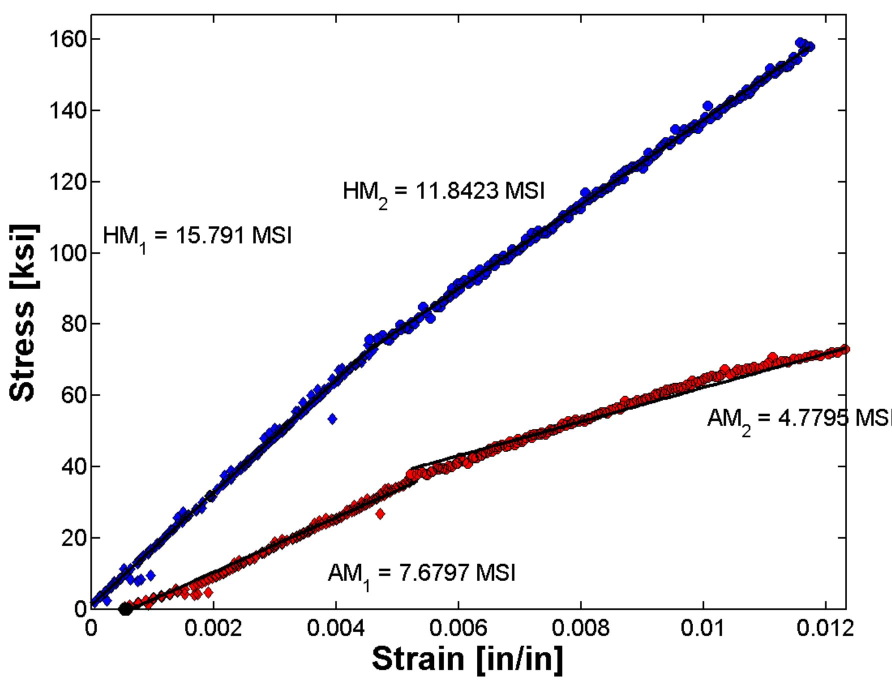

Figure C.38 Principal stress strain response of cylinder ALT695-4944. Note: Blue data points represent hoop response and red data points represent axial response.

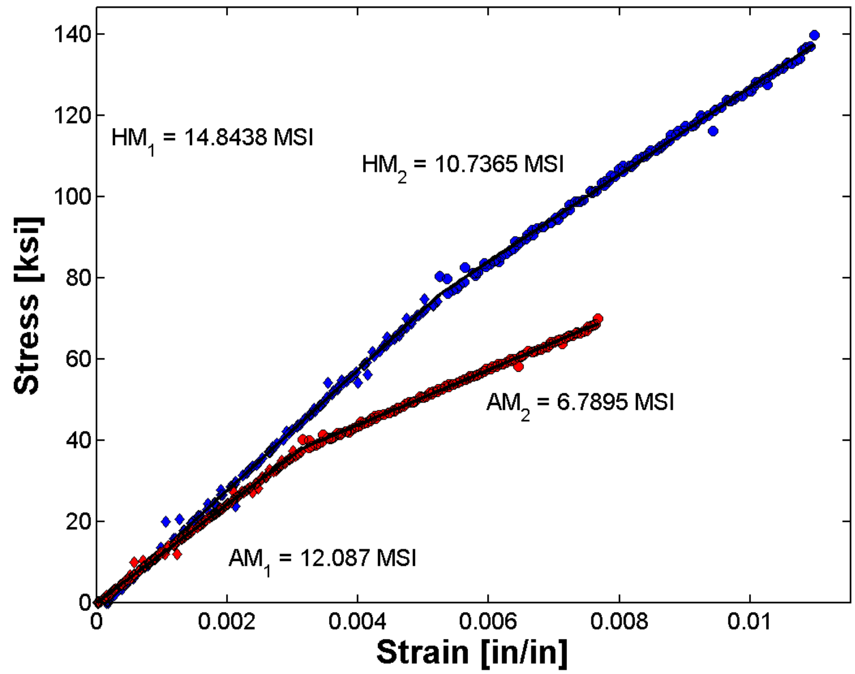

Figure C.39 Principal stress strain response of cylinder ALT695-5497. Note: Blue data points represent hoop response and red data points represent axial response.

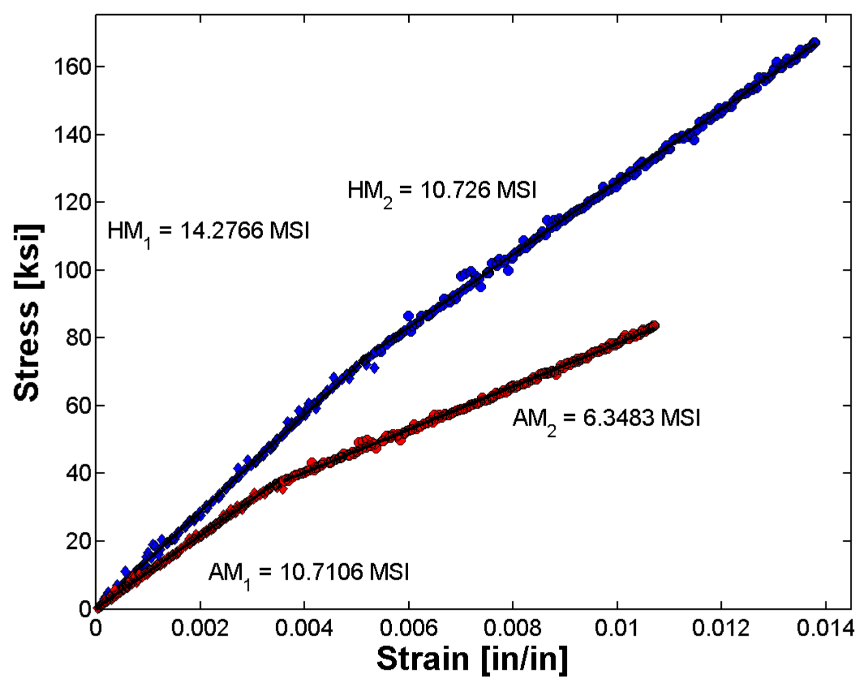

Figure C.40 Principal stress strain response of cylinder ALT695-5558. Note: Blue data points represent hoop response and red data points represent axial response.

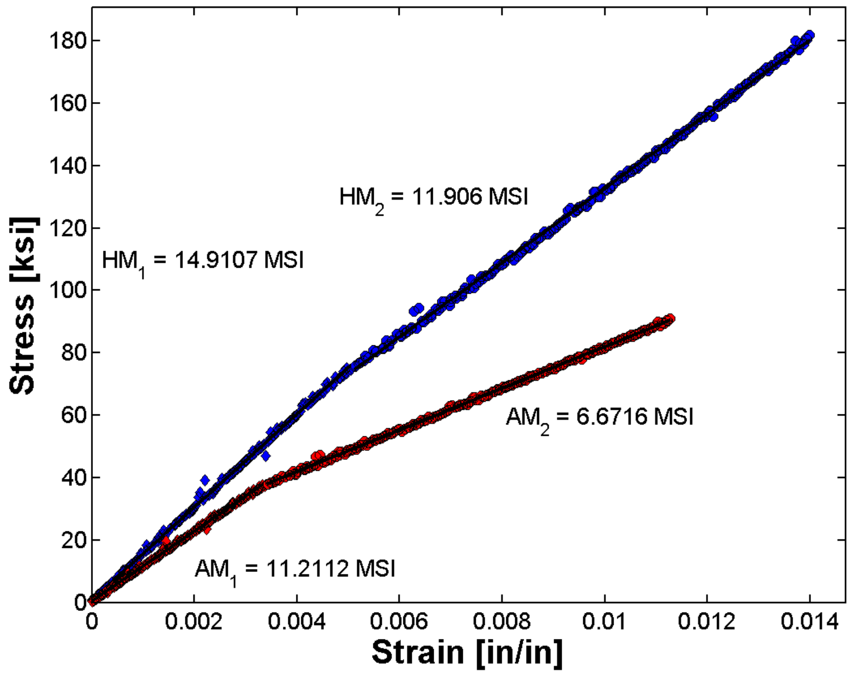

Figure C.41 Principal stress strain response of cylinder ALT695-5641. Note: Blue data points represent hoop response and red data points represent axial response.

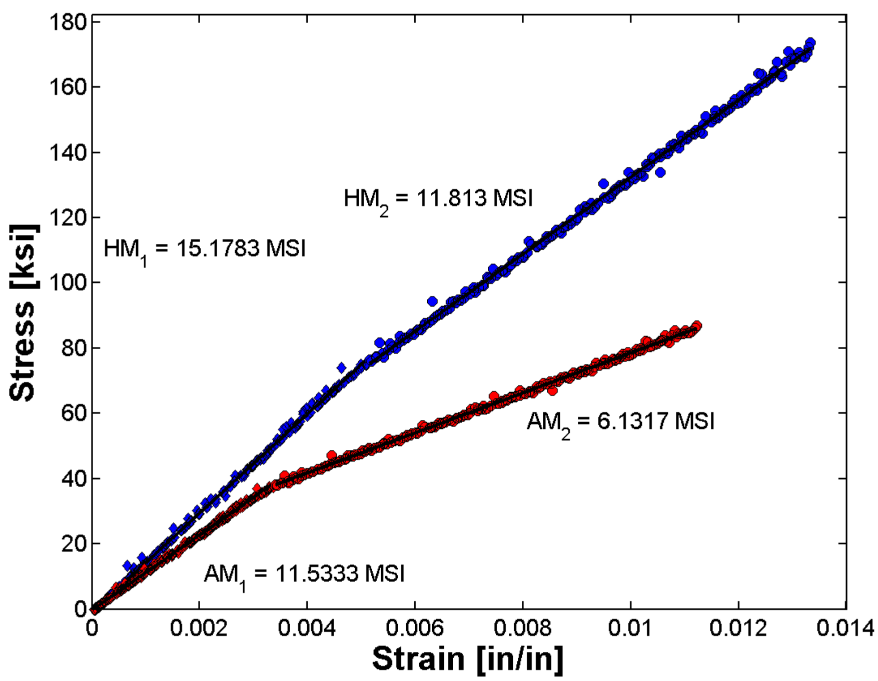

Figure C.42 Principal stress strain response of cylinder ALT695-6041. Note: Blue data points represent hoop response and red data points represent axial response.

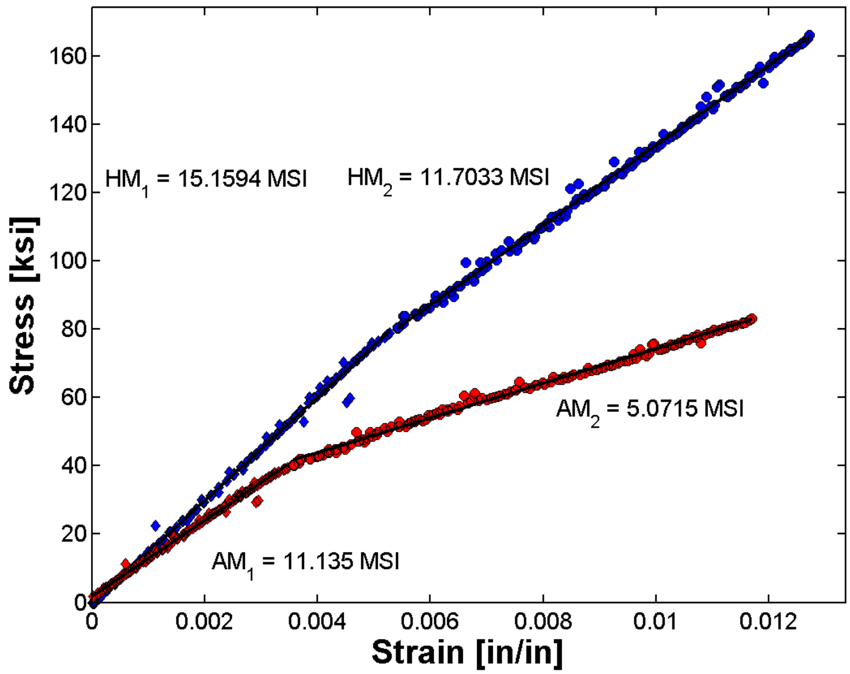

Figure C.43 Principal stress strain response of cylinder IH667. Note: Blue data points represent hoop response and red data points represent axial response.

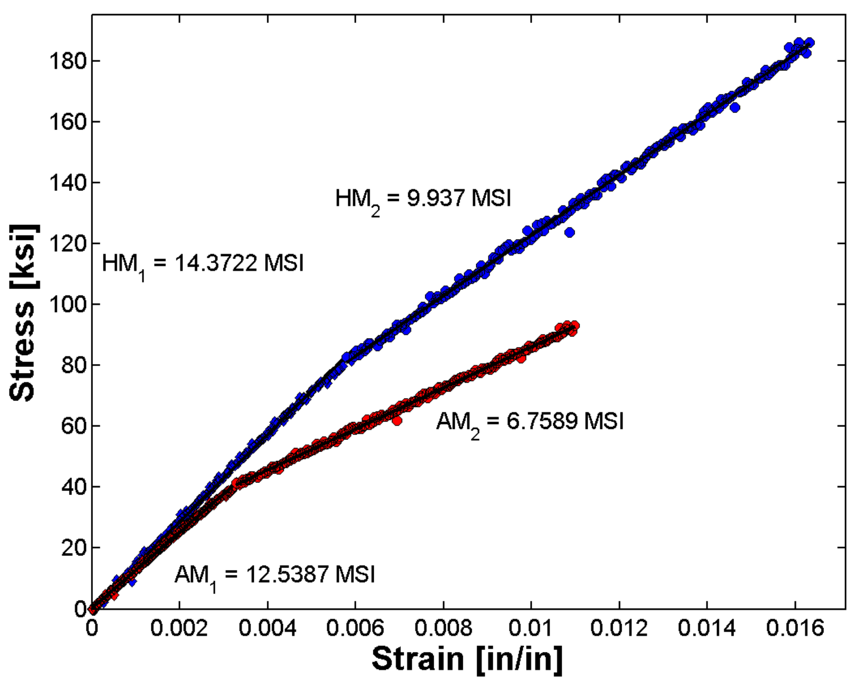

Figure C.44 Principal stress strain response of cylinder IL2705. Note: Blue data points represent hoop response and red data points represent axial response.

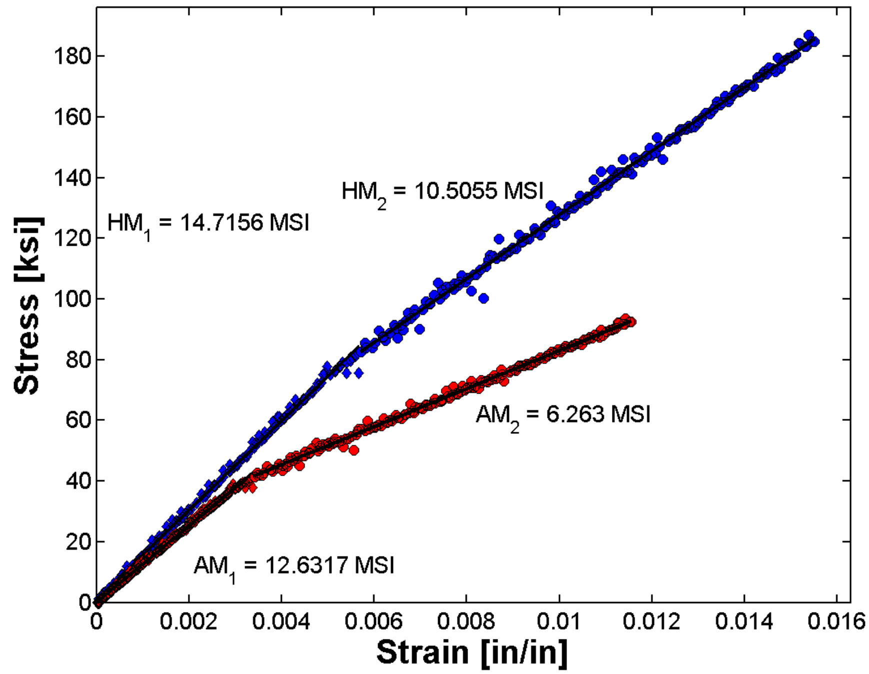

Figure C.45 Principal stress strain response of cylinder IL2722. Note: Blue data points represent hoop response and red data points represent axial response.

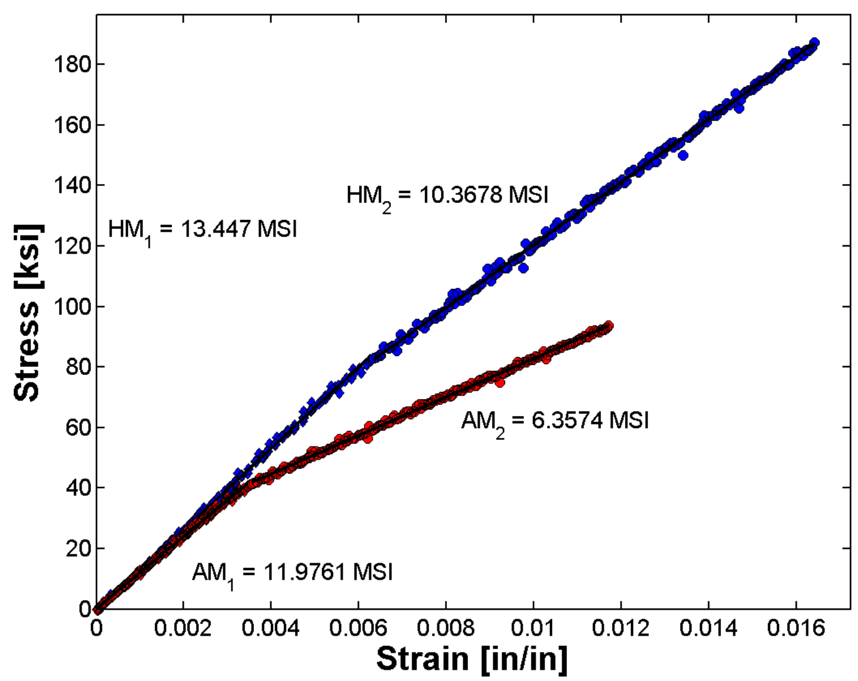

Figure C.46 Principal stress strain response of cylinder IL2933. Note: Blue data points represent hoop response and red data points represent axial response.

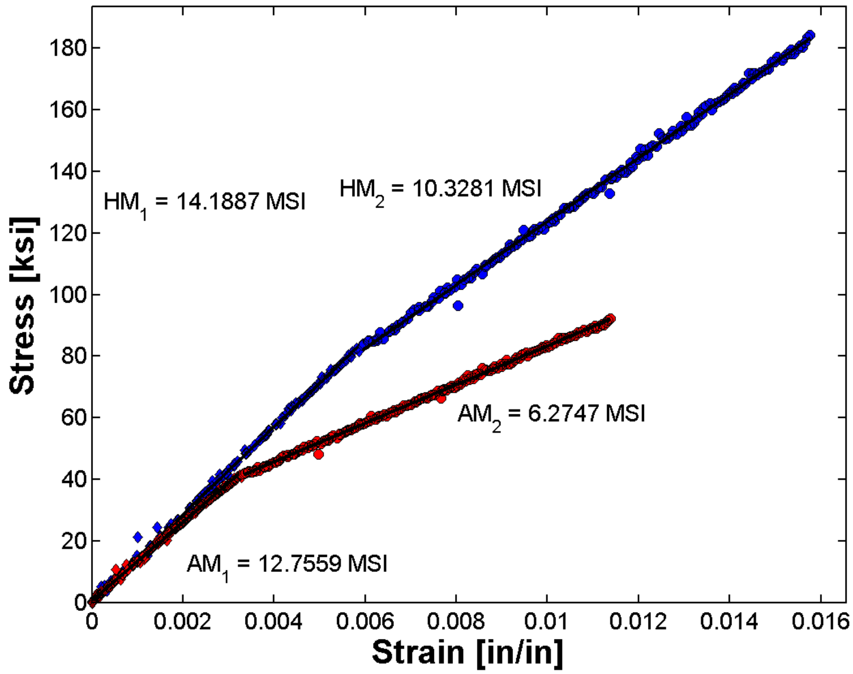

Figure C.47 Principal stress strain response of cylinder IL3334. Note: Blue data points represent hoop response and red data points represent axial response.

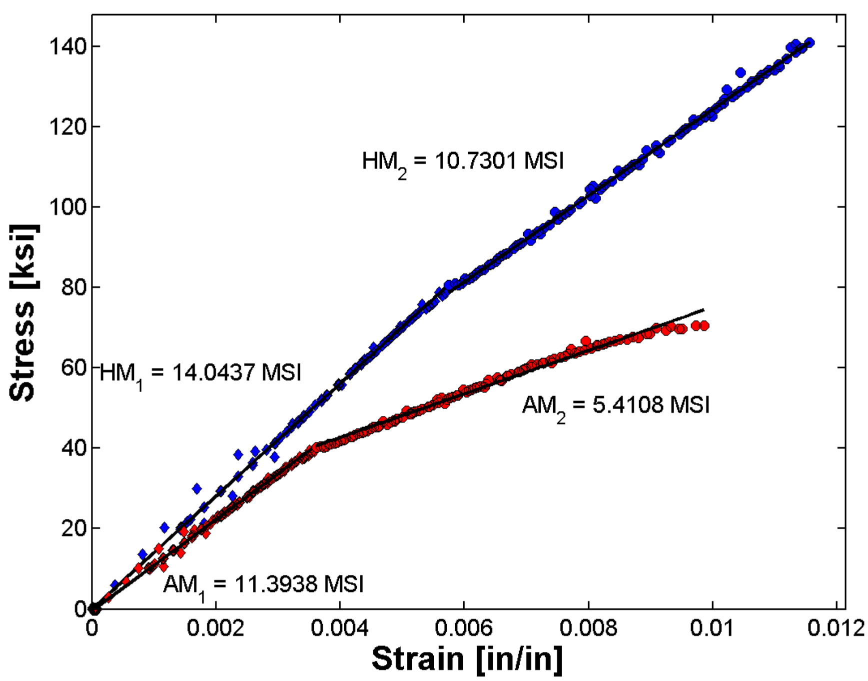

Figure C.48 Principal stress strain response of cylinder OK85342. Note: Blue data points represent hoop response and red data points represent axial response.

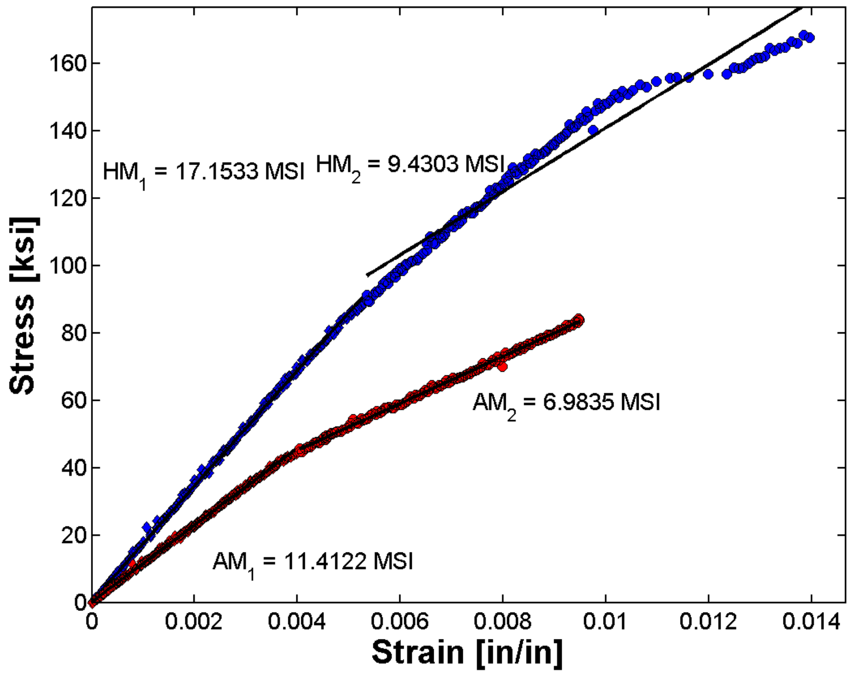

Figure C.49 Principal stress strain response of cylinder ON3077. Note: Blue data points represent hoop response and red data points represent axial response.

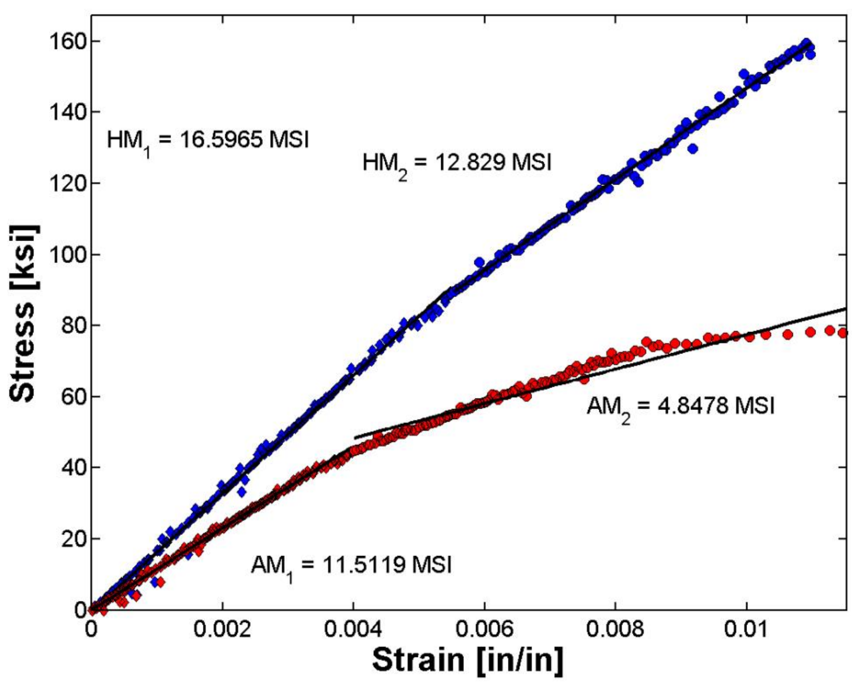

Figure C.50 Principal stress strain response of cylinder ON3146. Note: Blue data points represent hoop response and red data points represent axial response.

11. Appendix D – BEOP plots

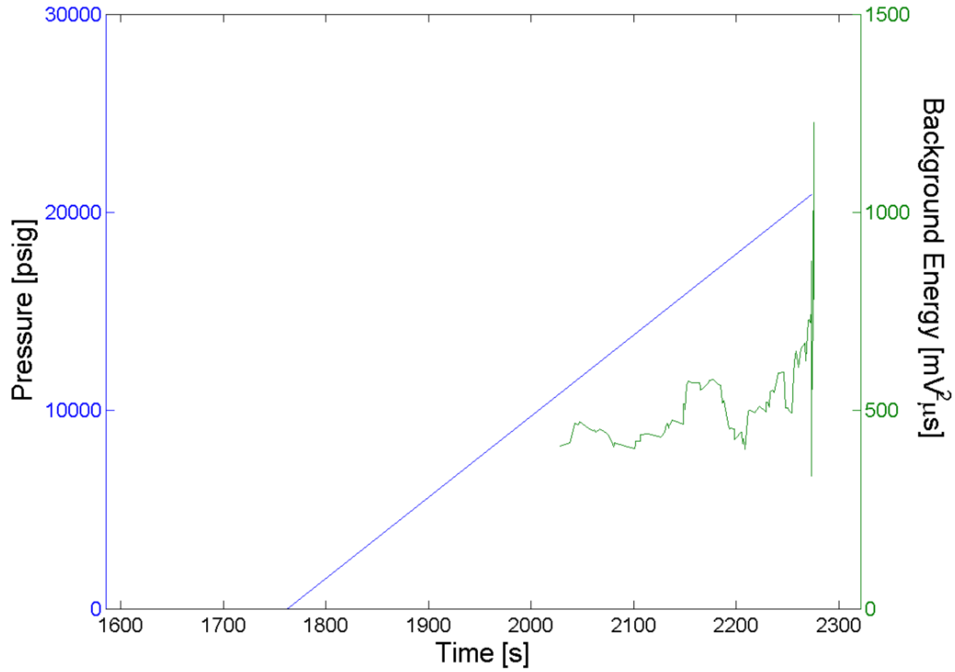

Figure D.1 – Background energy oscillation plot for cylinder ALT604-5155.

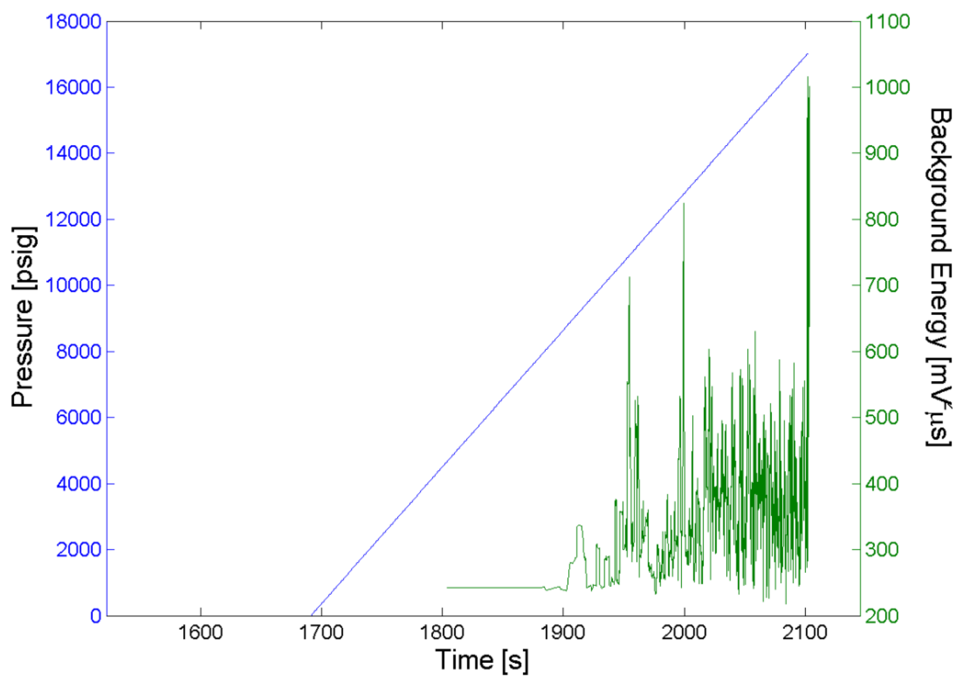

Figure D.2 – Background energy oscillation plot for cylinder ALT604-5553.

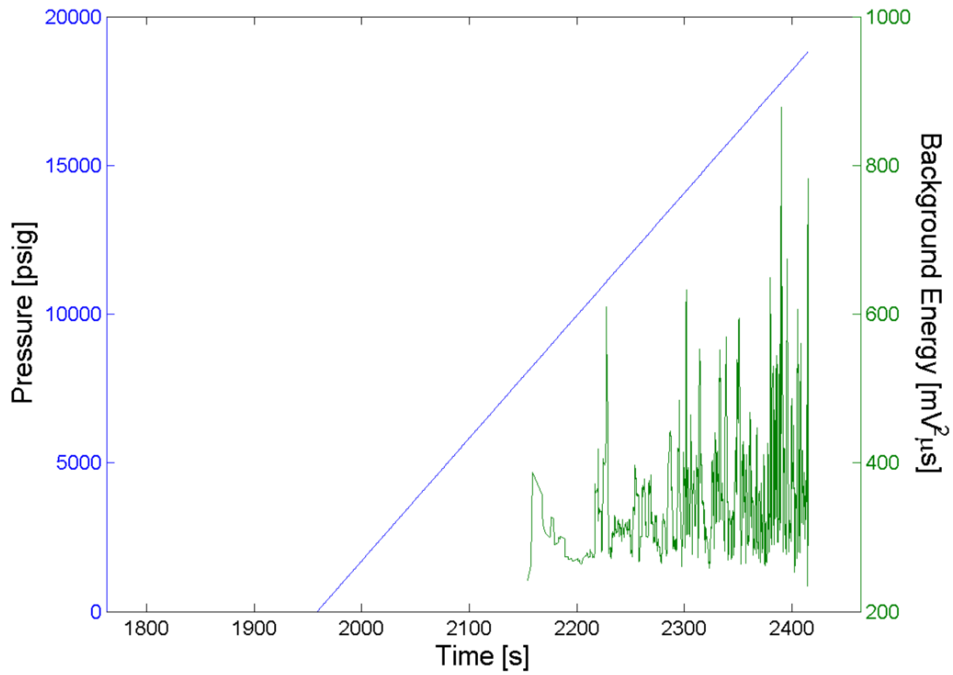

Figure D.3 – Background energy oscillation plot for cylinder ALT604-5561.

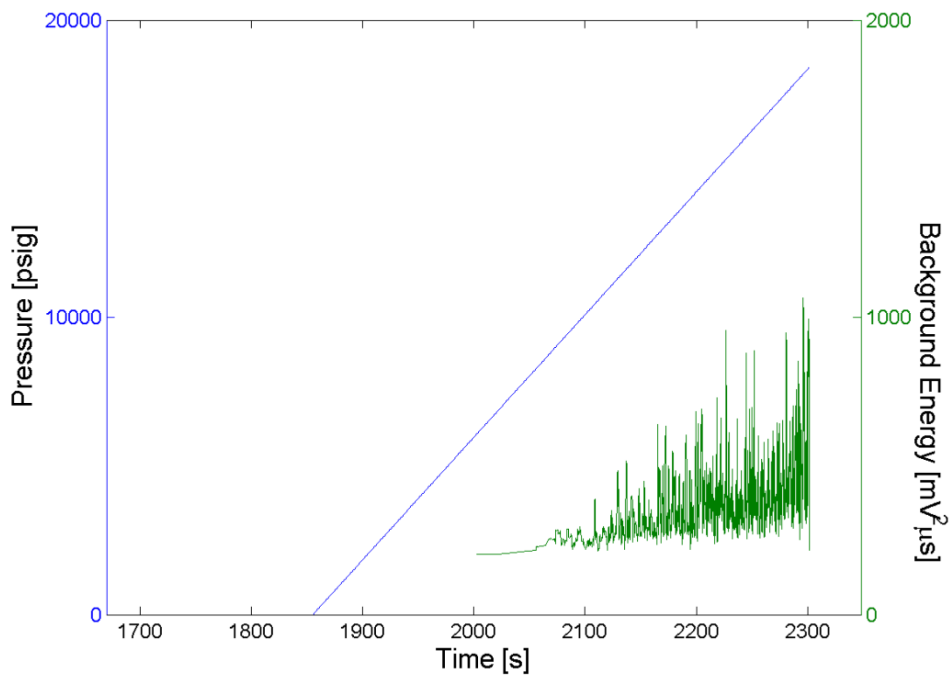

Figure D.4 – Background energy oscillation plot for cylinder ALT604-6707.

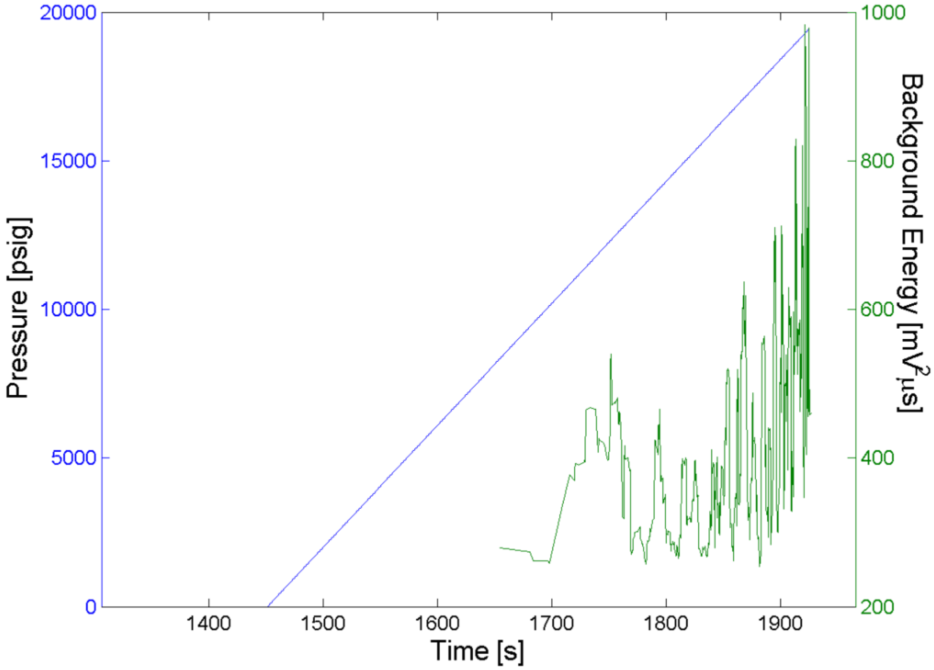

Figure D.5 – Background energy oscillation plot for cylinder ALT639-4101.

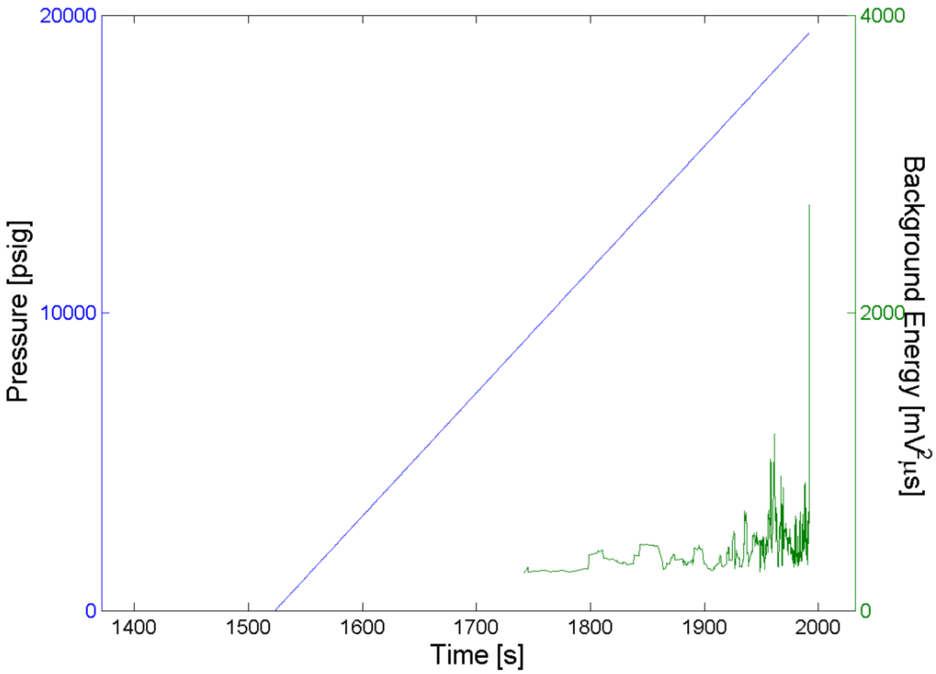

Figure D.6 – Background energy oscillation plot for cylinder ALT639-4610.

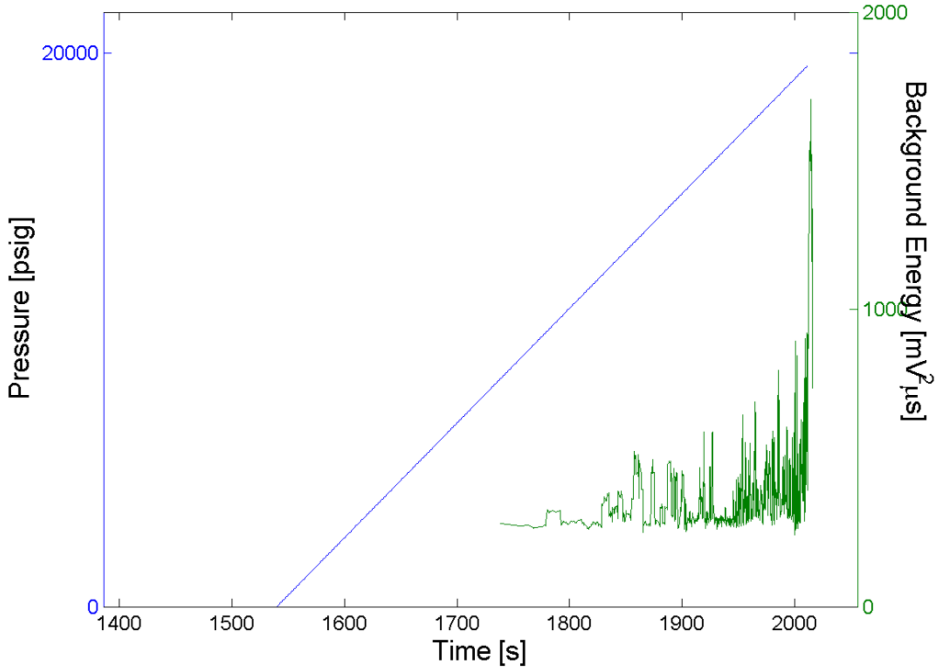

Figure D.7 – Background energy oscillation plot for cylinder ALT639-5224.

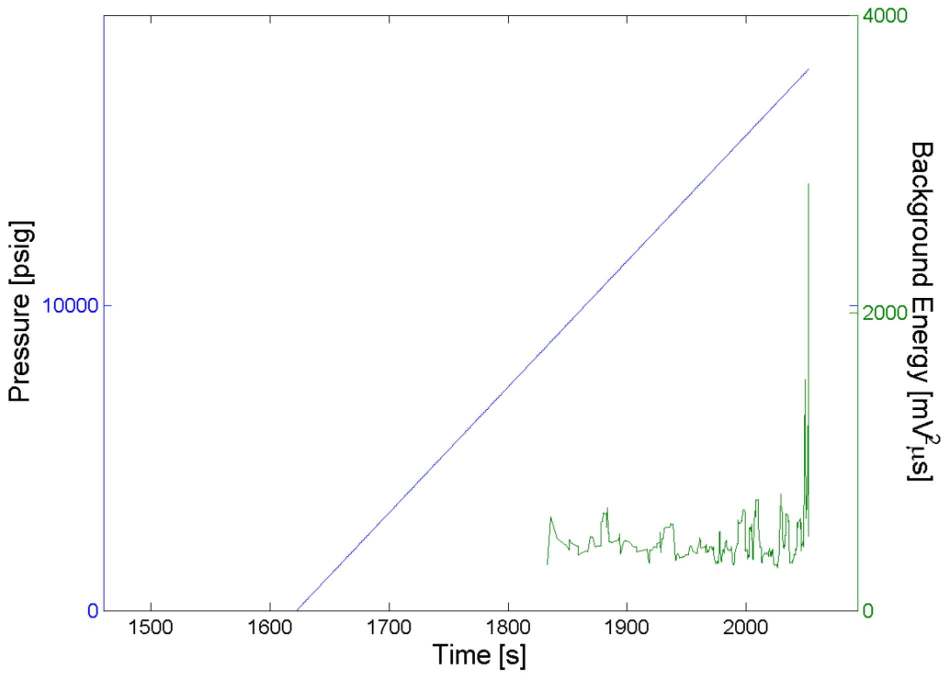

Figure D.8 – Background energy oscillation plot for cylinder ALT639-9435.

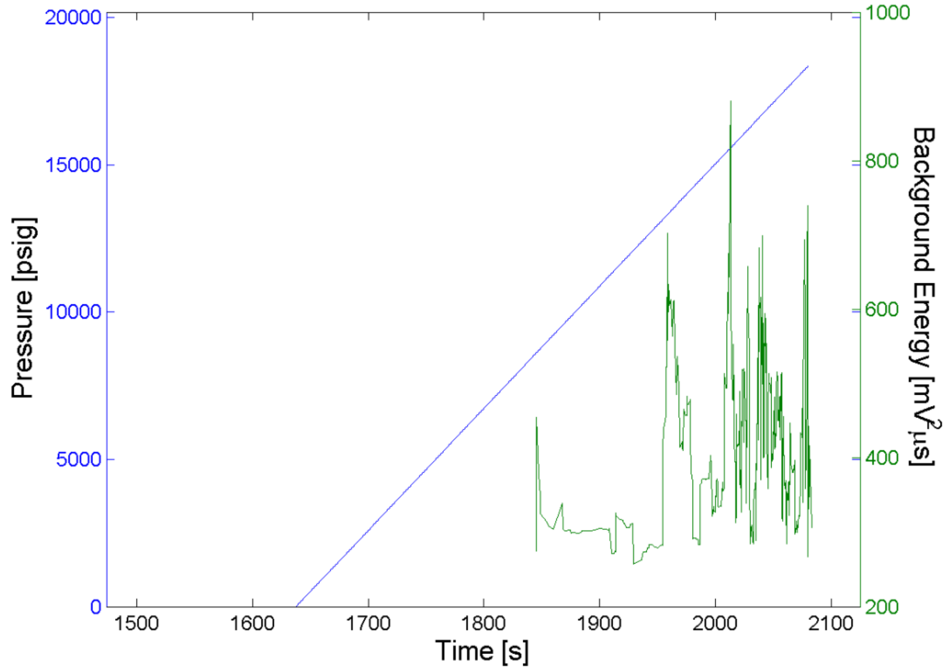

Figure D.9 – Background energy oscillation plot for cylinder ALT639-9528.

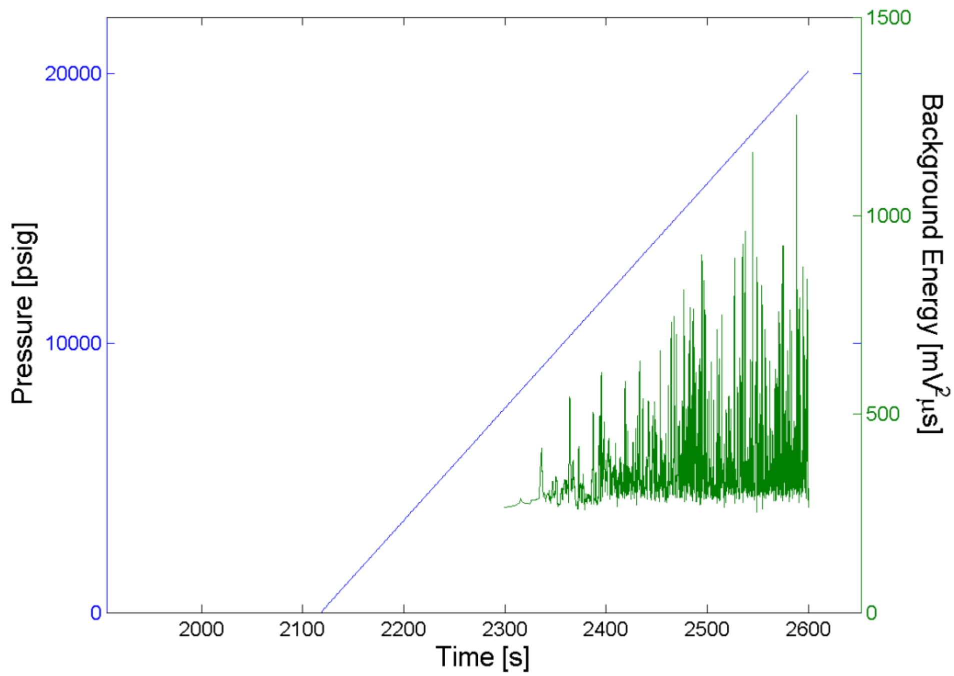

Figure D.10 – Background energy oscillation plot for cylinder ALT639-9941.

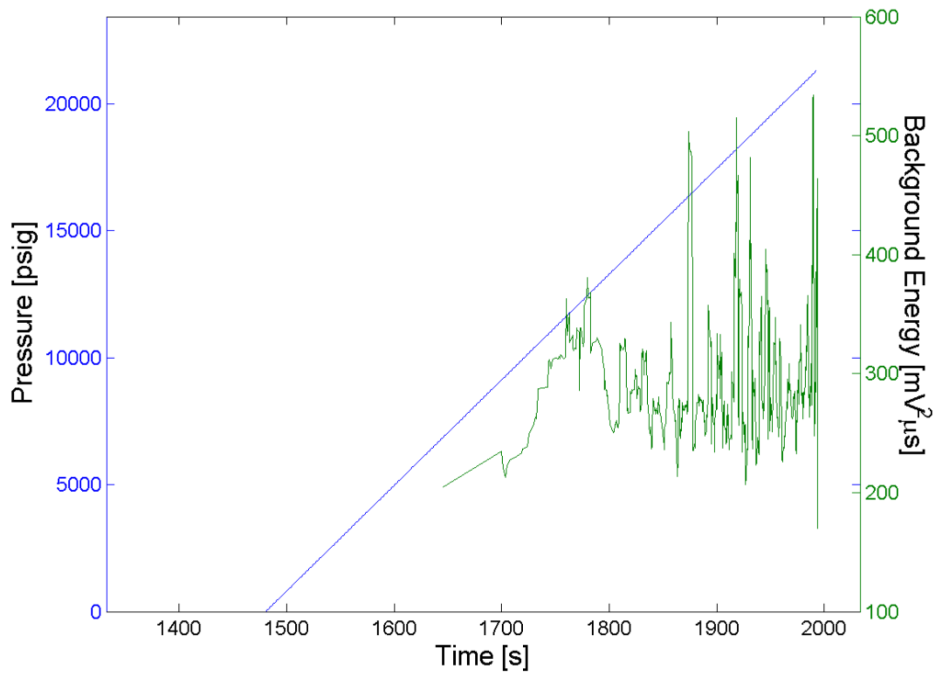

Figure D.11 – Background energy oscillation plot for cylinder ALT639-17714.

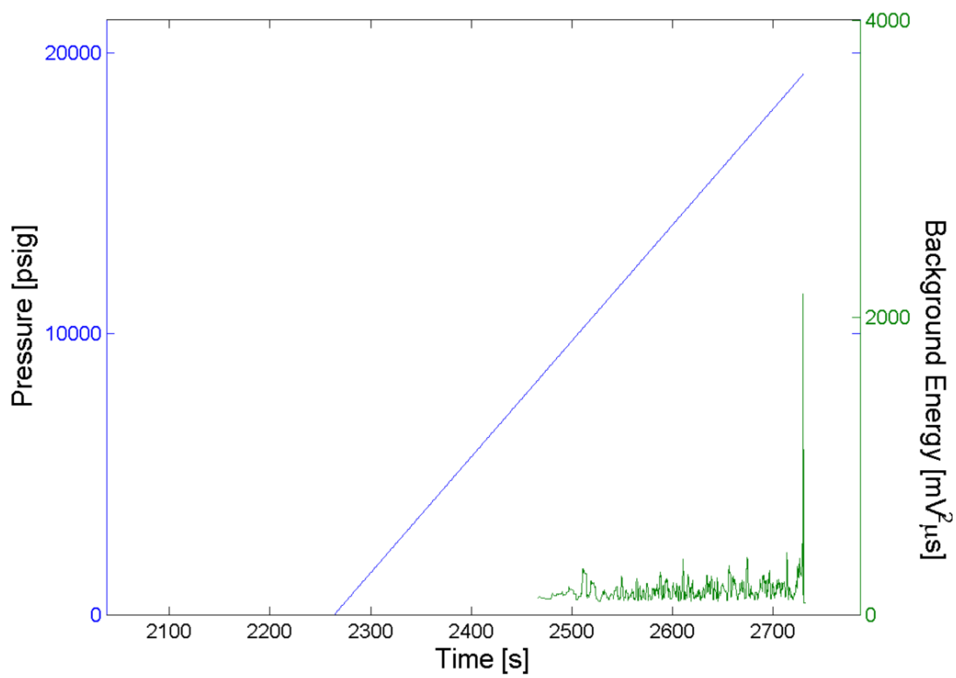

Figure D.12 – Background energy oscillation plot for cylinder ALT639-18594.

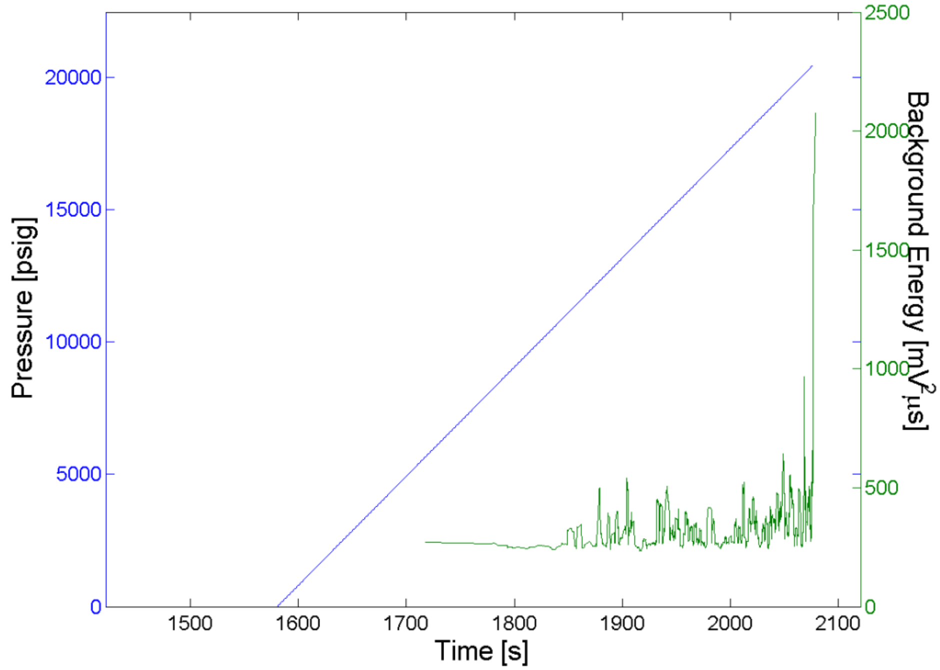

Figure D.13 – Background energy oscillation plot for cylinder ALT639-18682.

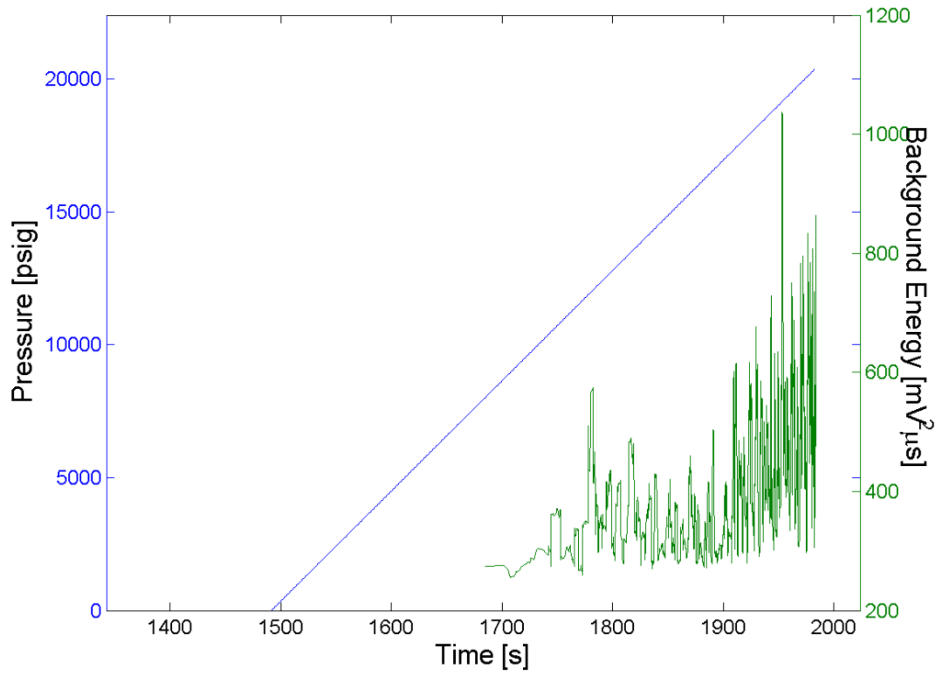

Figure D.14 – Background energy oscillation plot for cylinder ALT639-19008.

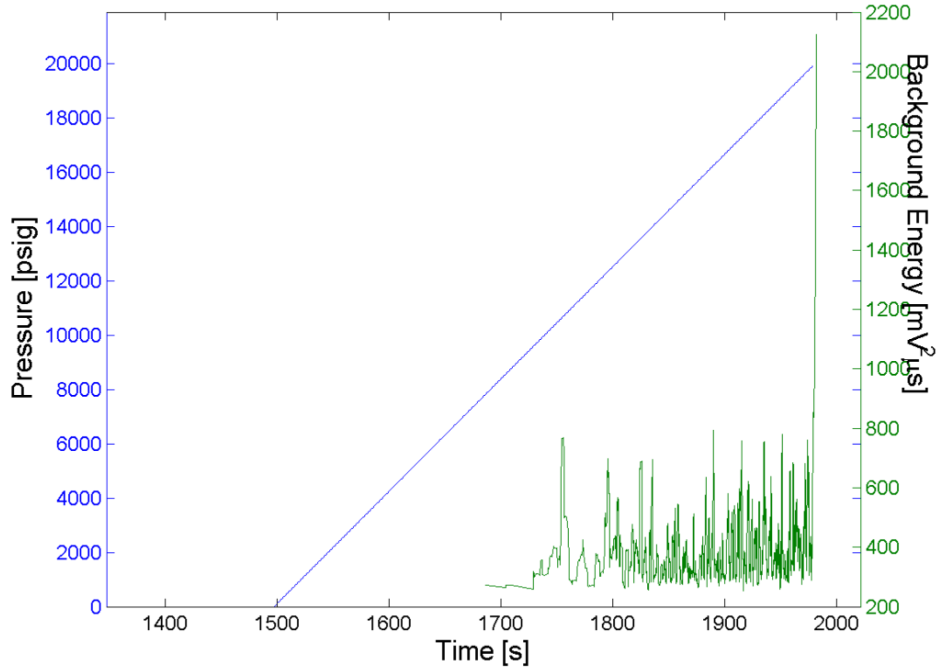

Figure D.15 – Background energy oscillation plot for cylinder ALT639-22931.

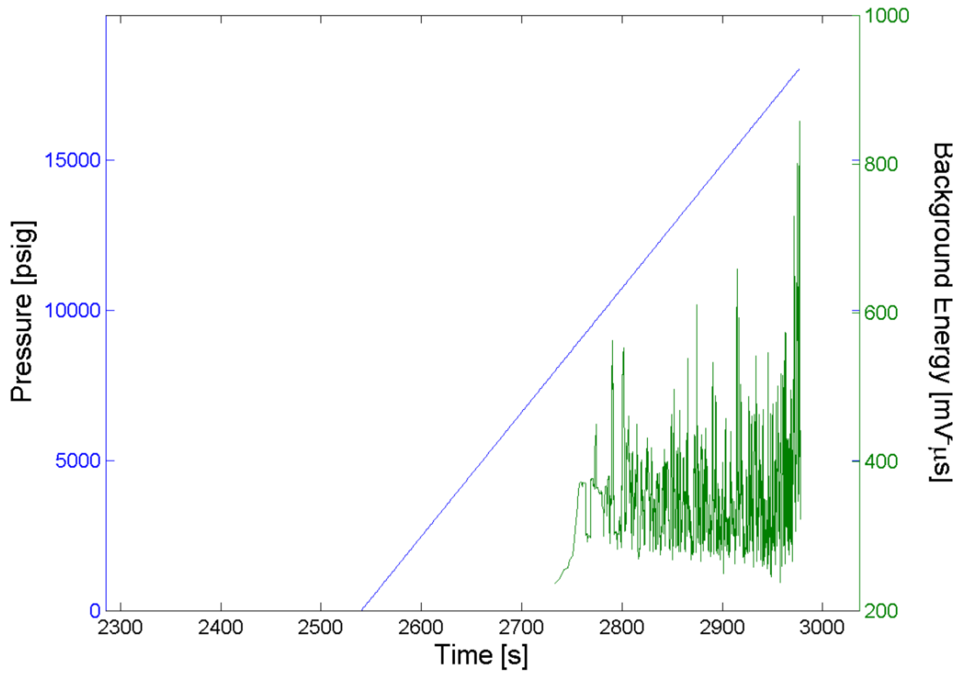

Figure D.16 – Background energy oscillation plot for cylinder ALT639-23993.

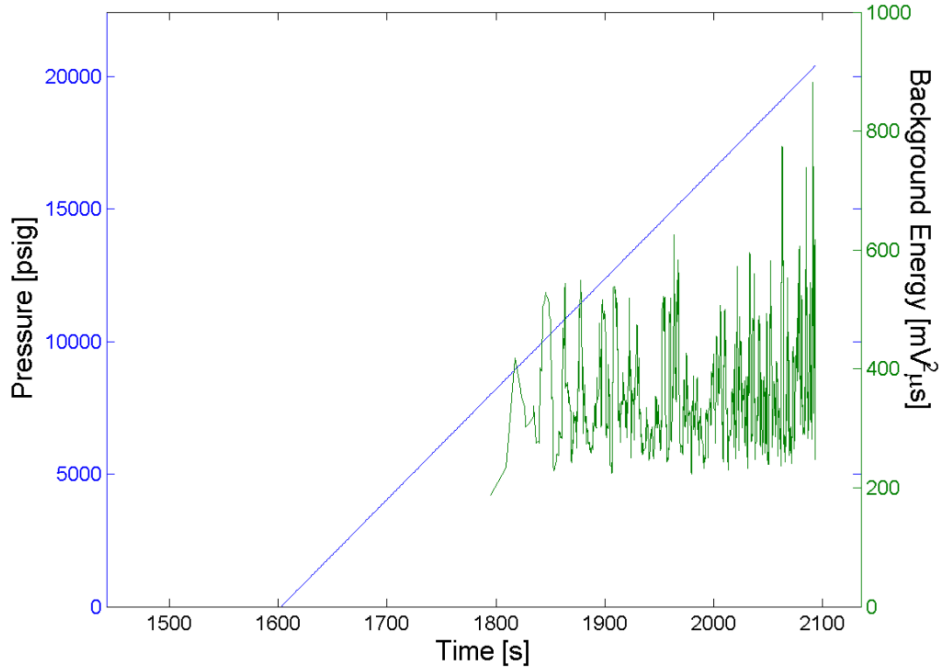

Figure D.17 – Background energy oscillation plot for cylinder ALT639-24574.

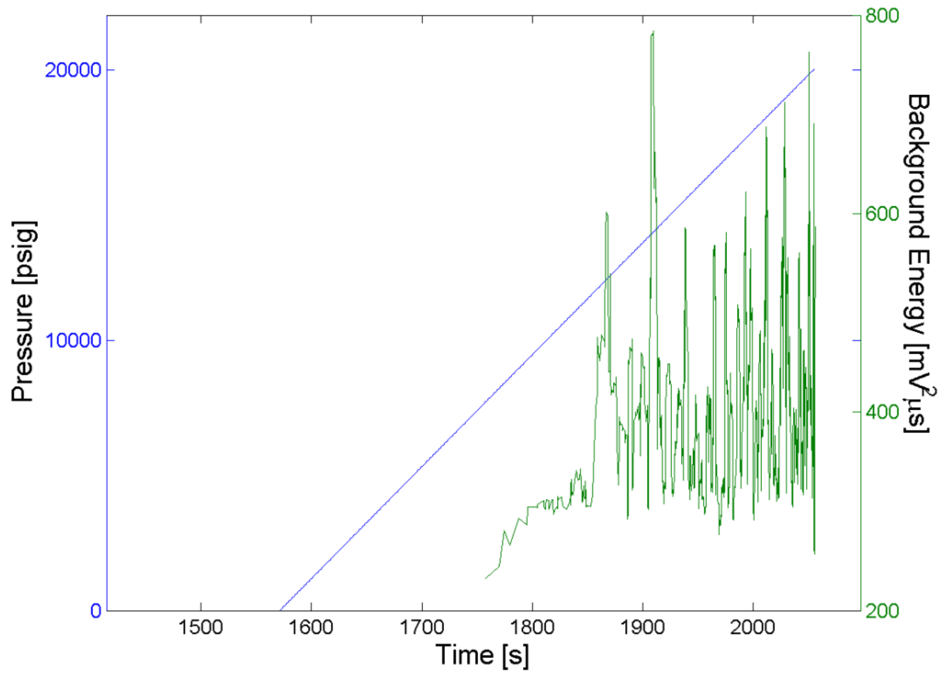

Figure D.18 – Background energy oscillation plot for cylinder ALT639-34005.

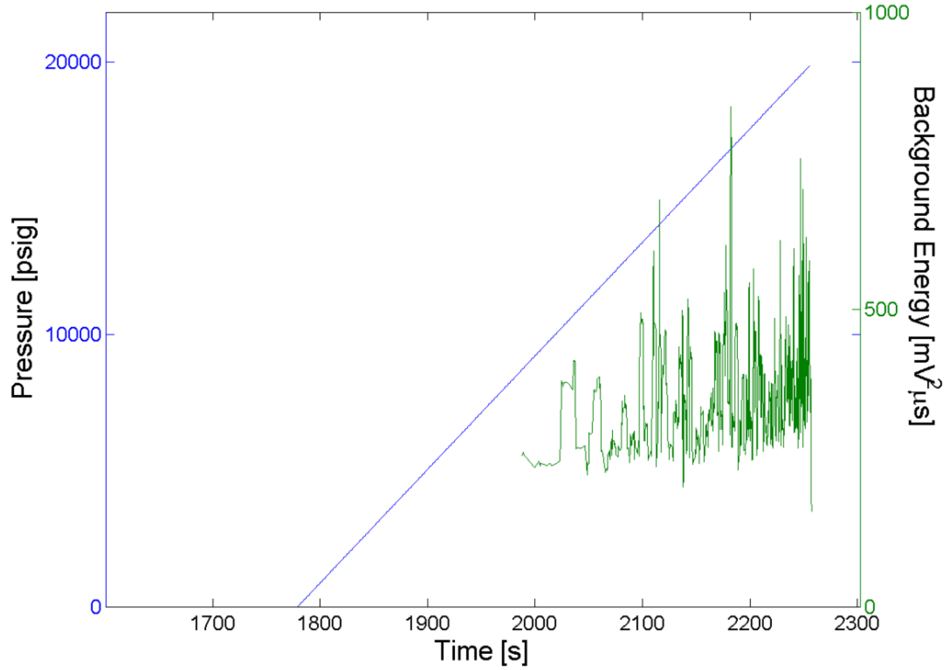

Figure D.19 – Background energy oscillation plot for cylinder ALT639-38566.

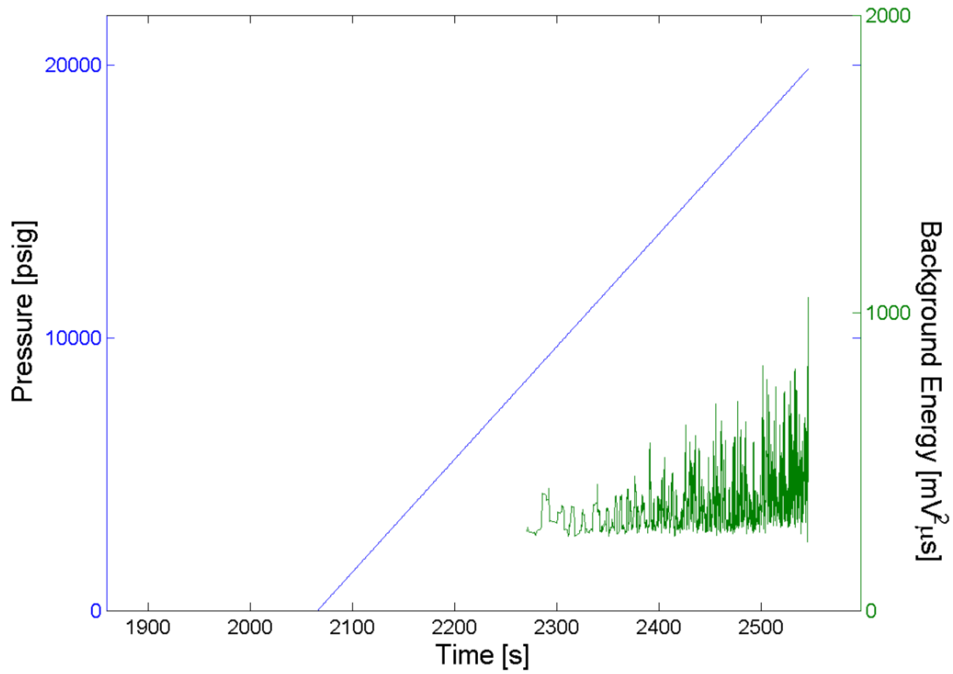

Figure D.20 – Background energy oscillation plot for cylinder ALT639-40136.

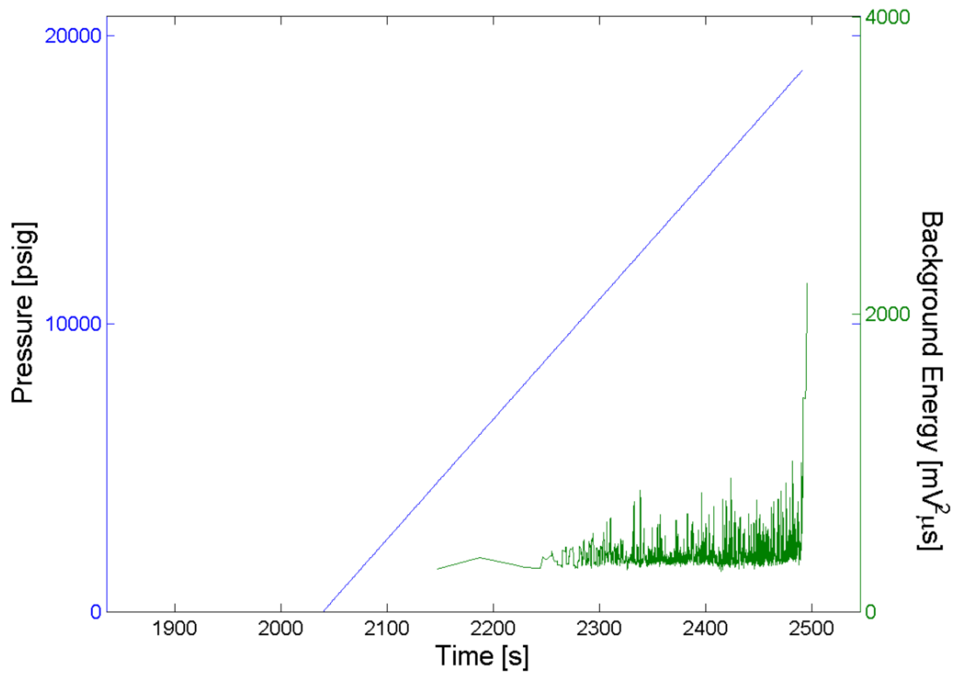

Figure D.21 – Background energy oscillation plot for cylinder ALT639-69988.

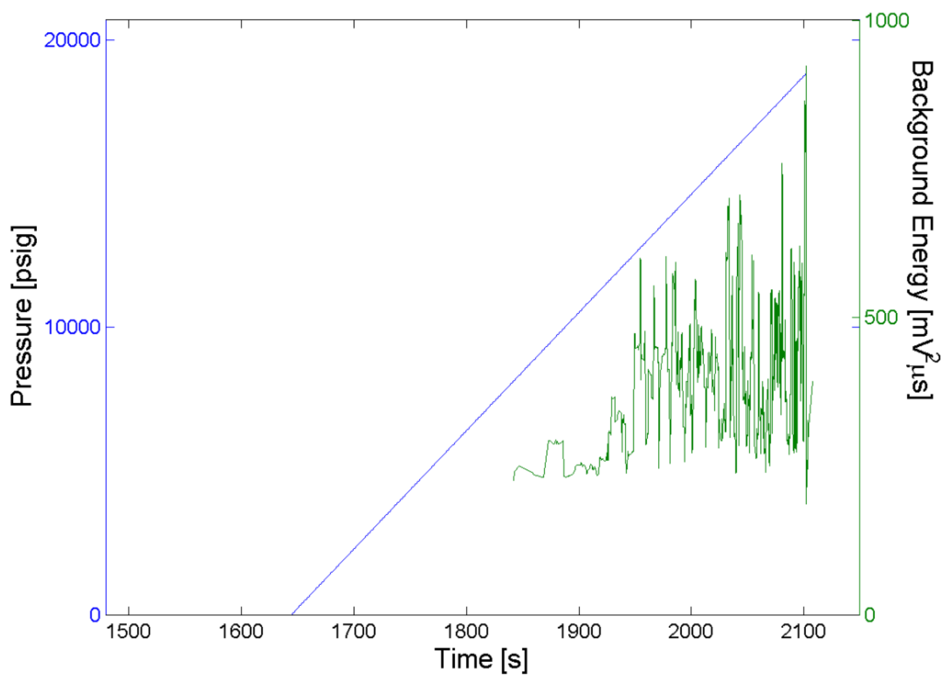

Figure D.22 – Background energy oscillation plot for cylinder ALT695-1862.

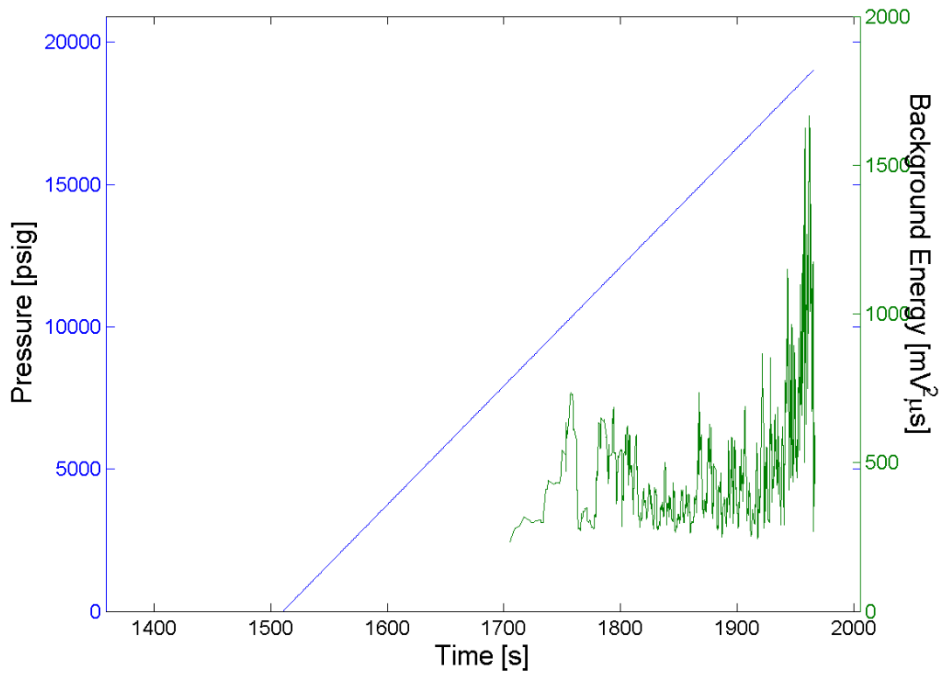

Figure D.23 – Background energy oscillation plot for cylinder ALT695-3224.

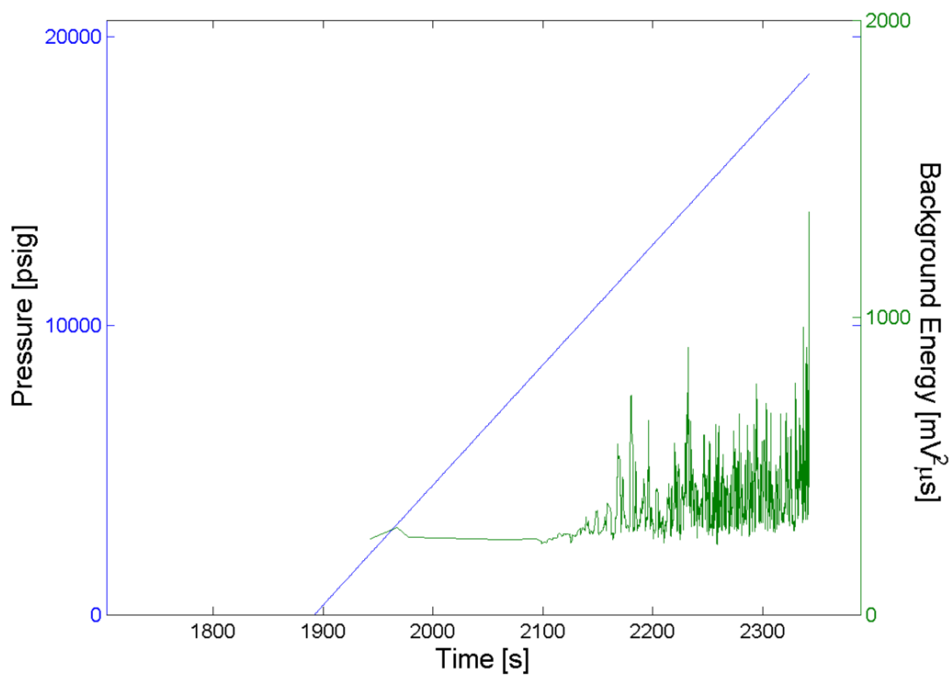

Figure D.24 – Background energy oscillation plot for cylinder ALT695-3313.

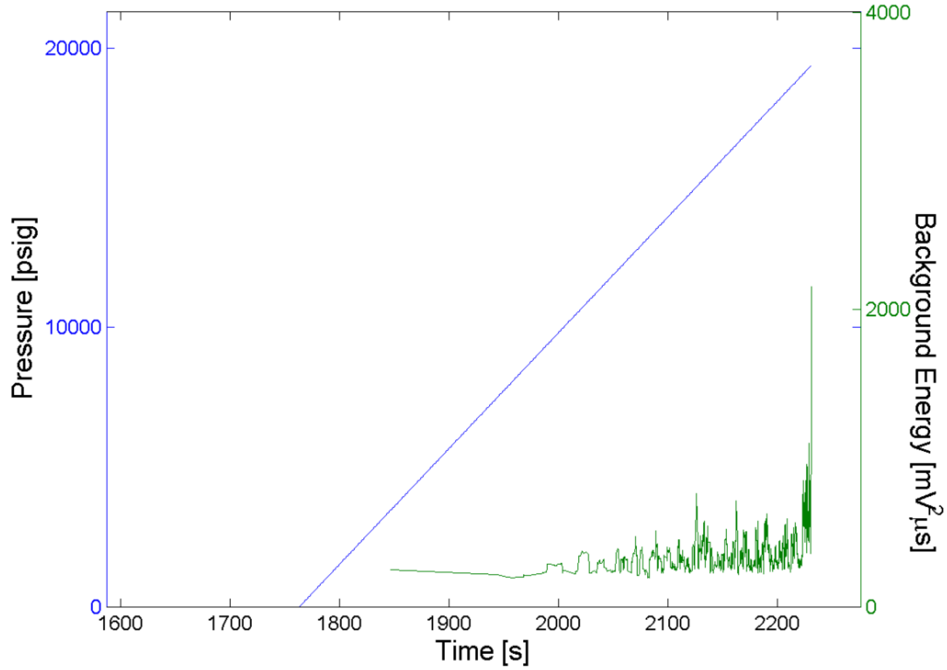

Figure D.25 – Background energy oscillation plot for cylinder ALT695-3575.

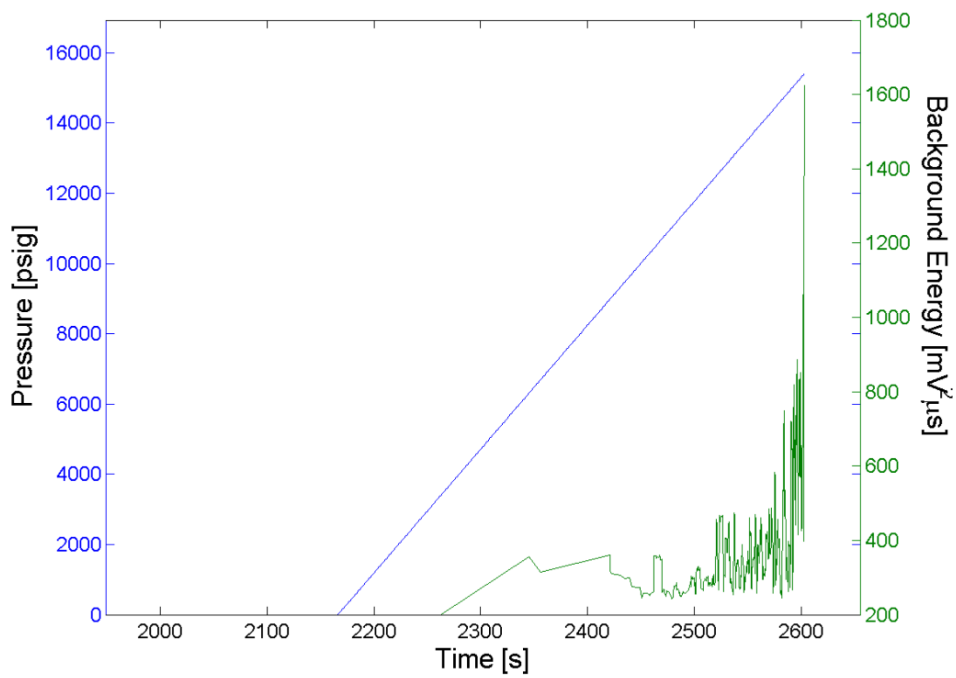

Figure D.26 – Background energy oscillation plot for cylinder ALT695-3646.

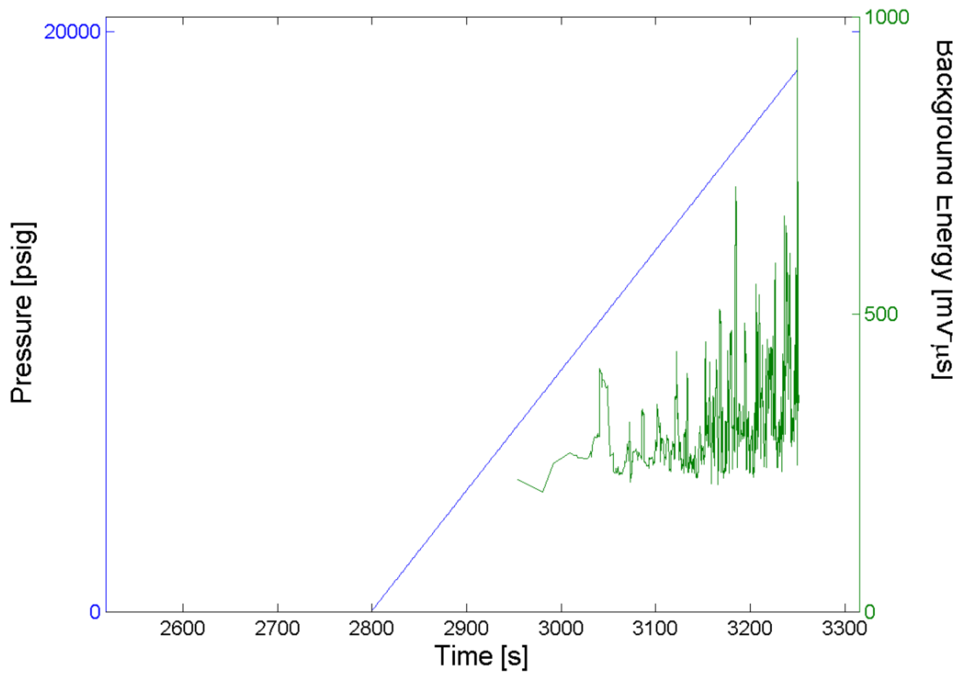

Figure D.27 – Background energy oscillation plot for cylinder ALT695-3771.

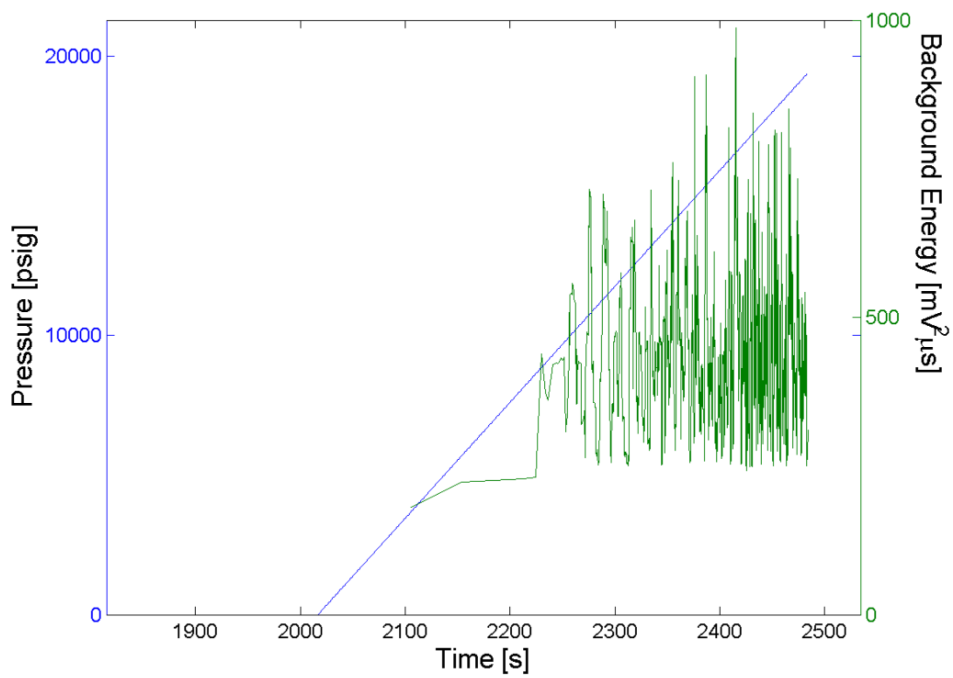

Figure D.28 – Background energy oscillation plot for cylinder ALT695-3798.

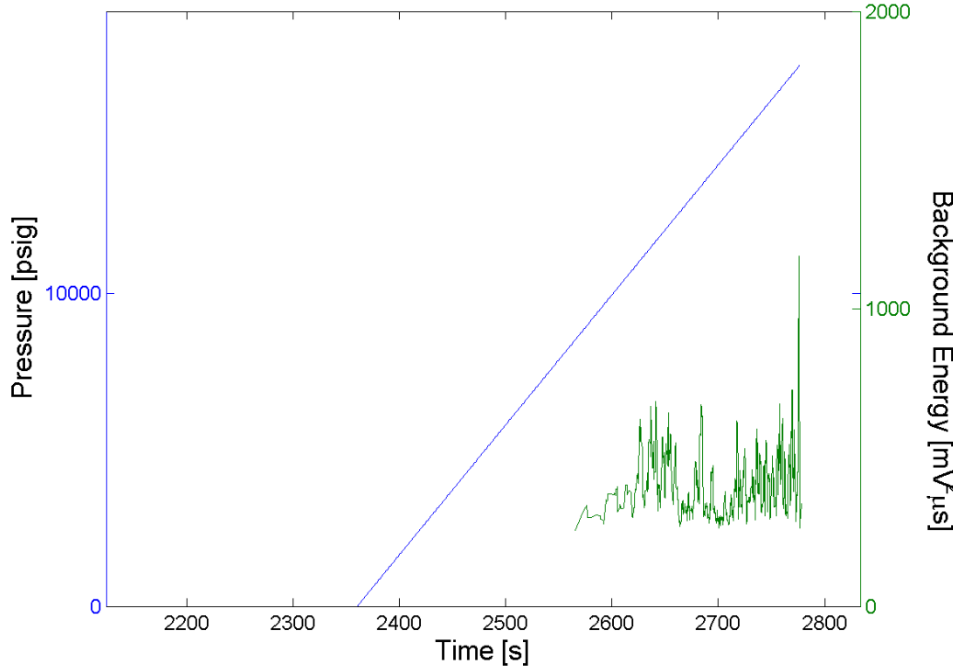

Figure D.29 – Background energy oscillation plot for cylinder ALT695-3881.

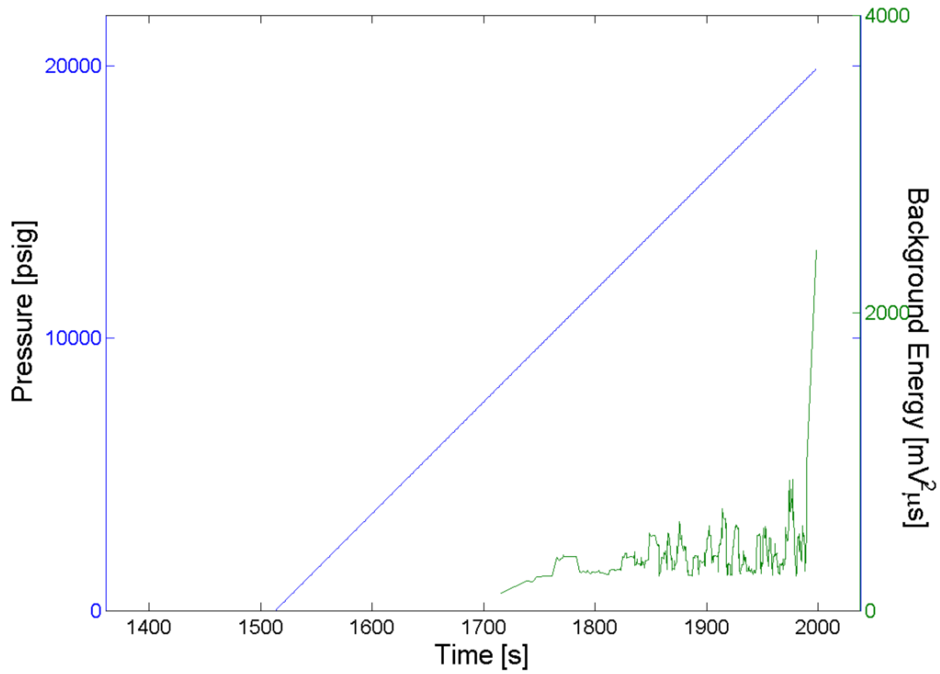

Figure D.30 – Background energy oscillation plot for cylinder ALT695-3936.

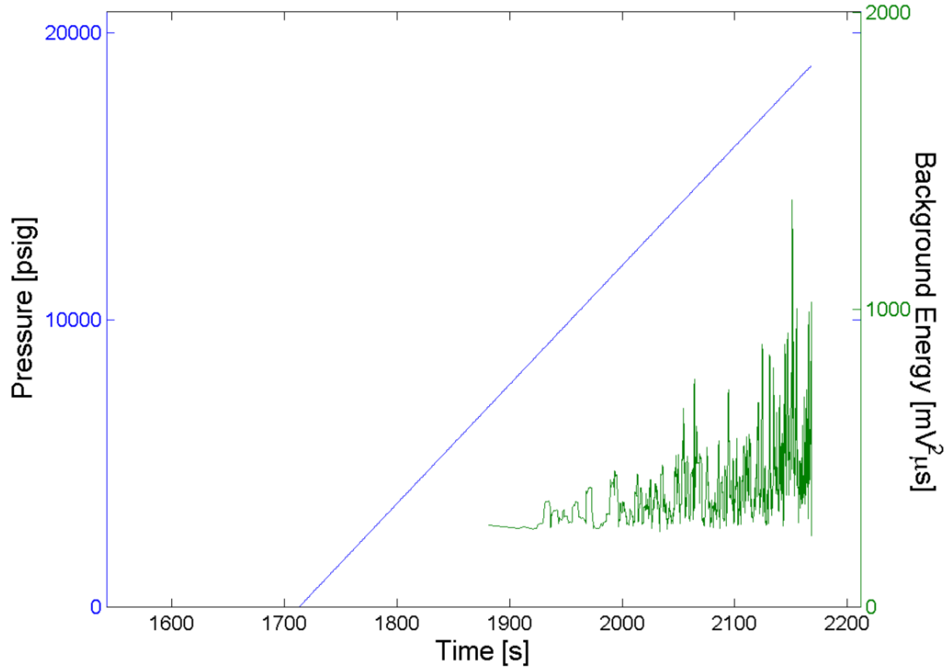

Figure D.31 – Background energy oscillation plot for cylinder ALT695-4379.

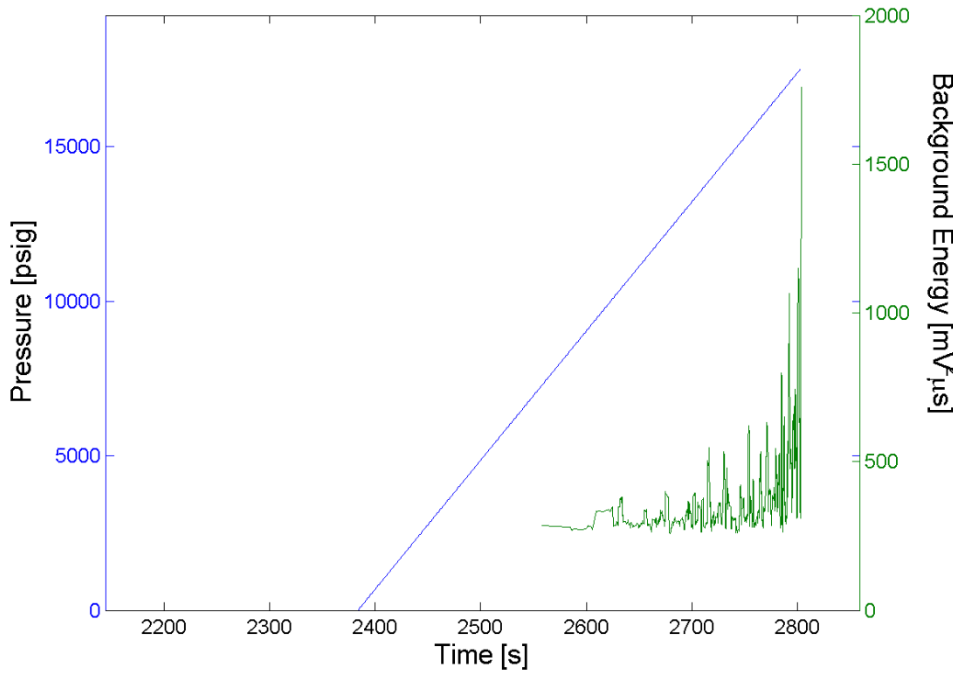

Figure D.32 – Background energy oscillation plot for cylinder ALT695-4396.

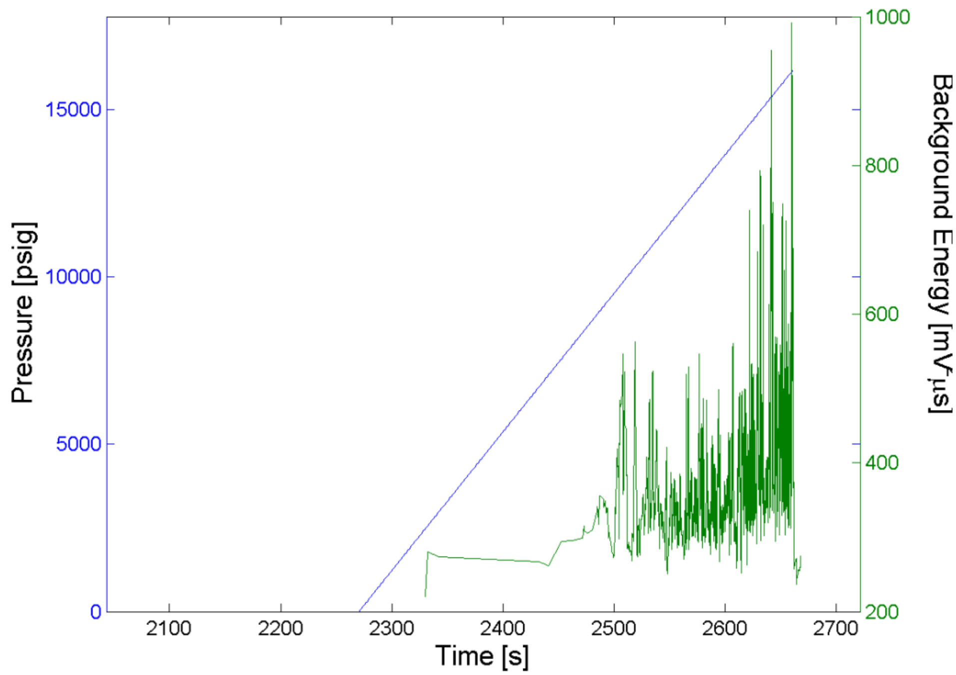

Figure D.33 – Background energy oscillation plot for cylinder ALT695-4469.

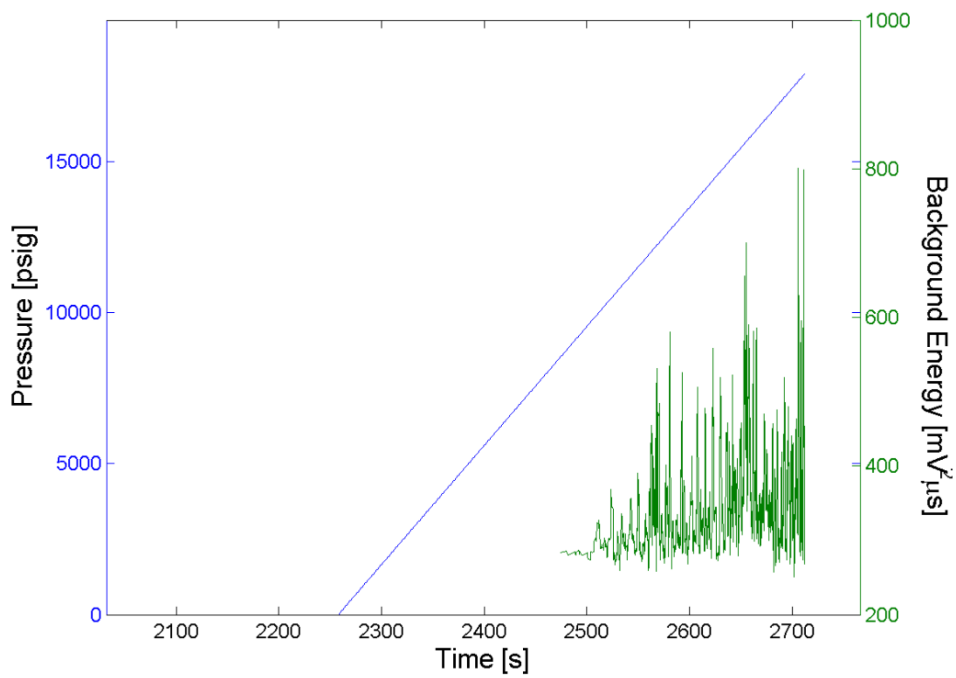

Figure D.34 – Background energy oscillation plot for cylinder ALT695-4482.

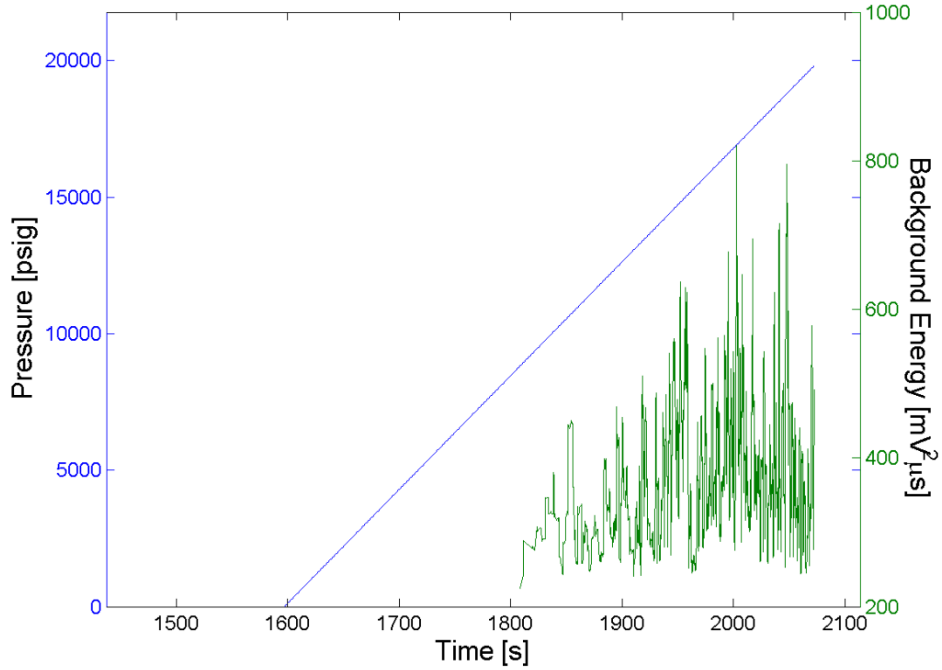

Figure D.35 – Background energy oscillation plot for cylinder ALT695-4492.

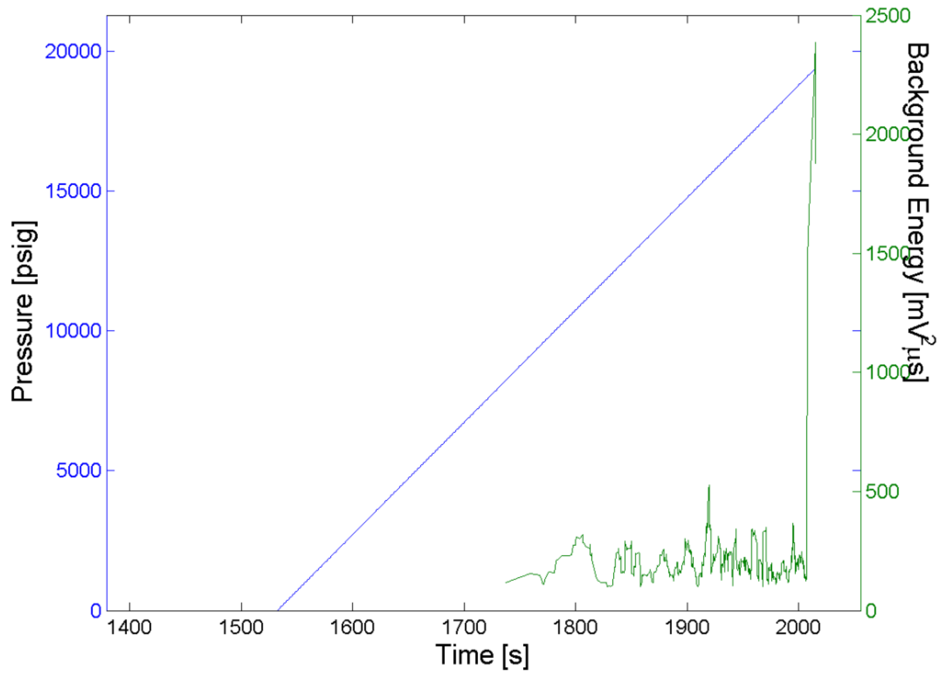

Figure D.36 – Background energy oscillation plot for cylinder ALT695-4734.

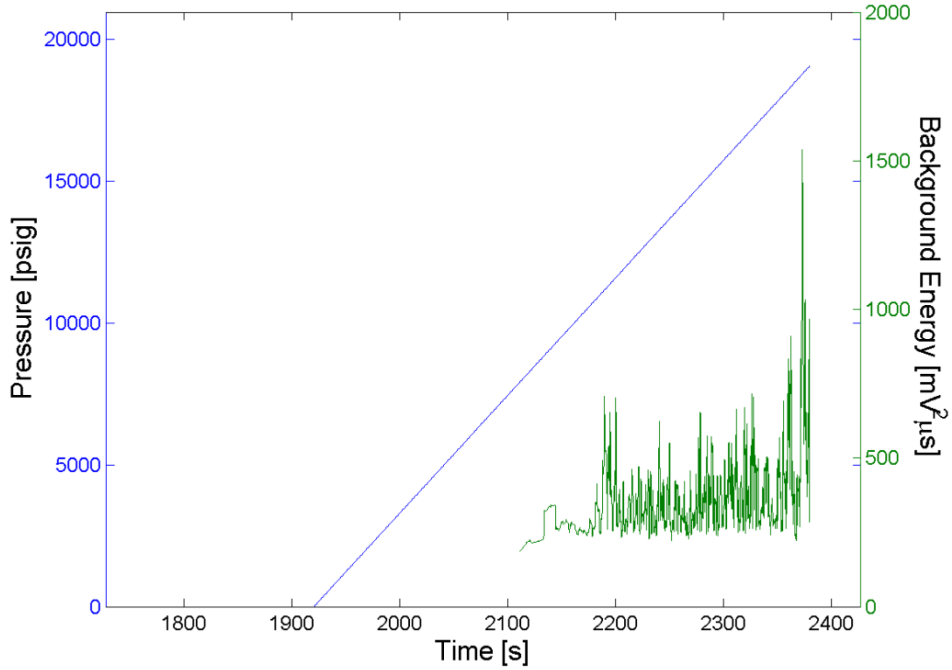

Figure D.37 – Background energy oscillation plot for cylinder ALT695-4775.

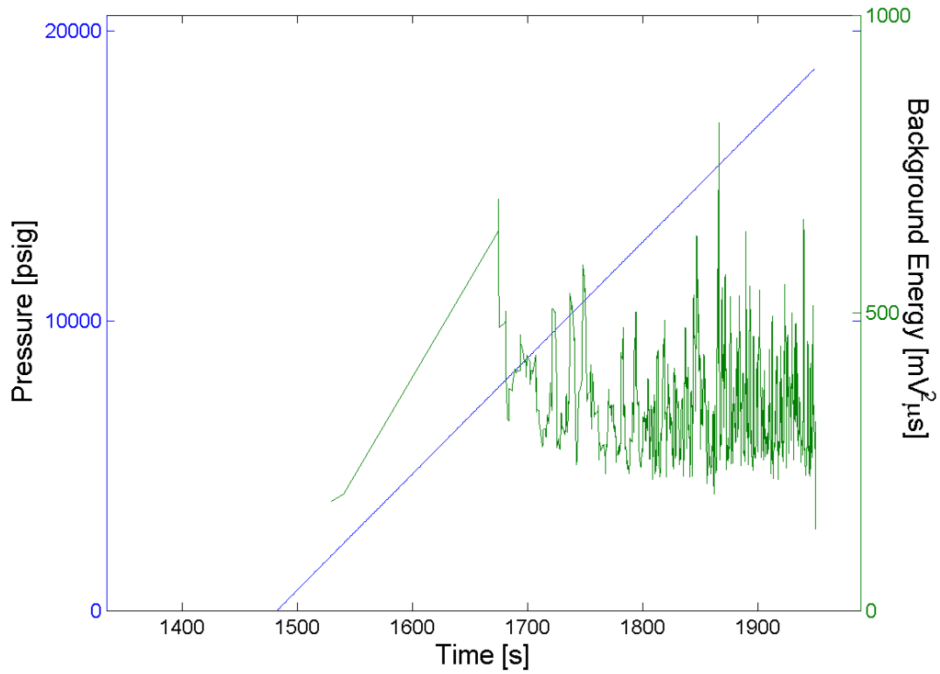

Figure D.38 – Background energy oscillation plot for cylinder ALT695-4944.

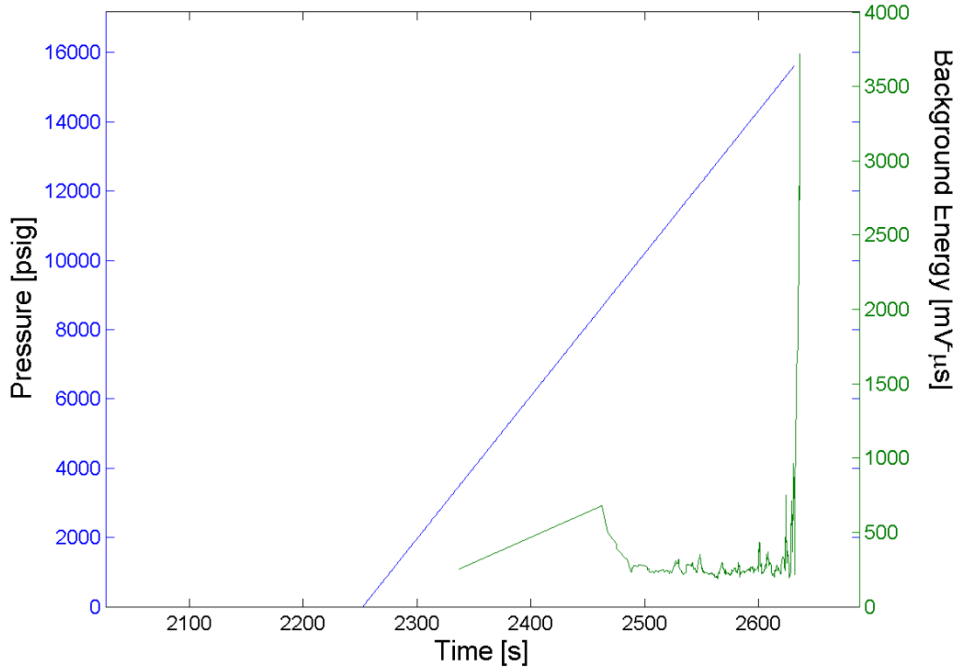

Figure D.39 – Background energy oscillation plot for cylinder ALT695-5497.

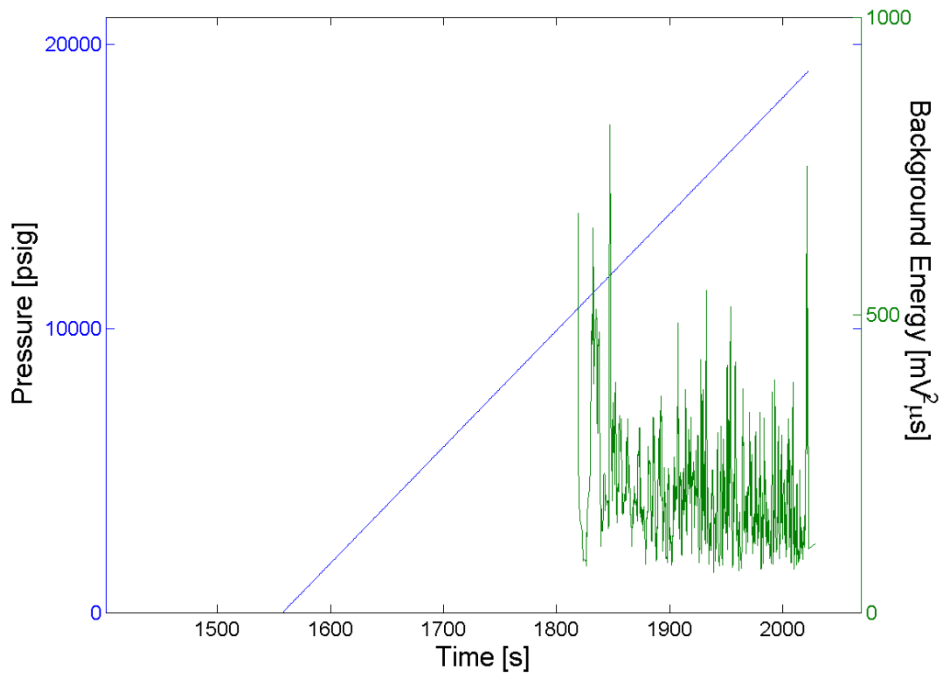

Figure D.40 – Background energy oscillation plot for cylinder ALT695-5558.

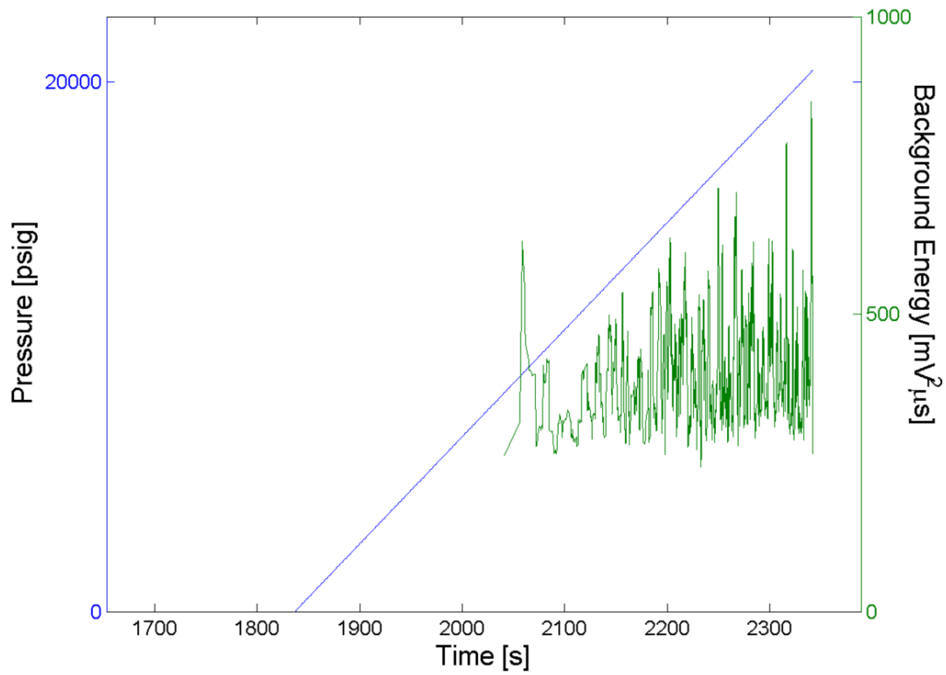

Figure D.41 – Background energy oscillation plot for cylinder ALT695-5641.

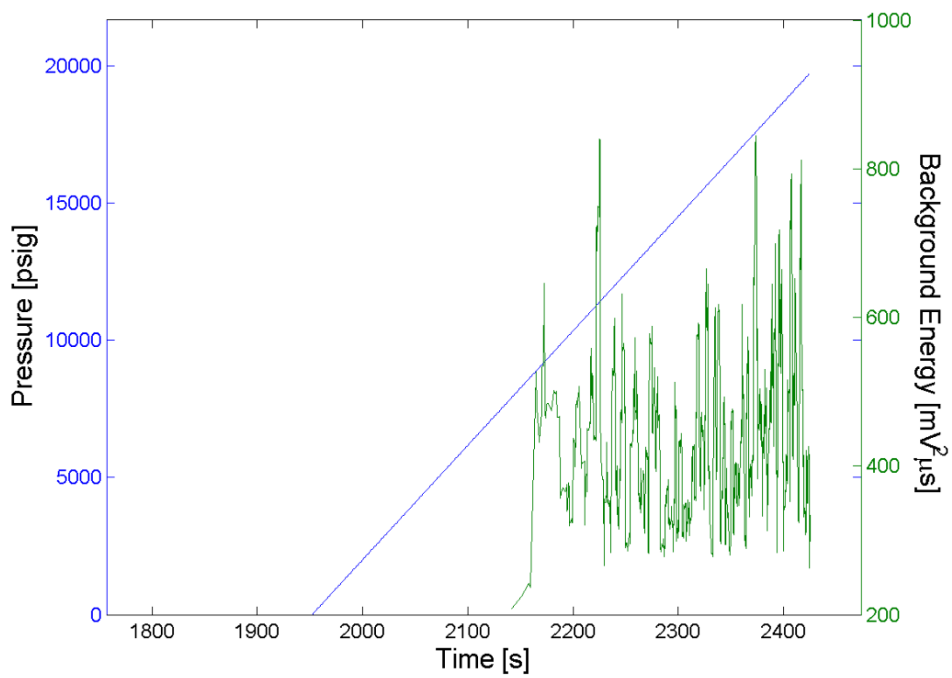

Figure D.42 – Background energy oscillation plot for cylinder ALT695-6041.

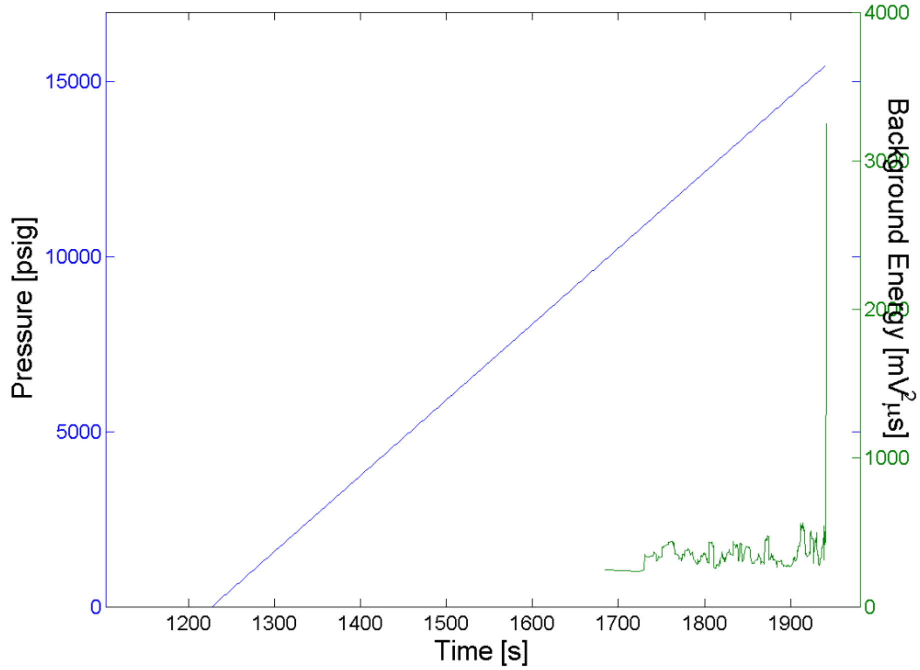

Figure D.43 – Background energy oscillation plot for cylinder IH667.

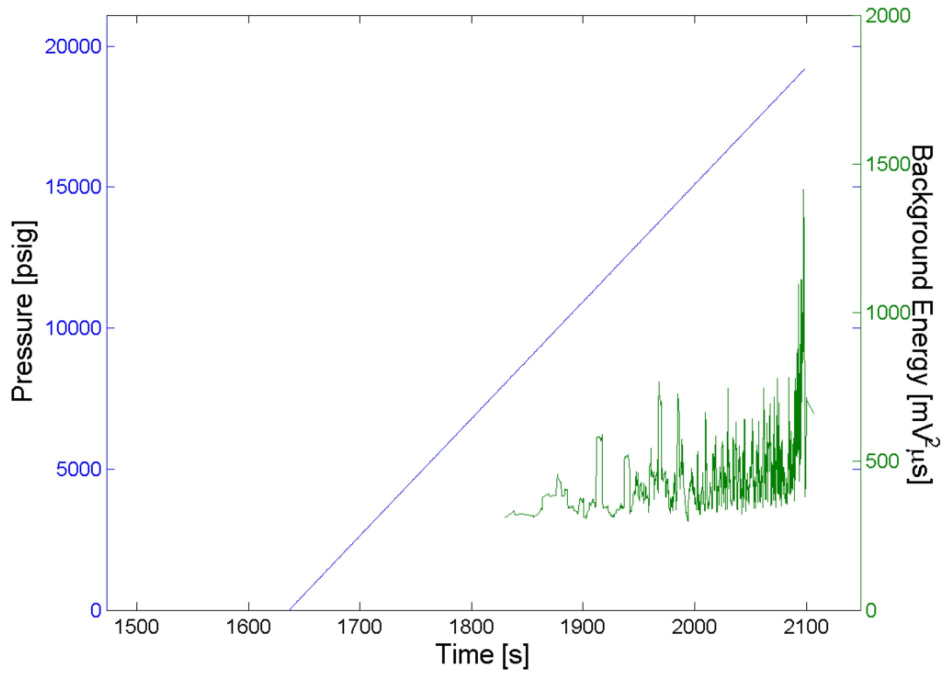

Figure D.44 – Background energy oscillation plot for cylinder IL2705.

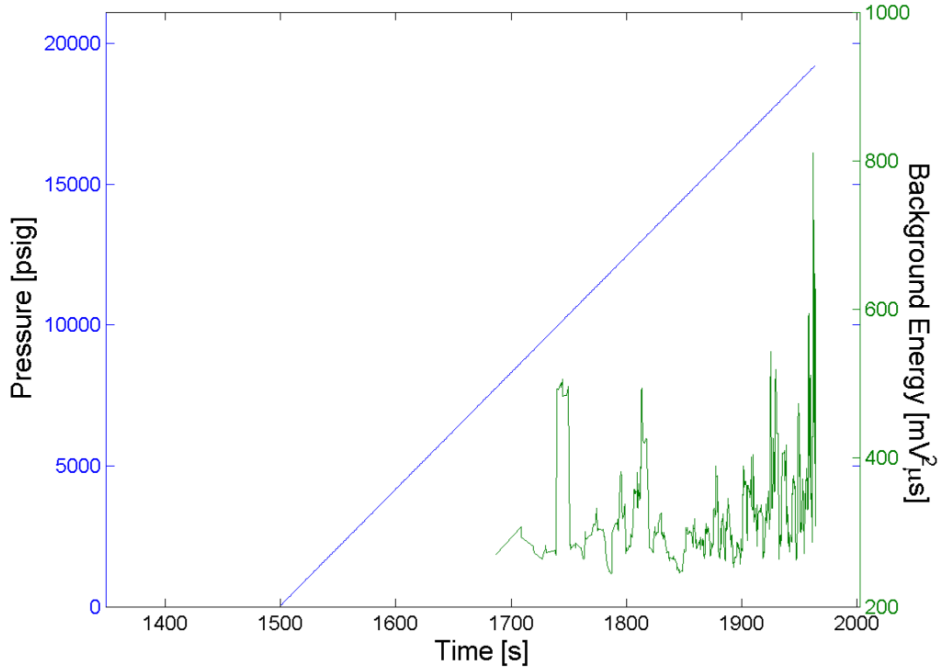

Figure D.45 – Background energy oscillation plot for cylinder IL2722.

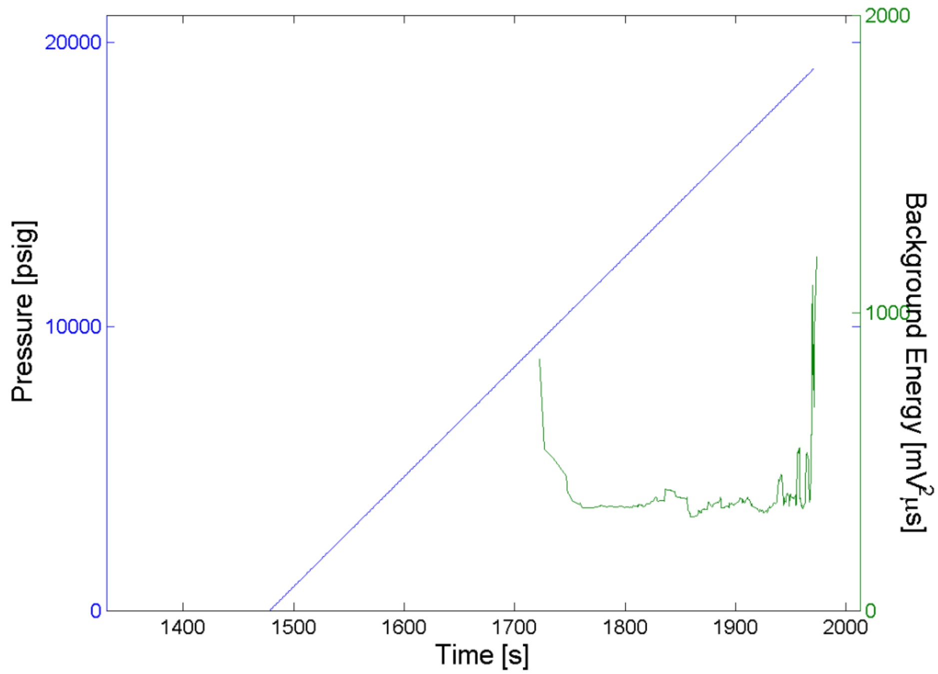

Figure D.46 – Background energy oscillation plot for cylinder IL2933.

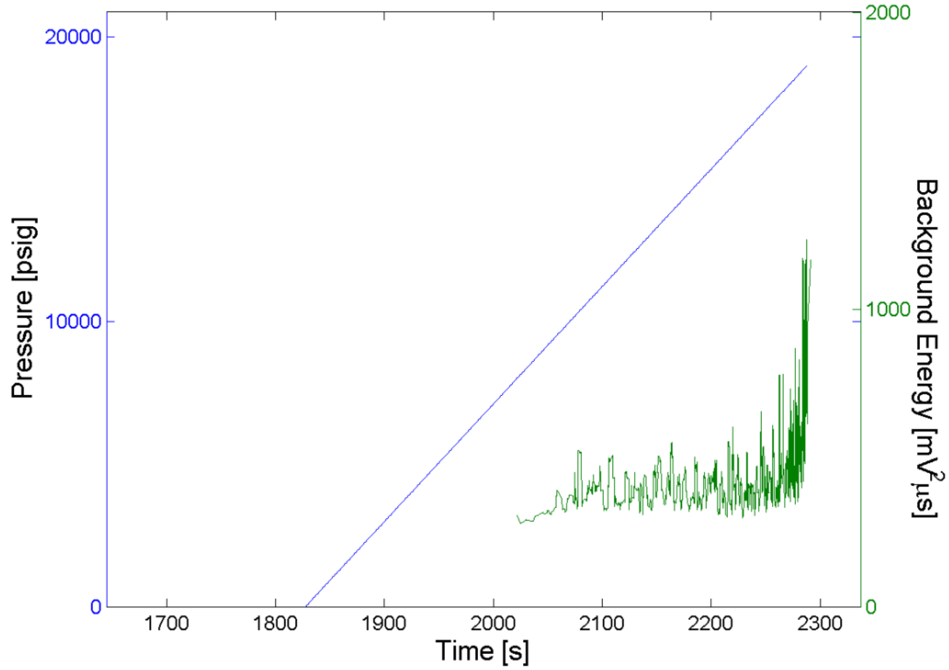

Figure D.47 – Background energy oscillation plot for cylinder IL3334.

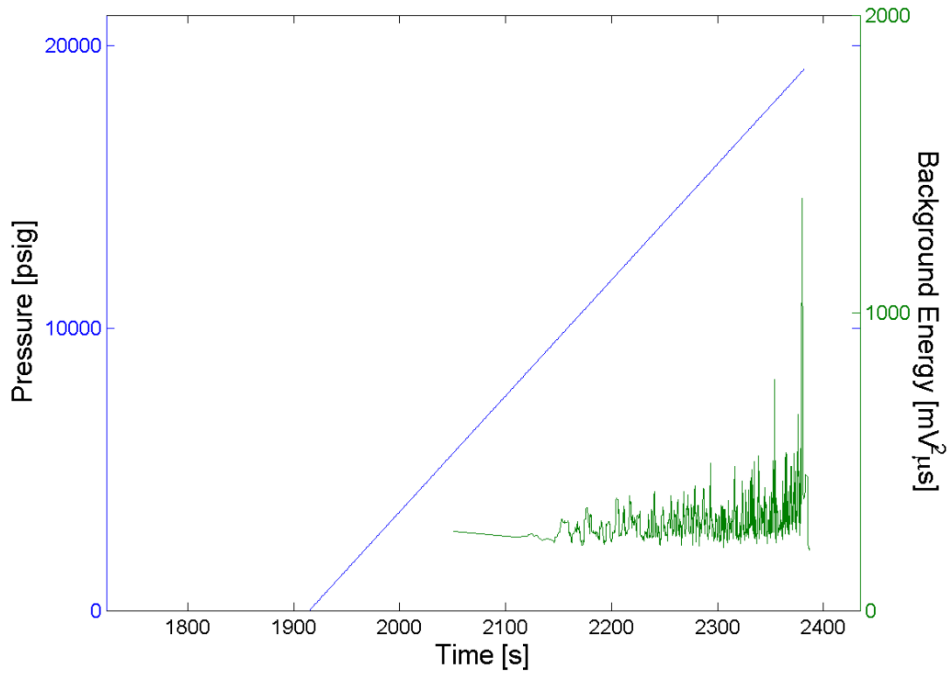

Figure D.48 – Background energy oscillation plot for cylinder OK85342.

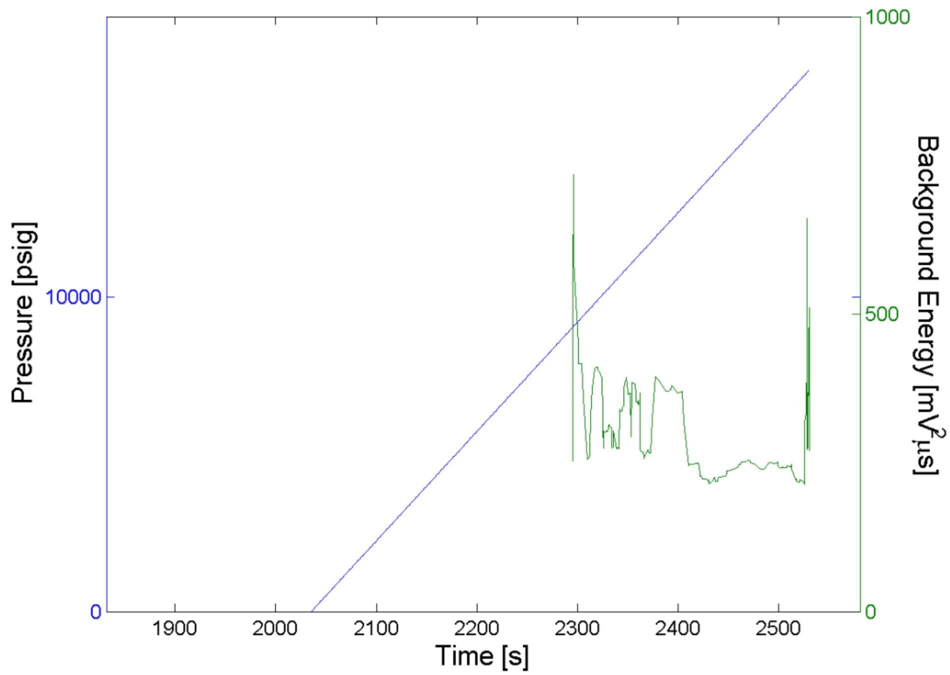

Figure D.49 – Background energy oscillation plot for cylinder ON3077.

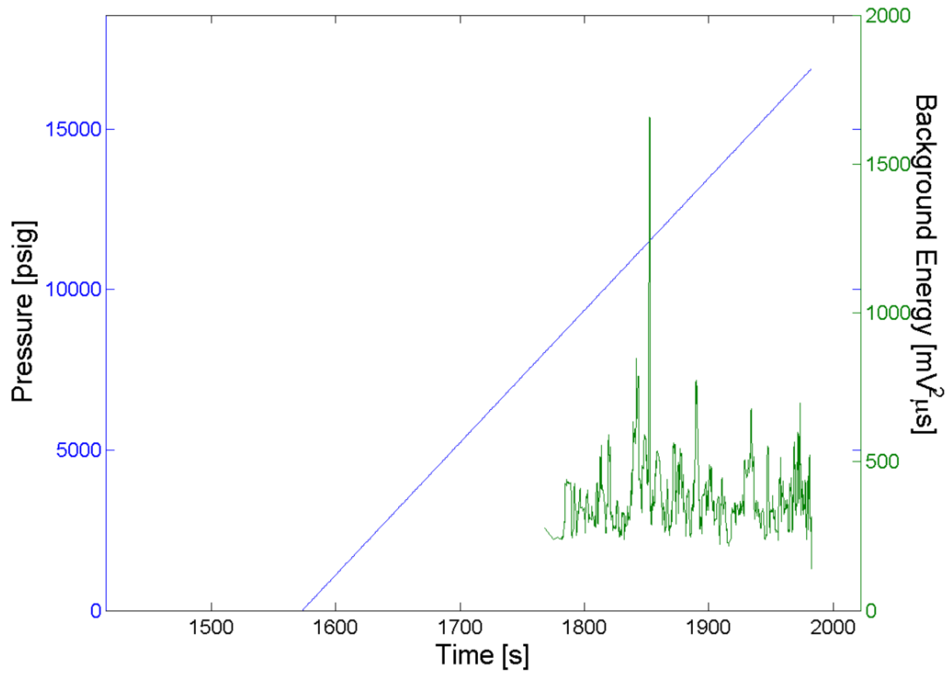

Figure D.50 – Background energy oscillation plot for cylinder ON3146.

12. Appendix E – MAE source mechanism plots

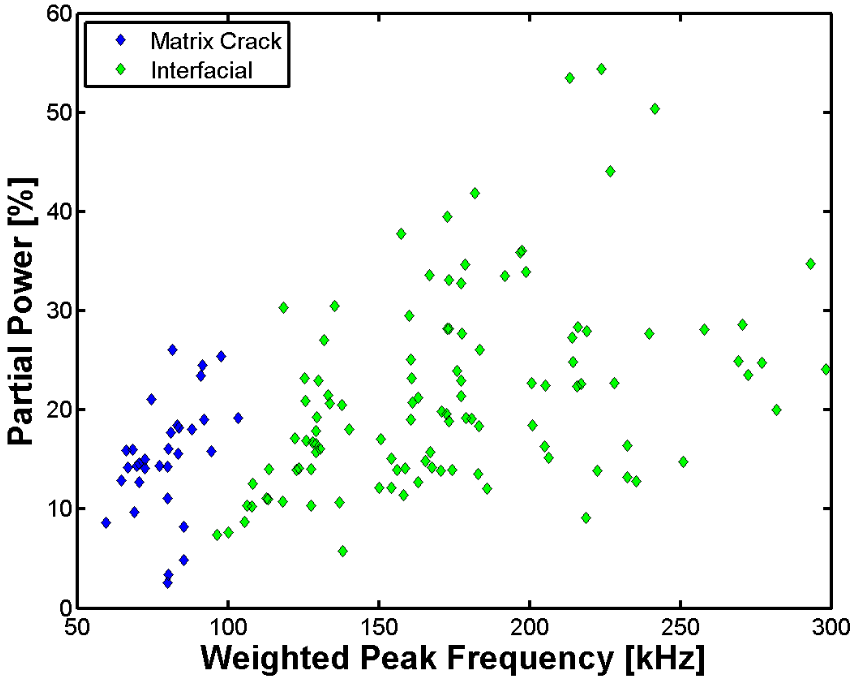

Figure E.1 – Source mechanism plot for cylinder ALT604-5155.

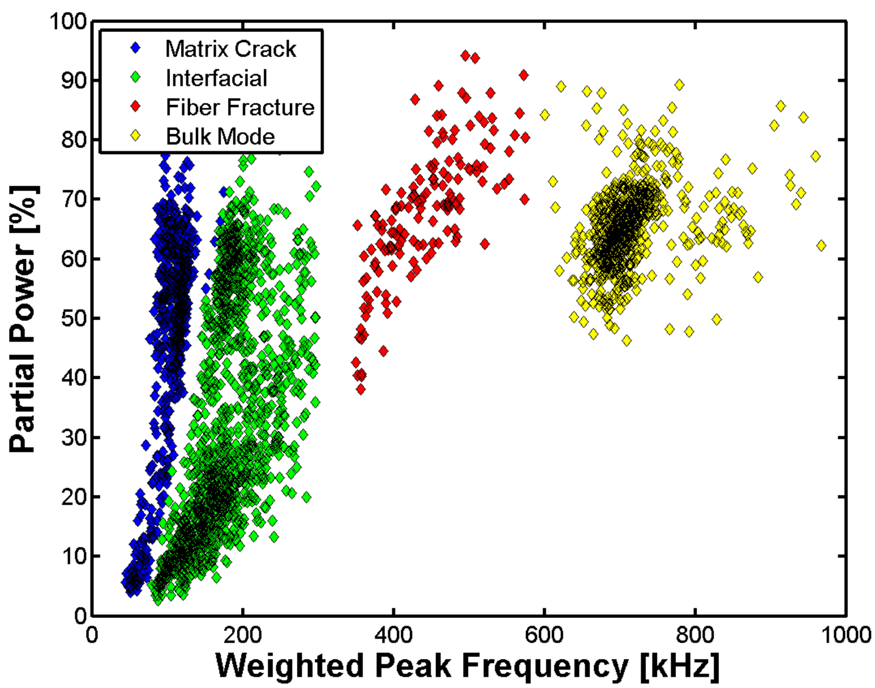

Figure E.2 – Source mechanism plot for cylinder ALT604-5553.

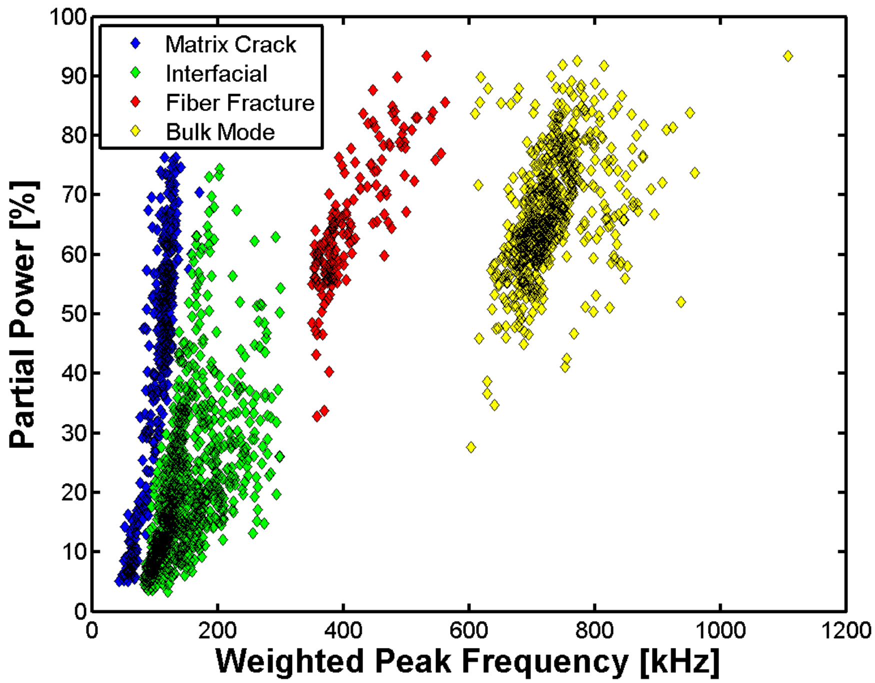

Figure E.3 – Source mechanism plot for cylinder ALT604-5561.

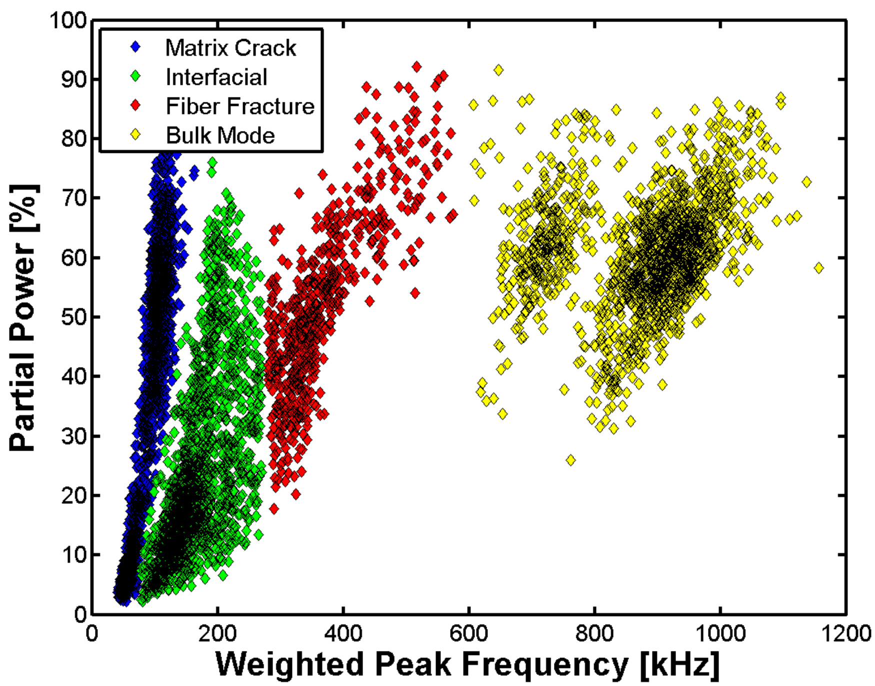

Figure E.4 – Source mechanism plot for cylinder ALT604-6707.

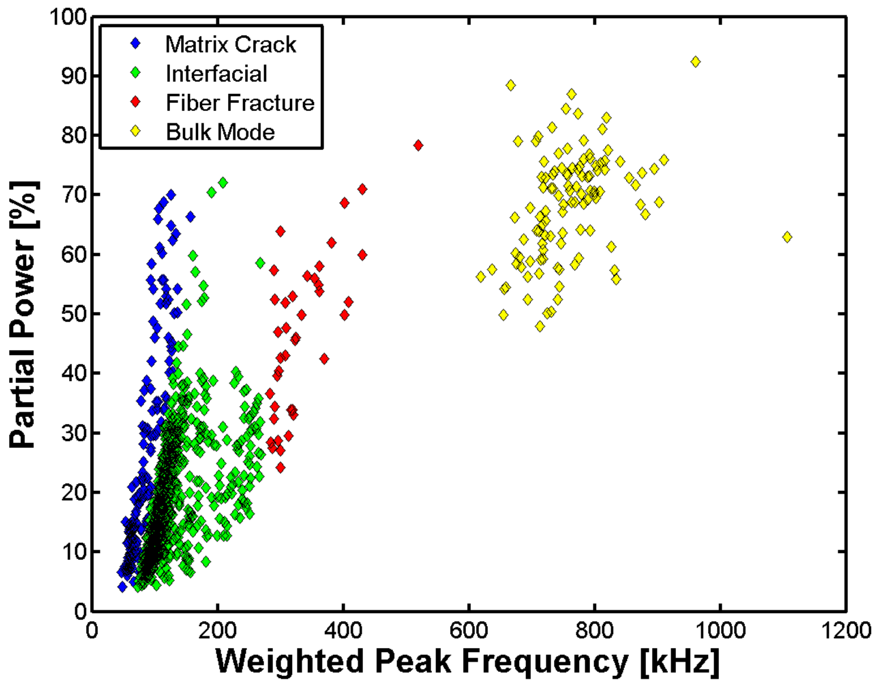

Figure E.5 – Source mechanism plot for cylinder ALT639-4101.

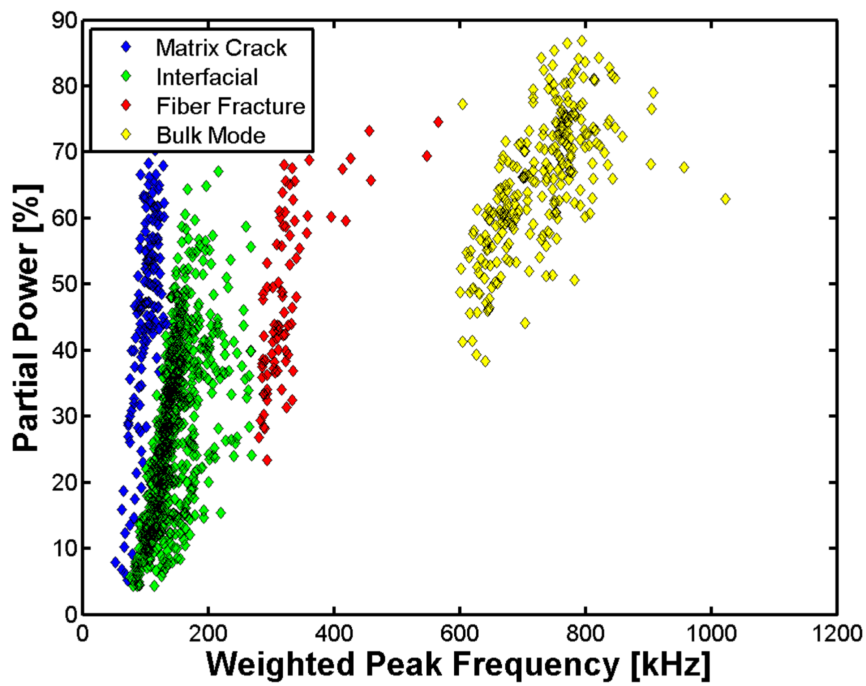

Figure E.6 – Source mechanism plot for cylinder ALT639-4610.

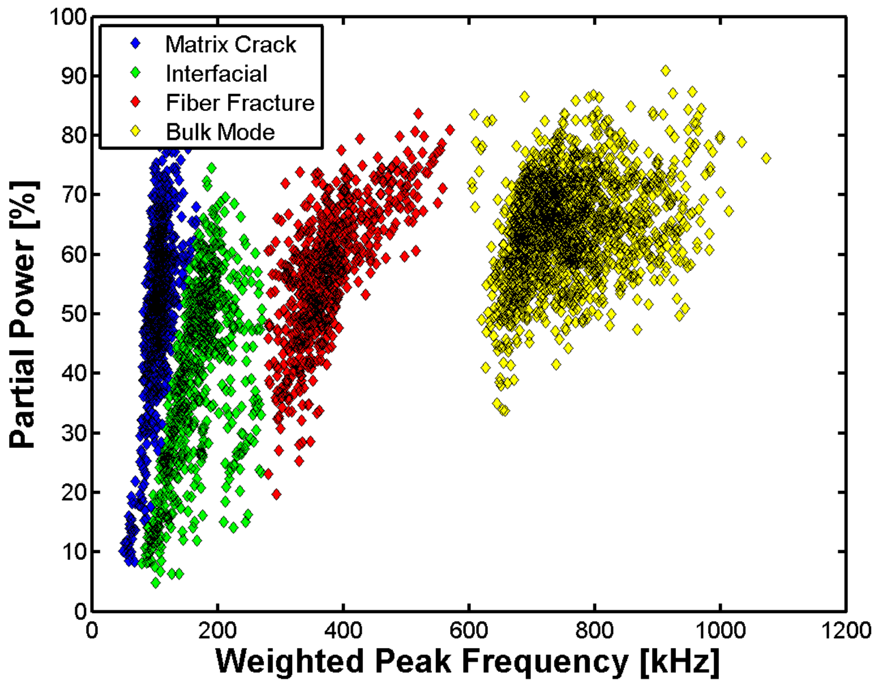

Figure E.7 – Source mechanism plot for cylinder ALT639-5224.

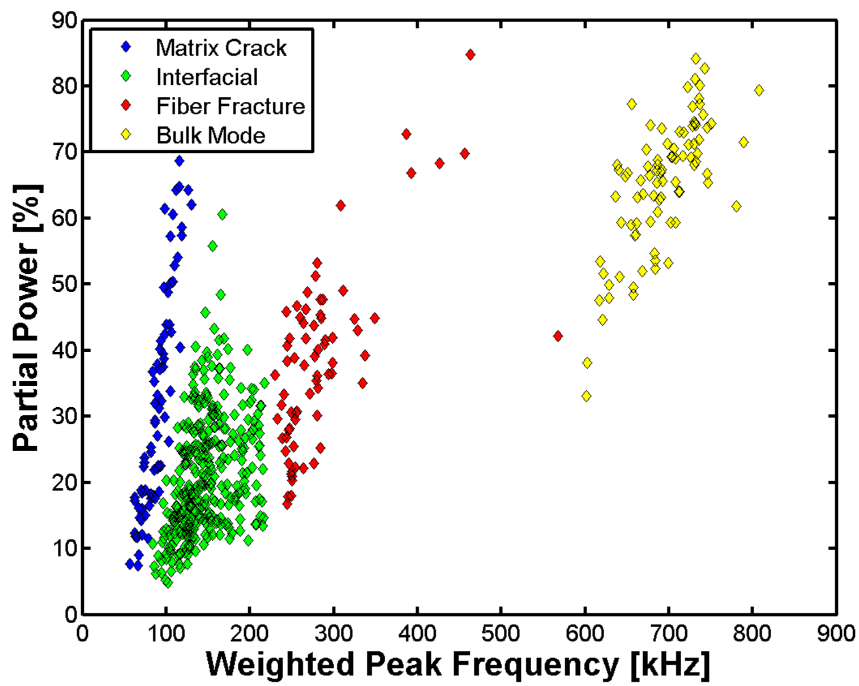

Figure E.8 – Source mechanism plot for cylinder ALT639-9435.

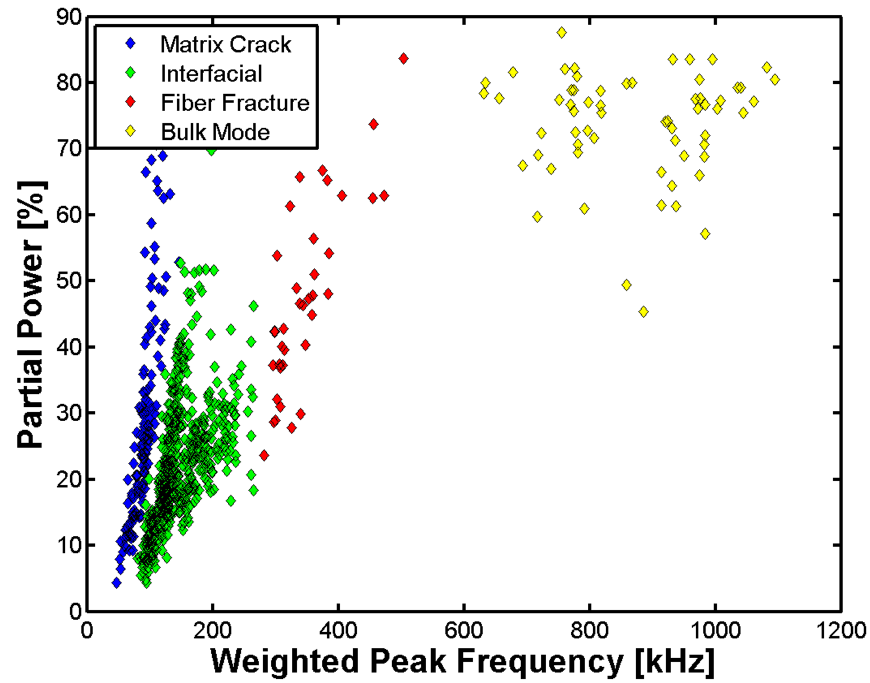

Figure E.9 – Source mechanism plot for cylinder ALT639-9528.

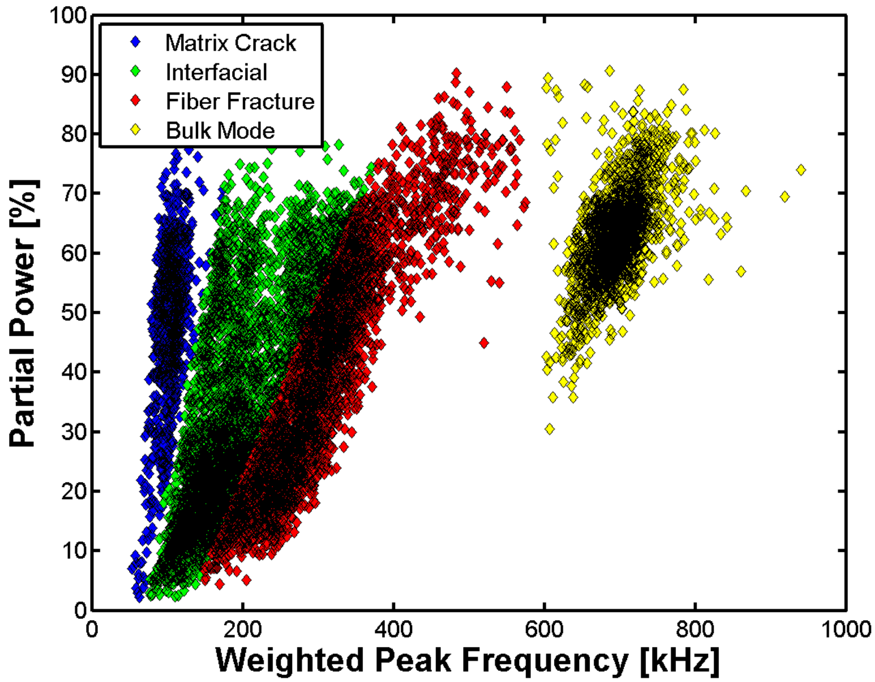

Figure E.10 – Source mechanism plot for cylinder ALT639-9941.

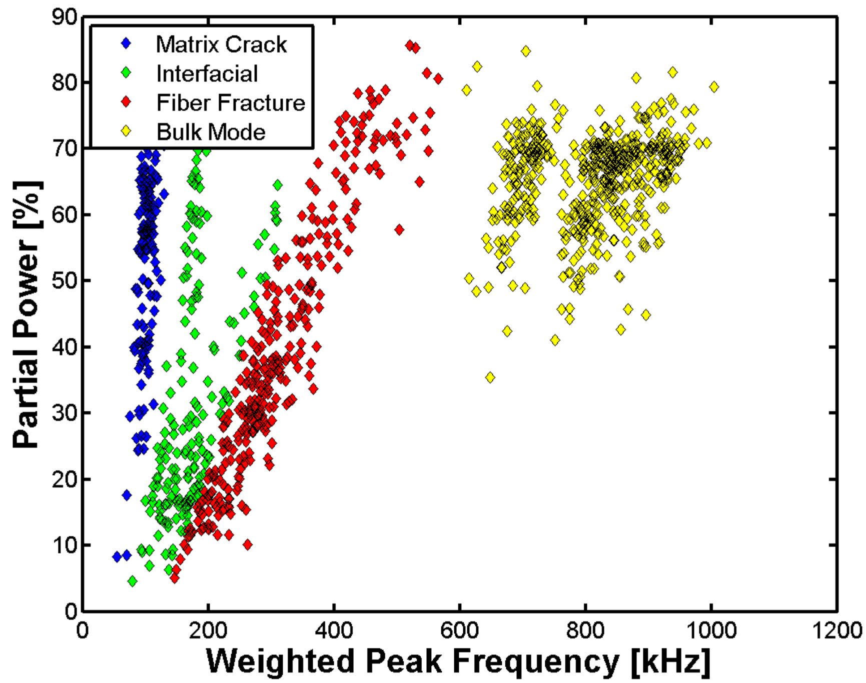

Figure E.11 – Source mechanism plot for cylinder ALT639-17714.

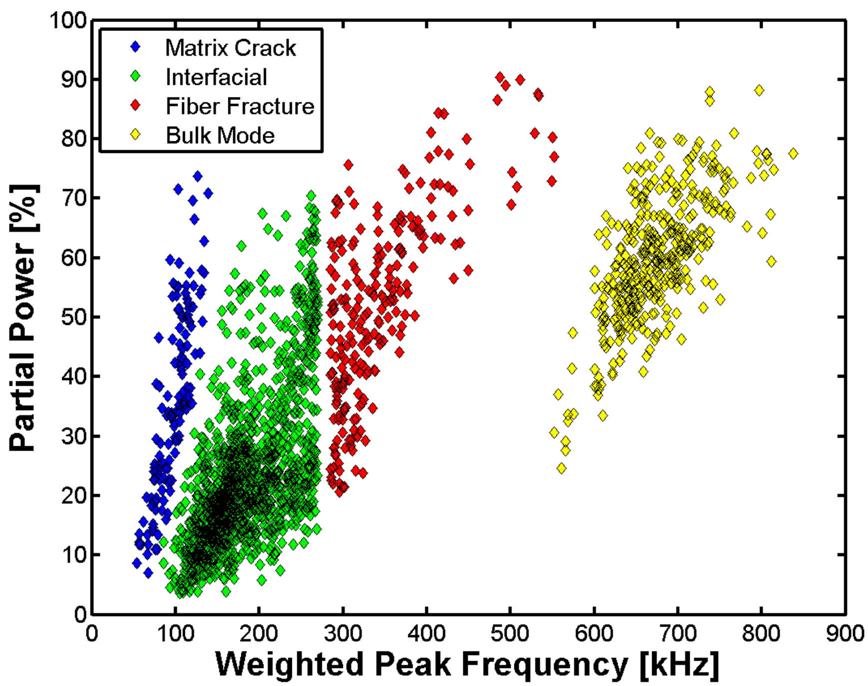

Figure E.12 – Source mechanism plot for cylinder ALT639-18594.

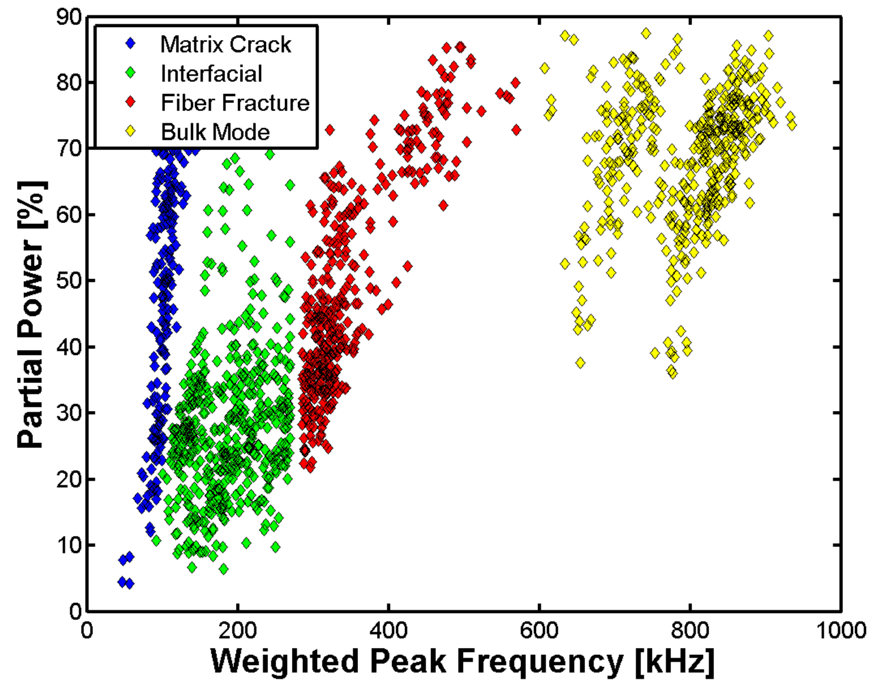

Figure E.13 – Source mechanism plot for cylinder ALT639-18682.

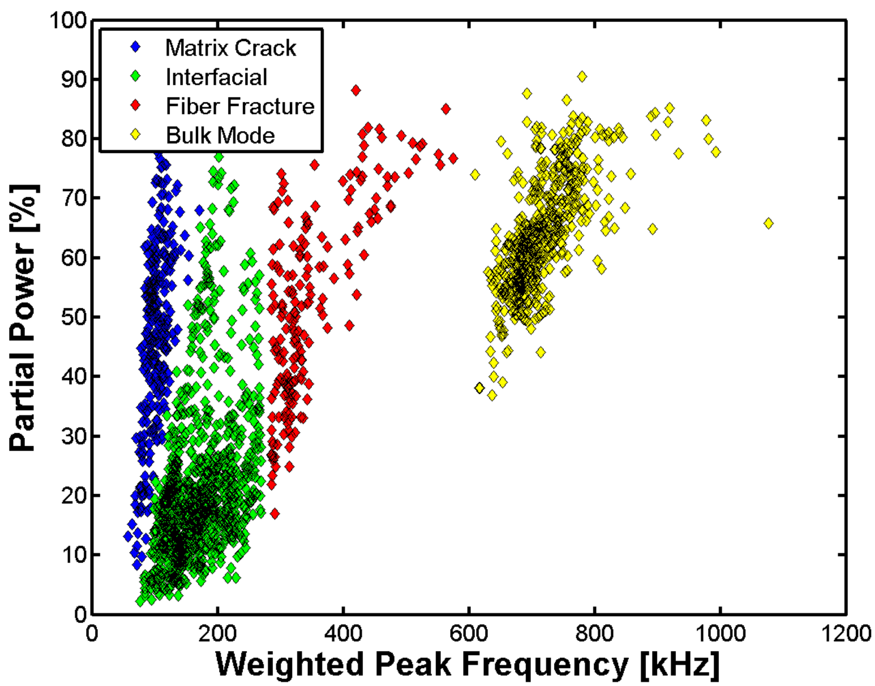

Figure E.14 – Source mechanism plot for cylinder ALT639-19008.

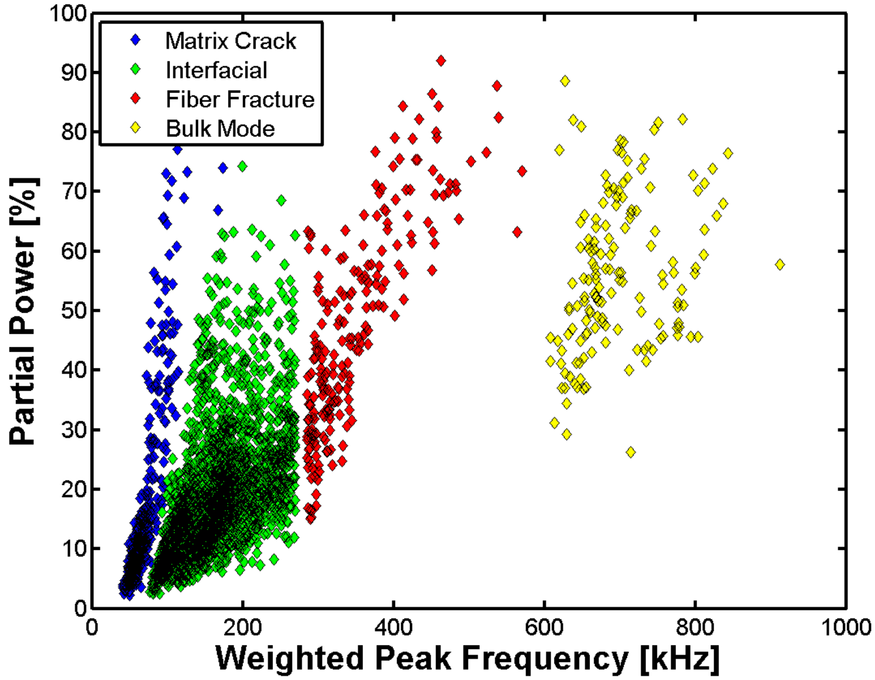

Figure E.15 – Source mechanism plot for cylinder ALT639-22931.

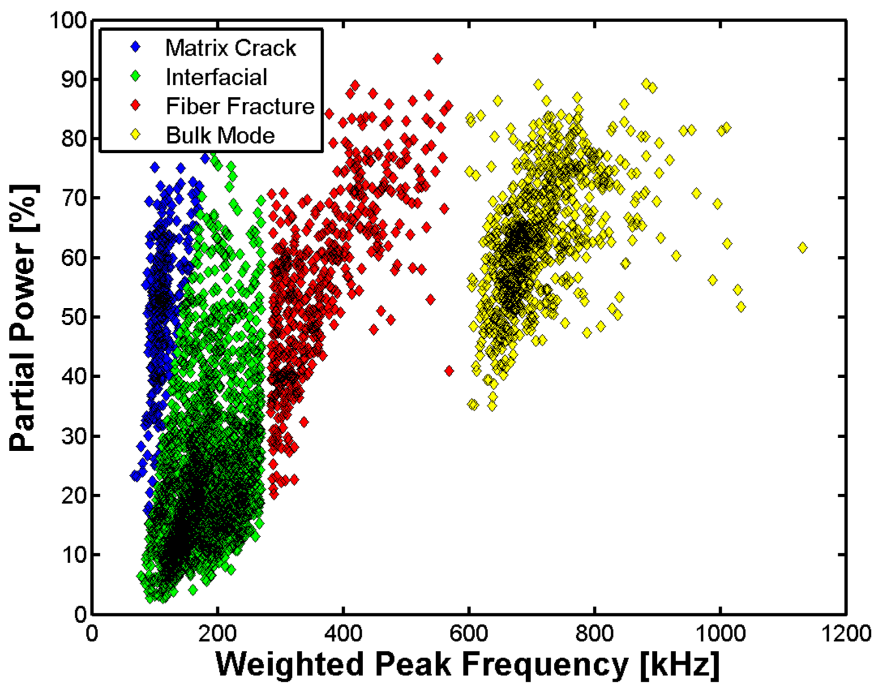

Figure E.16 – Source mechanism plot for cylinder ALT639-23993.

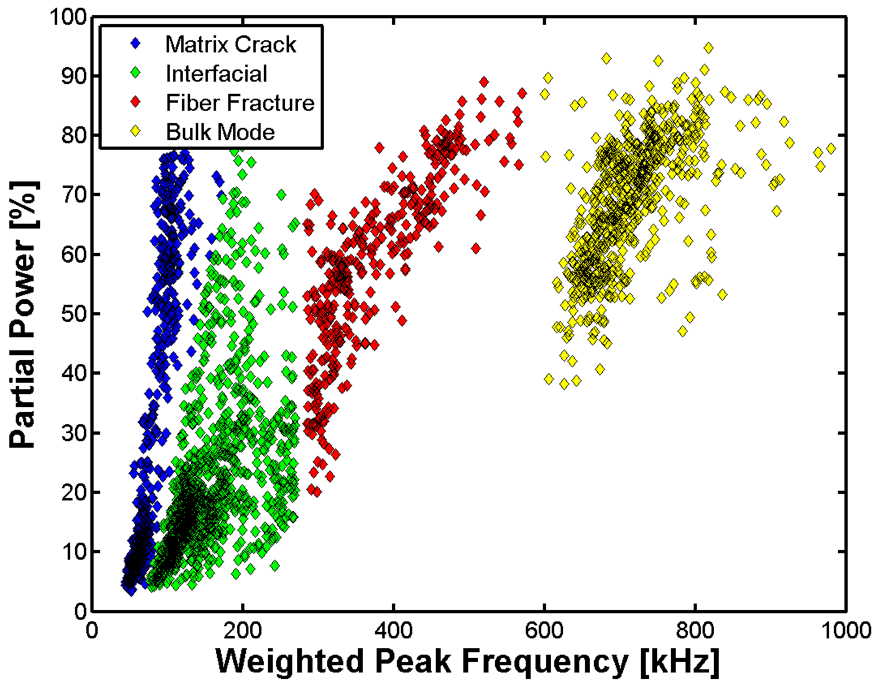

Figure E.17 – Source mechanism plot for cylinder ALT639-24574.

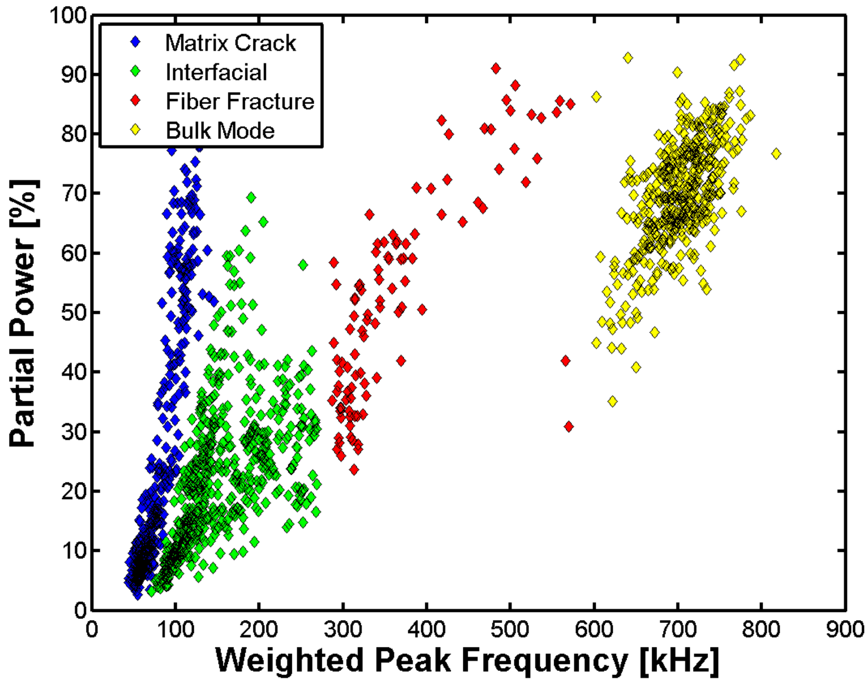

Figure E.18 – Source mechanism plot for cylinder ALT639-34005.

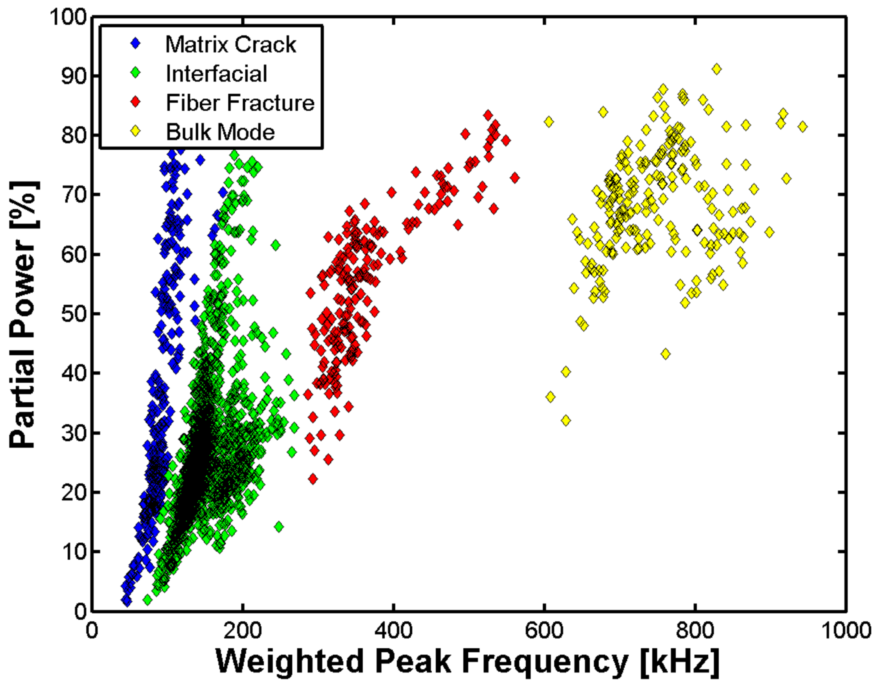

Figure E.19 – Source mechanism plot for cylinder ALT639-38566.

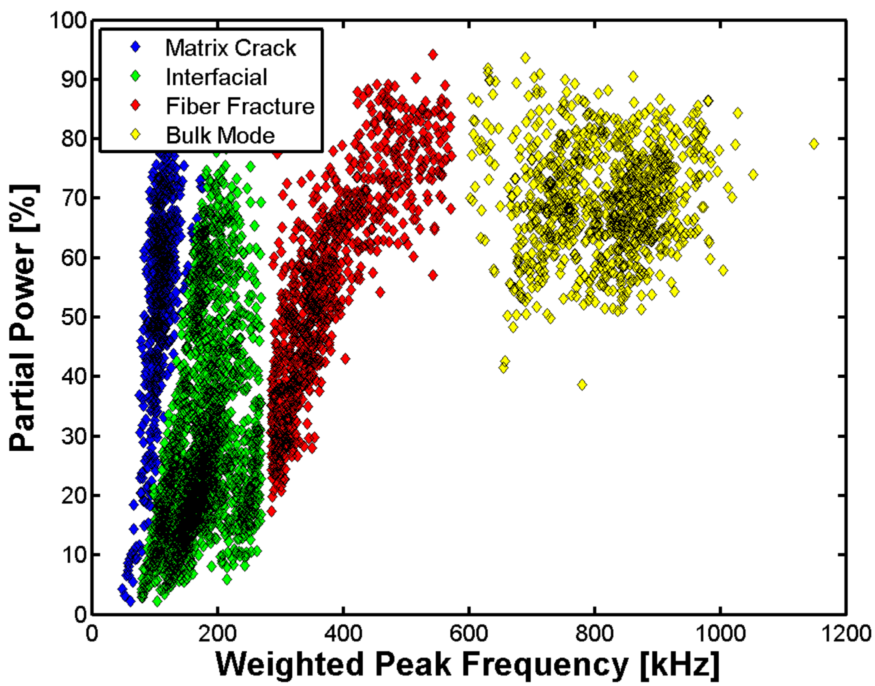

Figure E.20 – Source mechanism plot for cylinder ALT639-40136.

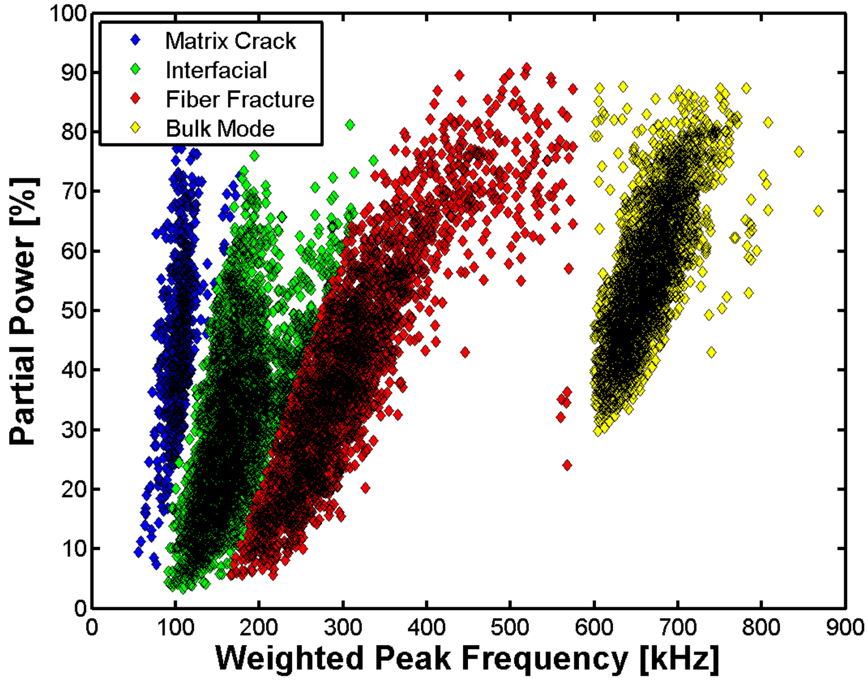

Figure E.21 – Source mechanism plot for cylinder ALT639-69988.

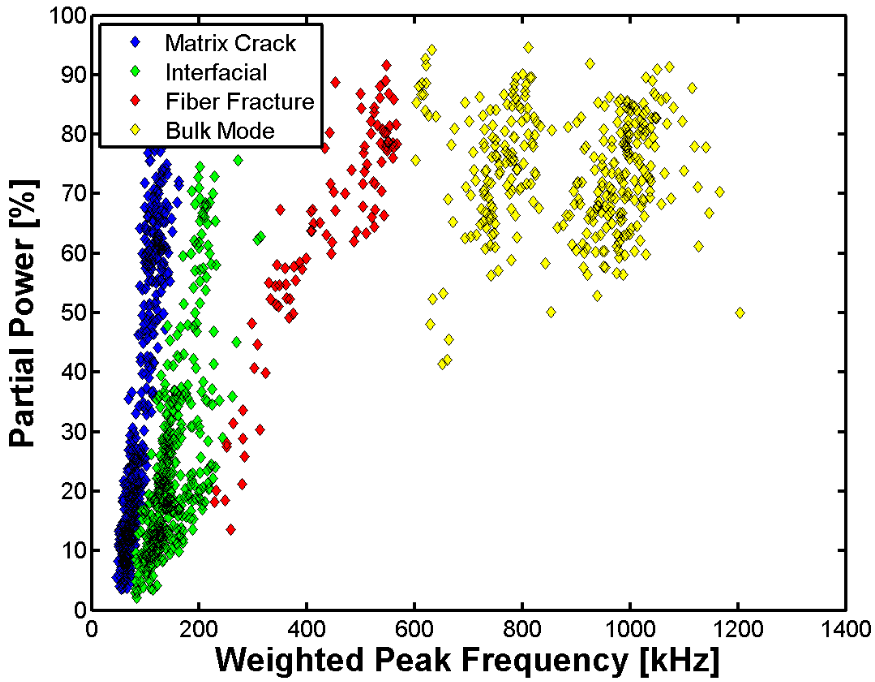

Figure E.22 – Source mechanism plot for cylinder ALT695-1862.

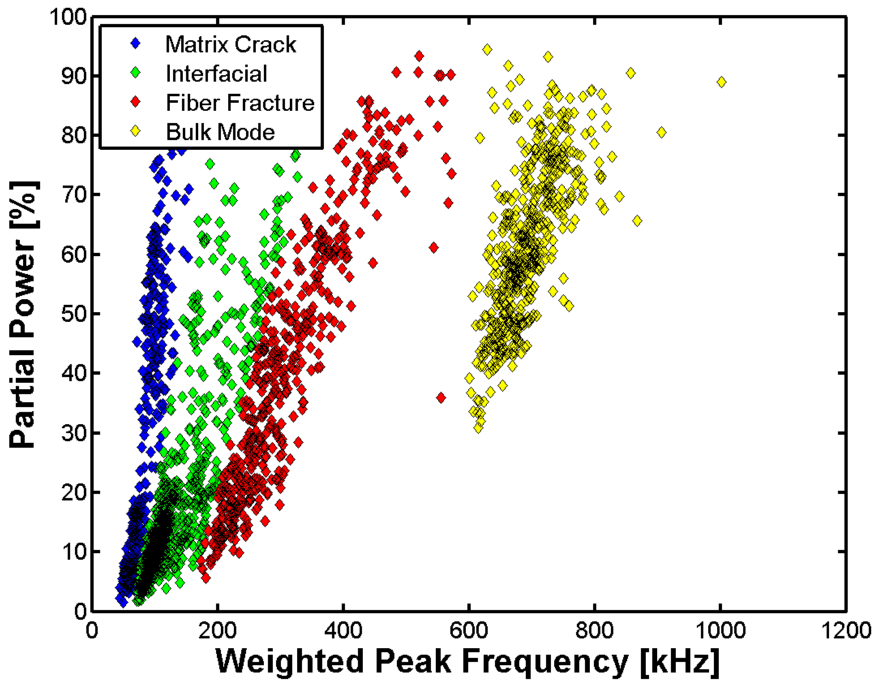

Figure E.23 – Source mechanism plot for cylinder ALT695-3224.

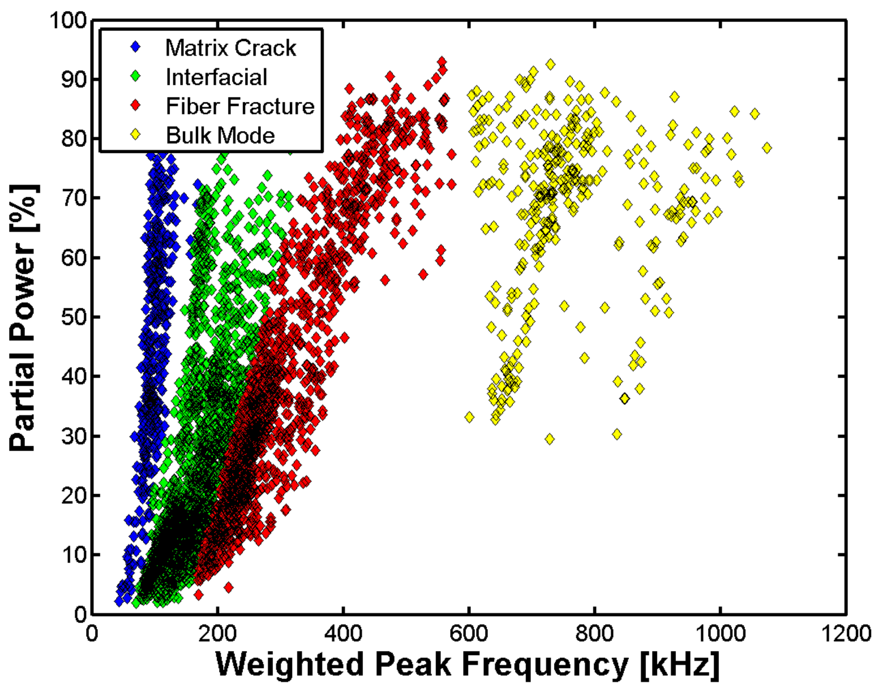

Figure E.24 – Source mechanism plot for cylinder ALT695-3313.

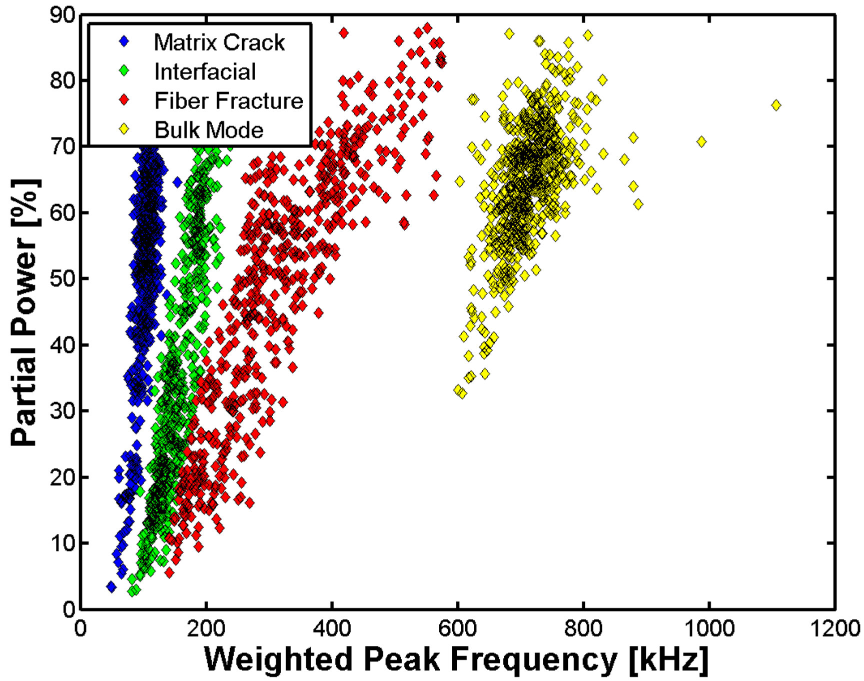

Figure E.25 – Source mechanism plot for cylinder ALT695-3575.

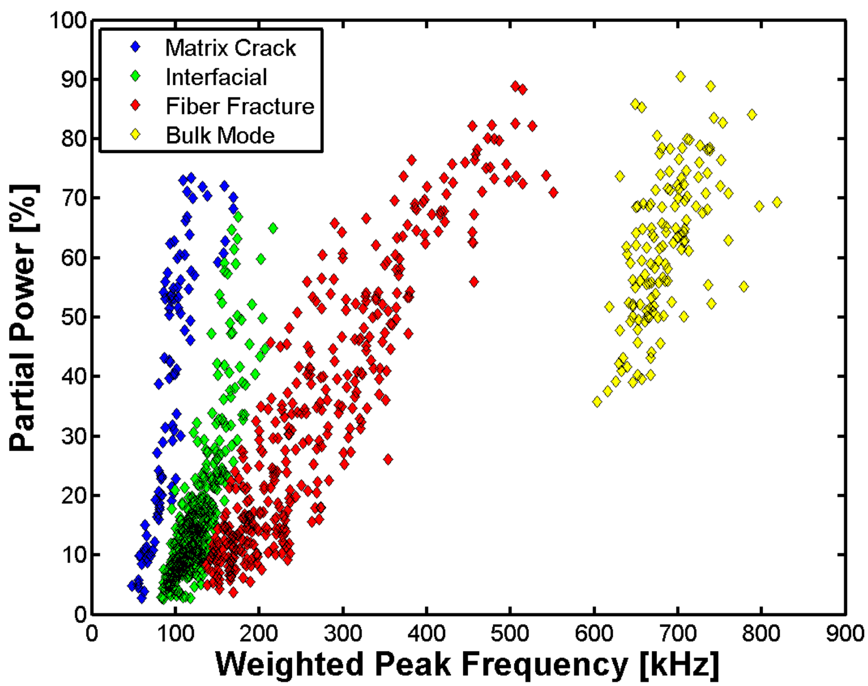

Figure E.26 – Source mechanism plot for cylinder ALT695-3646.

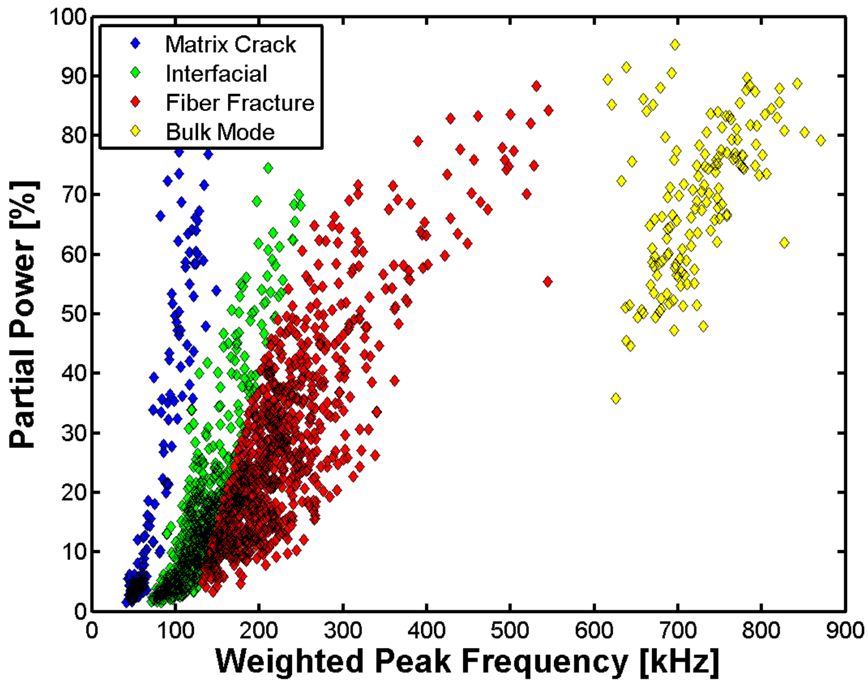

Figure E.27 – Source mechanism plot for cylinder ALT695-3771.

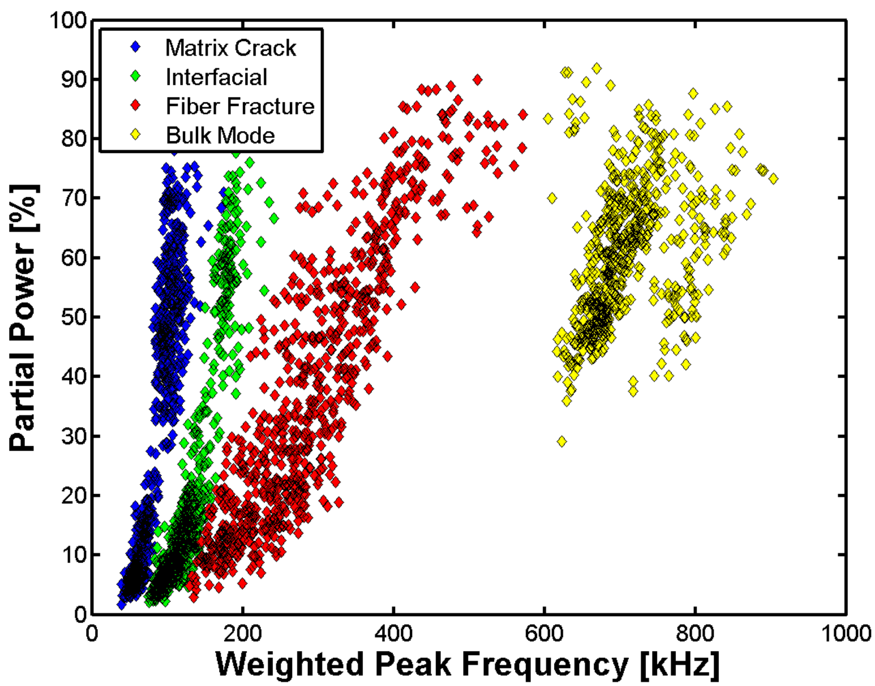

Figure E.28 – Source mechanism plot for cylinder ALT695-3798.

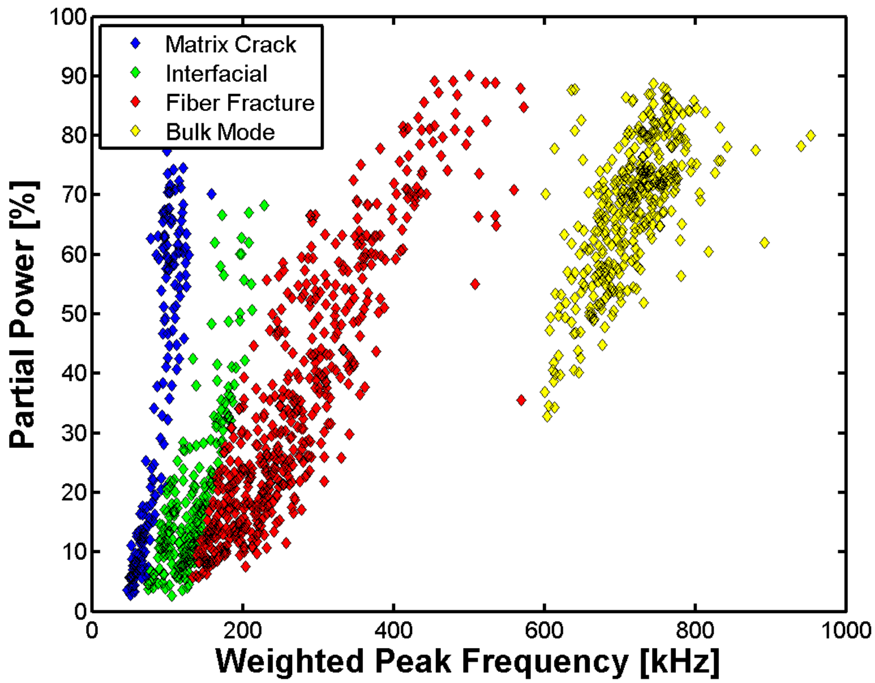

Figure E.29 – Source mechanism plot for cylinder ALT695-3881.

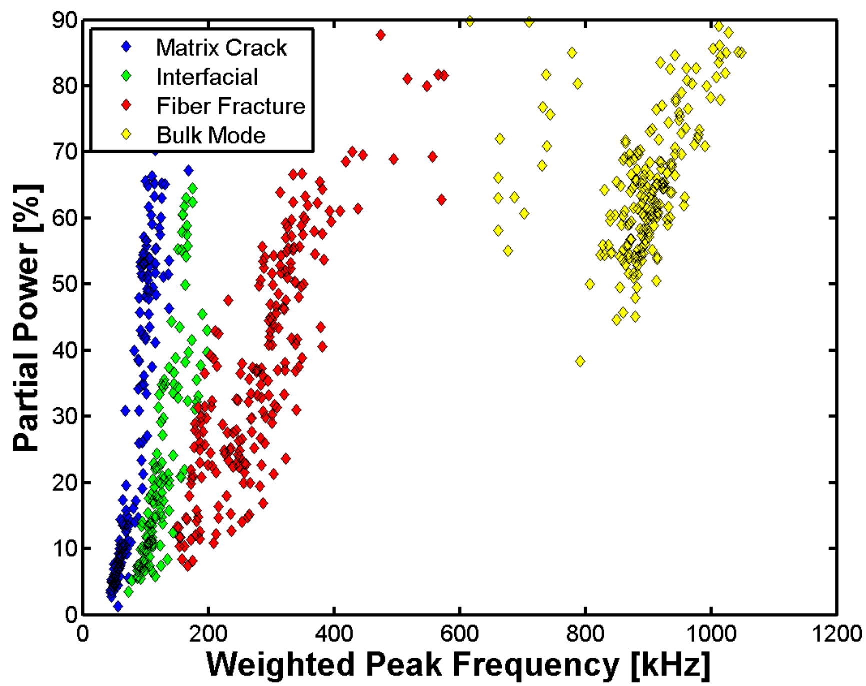

Figure E.30 – Source mechanism plot for cylinder ALT695-3936.

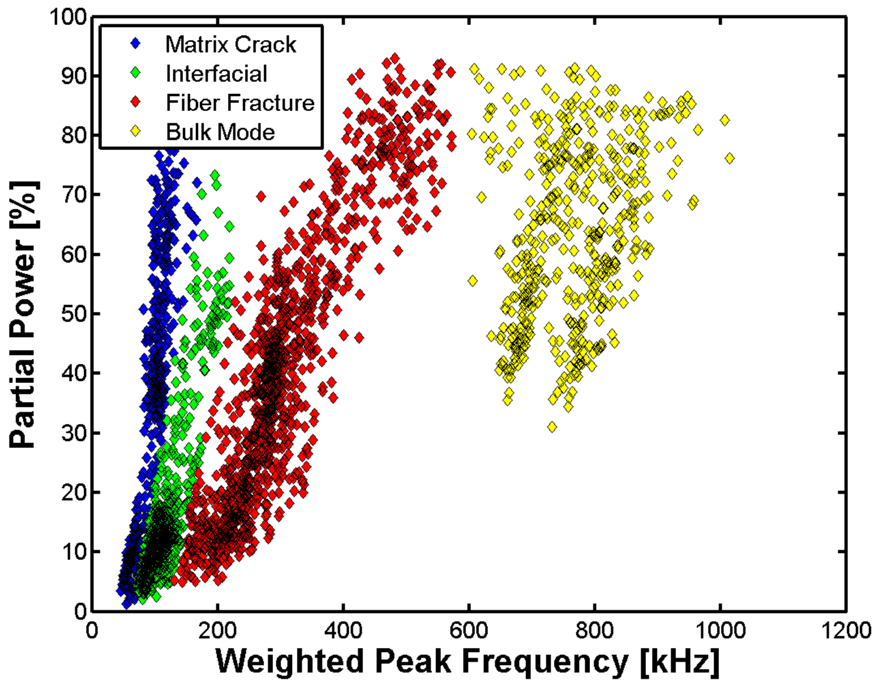

Figure E.31 – Source mechanism plot for cylinder ALT695-4379.

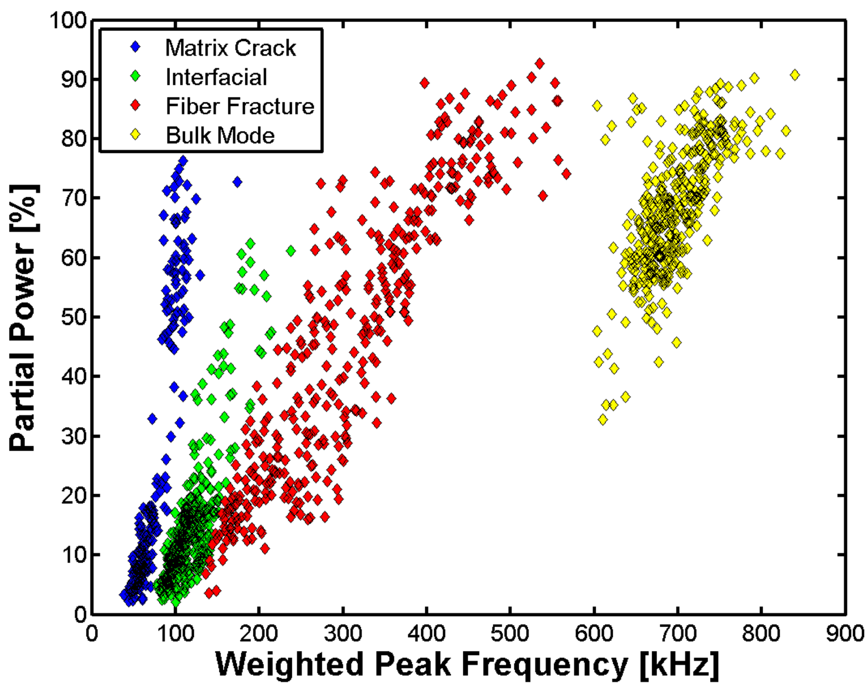

Figure E.32 – Source mechanism plot for cylinder ALT695-4396.

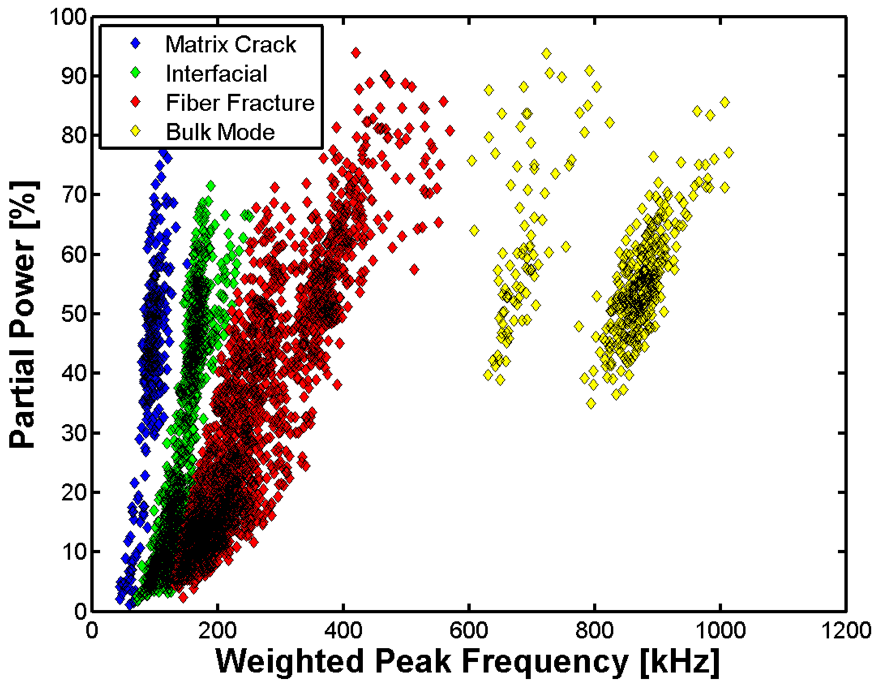

Figure E.33 – Source mechanism plot for cylinder ALT695-4469.

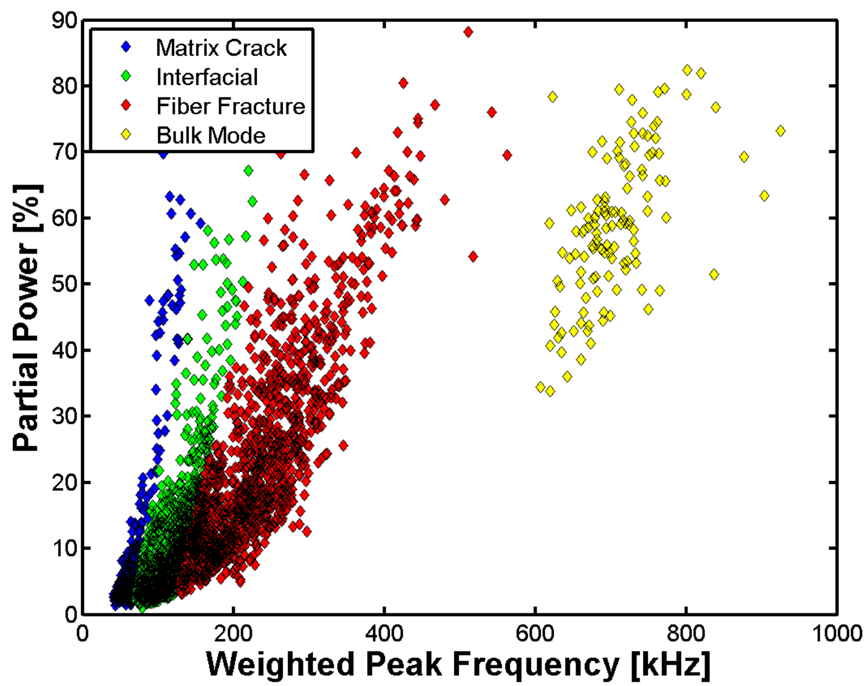

Figure E.34 – Source mechanism plot for cylinder ALT695-4482.

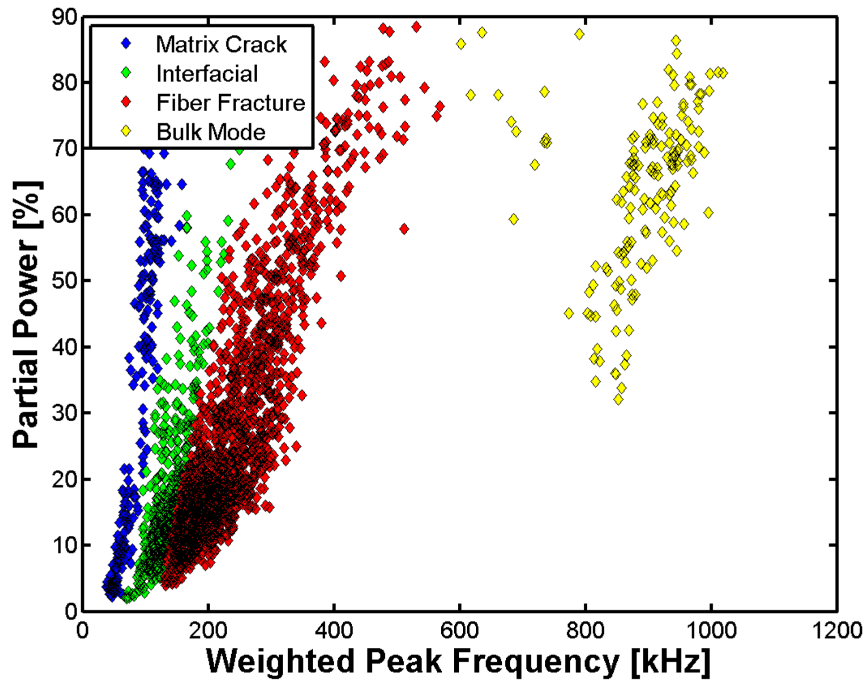

Figure E.35 – Source mechanism plot for cylinder ALT695-4492.

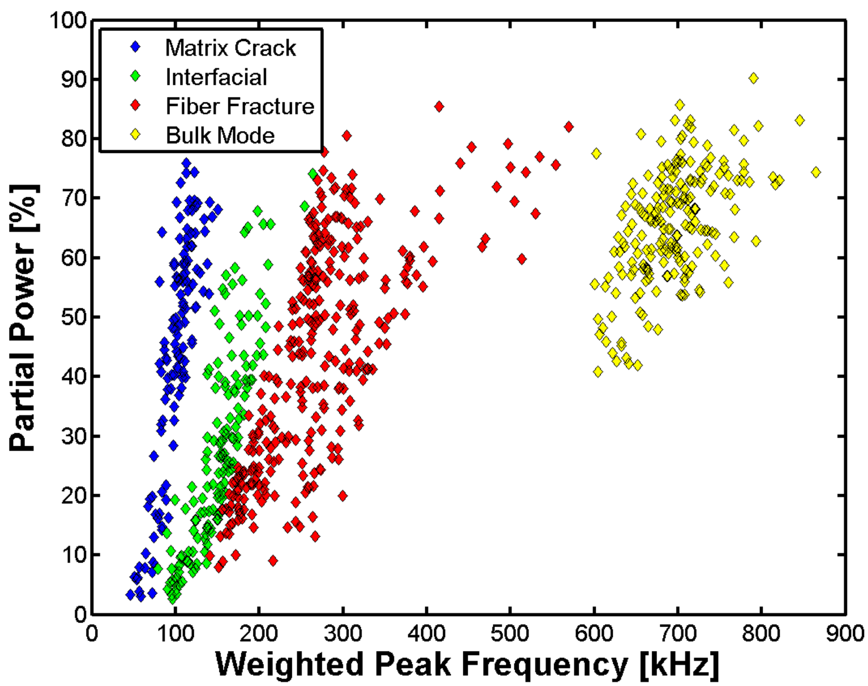

Figure E.36 – Source mechanism plot for cylinder ALT695-4734.

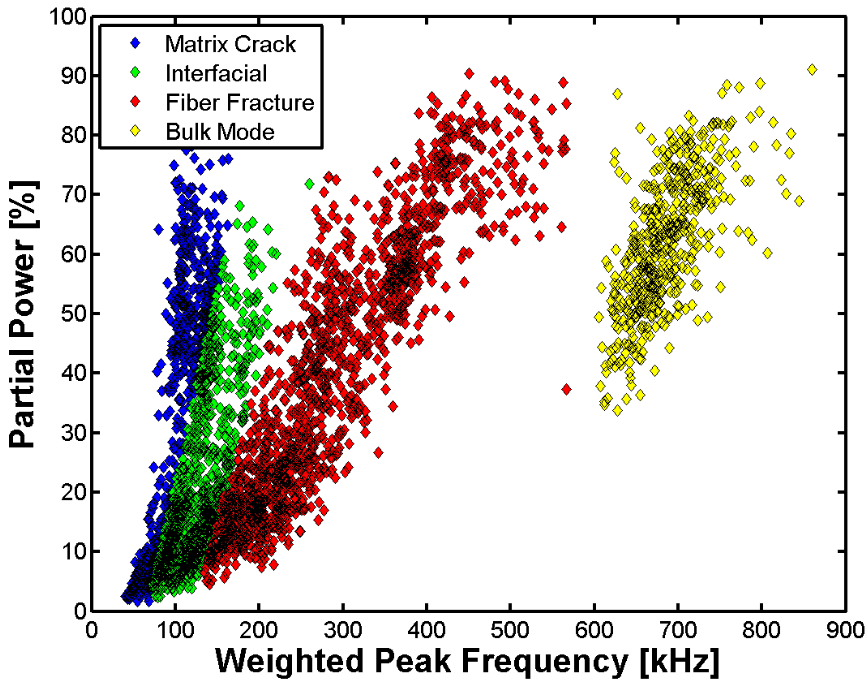

Figure E.37 – Source mechanism plot for cylinder ALT695-4775.

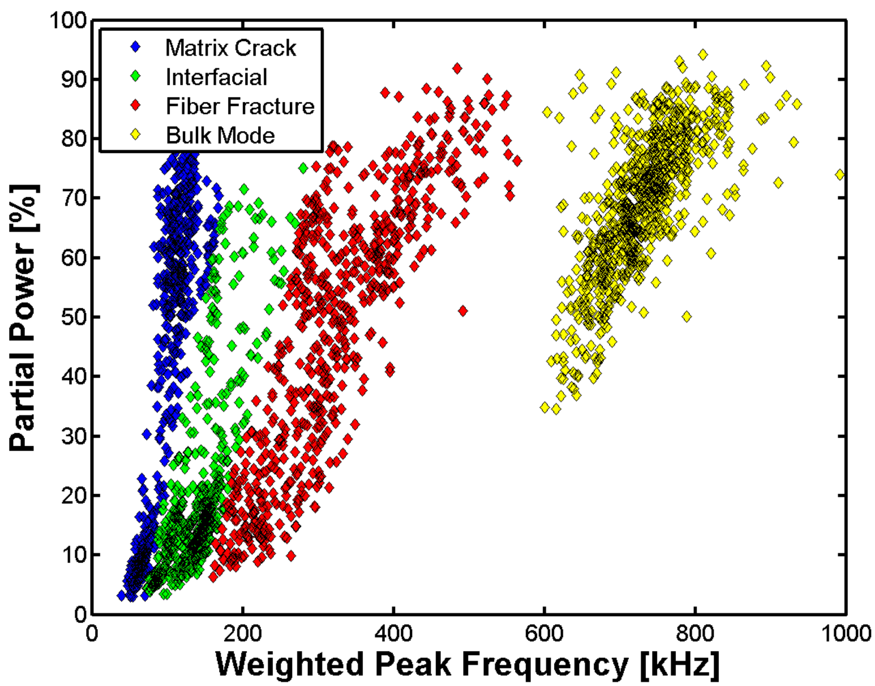

Figure E.38 – Source mechanism plot for cylinder ALT695-4944.

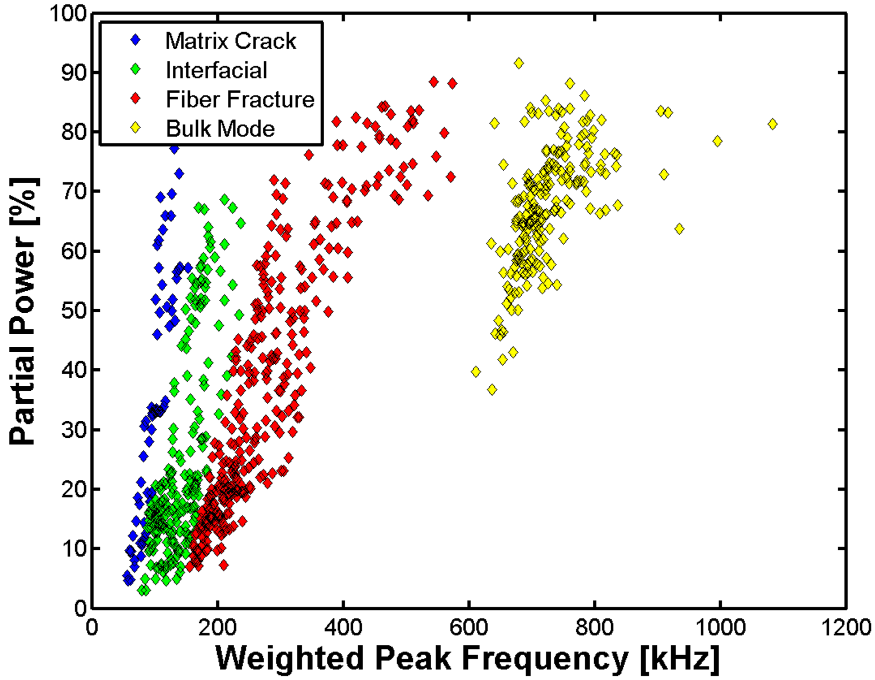

Figure E.39 – Source mechanism plot for cylinder ALT695-5497.

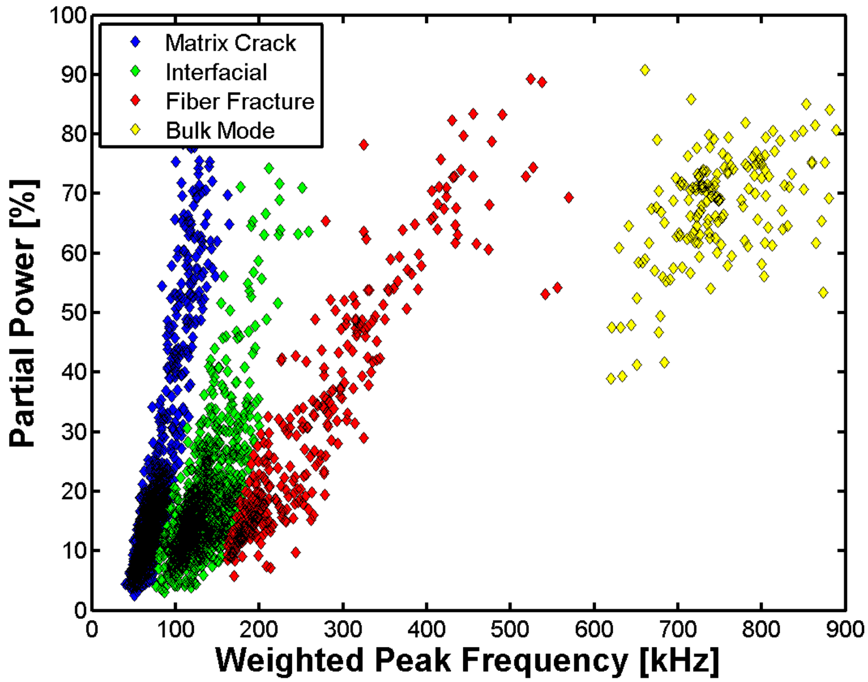

Figure E.40 – Source mechanism plot for cylinder ALT695-5558.

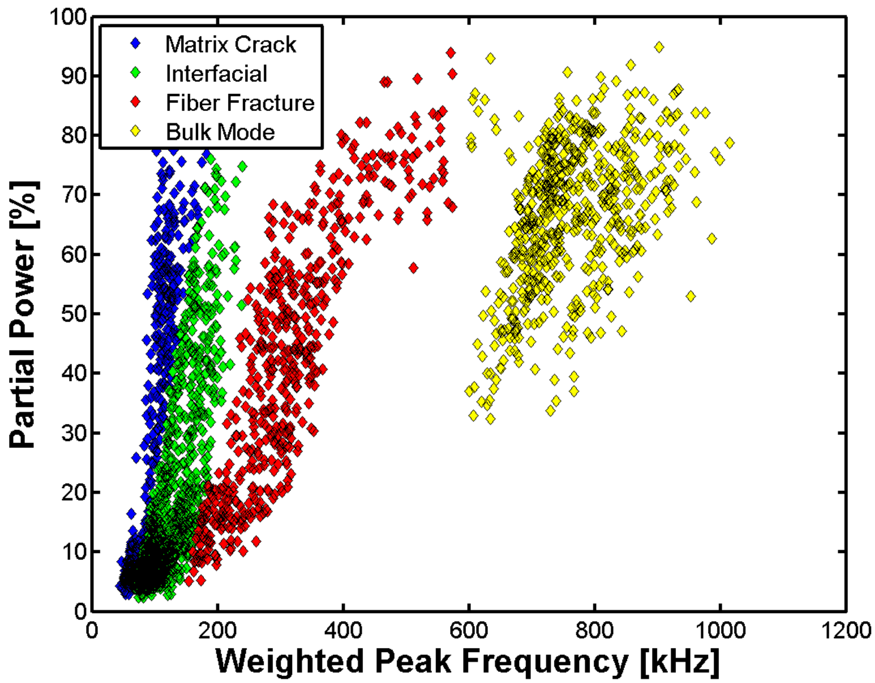

Figure E.41 – Source mechanism plot for cylinder ALT695-5641.

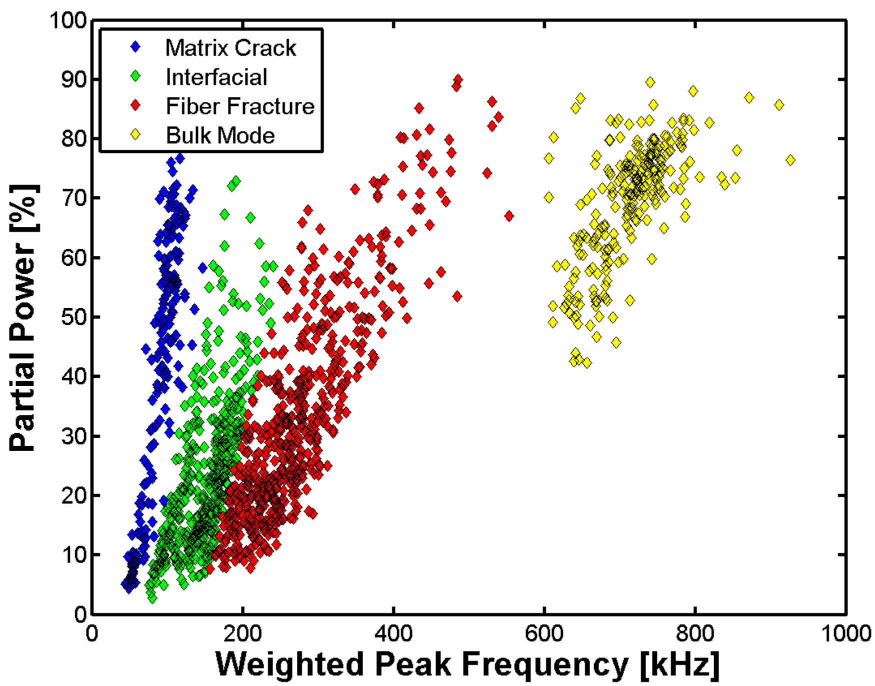

Figure E.42 – Source mechanism plot for cylinder ALT695-6041.

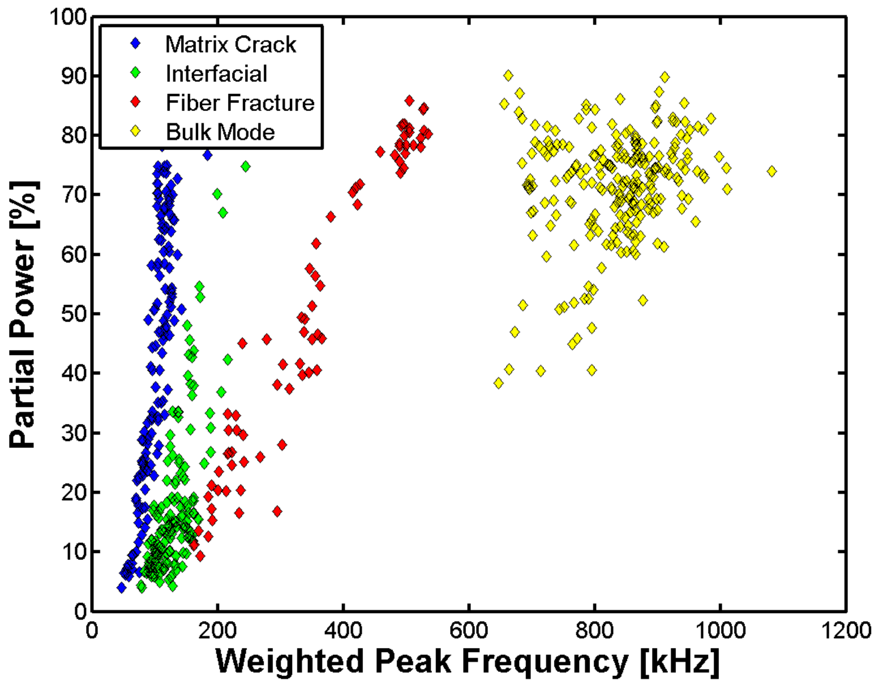

Figure E.43 – Source mechanism plot for cylinder IH667.

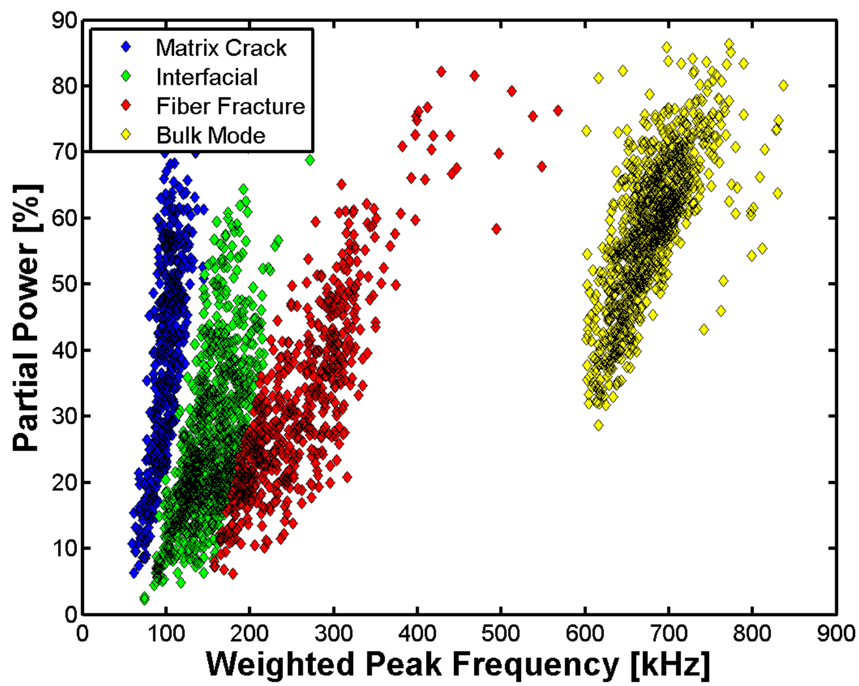

Figure E.44 – Source mechanism plot for cylinder IL2705.

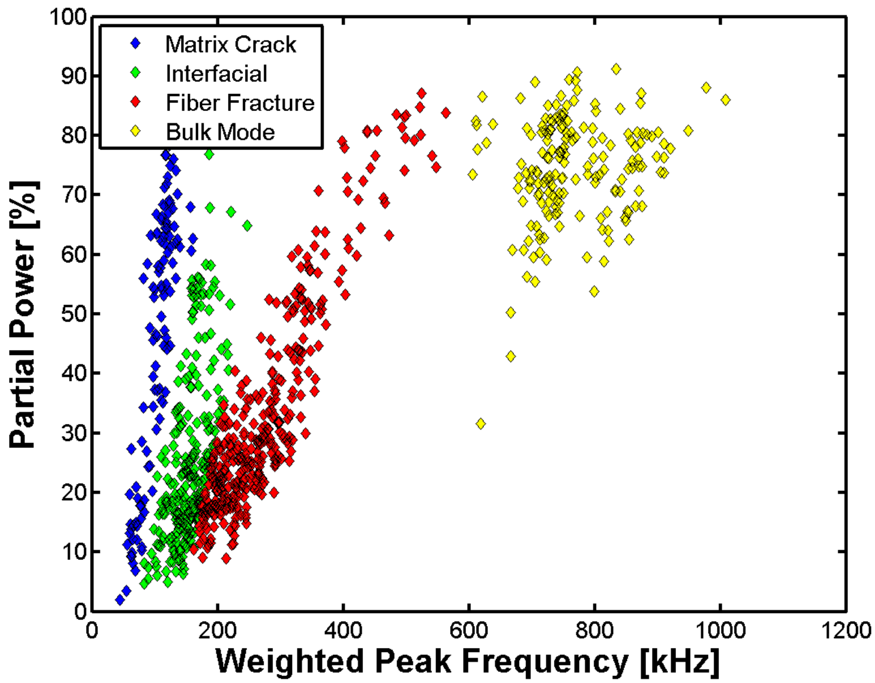

Figure E.45 – Source mechanism plot for cylinder IL2722.

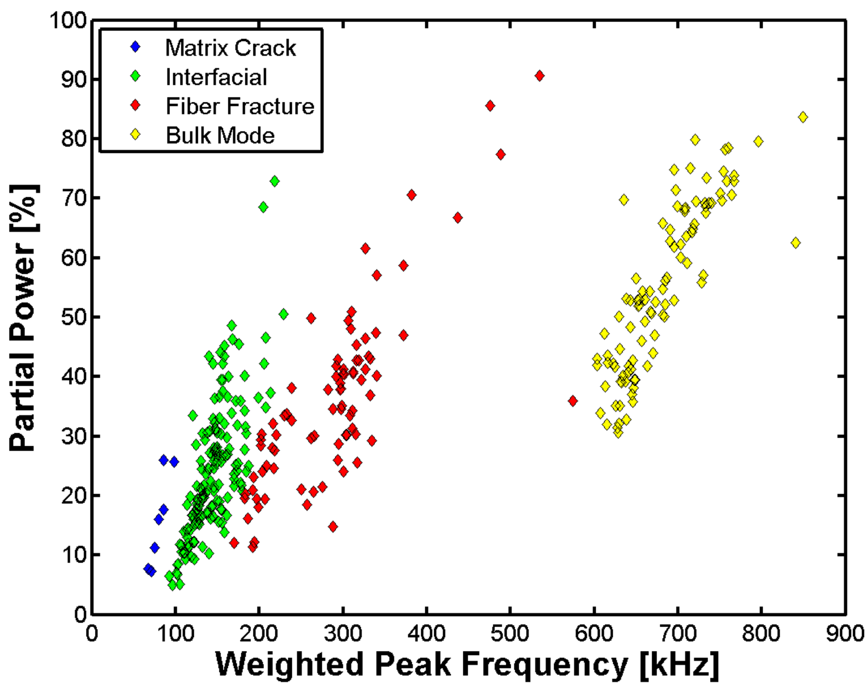

Figure E.46 – Source mechanism plot for cylinder IL2933.

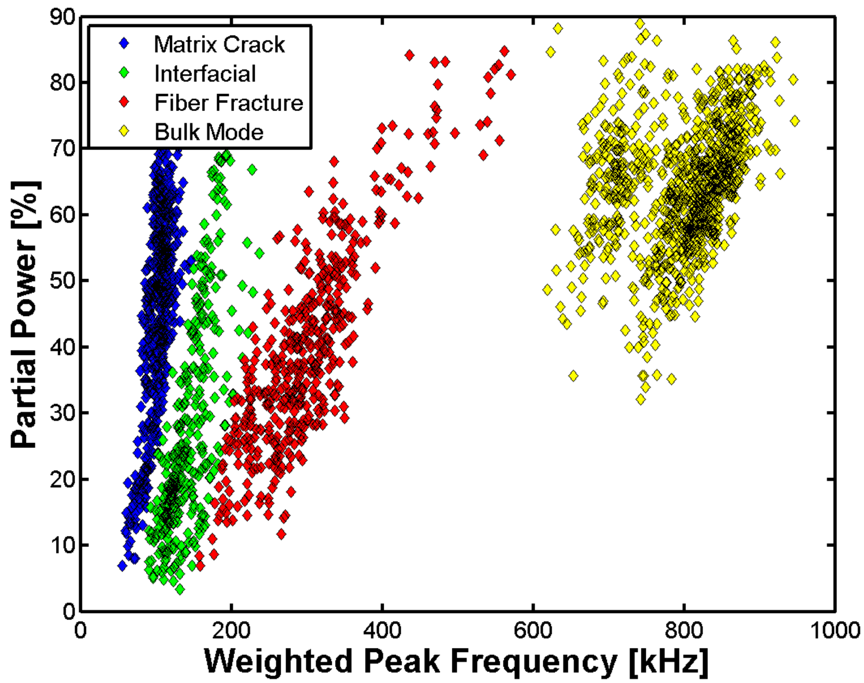

Figure E.47 – Source mechanism plot for cylinder IL3334.

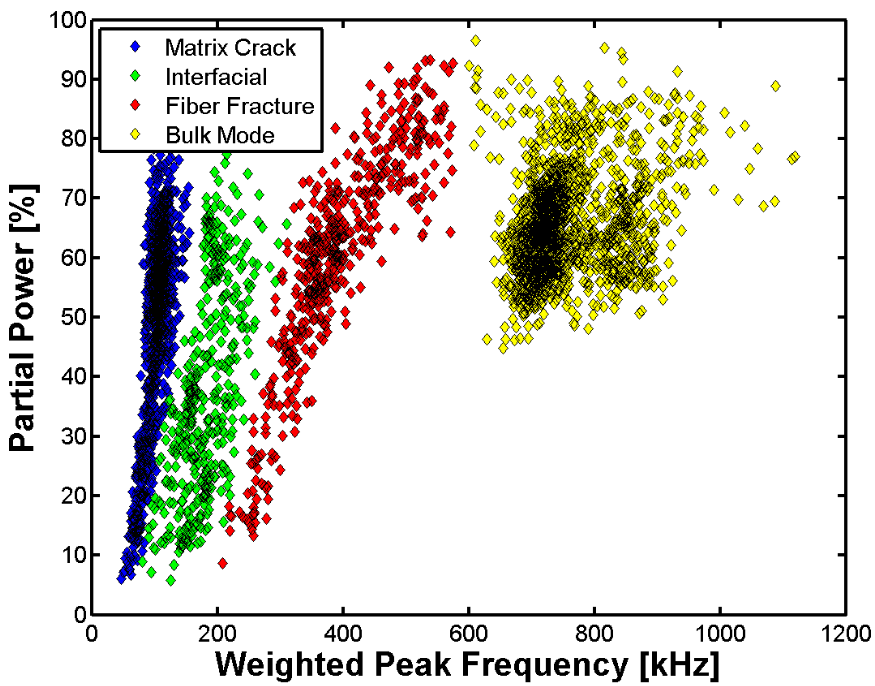

Figure E.48 – Source mechanism plot for cylinder OK85342.

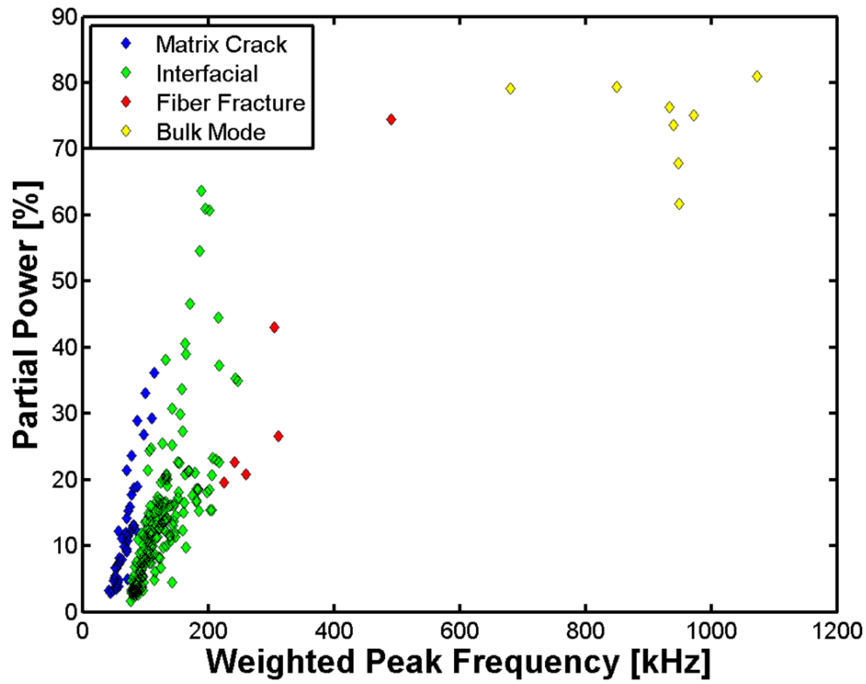

Figure E.49 – Source mechanism plot for cylinder ON3077.

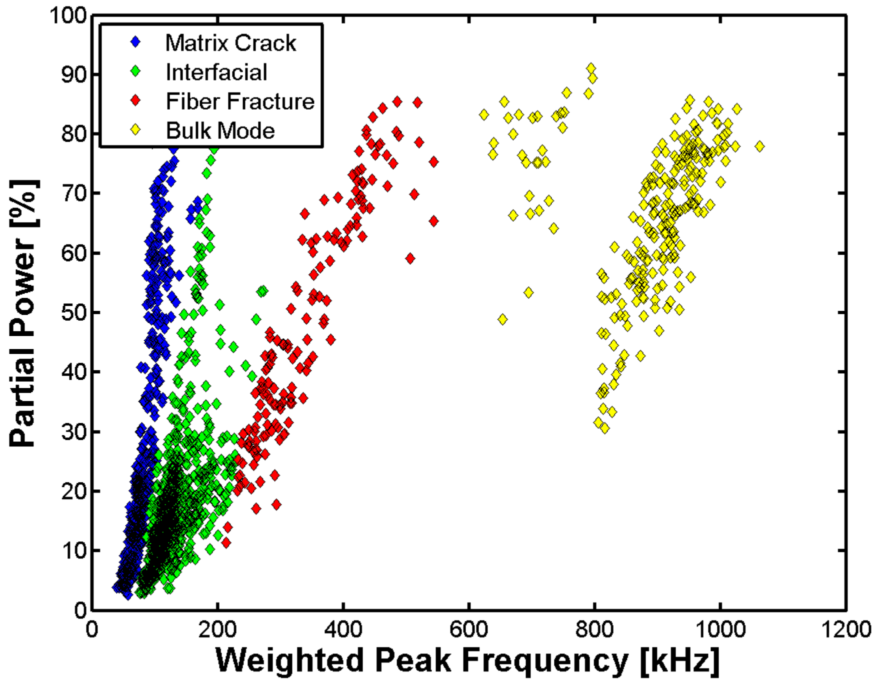

Figure E.50 – Source mechanism plot for cylinder ON3146.